"Antibody-mediated inhibition of Wnt-11 in prostate cancer"

Saray Sánchez Yagüe

Doctoral Thesis, 2021

Director: Robert Kypta, PhD
Co-director: Aitziber López Cortajarena, PhD
Tutor: Ana María Zubiaga Elordieta, PhD

Molecular Biology and Biomedicine Doctorate Program
Department of Genetics, Physical Anthropology and Animal Physiology
University of the Basque Country (UPV/EHU)

This work has been carried out at the Center for Cooperative Research in Biosciences (CIC bioGUNE) supported by the Basque Government Grant PRE_2018_2_0152

Table of contents

Table of contents **1**

List of figures **5**

List of tables **9**

Abbreviations **11**

Abstract **15**

Resumen **17**

Introduction **19**

1. Cancer 21
   - 1.1. Hypoxia in cancer 24
2. Therapeutic antibodies 26
3. Nanoparticles 29
4. The human prostate and prostate cancer 31
   - 4.1. Diagnosis and grading 31
   - 4.2. Prostate cancer progression and treatment 33
   - 4.3. Prostate cancer recurrent mutations 35
5. Wnt proteins 37
   - 5.1. Wnt modification and secretion 37
   - 5.2. Wnt structure 38
   - 5.3. Wnt signaling 40
     - 5.3.1. Wnt signaling regulators: antagonists and agonists 44
     - 5.3.2. Luciferase-based Wnt gene reporters 45
   - 5.4. Wnt receptors, coreceptors and DVL 46
     - 5.4.1. FZD receptors 47
     - 5.4.2. LRP5/6 coreceptors 47
     - 5.4.3. ROR/RYK coreceptors and others 48
     - 5.4.4. Dishevelled (DVL) 49
   - 5.5. Wnt in development and tissue homeostasis 50
   - 5.6. Wnt in cancer and prostate cancer 51

5.7. Wnt-based therapeutics 53
5.7.1. Inhibition of Wnt secretion 53
5.7.2. β-catenin interaction, stability, and activity modulators 53
5.7.3. Targeting Wnt pathway regulators 54
5.7.4. Wnt/receptor interaction modulators 55
6. Wnt-11 59
6.1. Wnt-11 in development and adult homeostasis 59
6.2. Wnt-11 in cancer and disease 60
6.2.1. Wnt-11 in prostate cancer 62
Hypothesis and aims 65
Materials and methods 69
1. Reagents 71
1.1. Anti-Wnt antibodies, recombinant proteins, peptides, and drugs 71
1.2. MNP functionalization 72
2. Cell culture 74
2.1. Cell lines 74
2.2. Cell transfection 75
2.2.1. Gene silencing 75
2.2.2. Plasmid transfection 76
2.2.3. Plasmid mutagenesis 76
2.2.4. E. coli transformation for plasmid amplification 78
2.3. Lentiviral transduction 78
2.4. Proliferation assay 79
2.5. Sphere assay 79
2.6. Transwell cell migration and invasion 80
2.7. Wound healing assay (Cell migration) 81
2.8. Gene reporter assay 81
3. mRNA analysis 83
3.1. RNA extraction 83
3.2. Retro-transcription reaction 83
3.3. Real-Time quantitative PCR (RT-PCR) 84
3.4. Primer design and sequences 84
4. Fluorescence activated cell sorting (FACS) 86
5. Protein analysis 87
5.1. Protein extraction 87
5.2. Western blot (WB) 87

5.3. Primary antibodies 88
5.4. Peptide ELISA 89
5.5. Dot blot 90
5.5.1. Peptide dot blot 90
5.5.2. Cell supernatant dot blot 90
5.6. Immunoprecipitation (IP) and pull-down 90
5.7. Immunofluorescence (IF) 92
5.8. Immunohistochemistry (IHC) 92
5.8.1. Prussian blue 93
6. Chick chorioallantoic membrane (CAM) model 94
7. Bioinformatics resources 97
7.1. Databases 97
7.2. Image analysis 97
8. Statistical analysis 99
Results 101
Chapter I: Characterization of anti-Wnt-11 antibodies and functionalized nanoparticles 103
I.1. Characterization of anti-Wnt-11 antibodies' recognition of Wnt-11 103
I.2. Functionalization of MNPs with anti-Wnt-11 antibodies 107
I.2.1. Recognition of prostate cancer cells by anti-Wnt-11-functionalized MNPs 108
Chapter II: Effects of anti-Wnt-11 monoclonal antibodies and MNP conjugates on prostate cancer cells *in vitro* 111
II.1. Anti-Wnt-11 monoclonal antibodies inhibit proliferation and sphere formation of prostate cancer cells 111
II.2. Anti-Wnt-11 monoclonal antibodies inhibit prostate cancer cell migration and invasion 114
II.3. Anti-Wnt-11 monoclonal antibodies inhibit hypoxia-induced migration of prostate cancer cells 118
II.4. Anti-Wnt-11 functionalized magnetic nanoparticles inhibit migration of prostate cancer cells 122
Chapter III: Effects of anti-Wnt-11 monoclonal antibodies and MNP-antibody conjugates on prostate cancer cells *in vivo* 125
III.1. Anti-Wnt-11 antibody E8 inhibits PC3 cell tumor growth in CAM assays 125
III.2. Anti-Wnt-11 functionalized magnetic nanoparticles partially inhibit PC3 cell tumor growth in CAM assays 130
Chapter IV: Mechanism of action of anti-Wnt-11 monoclonal antibodies 135

IV.1. Anti-Wnt-11 antibodies interfere with Wnt-11 signaling through DVL and ATF2 135
IV.2. The antibody epitope is required for Wnt-11 mediated migration and signaling 138
IV.2.1. Molecular characterization of the antibody epitope deletion mutant 138
IV.2.2. Functional role of the antibody epitope for Wnt-11-mediated prostate cancer cell migration 143
IV.2.3. The potential role of the antibody epitope in Wnt-11-mediated signaling 144
IV.3. The role of the antibody epitope in Wnt receptor and coreceptor binding 147
IV.3.1. Structural context 147
IV.3.2. Interaction of Wnt-11 and the antibody epitope mutant with FZD8 150
IV.3.3. Interaction of Wnt-11 and the antibody epitope mutant with LRP6 151
IV.4. Effect of the Wnt-11 antibody epitope mutation on signaling by Wnt receptors and coreceptors 156
Discussion 161
Chapter I: Characterization of anti-Wnt-11 antibodies and functionalized nanoparticles 165
Chapter II: Effects of anti-Wnt-11 monoclonal antibodies and MNP conjugates on prostate cancer cells *in vitro* 167
Chapter III: Effects of anti-Wnt-11 monoclonal antibodies and MNP-antibody conjugates on prostate cancer cells *in vivo* 171
Chapter IV: Mechanism of action of anti-Wnt-11 monoclonal antibodies 175
Conclusions 187
References 191
Resumen extendido 211
Introducción 211
Hipótesis y objetivos 212
Materiales y métodos 212
Resultados 213
Capítulo I: Caracterización de anticuerpos anti-Wnt-11 y sus conjugados con nanopartículas magnéticas (MNP) 213
Capítulo II: Efectos de los anticuerpos anti-Wnt-11 y sus conjugados con MNP en células de cáncer de próstata *in vitro* 214
Capítulo III: Efectos de los anticuerpos anti-Wnt-11 y sus conjugados con MNP en células de cáncer de próstata *in vivo* 215
Capítulo IV: Mecanismo de acción de los anticuerpos anti-Wnt-11 215
Conclusiones 217

List of figures

Figure 1. The hallmarks of cancer (a) and tumor microenvironment (b). 22
Figure 2. Transcription regulation induced by hypoxia. 25
Figure 3. Generic antibody structure and domains. 26
Figure 4. Representation of magnetic nanoparticles (MNP). 29
Figure 5. The Gleason grading system of prostate cancer. 32
Figure 6. Prostate cancer progression and treatment. 34
Figure 7. Wnt structure. 39
Figure 8. Wnt/β-catenin signaling. 41
Figure 9. β-catenin-independent Wnt signaling. 42
Figure 10. Domain organization of FZD, LRP and DVL. 46
Figure 11. Summary of selected Wnt-based therapeutic agents. 57
Figure 12. Wnt-11 in prostate cancer. 64
Figure 13. Generation of anti-Wnt-11 antibodies E8 and F10. 71
Figure 14. Scheme for MNP functionalization of anti-Wnt-11 antibodies E8, F10 and rat IgG control using sulfo-SMCC. 73
Figure 15. Scheme of protein analysis of FACS sorted cells. 86
Figure 16. Experimental designs for PA-tagged Wnt-11 (W11) or antibody epitope mutant (AE) immunoprecipitation (IP) or pull-down with VSV-G or Fc tagged LRP6. 91
Figure 17. Scheme of chick chorioallantoic membrane (CAM) assay of tumor growth. 96
Figure 18. Example images obtained for automated cell counting of migrating cells using the ImageJ macro shown in Table 12. 98
Figure 19. Detection of recombinant Wnt-11 protein and ectopic Wnt-11 in C4-2B cells with E8 antibody. 105
Figure 20. Detection of Wnt-11 protein levels of FACS-sorted HEK 293 cells overexpressing Wnt-11 transiently. 106
Figure 21. MNP aggregation under low fetal bovine serum (FBS) conditions in RPMI media. 108
Figure 22. Prussian Blue staining of VCaP cells incubated with MNP conjugates for 2 h at 37 °C and 4 °C. 109
Figure 23. Proliferation assays of PC3 (a) and DU145 (b) cells treated with E8 and F10. 111
Figure 24. Potential role of Wnt-11 in prostate cancer cell stemness. 112
Figure 25. Sphere formation assays for PC3 and DU145 cells treated with E8 and F10. 113
Figure 26. Wound healing assays for *WNT11* gene silencing and anti-Wnt-11 antibody treatment in PC3 cells. 115
Figure 27. Transwell migration assays for prostate cancer cells treated with E8 and F10. 116

Figure 28. Transwell invasion assays of C4-2B-V and C4-2B-WNT11 cells treated with E8 and F10. 117

Figure 29. Analysis of Wnt-11 protein expression upon treatment with the hypoxia mimetic DMOG. .. 118

Figure 30. mRNA expression analysis of selected Wnt signaling components upon treatment with the hypoxia mimetic DMOG. 120

Figure 31. Transwell migration assays of PC3 cells carried out under hypoxic conditions with E8 antibody treatment. 121

Figure 32. Proliferation and wound healing assays of PC3 cells treated with MNP nanoformulations. .. 123

Figure 33. Histology and Wnt-11 immunohistochemistry of PC3 CAM tumors. 126

Figure 34. Effect of E8 and IgG control antibodies in PC3 tumor growth on the CAM. 127

Figure 35. Proliferation marker Ki67 IHC staining of PC3 CAM tumors treated with E8 and IgG control antibodies. 129

Figure 36. Effect of MNP nanoformulations on PC3-GFP tumor growth on the CAM. 130

Figure 37. IHC of Ki67 and Prussian Blue stainings in PC3-GFP CAM tumors treated with MNP-IgG and MNP-E8. 133

Figure 38. DVL status upon anti-Wnt-11 antibodies treatment in PC3 cells. 136

Figure 39. Effect of Wnt-11 ectopic expression and E8 treatment on ATF2-luc reporter activity in PC3 cells. 137

Figure 40. Antibody epitope location in Wnt sequence and structure. 139

Figure 41. Antibody epitope mutant (AE) expression and secretion. 140

Figure 42. Cell surface immunofluorescence staining of Wnt-11 and antibody epitope mutant (AE). 141

Figure 43. Detection of Wnt-11 protein levels of FACS-sorted HEK 293 cells transfected with plasmids for Wnt-11 and antibody epitope mutant (AE) expression. 142

Figure 44. Transwell migration assays of PC3M cells transfected for the expression of Wnt-11 (W11) and antibody epitope mutant (AE). 143

Figure 45. Effect of Wnt-11 (W11) and antibody epitope mutant (AE) ectopic expression on DVL status. 144

Figure 46. Effect of Wnt-11 (W11) and antibody epitope mutant (AE) ectopic expression on TOP-luc reporter activity stimulated with Wnt-3a conditioned media (CM). 145

Figure 47. Structure of Wnt-3 in complex with FZD8-CRD highlighting the Wnt-11 antibody epitope region. 148

Figure 48. Juxtaposition of Wnt-3 with Fab structures. 149

Figure 49. Immunoprecipitation of Wnt-11 (W) and antibody epitope mutant (AE) with FZD8-CRD in PC3 cells. 150

Figure 50. Analysis of Wnt-11 and LRP6 interaction and co-expression. 151

Figure 51. Immunoprecipitation of Wnt-11 (W) and the antibody epitope mutant (AE) with VSV-G tagged LRP6 in HEK 293 cells. 152

Figure 52. Immunoprecipitation of Wnt-11 (W) and the antibody epitope mutant (AE) with the Fc-tagged extracellular domain of LRP6 (LRP6N) in HEK 293 and PC3 cells. 153

Figure 53. Imunofluorescence co-localization of Wnt-11 and antibody epitope mutant (AE) with VSV-G-tagged full length LRP6 in PC3 cells. 154

Figure 54. Effects of Wnt-11 (W11) and antibody epitope mutant (AE) on LRP6-mediated activation of β-catenin/TCF-mediated signaling. 156

Figure 55. Effects of Wnt-11 (W11) and LRP6 expression in ATF2-depedent transcription. 157

Figure 56. Effects of Wnt-11 (W11) and antibody epitope mutant (AE) in combination with FZD8 and LRP6 in ATF2-dependent transcription in HEK 293 LRP5/6 $^{-/-}$ knock-out cells.....158

Figure 57. Modeled Wnt-11 and antibody epitope mutant (AE) structures using AlphaFold.....177

Figure 58. Working model of anti-Wnt-11 antibodies and MNP nanoformulations strategy in the treatment of advanced prostate cancer.....184

List of tables

Table 1. Characteristics of the MNP-Ab conjugation batches generated. 74
Table 2. Cell lines characteristics and culture conditions. 75
Table 3. LTX/Plus plasmid transfection volume and concentrations. 76
Table 4. Plasmids used for ectopic expression. 77
Table 5. Details of the protein tags carried in some of the exogenous expression plasmids shown in Table 4. 77
Table 6. Plasmids specific for gene reporter assays. 77
Table 7. Plasmids used for lentiviral transduction. 79
Table 8. Volumes and concentrations of reagents for retro-transcription reactions. 84
Table 9. Details of primers used for RT-PCR. 85
Table 10. SDS-polyacrylamide gel information. 88
Table 11. List of primary antibodies and experimental details. 89
Table 12. Example ImageJ macro used for automated cell counting of migrating cells. 98
Table 13. *WNT11* mRNA expression in the prostate cancer cell lines used. 104
Table 14. Dynamic light scattering (DLS) measurements of the MNP nanoformulations, 2020 batch. 108
Table 15. Statistical analysis of PC3 CAM tumor weight upon treatment with E8 and IgG control antibodies. 128
Table 16. Statistical analysis of PC3 CAM tumor area upon treatment with E8 and IgG control antibodies. 128
Table 17. Statistical analysis of Ki67 IHC staining of PC3 CAM tumors treated with E8 and IgG control. 129
Table 18. Statistical analysis of PC3-GFP CAM tumor area upon treatments with MNP nanoformulations. 132
Table 19. Statistical analysis of PC3-GFP CAM tumor weight upon treatments with MNP nanoformulations. 132
Table 20. Statistical analysis of data presented in Figure 56. 159

Abbreviations

1x	ATF2-Luc reporter 1 copy
2D	Two-dimensional
3D	Three-dimensional
95 CI	95% confidence intervals
A	Ampere
A_{370}	Absorbance at 370 nm
Ab	Antibody
ADT	Androgen Deprivation Therapy
AE	Antibody Epitope mutant
ANOVA	Analysis of variance
AP-1	Activator protein 1
APC	Adenomatous polyposis coli gene product
APS	Ammonium persulfate
AR	Androgen receptor
ATCC	American Type Culture Collection
ATF2	Activating transcription factor
bp	Base pairs
CAM	Chick chorioallantoic membrane
cDNA	Complementary DNA
CDS	Coding sequence
C_H	Heavy chain constant domain (Ab)
CK1	Casein kinase 1
C_L	Light chain constant domain (Ab)
CM	Conditioned media
CRD	Cysteine-rich domain
CRPC	Castration resistant prostate cancer
CT	Cycle threshold (RT-PCR)
C-ter	C-terminal, carboxyl-terminus (protein)
DAB	3,3'-diaminobenzidine (IHC)
ddH_2O	Double distilled water
DEP	DVL, Egl-10, Pleckstrin domain (DVL)
DIX	DVL and Axin domain
DKK	Dickkopf-related proteins
DMOG	Dimethyloxaloylglycine
DMSO	Dimethyl sulfoxide
DNA	Deoxyribonucleic acid
dNTP	Nucleoside triphosphate
DVL	Dishevelled
EDD	Embryo development day (CAM)
EDTA	Ethylenediaminetetraacetic acid
ELISA	Enzyme linked immunosorbent assay
EMT	Epithelial to mesenchymal transition
EPR	Enhanced permeability and retention
ERG	ETS-related gene
EtOH	Ethanol
F12	Ham's F12 culture medium
Fab	Antigen-binding fragment (Ab)
FACS	Fluorescence-activated cell sorting
FBS	Fetal bovine serum
Fc	Fragment crystallizable (Ab)
FDA	Food and Drug Administration
Fe	Iron
FIH-1	Factor inhibiting HIF-1α
FZD	Frizzled
g	Times gravity (centrifugation)
G418	Geneticin
GFP	Green fluorescent protein

GSK3	Glycogen synthase kinase 3
h	Hours
HBS	HEPES-buffered solution
HER2	Receptor tyrosine-protein kinase erbB-2
HIF	Hypoxia-inducible factor
HRP	Horseradish peroxidase
HSP60	60 kDa heat shock protein, mitochondrial
IF	Immunofluorescence
Ig	Immunoglobulin
IHC	Immunohistochemistry
IP	Immunoprecipitation
IQR	Interquartile range
IV	Intravenous
JNK	Jun-N-terminal kinase
Jun	Transcription factor AP-1
kDa	Kilodalton
LEF/LEF1	Lymphoid enhancer-binding factor 1
LGR	Leucine-rich repeat-containing G protein-coupled receptors
LRP	Low-density lipoprotein receptor-related proteins (5/6)
M	Molar
mAb	Monoclonal antibody
MAD	Median absolute deviation
mg	Miligram
min	Minute
ml	Mililiter
mm	Milimeter
MMTV	Mouse mammary tumor virus
MNP	Magnetic nanoparticle
mRNA	Messenger RNA
mt5	Mutant 5 of ATF2-Luc reporter
mV	Millivolts
NE	Neuroendocrine
NED	Neuroendocrine differentiation
NFAT	Nuclear factor of activated T-cells
ng	Nanogram
NIH	National Institutes of Health
NKD1	Naked-1
nm	Nanometer
nM	Nanomolar
NP	Nanoparticle
N-ter	N-terminal, amino-terminus
°C	Degree Celsius
PAM	Palmitoleic acid
PBS	Phosphate-buffered saline
PCP	Planar cell polarity
PCR	Polymerase chain reaction
PDZ	Postsynaptic density 95, discs large, zonula occludens-1 domain (DVL)
PEG	Polyethylene glycol
PFA	Paraformaldehyde
PHD	Prolyl hydroxylase
PI3K	Phosphatidylinositol 3-kinase
PIN	Intraepithelial neoplasia
PKC	Protein kinase C
PSA	Prostate-specific antigen
Q1	Quartile 1
Q3	Quartile 3
Rel.	Relative
RIPA	Radioimmunoprecipitation assay
RNA	Ribonucleic acid
RNF43	E3 ubiquitin-protein ligase RNF43
ROCK	Rho-associated protein kinase
ROR	Inactive tyrosine-protein kinase transmembrane receptor (1/2)
RSPO	R-spondins
RT	Room temperature
RT-PCR	Real-time polymerase chain reaction
RYK	Tyrosine-protein kinase
SDS	Sodium dodecyl sulfate

SDS-PAGE	Sodium dodecyl sulfate polyacrylamide gel electrophoresis
sec	Second
SEM	Standard error of the mean
sFRP	Secreted frizzled-related proteins
siRNA	Small interfering RNA (gene silencing)
SOX2	SRY-box transcription factor 2
SPION	Superparamagnetic iron oxide nanoparticle
TAZ	WW domain containing transcription regulator 1
TBS	Tris (hydro methyl) aminomethane-buffered saline
TBST	Tris (hydro methyl) aminomethane-buffered saline 0.5% Tween20
TCF	T-cell factor
TEMED	Tetramethylethylenediamine
TGF-β	Transforming growth factor beta
TMPRSS2	Transmembrane protease serine 2
V	Volts
v/v	Volume-volume (concentration)
V_H	Heavy chain variable domain (Ab)
V_L	Light chain variable domain (Ab)
VSV-G	Vesicular stomatitis virus (VSV) glycoprotein (G)
w/v	Weight-volume (concentration)
W11	Wnt-11
WB	Western blot
WLS	Wntless
YAP	Yes-associated protein 1
ZNRF3	E3 ubiquitin-protein ligase ZNRF3
µg	Microgram
µl	Microliter
µm	Micrometer
µM	Micromolar

Abstract

Wnt-11 is highly expressed in metastatic prostate cancer, where it is known to promote neuroendocrine-like differentiation, survival, and migration by activating β-catenin-independent signals, in part via AP-1/ATF family transcription factors. To characterize the effects of selectively blocking Wnt-11 signaling, two monoclonal anti-Wnt-11 antibodies generated *in house* to human Wnt-11 peptides were tested, named E8 and F10. Both antibodies recognize the same epitope in a region of Wnt-11 that is located outside known Wnt receptor binding sites.

The antibodies recognize Wnt-11 in multiple assays, including in a cellular context, reduce prostate cancer cell sphere formation, inhibit cancer cell migration and invasion, and inhibit migration in cells cultured under hypoxic conditions, where Wnt-11 expression is found to be upregulated. Magnetic nanoparticle (MNP) conjugates of E8 and F10 were generated as potential therapeutic agents and tested in parallel with a control rat IgG conjugate. Anti-Wnt-11 MNP conjugates reduced prostate cancer cell migration without affecting viability. Both naked E8 antibody and MNP-E8 nanoformulation reduced PC3 cell tumor growth in the chick chorioallantoic membrane (CAM) *in vivo* model, and this was accompanied by a reduction in the intensity of the proliferation marker Ki67 in the tumors. An antibody epitope deletion mutant (AE) of Wnt-11 was generated to characterize the impact of this region on Wnt-11 signaling and function. Targeting this hotspot, in an antibody-mediated manner or by deletion mutation, reduces the phosphorylation level of the Wnt effector DVL. It also interferes with ATF2-dependent transcription and blocks the ability of Wnt-11 to inhibit Wnt-3a activation of β-catenin/TCF-dependent transcription. Immunoprecipitation and immunofluorescence co-localization assays demonstrated that the epitope mutation resulted in a reduced interaction of Wnt-11 with the Wnt coreceptor LRP6. Furthermore, the antibody epitope mutation compromised Wnt-11 inhibition on LRP6-induced β-catenin/TCF-dependent transcription and Wnt-11/FZD8 activation of ATF2-dependent transcription.

Together, these results highlight Wnt-11 as a therapeutic target and anti-Wnt-11 antibodies and their nanoformulations as potential therapeutic agents to treat patients with advanced prostate cancer.

Resumen

Wnt-11 es una proteína que se encuentra altamente expresada en el cáncer de próstata metastático, donde favorece la diferenciación neuroendocrina, la supervivencia y migración celular activando señales a través de la familia de factores de transcripción AP-1/ATF, independientes de β-catenina. Para caracterizar los efectos de inhibición selectiva de Wnt-11, se generaron dos anticuerpos monoclonales anti-Wnt-11, E8 y F10. Ambos anticuerpos reconocen el mismo epítopo en Wnt-11 en una región con función desconocida.

Los anticuerpos reconocen Wnt-11 en múltiples ensayos, incluyendo en contexto celular, reducen la proliferación en esferas de células de cáncer de próstata, inhiben la migración e invasión celular y la migración de células en hipoxia, donde la expresión de Wnt-11 se ve aumentada. La conjugación de E8 y F10 a nanopartículas magnéticas (MNP) fue llevada a cabo para su uso como potenciales agentes terapéuticos. Las nanoformulaciones anti-Wnt-11 reducen la migración celular sin afectar a la viabilidad. Tanto E8 como la nanoformulación MNP-E8 reducen el crecimiento tumoral de células PC3 en el modelo *in vivo* de la membrana corioalantoidea de pollo (CAM), provocando una disminución en la intensidad del marcador de proliferación Ki67. Un mutante de Wnt-11 en el que se ha delecionado parte del epítopo fue generado para caracterizar el impacto que tiene esta región en la función y señalización por Wnt-11, llamado AE. La inhibición del epítopo tanto por los anticuerpos como por deleción reduce la fosforilación del efector de Wnt, Dishevelled (DVL). También interfiere con la activación de transcripción dependiente de ATF2 y bloquea la capacidad de Wnt-11 de inhibir la señalización por Wnt-3a/β-catenina/TCF. Ensayos de inmunoprecipitación y co-localización por inmunofluorescencia indican que la mutación de deleción de epítopo produce una reducción significativa en la interacción de Wnt-11 con el correceptor de Wnt LRP6. Además, esta mutación impide la capacidad de Wnt-11 de inhibir la transcripción inducida por LRP6/β-catenina/TCF y la capacidad de LRP6 de potenciar la transcripción dependiente de ATF2.

En conjunto, los resultados indican que Wnt-11 puede ser una diana terapéutica adecuada en el cáncer de próstata metastático y que los anticuerpos anti-Wnt-11 y sus nanoformulaciones podrían tener uso como potenciales agentes terapéuticos en su tratamiento.

Introduction

1. Cancer

Cancer is a disease characterized by aberrant and uncontrolled cell growth that has the potential to invade healthy tissues and disrupt their function. It is also referred to as a malignancy, tumor or neoplasm and can originate from any body tissue. A neoplasm will naturally tend to invade adjacent or distant healthy tissues (a process known as metastasis), propagating through the organism until its burden becomes incompatible with life. It is now well recognized the "many diseases" nature of cancer as a result of not only the heterogeneity of cancer types but also the heterogeneity among the cells found within a tumor (American cancer society, 2021; NIH National Cancer Institute, 2021; World Health Organization, 2021).

According to the tissue origin, cancer can be classified as hematologic (e.g., leukemia, lymphoma, myeloma) and solid tumors. The latter can be subclassified into carcinomas, for tumors with an epithelial origin, and sarcomas, which originate from connective tissues. More than 90% of diagnosed tumors are carcinomas, with the main subtype being adenocarcinomas. This subtype affects tissues with secretory function, like most (but not all, as it depends on the specific tissue of origin) prostate, breast, lung, and colorectal cancers.

Cancer has been known for over 5 000 years, with the earliest recorded description in the Edwin Smith Papyrus, where it was reported as an untreatable disease (Hajdu, 2004). Since then, cancer therapy has come a long way always in hand with surgical advancements, with surgery continuing to be its main treatment. It was not until the late 19th century when Marie Curie discovered what later came to be the first non-surgical anti-cancer therapy, radiation (Gianfaldoni et al., 2017). In the 1970s, chemotherapy first showed its potential as treatment of acute childhood leukemia and advanced Hodgkin's disease (DeVita & Chu, 2008). Now, chemotherapy refers mainly to the use of chemical agents that impact all dividing cells in the organism without tumor specificity, therefore its use carries important adverse effects.

It was noticed early that cancer is a disease involving mutations in the genome and studies focused on those that activated oncogenes or that abolished the function of tumor suppressor genes. In 1996 the first targeted therapy came to be, with Imatinib, a BCR-ABL1 tyrosine kinase inhibitor used in the treatment of chronic myelocytic leukemia. The sequencing of the human genome in the early 2000s accelerated cancer research greatly (Craig Venter et al., 2001; Lander et al., 2001).

In addition, the publication of the seminal *Hallmarks of cancer* paper by Hanahan & Weinberg (2000) provided a theorical framework by rationalizing the diversity of neoplastic diseases. They predicted that the cancer field would evolve into a logical science, where the complexities of the disease could become "understandable in terms of a small number of underlying principles". Not exempted from criticism, they provided the six hallmarks of cancer, a sort of multistep rules governing the transformation of normal cells into malignant cancers. These compiled the cancer-associated properties into six categories, namely: self-sufficiency in growth signals, insensitivity to growth-inhibitory (antigrowth) signals, evasion of programmed cell death (apoptosis), limitless replicative potential, sustained angiogenesis, and tissue invasion and metastasis. Hanahan & Weinberg revisited this work in 2011 (Hanahan & Weinberg, 2011), adding two emerging hallmarks: deregulating cellular energetics and evading immune destruction. Furthermore, they included the enabling characteristics that allow the arising of the other hallmarks: genomic instability and mutations and the tumor promoting inflammation. Here, the contribution of the tumor microenvironment for the development of the disease was also highlighted. This work has been very influential and continues to constitute the theoretical framework for cancer research. A graphic summary of the hallmarks of cancer and a depiction of the tumor microenvironment is provided in Figure 1.

Figure 1. The hallmarks of cancer (a) and tumor microenvironment (b). A) The hallmarks of cancer adapted from (Hanahan & Weinberg, 2011), with the original and emerging hallmarks in the top two rows and the enabling factors at the bottom. B) Representation of the tumor microenvironment, with vessels, blood and immune cells, cancer associated stroma and cancer cells. The process of intravasation and extravasation of cancer cells from blood vessels is also depicted. CTC – circulating tumor cell.

a The hallmarks of cancer

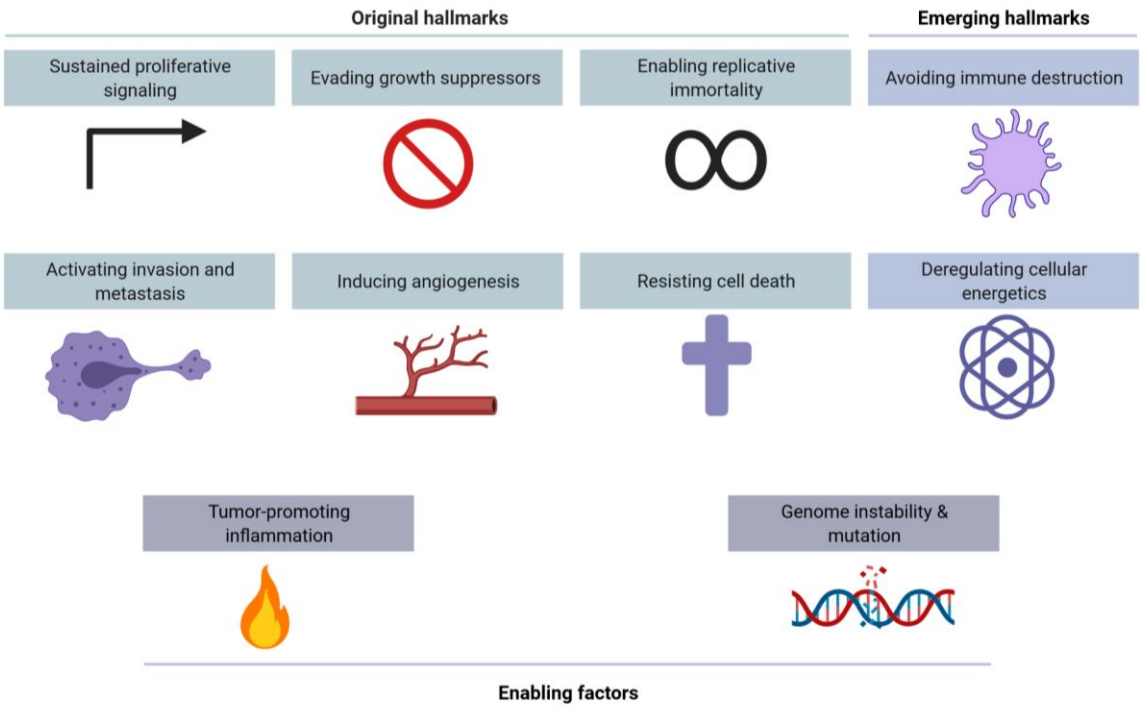

b Tumor microenvironment

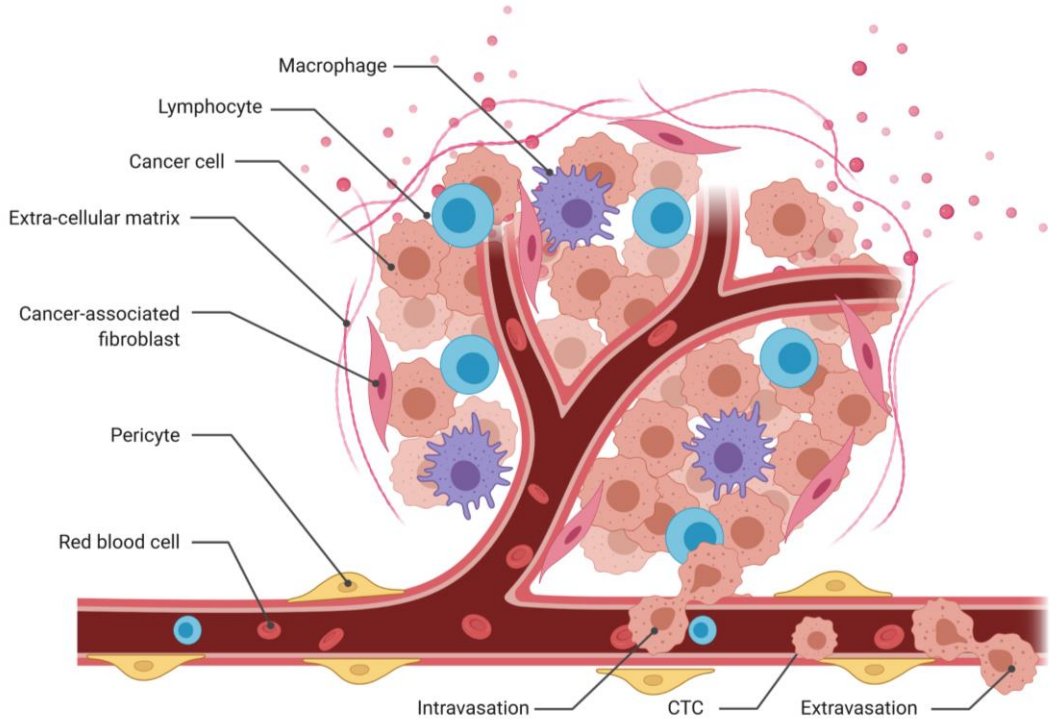

1.1. Hypoxia in cancer

Hypoxia refers to a status of oxygen deprivation. This condition has evolved as a normal response to certain physiological stimuli, but it is also a common event in the biology of solid tumors. Tumor growth is accompanied by the establishment of a tumor microenvironment that supports the expanding nature of the malignancy, but this does not always happen in a balanced way. Some tumor regions can be left with limited access to the bloodstream and therefore are deprived of oxygen and nutrients, which induces cellular adaptations to hypoxia. The restricted access to the bloodstream is also relevant for therapeutic agents, as these may be unable to reach hypoxic regions in tumors. Hypoxia has been associated with tumor progression and poor prognosis in patients (Brahimi-Horn, Chiche, & Pouysségur, 2007).

The hypoxia response activates hypoxia-inducible factors (HIF)-induced transcription. HIFs are heterodimers composed of an inducible α-subunit (HIF-1α, HIF-2α or HIF-3α) and a constitutively-expressed β-subunit (HIF-1β) (P. Lee, Chandel, & Simon, 2020). In normoxia, HIFα subunits are poly-ubiquitinated and targeted for degradation by the Von Hippel-Lindau (VHL) complex. This interaction is dependent on hydroxylation of two proline residues of HIFα by prolyl hydroxylases (PHD), a reaction that is coupled to the oxidative decarboxylation of α-ketoglutarate (Figure 2). PHDs have low affinity for oxygen making them particularly sensitive to changes in the intracellular oxygen concentration. Therefore, under hypoxia, PHDs are inhibited by lack of substrate (O_2) and turn off HIFα hydroxylation, resulting in its stabilization and nuclear translocation. HIFα together with HIF-1β activate their target genes by binding to HRE (hypoxia response elements). There is an additional level of regulation of HIF transcriptional activity by the factor inhibiting HIF-1α (FIH-1). FIH-1 is an α-ketoglutarate-dependent dioxygenase that hydroxylates an asparagine residue in a transactivating domain of HIFs under normoxia, preventing the recruitment of the transcriptional cofactors p300 and CBP, thereby inhibiting HIF transcriptional output (Figure 2). Dimethyloxalylglycine (DMOG) is a synthetic analogue of α-ketoglutarate that acts as a PHD and FIH inhibitor, allowing HIF-1α stabilization in a O_2-independent manner. It is frequently used to increase HIF stabilization and signaling; however, care must be taken as PHDs have been shown to control multiple biological processes independently of HIFs (Nguyen & Durán, 2016).

Hypoxia induces many responses in context-dependent conditions that are tightly balanced and can eventually lead to the induction or repression of the same cellular processes. In a first

stage, HIF activation can induce proliferation, survival, and angiogenesis, however when prolonged, the same mechanism can promote necrosis and apoptosis (Greijer & Van Der Wall, 2004). Hypoxia can promote tumor cell migration and invasion, which is often associated with a metastatic-promoting phenotype and can induce active tumor microenvironment remodeling (Petrova, Annicchiarico-Petruzzelli, Melino, & Amelio, 2018). Therefore, several groups have studied hypoxic gene signatures, as these may be useful for cancer prognosis (Buffa, Harris, West, & Miller, 2010).

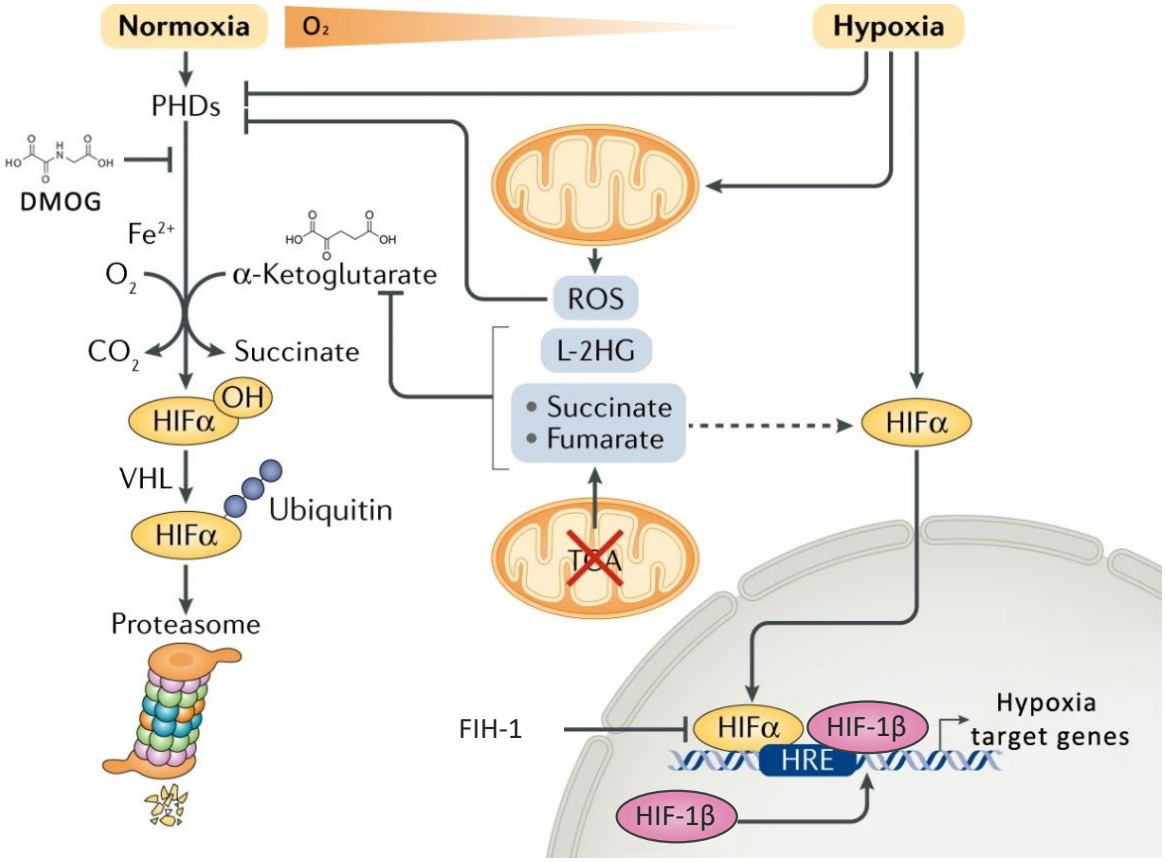

Figure 2. Transcription regulation induced by hypoxia. Under normoxia HIFα is targeted for degradation. In contrast in hypoxic situation HIFα is stabilized and can activate its nuclear target genes. Abbreviations: HIF – hypoxia-inducible factor, VHL - von Hippel– Lindau tumor suppressor protein, FIH-1 - Factor inhibiting HIF-1α, HRE - hypoxia response elements, TCA - Tricarboxylic acid cycle, ROS – Reactive oxygen species, L-2HG - l-2-hydroxyglutarate, Fe2+ - iron, O_2 – oxygen, CO_2 - carbon dioxide, OH - hydroxide. DMOG – Dimethyloxalylglycine. Adapted from (P. Lee et al., 2020).

2. Therapeutic antibodies

Antibodies (Ab), also known as immunoglobulins (Ig), are specialized secreted glycoproteins that aid the immune system in the identification of targets that are potentially pathogenic. They are composed of 4 polypeptides: 2 identical light chains (L) each bound by disulfide bonds to 2 identical heavy chains (H). The latter are also bound to each other, conferring the protein a Y-shape with a total molecular mass of about 150 kDa (Figure 3a) (Moorthy et al., 2015). Abs present a modular structure, with each chain divided into globular domains that can be variable (V) or constant (C), according to their sequence diversity. Light chains are composed of one variable and one constant domain (V_L-C_L), and heavy chains have one variable followed by three constant domains (V_H-C_H1-C_H2-C_H3). The variable regions together with adjacent constant chains, are grouped into the antigen-binding fragment (Fab) regions (V_L-C_L and V_H-C_H1 form one Fab), while the remaining two constant domains in the heavy chains are referred to as the fragment crystallizable (Fc) region (C_H2-C_H3 from the 2 heavy chains).

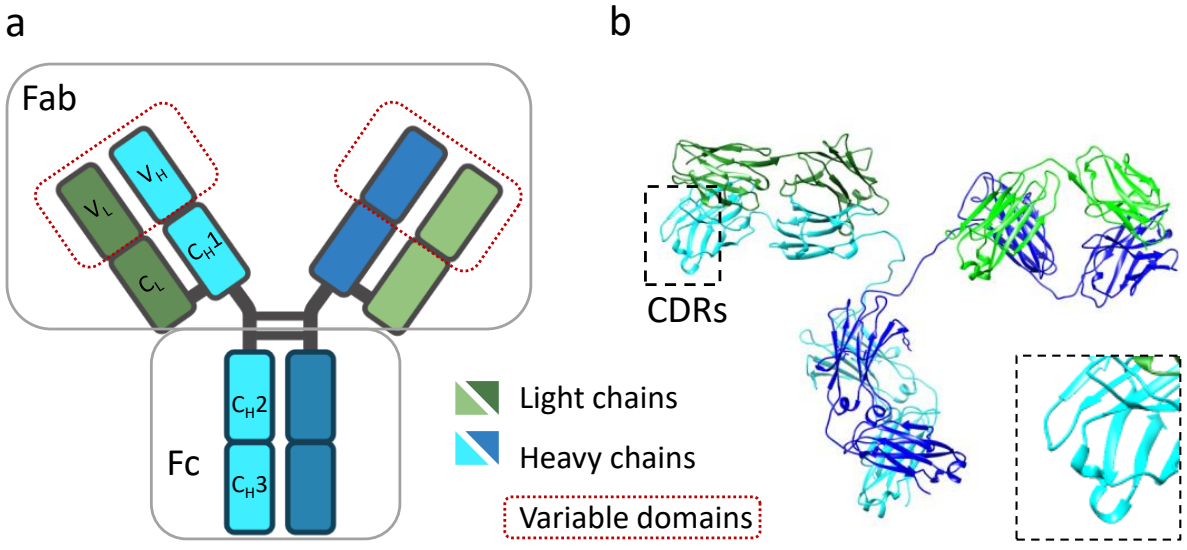

Figure 3. Generic antibody structure and domains. A) Graphical representation of the domains of a generic IgG antibody. Light chains in green with indicated domains (V_L - variable light chain, C_L – constant light chain), heavy chains (H) in blue with their respective variable and constant domains (V_H-C_H1-C_H2-C_H3). Variable domains are also highlighted with a red dotted line. Fab and Fc regions are indicated by grey squares. B) Crystal structure of a mouse IgG2a monoclonal antibody depicted in similar colors to the representation of (A). CRD - complementarity-determining region is highlighted by black dotted square. PBD: 1IGT (L. J. Harris, Larson, Hasel, & McPherson, 1997).

These proteins are specialized in binding with high affinity and avidity to peptides (epitopes) present in their target proteins (antigens). For specific binding, antibodies use their variable domains. Specifically, the interaction is mediated by three hypervariable regions, the complementarity-determining regions (CDRs), which contain the few residues directly involved in the binding to the epitope (Figure 3b).

The Fc are the effector regions of antibodies, which are composed by heavy chains that can be of diverse types: α, γ, δ, ε and μ which confers the antibodies their isotype or class: IgA, IgG, IgD, IgE, IgM, respectively (Moorthy et al., 2015). Different isotypes mediate different biological properties and bind to Fc receptors (FcR) in immune cells. Abs exert their function through the Fab-fragments, which can block and agglutinate (neutralize) pathogens, and via the Fc region, that can enhance phagocytosis (opsonization) and can induce cytotoxic responses via complement activation among others (Mix, Goertsches, & Zett, 2006).

Ab production is a type of adaptive immunity that occurs in vertebrate B cells. Ab variety is created during B cell maturation in peripheral lymphatic tissues by isotype class switching and somatic hypermutation with each B cell producing only one type of antibody (Mix et al., 2006). Abs have many applications and can be generated to specific desired targets by immunizing research mammal animals to produce polyclonal antibodies.

In 1975, hybridomas were first described as a powerful tool to produce antibodies. The method requires plasma Ab-producing cells to be fused to myeloma immortalized cells, forming hybridoma cells. Each hybridoma clone will produce Abs with the same sequence, this is monoclonal antibodies (mAb), which can be retrieved and purified. Phage display is another method for antibody production *in vitro*. The approach is based on the fusion of peptides to the phage envelope proteins, which allows phenotypic selection of the phage particle of interest (Frenzel, Schirrmann, & Hust, 2016).

Abs generated by these technologies are of utility for research purposes, but their properties made them also interesting from a clinical point of view. For their application as a therapy in humans, antibodies need to undergo a process to make them less immunogenic (R. M. Lu et al., 2020). This process creates chimeric antibodies, obtained by combining the variable regions with human-specific constant regions, and humanized antibodies, completely human antibodies except for the CDR regions. ‘Humanized’ mice can also be used to generate fully human antibodies, by replacing the entire IgG repertoire of the mouse with the human one,

although these have their own disadvantages, such as the inability to use a toxic immunogen or a immunogen that has a striking similarity to its mouse ortholog (Sneha et al., 2017). In 1986, the first therapeutic antibody was approved, Orthoclone OKT3, for the prevention of kidney transplant rejection (Ecker, Jones, & Levine, 2015; Gordon et al., 1988). In December 2019, there were 79 therapeutic mAbs approved by the Food and Drug Administration (FDA) and in 2021 the 100th monoclonal antibody product has been granted FDA-approval (R. M. Lu et al., 2020; Mullard, 2021).

The target molecule of the therapeutic antibody needs to be readily accessible, preferably located on the cell surface or extracellular compartment; however intracellular proteins can also be targeted (Redman, Hill, AlDeghaither, & Weiner, 2015; Trenevska, Li, & Banham, 2017). The interaction of the Fab region with the epitope can neutralize the target protein, by steric and/or allosteric means, which may result in its function being impaired. This is one of the mechanisms of action of function-blocking or neutralizing Abs. Additionally, the Fc-mediated interaction with immune effector cells can play additional roles in anti-tumor activity by the induction of antibody-dependent cell-mediated cytotoxicity (ADCC) and complement-dependent cytotoxicity (CDC). This is dependent on the Ab isotype, for example, human IgG2 activates only ADCC, human IgG4 does not activate ADCC nor CDC, and human IgG1 can activate both (Redman et al., 2015).

One example of a therapeutic antibody in cancer is trastuzumab (Herceptin), a humanized IgG1 antibody that recognizes HER2 receptor tyrosine-kinase, which is overexpressed in 20-25% of breast cancers worldwide (Jiani Wang & Xu, 2019). To exert its effect, trastuzumab induces receptor dimerization, promoting its internalization and endocytic destruction; and it can also activate ADCC (Redman et al., 2015). A successful therapeutic antibody against a secreted protein ligand is adalimumab (Humira), which targets tumor necrosis factor (TNF) and is used for the treatment of rheumatoid arthritis (Frenzel et al., 2016).

However, the clinical use of antibody-based therapies has some disadvantages: they show limited membrane permeability and poor gastrointestinal stability and therefore they cannot be delivered orally (Castelli, McGonigle, & Hornby, 2019). Most approved therapeutic antibodies require intravenous (IV) administration of large doses by slow infusions, increasing costs (L. Liu, 2018). In contrast, compared to small molecules, antibodies have an exceptionally long half-life in circulation, estimated to be of 21 days for IgG1 (Sousa et al., 2017).

3. Nanoparticles

Nanoparticles (NPs) are 10–100 nm particles that can be made of lipids, polymers, and metals, which have been used in biomedical applications for decades due to their attractive physical and chemical properties (Farzin, Etesami, Quint, Memic, & Tamayol, 2020). Magnetic nanoparticles (MNPs) are one class of NPs, the core of which can be formed by pure or mixed metals (Fe, Co, Ni, and others), their alloys, and oxides (Figure 4). Iron oxide nanoparticles can be conveniently coated with various compounds, such as polymers (e.g., polyethylene glycol (PEG), chitosan) and dendrimers, and they can also be encapsulated in silane or gold shells (Wilczewska, Niemirowicz, Markiewicz, & Car, 2012). This is in order to improve the properties of the nanomaterials, such as their stability, interaction with biological molecules, and bioconjugation capabilities.

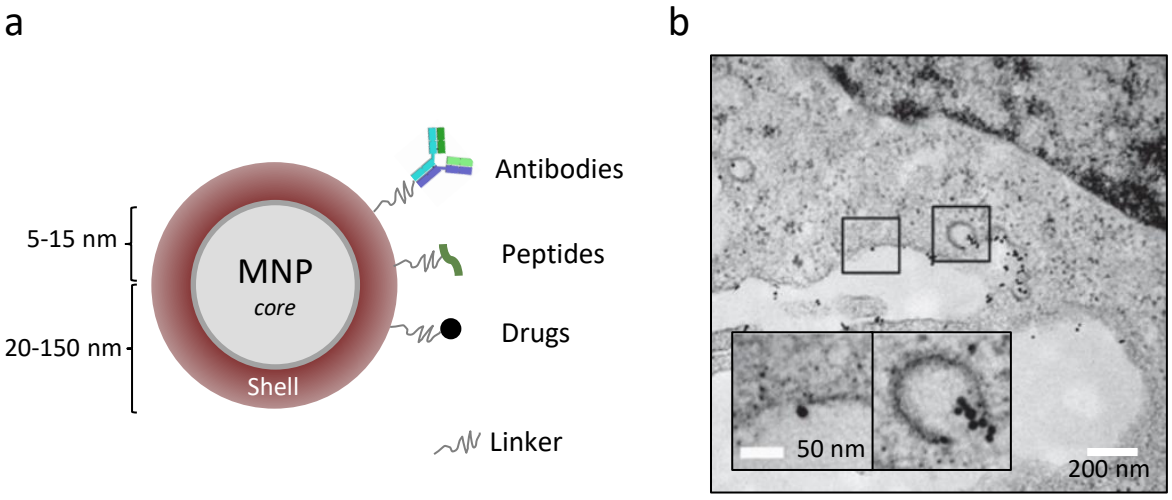

Figure 4. Representation of magnetic nanoparticles (MNP). A) Scheme showing the components of MNPs/SPIONs: core of 5-15 nm radius and shell, with hydrodynamic radius of about 20-150 nm. Indication of potential functionalization agents (antibodies, peptides, and drugs). B) Electron microscopy images of thin sections of MDA-MB-231 cells incubated with MNP-antiCD44 SPIONs. The insets show MNPs interacting with plasmatic membrane (left) or incorporated into vesicles (right). Adapted from (Aires et al., 2016).

MNPs have gained immense attention for their potential for cancer diagnosis and therapy, i.e., theranostic applications (Mukherjee, Liang, & Veiseh, 2020). In cancer, MNPs can be used for inducing tumor hyperthermia, controlled drug delivery and release, magnetic resonance imaging (MRI), and other applications (Farzin et al., 2020). Among MNPs, superparamagnetic iron oxide nanoparticles (SPIONs) show good biocompatibility, low toxicity and have an easy single step synthesis (Wilczewska et al., 2012).

Specific tumor targeting by the MNPs can be achieved by passive or active mechanisms. The enhanced permeability and retention (EPR) effect is a controversial concept that has been proposed to allow passive tumor targeting for MNPs. The EPR effect was first described in 1986 (Matsumura & Maeda, 1986) and it is based on the notion that solid tumors have a faulty vascular architecture, different from that of healthy tissue, that permits enhanced extravasation of macromolecules into the tumor tissue interstitium. This effect can theoretically be exploited for MNP delivery because they possess the appropriate size: higher than 50 nm to evade the liver and renal clearance and less than 200 nm (Farzin et al., 2020). However, the EPR effect displays a large heterogeneity between patients and cancer types and may not be present in all types of human tumors (Wolfram et al., 2015).

MNPs are suitable platforms for functionalization and conjugation of cell-specific targeting ligands, such as antibodies, which may increase tumor selectivity (Trabulo, Aires, Aicher, Heeschen, & Cortajarena, 2017). Moreover, MNPs allow multi-functionalization of several bioactive molecules, such as antibodies with different targets or cytotoxic drugs. Also, the conjugation linker can be engineered based on the desired stability, and some can be cleaved by lysosomal proteases for intracellular delivery of drugs.

The use of NPs as a delivery system for antibodies helps increase their stability, tumor selectivity and can lead to reduced dosing in patients (Sousa et al., 2017). In general, antibody functionalization of SPIONs does not diminish their targeting properties in a significant way (Dulińska-Litewka et al., 2019). With appropriate functionalization, SPIONs can show enhanced accumulation in tumor tissues by passive or active targeting mechanisms, while significantly reducing nonspecific accumulation in the liver and spleen (L. Zhu, Zhou, Mao, & Yang, 2017).

4. The human prostate and prostate cancer

The prostate is a male specific gland that surrounds the urethra at the base of the bladder that produces important components of the seminal fluid (Prostate cancer foundation, 2021, pp. 12–13; Shen & Abate-Shen, 2010). Prostate-specific antigen (PSA) is a kallikrein-related serine protease that is produced in normal prostate secretions and in a healthy situation, only small quantities are released into the bloodstream. The prostate displays a lobular structure that can be classified into four anatomical zones: the central zone, that surrounds the ejaculatory ducts; the peripheral zone, which is located in the posterior and lateral parts of the gland and is where most prostate tumors originate (~60%-75%); the transition zone, that partially surrounds the proximal prostatic urethra; and the anterior fibromuscular stroma, that forms the anterior external surface and lacks glandular tissues (Dehm & Tindall, 2019, p. 63; G. Wang, Zhao, Spring, & Depinho, 2018). Androgen hormones (testosterone and dihydrotestosterone, or DHT) are essential for the prostate function and crucial for the development of secondary genre characteristics and prostate growth during adolescence.

As of 2020, prostate cancer was the second most diagnosed cancer in the male population worldwide, with more than 1.4 million new cases. Prostate cancer incidence rates are variable worldwide, age-standardized rate (ASR) annual incidence are higher in developed countries accounting for over 60 cases per 100 000 in Europe (Global Cancer Observatory (GCO) IARC, 2021; Rawla, 2019). The mortality rate of prostate cancer is also variable worldwide, with an average mortality rate of 7 per 100 000 people and accounting for more than 300 000 total deaths per year. The main risk factor for the development of prostate cancer is age, but other important risk factors include race, lifestyle, and diet. Multiple genetic studies have demonstrated a strong genetic component in the etiology of prostate cancer, which is among the most heritable cancers (G. Wang et al., 2018).

4.1. Diagnosis and grading

Screening nowadays, and since it was approved in 1994 by the FDA, involves PSA determination in blood (Prostate cancer foundation, 2021, pp. 10–11; Rawla, 2019). An increased PSA presence in the bloodstream is an indicator of prostate malfunction, that can be due to prostate cancer or to other non-malignant lesions of the prostate, such as benign prostate hyperplasia or a urinary tract infection. This, and the fact that prostate tumors are in many cases slow-growing and confined to the gland at the time a diagnosis, has prompted a debate over

the risks and benefits of PSA screening in the healthy adult population, with concerns of over-vigilance and over-treatment (Attard et al., 2016; Rawla, 2019). Most prostate cancers initiate in the peripheral zone, which is exploited in the diagnosis based on digital rectal exam, a test that usually accompanies a positive PSA result.

However, for a prostate cancer diagnosis, a histopathological examination of a biopsy is needed. This enables grading the tumor, an indication of the aggressiveness and prognosis of the cancer, which in prostate cancer is called the Gleason score (Gleason, 1992). By this system, a tumor can be graded from ≤6 (low) to 9-10 (very high), where this number refers to the sum of the two most frequent histological patterns found in the tumor, e.g., Gleason score 3+4 or 7 (Figure 5).

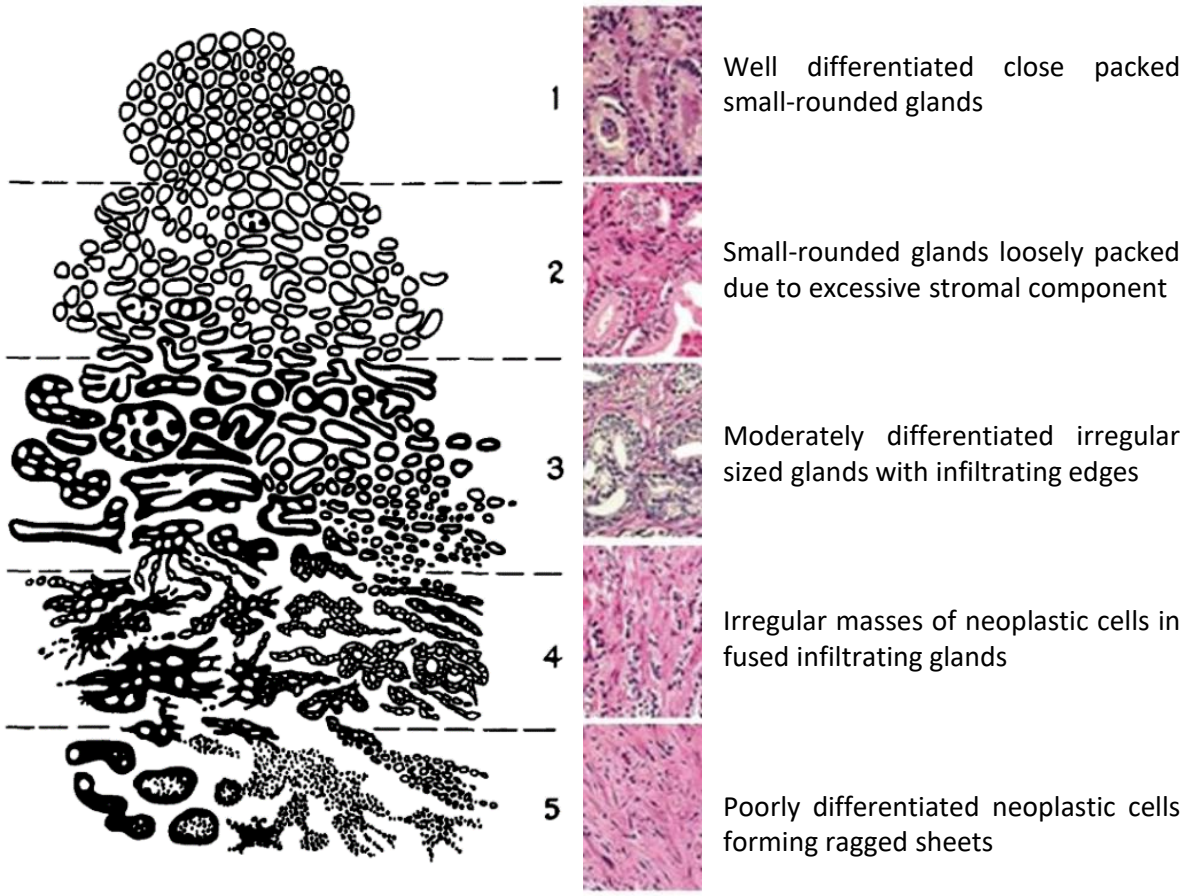

Figure 5. The Gleason grading system of prostate cancer. Standardized drawing for grading system of prostatic adenocarcinoma (histologic patterns) described in (Gleason, 1992), with representative histological images, adapted from (Harnden, Shelley, Coles, Staffurth, & Mason, 2007) and a brief description of each score.

Additional to the Gleason score, a prostate tumor can be classified by the TNM (tumor, lymph nodes, metastasis) stage (Schröder et al., 1992). In 2020, the FDA approved the Radiolabeled prostate-specific membrane antigen (PSMA) ligand Glu-NH-CO–NH-Lys-(Ahx)-[68Ga (HBED-CC)], also known as 68Ga-PSMA-11 as a radiotracer for positron emission tomography (PET) scanning to help in the detection of metastatic lesions (Kurash, Gill, Khairulin, Harbosh, & Keidar, 2020; Prostate cancer foundation, 2021, pp. 62–63).

4.2. Prostate cancer progression and treatment

The malignant transformation towards prostate cancer is thought to follow a multistep process, initiating as prostatic intraepithelial neoplasia (PIN). PIN is characterized at the histological level by the appearance of luminal epithelial hyperplasia and, although PIN is not considered malignant, is regarded as a precursor of prostate cancer (Shen & Abate-Shen, 2010). PIN may progress to localized prostate cancer, which in most cases are acinar adenocarcinomas that express androgen receptor (AR). Although primary tumors that are classified as neuroendocrine prostate cancer represent less than 2% of prostate cancers, they are considered highly aggressive (Shen & Abate-Shen, 2010). Prostate cancers can be in a latent state or progress to be a clinically detectable disease (Figure 6, upper panel).

Upon a prostate cancer diagnosis, active surveillance constitutes the standard of care for low-grade (Gleason score ≤ 6) localized prostate cancers (Attard et al., 2016; Prostate cancer foundation, 2021, p. 35). For men with intermediate or high-risk cancer that has not spread, surgical removal of the prostate and seminal vesicles, referred to as radical prostatectomy, is usually performed. This may be accompanied by adjuvant radiation therapy and hormone therapy for cases where lymph nodes are found affected. When the cancer cells invade other tissues and organs, a metastatic disease is present.

In advanced disease, hormone therapy is the most used, also known as castration therapy, androgen deprivation therapy or ADT (Prostate cancer foundation, 2021, p 67). Meanwhile androgens are important for the normal function of the prostate, they usually also drive the growth of prostate tumors. ADT therapy can consist of orchiectomy (surgical castration) or in the blockade of testosterone production by pharmacological means using Gonadotropin-releasing hormone (GnRH) agonists (e.g., leuprolide) and antagonists (e.g., degarelix, relugolix). These may be used in combination with anti-androgens e.g., bicalutamide, flutamide, and nilutamide, that block the action of the hormone in recipient cells. For advanced

prostate cancer second-generation hormone therapy, referred to as androgen-directed therapies, can be employed, including drugs such as androgen receptor antagonists apalutamide and enzalutamide; and abiraterone, a potent CYP17A1 inhibitor that blocks androgenic steroid synthesis (Attard et al., 2016).

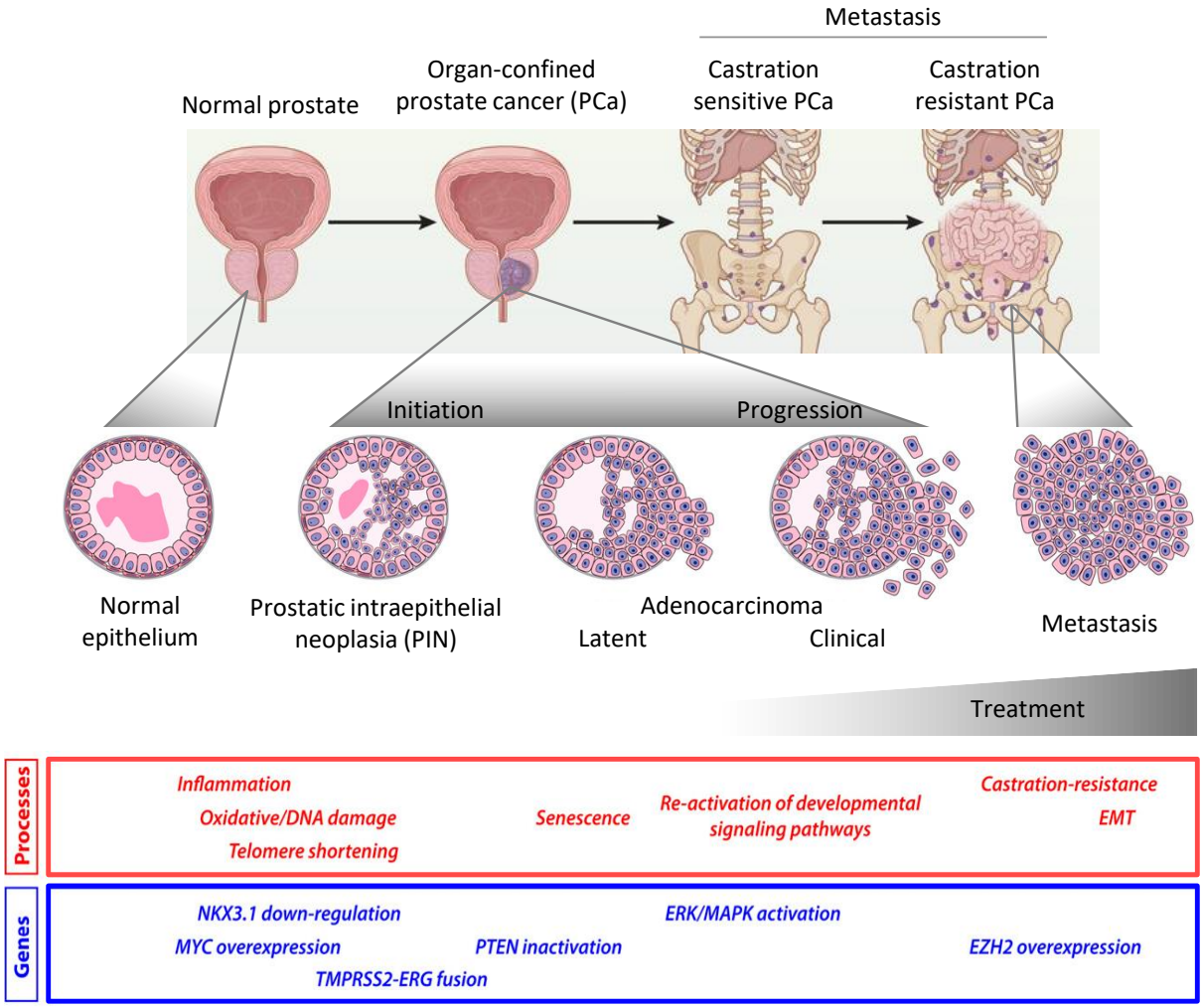

Figure 6. Prostate cancer progression and treatment. Stages of prostate cancer progression are shown, together with a gland depiction of histological features (upper panel). Molecular processes and genes/pathways considered to be significant at each stage is provided in the bottom panel. Abbreviations: EMT – Epithelial to mesenchymal transition, PCa – prostate cancer. Adapted from (Arap, Pasqualini, & Costello, 2020; Shen & Abate-Shen, 2010).

Although most prostate tumors initially respond well to ADT, treatment-induced selective pressure promotes the acquisition of resistance with the disease progressing to castration resistant prostate cancer (CRPC) (G. Wang et al., 2018). However, most cancers remain being hormone-driven despite castration resistance and second generation androgen-directed therapies can be used for CRPC treatment (Attard et al., 2016). Among those, darolutamide

was approved in 2019 for the treatment of non-metastatic CRPC (Fizazi et al., 2019). Non-hormonal treatment options for metastatic CRPC include the use of taxane and platinum-based chemotherapies (G. Wang et al., 2018). Pembrolizumab, an anti-PD-1 therapeutic antibody was FDA-approved in 2017 for multiple solid tumors, including prostate tumors with high tumor mutational burden and has been proposed to be beneficial for a broaden subset of metastatic CRPC (Antonarakis et al., 2020; Prostate cancer foundation, 2021, p. 74). In 2020 the FDA approved the PARP inhibitors olaparib and rucaparib for metastatic CRPC carrying inactivating mutations in DNA damage repair genes, which may comprise up to 20% of patients (Prostate cancer foundation, 2021, p. 75; Ratta et al., 2020).

In some cases CRPC can transdifferentiate to a neuroendocrine phenotype (CRPC-NE), which represents a major clinical challenge for which experimental models are lacking (Faugeroux et al., 2020). It has been proposed that selective pressure induced by ADT can induce neuroendocrine differentiation (NED) and that NED is associated with increased aggressiveness (Beltran et al., 2016; D. Lin et al., 2014). This highlights that CRPC is a complex and heterogeneous disease in which patients could benefit from stratification for the use of targeted therapies.

4.3. Prostate cancer recurrent mutations

The most prevalent and recurrent mutations in prostate cancer have been thoroughly investigated (Armenia et al., 2018; Shen & Abate-Shen, 2010). Main early events in prostate cancer progression are thought to involve downregulation of the *NKX3.1* homeobox gene and the upregulation of the *MYC* oncogene (Figure 6, bottom panel). In addition, there are chromosomal rearrangements that lead to aberrant expression of several members of the ETS family of transcription factors (ERG, ETV1, and ETV4), which is a common event across many cancer types (Sizemore, Pitarresi, Balakrishnan, & Ostrowski, 2017). Approximately 50% of localized prostate cancers display the TMPRSS2–ERG fusion which results in the expression of a truncated ERG protein under the control of the androgen-responsive promoter of TMPRSS2 (Tomlins et al., 2007, 2008; G. Wang et al., 2018).

Tumor suppressor phosphatase and tensin homolog (PTEN) reduction or loss is another common event in the progression of prostate cancer (Shen & Abate-Shen, 2010). This leads to activation of AKT1, also known as protein kinase B (PKB), which promotes mechanistic target of rapamycin (mTOR)/AKT signaling. In addition, ERK (p42/44) MAP Kinase signaling is

also frequently activated in prostate cancer. Together, these events promote tumor progression and development of CRPC. Upregulation of EZH2, a histone lysine methyltransferase, and subsequently of its target genes, is associated specifically with metastasis. Other studies have shown that mutations in genes involved in DNA repair, PI3K signaling, cell cycle and Wnt/CTNNB1 pathways are specifically found enriched in metastatic samples (Armenia et al., 2018; Robinson et al., 2015).

The reactivation of developmental signaling pathways is also important in prostate cancer progression, particularly the reactivation of the Wnt signaling pathway has been associated with metastatic disease (Pomerantz et al., 2020). This has been suggested to be driven by the activation of developmental epigenomic programs. In addition, recently it has been reported that lesions displaying hypoxia show correlation with biochemical relapse and metastasis rate and are often associated with disease progression factors, such as genomic instability and loss of PTEN (C. Q. Yao et al., 2019).

5. Wnt proteins

Wnts are a family of signaling proteins that coordinate complex cellular processes during embryonal development, such as neural patterning, organogenesis, cell polarity, migration, self-renewal, and cell survival. Wnt expression, localization, and activity are tightly regulated and an imbalance in Wnt signaling activity can result in embryonal defects and cancer (Anastas & Moon, 2013; van Amerongen & Berns, 2006).

Wnt proteins are present in all metazoan species (Loh, van Amerongen, & Nusse, 2016). In humans, the Wnt family comprises 19 different *WNT* genes (Willert & Nusse, 2012): *1*, *2*, *3*, *3A*, *4*, *5A*, *5B*, *6*, *7A*, *7B*, *8A*, *8B*, *9A*, *9B*, *10A*, *10B*, *11*, *16* (MacDonald, Tamai, & He, 2009; Wiese, Nusse, & van Amerongen, 2018; Willert & Nusse, 2012). The first reported Wnt was mouse *Wnt1* (then designated *Int1*), which was found to be aberrantly overexpressed as a result of the insertion of the mouse mammary tumor virus (MMTV) at its locus producing spontaneous mammary tumors (Nusse & Varmus, 1982). Sequence analysis later showed this was the ortholog of the Drosophila segment polarity gene *Wingless* (*Wg*) (R. P. Sharma & Chopra, 1976). The term *Wnt* is an amalgam of *Wg* and *Int-1* (Nusse & Varmus, 2012, 1992).

5.1. Wnt modification and secretion

Wnt proteins carry a signal peptide of approximately 20 hydrophobic amino acids in the amino-terminal region, which targets them for secretion and is cleaved upon processing. However, Wnts have shown to be less soluble than sequence alone predicts. This is in part due to heavy post-translational modifications, which include lipidation and glycosylation (R. Takada et al., 2006; Willert & Nusse, 2012). These modifications occur in the endoplasmic reticulum and Golgi and have been shown to be important for the secretion and function of most Wnts, although their strict requirement for some Wnts is still a matter of debate (e.g., Wnt-4) (Rao et al., 2019).

Wnt glycosylation is mediated by the oligosaccharyltransferase complex that modifies certain asparagine residues, the locations of which vary among Wnts (Coudreuse & Korswagen, 2007; Hideki Yamamoto et al., 2013). Wnt lipidation consists of the addition of a palmitoleic acid (PAM) to a conserved serine residue by porcupine, a membrane-tethered O-acetyltransferase. Later, cargo proteins are responsible for the transport of Wnts to the Golgi and then to the plasma membrane for their release. Among those, Wntless (WLS), a sorting

receptor, plays a prominent role. Recently, a cryogenic electron microscopy (cryo-EM)-solved structure has been reported for the Wnt-3a/WLS complex, showing multiple interfaces for their interaction, with the lipid moiety on Wnt-3a traversing a hydrophobic tunnel of the WLS transmembrane domain (Zhong et al., 2021).

Once on the cell surface, Wnts can be retained attached to the cell matrix, solubilized or incorporated into lipoprotein complexes or extracellular vesicles (S. Takada, Fujimori, Shinozuka, Takada, & Mii, 2017). Because lipid-modified Wnts are poorly soluble, long-range spreading by diffusion is unlikely (Janda, Waghray, Levin, Thomas, & Garcia, 2012; Stanganello & Scholpp, 2016). They may travel on signaling filopodia, also known as cytonemes, which are membrane protrusions of approximately 1 μm that allow cell-cell transfer of Wnt proteins (Moti, Yu, Boncompain, Perez, & Virshup, 2019; Stanganello & Scholpp, 2016). Other transport mechanisms have been reported that would enable Wnts to signal long-distance, e.g., by their lipid moiety being shielded by Glypican, a heparan sulfate proteoglycan (McGough et al., 2020).

5.2. Wnt structure

Wnt proteins are about 350-400 amino acids in length and share a core of 22 cysteine residues forming disulfide bridges that maintain their structure (Coudreuse & Korswagen, 2007; Willert & Nusse, 2012). Wnt orthologs are highly conserved. For example, in vertebrate species, mouse and human Wnt-11 proteins share a 97% sequence identity and those of human and Xenopus share a 79%. Sequence identity among different Wnt family members is lower (27-83%) but still allows a similar protein folding. For instance, human Wnt-3 shares a 33% sequence identity with Xenopus Wnt-8 but has been reported to have a very similar structure (Hirai, Matoba, Mihara, Arimori, & Takagi, 2019; Janda et al., 2012).

The first Wnt structure was solved in 2012 (Janda et al., 2012). It showed Xenopus Wnt-8 (XWnt-8) in complex with mouse Frizzled-8 cysteine-rich domain (Fz-8-CRD) (Figure 7a). In this work the Wnt was described to resemble a hand with a “palm” as the core region from which the “thumb” and “index finger” were extended to interact with the Fz-8-CRD at two distinct binding sites. One is located in the tip of the “thumb”, where the lipid modification (PAM) inserts into a deep groove in the Fz-8-CRD. In the second binding site, the Wnt “index finger” forms hydrophobic patches with a depression on the opposite side of the Fz-8-CRD. XWnt-8 can be divided into an N-terminal α-helical domain (NTD) comprising residues ~1–250 (including the thumb) and a C-terminal cysteine-rich region (CTD) formed by residues

261–338. The structure shows two asparagine-linked glycosylation sites on XWnt-8. A potential coreceptor binding site was also identified as a solvent-exposed conserved patch located at the opposing end of XWnt-8/Fz-8 binding region.

Recently, the structure of human Wnt-3 in complex with mouse Fz-8-CRD was solved, showing an almost identical structure to the one described for XWnt-8 (Hirai et al., 2019) (Figure 7b, c). A putative low-density lipoprotein receptor-related protein 6 (LRP6) interacting region was proposed, based on surface plasmon resonance (SPR) studies, to be in the "linker" region, located close but different to the previously predicted one by Janda et al., 2012 (Figure 7b, c). Nonetheless this "linker" region had been proposed before as an LRP6 binding site by structure-based mutational analysis (Chu et al., 2013).

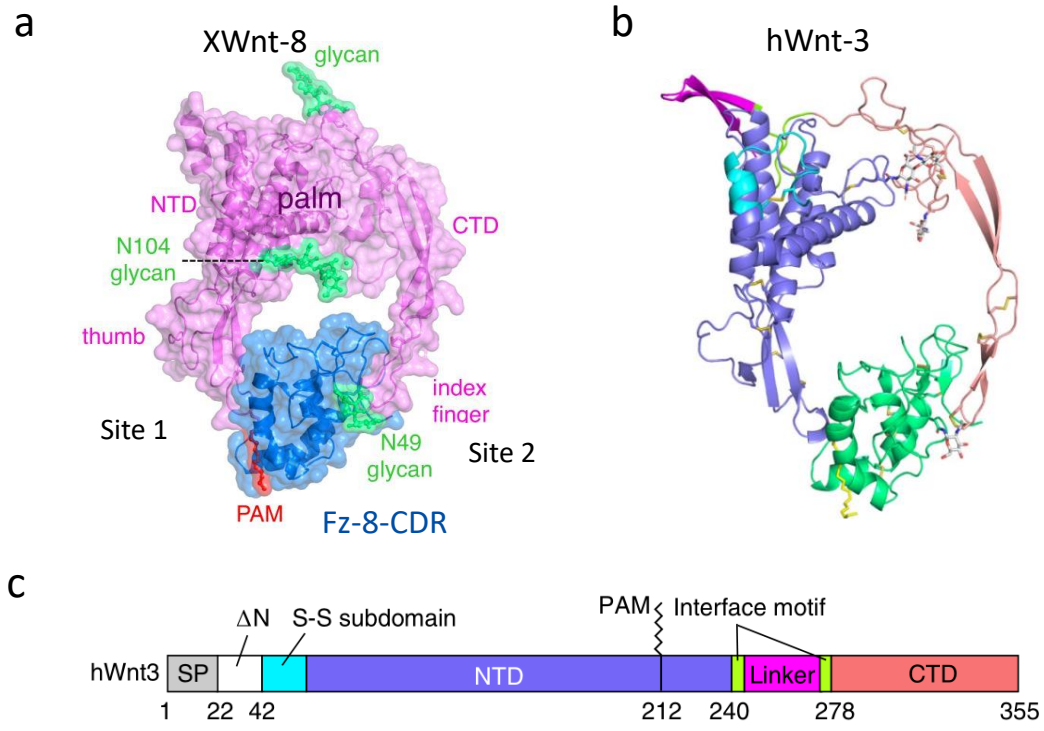

Figure 7. Wnt structure. A) XWnt-8 structure reported in Janda et al., 2012 with surface representation of XWnt-8/Fz-8-CRD complex structure, location of "palm", "thumb", "index finger" and PAM shown in red. B) Crystal structure of hWnt-3/mFz-8-CRD complex in ribbon representation reported in Hirai et al., 2019 with each domain color coded as in (C). C) Schematic diagram color-coded of the primary structure of human Wnt-3, highlighting signal peptide (SP), deleted N-terminal segment (ΔN), S-S subdomain, N-terminal domain (NTD), interface motif, linker region and C-terminal domain (CTD). PAM - Palmitoleic acid, CRD – Cysteine-rich domain.

5.3. Wnt signaling

One of the first milestones in Wnt research was achieved when β-catenin was established as a mediator of the pathway (Munemitsu, Albert, Souza, Rubinfeld, & Polakis, 1995; Yost et al., 1996). However, soon enough it was realized that some Wnt transduction pathways take place independently of β-catenin activation (Moon et al., 1993). This prompted the division of Wnt signaling into canonical and noncanonical, respectively. This simple separation has been challenged repeatedly, with the appearance of additional novel Wnt signaling branches and the discovery of intricate crosstalk (Chien, Conrad, & Moon, 2009), and it has been proposed that Wnt signaling should be better considered as a network rather than as individual pathways (Kestler & Kühl, 2008). In particular, the classification of Wnt ligands as being canonical or noncanonical has proven to be problematic. For instance, the prototypical canonical Wnt-3a can activate β-catenin-independent signaling (Bengoa-Vergniory, Gorroño-Etxebarria, González-Salazar, & Kypta, 2014; Qiu, Chen, & Kassem, 2011; Siman-Tov et al., 2021) and *vice versa*, Wnt-5a has been found to activate β-catenin-dependent signaling (Cha, Tadjuidje, Tao, Wylie, & Heasman, 2008). In addition, it has long been accepted that Wnt signal transduction pathways are highly cell-context dependent (Mikels & Nusse, 2006).

Wnt signaling initiates with the engaging of a Wnt ligand with its receptors and coreceptors at the cell surface. Frizzleds (FZD) are the main class of Wnt receptors and low-density lipoprotein receptor-related proteins 5 and 6 (LRP5/LRP6) are prominent coreceptors. In the absence of Wnt signals (Wnt off, Figure 8), the cytoplasmic pool of β-catenin is tightly controlled by several associated proteins that form the "destruction complex", which targets β-catenin for proteasomal degradation. These include the scaffolding protein Axin, casein kinase 1 (CK1), glycogen synthase kinase 3 (GSK3) and the adenomatous polyposis coli gene product (APC) (MacDonald et al., 2009). Kinases in the destruction complex phosphorylate β-catenin at certain serine/threonine residues, promoting its ubiquitination and subsequent degradation (Stamos & Weis, 2013). Certain Wnt signals (Wnt on, Figure 8) lead to sequestration of some of the destruction complex proteins to the plasma membrane (e.g., Axin, GSK3), disrupting the function of the destruction complex and allowing β-catenin cytoplasmic stabilization and accumulation, which is followed by its translocation to the nucleus.

In the nucleus, β-catenin associates with transcription factors to induce the expression of so-called Wnt target genes (Valenta, Hausmann, & Basler, 2012). T-cell factor (TCF)/lymphoid enhancer-binding factor (LEF) family of transcription factors are the main nuclear partners of

β-catenin. These, together with cofactors, such as cAMP response element binding protein (CREB) binding-protein (CBP)/p300 and B-cell CLL/lymphoma 9 (BCL9) and B Cell CLL/Lymphoma 9-Like (BCL9L), allow β-catenin-mediated regulation of gene expression (Valenta et al., 2012). There is now a great number of known β-catenin target genes, in human cells these include c-MYC, AXIN2, LEF1, NKD1, DKK1, RNF43 and ZNRF3, among others, which show differential tissue-specific expression patterns (Doumpas et al., 2019; Nakamura, De Paiva Alves, Veenstra, & Hoppler, 2016; Nusse Lab, 2021). These genes are often involved in cell proliferation, cell survival and stem cell maintenance (Valenta et al., 2012). Importantly, many target genes act as negative feedback regulators of β-catenin signaling, permitting both a potent and transient signal.

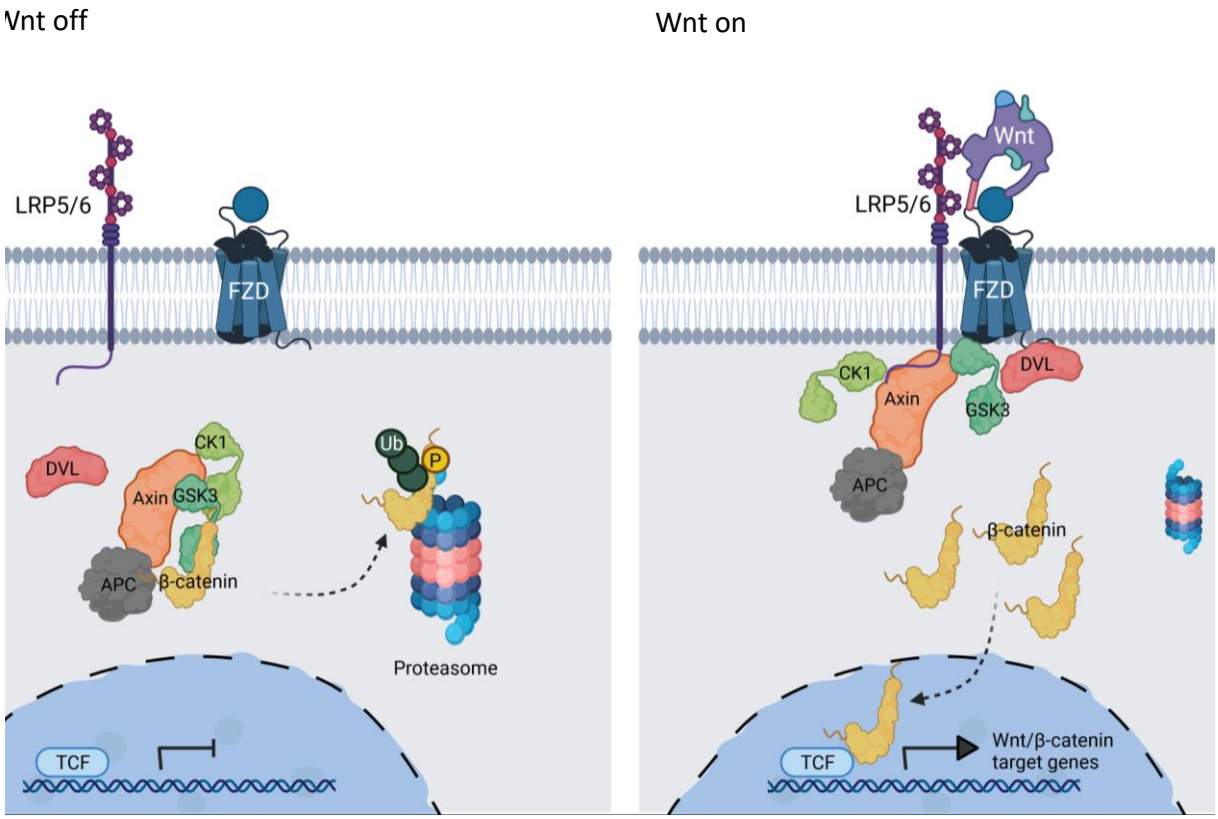

Figure 8. Wnt/β-catenin signaling. Wnt off state (left): the destruction complex formed by Axin, CK1, GSK3 and APC targets β-catenin for proteasomal degradation. Wnt on state (right): Wnt mediated signaling disrupts the function of the destruction complex and allows β-catenin stabilization and nuclearization to promote target gene expression. Abbreviations: FZD – Frizzled, LRP5 /LRP6 - low-density lipoprotein receptor-related proteins 5 and 6, DVL – Dishevelled, CK1 – casein kinase 1, GSK3 - glycogen synthase kinase 3, APC - adenomatous polyposis coli gene product, TCF - T-cell factor (TCF)/Lymphoid enhancer-binding factor (Lef), P - phosphate group, Ub – Ubiquitin.

Wnt signals that occur without the activation of β-catenin have been termed noncanonical (Veeman, Axelrod, & Moon, 2003) (Figure 9). These signaling pathways are many and less well understood than β-catenin-dependent Wnt signaling. The two best established, are the planar cell polarity (PCP) and the Calcium (Ca^{2+}) pathways. For these, Wnt ligands need to engage with FZD receptors and/or coreceptors, such as inactive tyrosine-protein kinase transmembrane receptor 1 and 2 (ROR1/2). This interaction also leads to the intracellular recruitment of Dishevelled (DVL), which acts as hub for Wnt signaling controlling both canonical and noncanonical signaling (Boutros & Mlodzik, 1999; Gao & Chen, 2010; M. Sharma, Castro-Piedras, Simmons, & Pruitt, 2018).

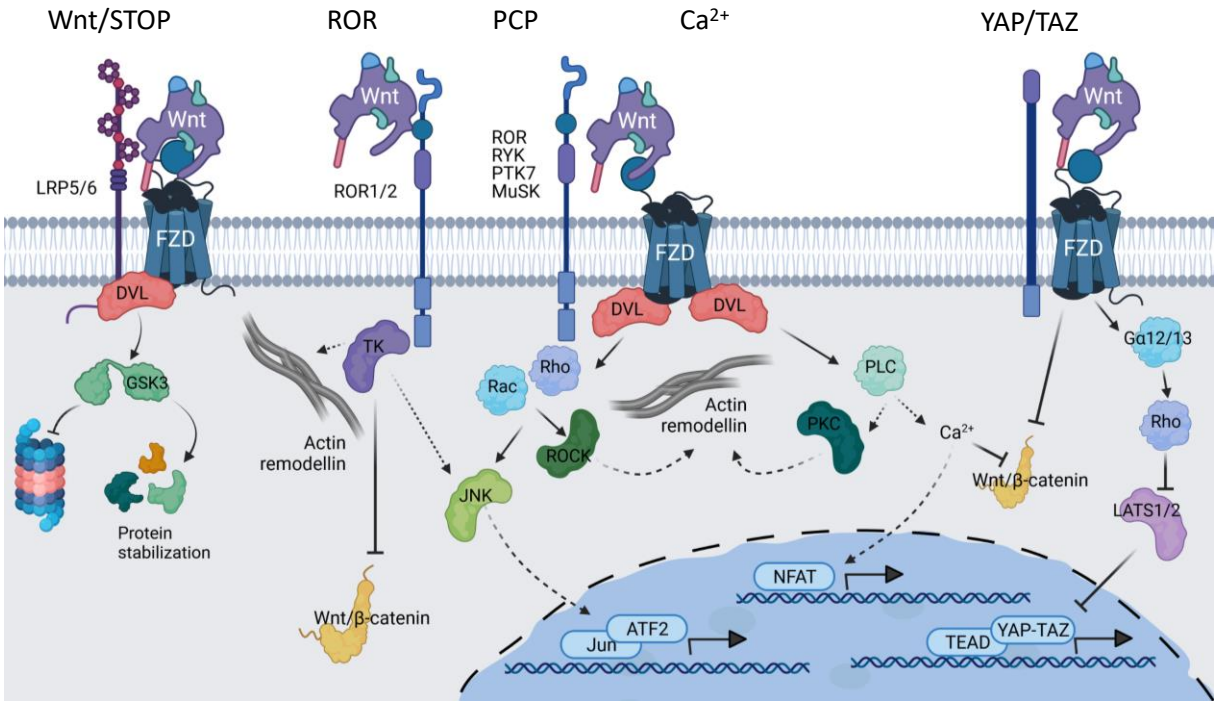

Figure 9. β-catenin-independent Wnt signaling. Selected noncanonical Wnt pathways from left to right: Wnt/STOP, ROR, PCP, Ca^{2+} and YAP/TAZ signaling. Wnts initiate signaling binding to receptors and coreceptors and intracellular signal mediators induce cytoplasm responses, such as protein stabilization and cytoskeleton remodeling and/or nuclear responses, with transcription factors and cofactors activating specific transcription programs. Abbreviations grouped by location in the pathway. Receptors/coreceptors: FZD – Frizzled, LRP5/LRP6 - Low-density lipoprotein receptor-related proteins 5 and 6, ROR1/2- inactive tyrosine-protein kinase transmembrane receptor 1 and 2. Intracellular mediators: DVL – Dishevelled, GSK3 - Glycogen synthase kinase 3, TK – Tyrosine kinase, JNK - Jun-N-terminal kinase, ROCK – Rho-associated protein kinase, PLC - Phospholipase C, PKC - Protein kinase C, Ca^{2+} - calcium ion. LATS1/2 - Large tumor suppressor kinase 1/2, CaMKII - Calcium/Calmodulin-dependent kinase 2. Nuclear factors: Jun – Transcription factor AP-1, NFAT - Nuclear factor of activated T-cells, YAP - Yes-associated protein 1; TAZ - WW domain containing transcription regulator 1, TEAD - TEA domain.

In the PCP pathway, DVL activates the small guanosine triphosphate hydrolase (GTPase) Rho and Rho-associated kinase (ROCK) to induce actin cytoskeleton remodeling. In parallel, there may be activation of the GTPase Rac, which activates Jun-N-terminal kinase (JNK), which in turn phosphorylates and activates members of the activator protein-1 (AP-1) family of transcription factors. AP-1 is a heterodimer composed of proteins from the Fos, Jun and activating transcription factor (ATF) families (Murillo-Garzón & Kypta, 2017; van Amerongen, 2012; Veeman et al., 2003).

In contrast, in the Wnt/Ca^{2+} pathway, DVL transduces signaling to phospholipase C (PLC), which promotes calcium mobilization and activation of the calcium-sensitive protein kinase C (PKC) and Calcium/Calmodulin-dependent kinase 2 (CaMKII). Subsequently, the nuclear factor of activated T-cells (NFAT) family transcription factors can be activated to promote processes such as growth, survival, invasion and angiogenesis (van Amerongen, 2012).

Nonetheless, there are additional noncanonical Wnt pathways, like those mediated by other protein tyrosine kinases. Fyn, a non-receptor tyrosine-protein kinase, has been shown to directly associate with Wnt-5a/b and FZD2 complex to induce signal transducer and activator of transcription 3 (STAT3)-mediated epithelial to mesenchymal transition (EMT). This pathway is known as the Fyn/STAT pathway and has been shown to be important in the progression of some malignancies (Gujral et al., 2014). RYK and ROR family receptor tyrosine kinases can function as stand-alone Wnt receptors, or as coreceptors in combination with FZDs to promote noncanonical Wnt signaling activating actin remodeling and AP-1 transcription factors (Green, Nusse, & van Amerongen, 2014). It is widely appreciated that Wnt-5a can be a ligand for ROR2, and this interaction has been shown to activate JNK and AP-1-mediated signaling (Nishita et al., 2010). Many of these noncanonical pathways have the ability to inhibit β-catenin-mediated signaling through different mechanisms, such as via receptor competition (Maye, Zheng, Li, & Wu, 2004; van Amerongen, 2012).

The crosstalk between Wnt and other pathways has been extensively studied, especially with the Hippo pathway (Azzolin et al., 2014; N. Li, Lu, & Xie, 2019; H. Liu et al., 2018). Inhibition of the Hippo tumor-suppressor pathway leads to the activation and nuclear entry of yes-associated protein 1 (YAP1) and its close paralog WW domain containing transcription regulator 1 (TAZ) to bind TEA domain (TEAD) family transcription factors, promoting tumorigenesis. It has been reported that the Hippo pathway antagonizes Wnt/β-catenin

signaling by interfering with the destruction complex (Azzolin et al., 2014). But not only that, a direct Wnt stimulus activating FZD/ROR receptors can induce Rho-mediated inhibition of large tumor suppressor kinase 1/2 (LATS1/2) which in turn induces YAP/TAZ/TEAD-mediated transcription (Hyun Woo et al., 2015). This occurs in a β-catenin independent manner and has been reported to promote cell migration and to antagonize Wnt/β-catenin signaling. Recently, LRP6 was reported to bind Merlin, a tumor suppressor that mediates signaling through the Hippo pathway, with LRP6 acting as a nutrient sensor to regulate Hippo signaling (Jeong et al., 2020).

In the Wnt/STOP pathway, LRP6-mediated Wnt signaling can initiate β-catenin-independent responses that promote protein stabilization, in a Cyclin-Y-dependent fashion, thereby inducing growth and promotion of cell cycle progression (Acebron & Niehrs, 2016). Recently, Wnt-10b-GSK3β–dependent Wnt/STOP has been shown to play an important role during mitosis, ensuring karyotype stability in human somatic cells (Y. C. Lin et al., 2021).

5.3.1. Wnt signaling regulators: antagonists and agonists

Given their potency as signaling molecules, the availability of active Wnts in the extracellular region is tightly controlled by activator and inhibitor proteins that associate with Wnts, Wnt receptors, coreceptors or other regulators of Wnt signaling. Wnt-binding regulators include secreted frizzled-related proteins (sFRP), WIF-1 and Cerberus (Malinauskas & Jones, 2014; Murillo-Garzón & Kypta, 2017).

Dickkopf-related proteins (DKK) and sclerostin (SOST) can associate with the LRP family coreceptors, antagonizing Wnt binding and signaling (Holdsworth et al., 2012; Kawano & Kypta, 2003; Malinauskas & Jones, 2014). Adenomatosis polyposis down-regulated 1 (APCDD1), a membrane-bound glycoprotein, can inhibit Wnt signaling by binding both Wnt and LRP5; it is found mutated in hereditary hypotrichosis simplex, a condition characterized by hair follicle miniaturization (Shimomura et al., 2010).

The availability of FZD receptors and coreceptors is regulated by endocytosis and by ubiquitination-mediated targeting for degradation, through the E3 ubiquitin ligases ZNRF3 and RNF43 (Hao et al., 2012; Koo et al., 2012). R-spondins (RSPO1–RSPO4), can bind ZNRF3 and RNF43 and leucine-rich repeat-containing G protein-coupled receptors (LGR4–LGR6) to enhance Wnt signaling by inducing membrane clearance of ZNRF3 and RNF43, enabling FZD

receptor stabilization, albeit the precise molecular mechanisms involved are still under investigation (Tsukiyama, Koo, & Hatakeyama, 2021).

Norrin (Norrie Disease Protein), can activate the Wnt/β-catenin pathway by binding to FZD4 (Chang et al., 2015). Although Norrin does not bear any sequence similarity to Wnt proteins, it does show structural similarity, mimicking Wnt for site 2 binding surfaces on FZD (see Wnt structure, page 38).

5.3.2. Luciferase-based Wnt gene reporters

Wnt signaling gene reporters have been of paramount importance in the development of the Wnt field. The TOP-Flash luciferase gene reporter assay has provided a robust and reliable way to measure activation of TCF/LEF-dependent transcription induced by β-catenin activation for many years. Its use is usually accompanied by a control reporter, FOP-Flash, that has mutations in the TCF/LEF binding sites (Korinek et al., 1997; Molenaar et al., 1996). There are several versions of this reporter, with different numbers of TCF/LEF binding sites. Analogous reporters of noncanonical Wnt signaling have been more difficult to obtain (van Amerongen, 2012).

Noncanonical Wnt signaling generally involves cytoskeletal and morphological changes that then lead to transcriptional responses involving molecular mediators that are not exclusive to Wnt signaling (e.g., small Rho GTPases, JNK/AP-1, NFAT). However, luciferase reporters for AP-1 and NFAT exist and are at least partially inducible by Wnt, FZDs and/or DVL (van Amerongen, 2012). Additionally, there is a luciferase reporter containing ATF2 response elements that, in Xenopus embryos, has been shown to provide a measure of noncanonical Wnt signaling in response to both gain and loss-of-function Wnt signaling components, including Wnt, FZD, ROR2, DVL, Rac1, and JNK (Ohkawara & Niehrs, 2011). Its use in Xenopus embryos has been further confirmed (Vitorino et al., 2015) and it was shown to be useful in monitoring Wnt-11 and Wnt-5a noncanonical signaling in chicks, which occurs in a DVL-dependent manner (Geetha-Loganathan, Nimmagadda, Fu, & Richman, 2014). However, it has been a matter of debate whether this reporter can be used reliably for monitoring noncanonical Wnt responses in mammalian cells. Nonetheless, this reporter has been used in human HEK 293 cells, where XWnt-5a activates it only in a short-range, autocrine manner, and this was further shown to be dependent on receptor complex internalization (Veronika et al., 2014). Also in HEK 293 cells, this ATF2-luc reporter has aided in the identification of noncanonical

Wnt receptors in Wnt-3a-induced neural differentiation (Bengoa-Vergniory et al., 2017). It has also been reported to be useful in measuring Wnt-11-mediated activation in colorectal and prostate cancer cells (Gorroño-Etxebarria et al., 2019; Murillo-Garzón et al., 2018). Moreover, similar ATF2-based constructs have been used to monitor other noncanonical Wnt signals (Boitard et al., 2015; C. Chen et al., 2018). In addition, as noncanonical Wnt activation often results in inhibition of Wnt/β-catenin signaling, inhibition of the TOP-Flash reporter has been useful as a readout for noncanonical Wnt signaling activity (van Amerongen, 2012).

5.4. Wnt receptors, coreceptors and DVL

Wnt receptors and coreceptors are key proteins that mediate the initiation of Wnt signaling. These are thought to consist of heterodimeric complexes, where Wnt can simultaneously bind both receptors and coreceptors, a well-studied case is the Wnt/FZD/LRP5/6 complex (Nusse & Clevers, 2017). The ability of DVL and Axin to multimerize and bind Wnt receptors and coreceptors makes them ideal to support the formation of these complexes. The availability of the receptors and coreceptors at the cell surface is tightly controlled by internalization, degradation and turn-over, and these events are important for controlling Wnt signal transduction. The domain organizations of FZD, LRP and DVL are depicted in Figure 10.

Figure 10. Domain organization of FZD, LRP and DVL. A) FZD (Frizzled) domains: CRD – Cysteine rich domain, linker, 7TM – 7-pass transmembrane, intracellular 8th domain. B) LRP (Lipoprotein receptor-related proteins) domains: EGF - Epidermal growth factor, LDLR-A - Low-density lipoprotein receptor class A, PPPSPxS - P, proline; S, serine or threonine, x, a variable residue. C) DVL DIX, PDZ and DEP domains. Adapted from (MacDonald & He, 2012). C-ter – C-terminal, N-ter – N-terminal.

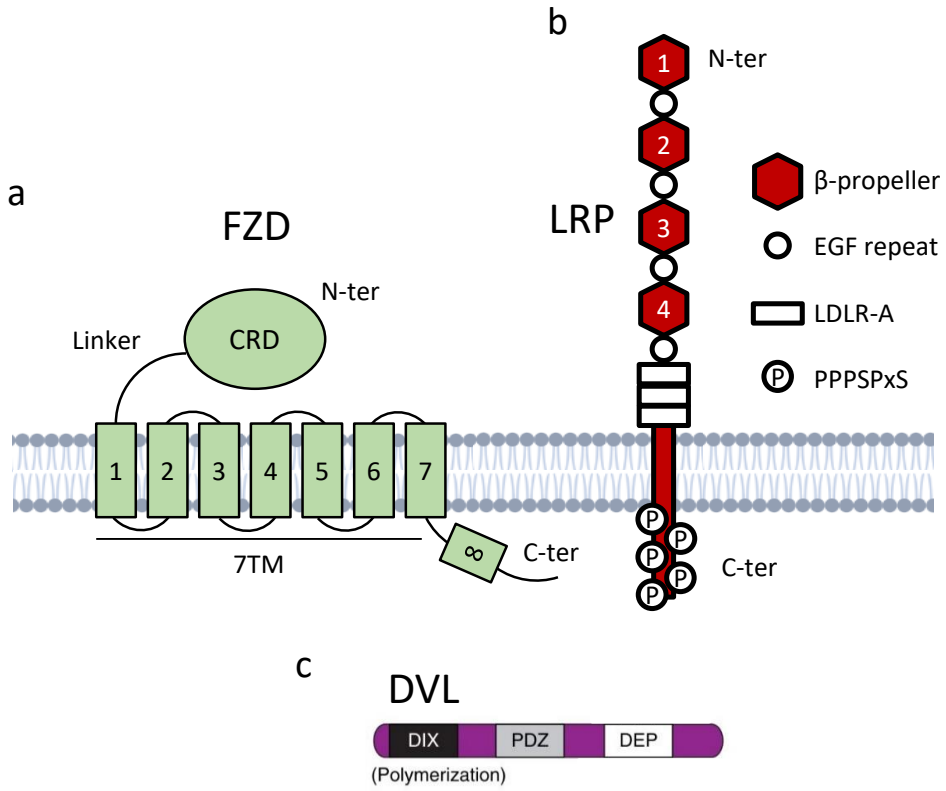

5.4.1. FZD receptors

FZDs are a family of 7-pass transmembrane (7TM) receptors of 500-700 amino acids in length. The family consists of 10 members in mammals. They are related to G-protein coupled receptors but are considered an independent family (Schulte & Bryja, 2007). Most members are codified in a single exon. Their N-terminal region contains a cysteine-rich domain (CRD) that is extracellular and highly conserved, a linker of variable size to the 7TM connected through several intracellular and extracellular loops and it has an additional intracellular domain that contains conserved KTxxxW (lysine-threonine-x-x-x-tryptophan, x - variable residues) motifs that are crucial for DVL interaction (Figure 10a). Structural studies have shown that Wnt binds to two distinct sites of the FZD-CRD (see Wnt structure, page 38).

5.4.2. LRP5/6 coreceptors

Mammalian low-density lipoprotein (LDL)-receptor-related proteins 5 and 6 (LRP5/6) are single-pass transmembrane receptors that were discovered as orthologs of the Drosophila *Arrow*. They were early recognized as key mediators of Wnt signaling acting as Wnt receptors (Pinson, Brennan, Monkley, Avery, & Skarnes, 2000; Tamai et al., 2000; Wehrli et al., 2000). They are part of the LDLR family, which also includes the LDL receptor, LRP (or LRP1),

megalin (LRP2), VLDL receptor, apoER2 (LRP8), SorLA/LR11, LRP1b, LRP3 and MEGF7 (LRP4) (Q. Ren, Chen, & Liu, 2021). LRP5 and LRP6 are unique with respect to the number and arrangement of LDLR repeats and share 71% sequence identity (Joiner, Ke, Zhong, Xu, & Williams, 2013). They have an extracellular domain containing four tandem β-propeller/epidermal growth factor (EGF) repeats followed by three LDLR type A repeats (MacDonald & He, 2012; Figure 10b). The C-terminal intracellular tail has 5 PPPSPxS (P, proline; S, serine or threonine, x, a variable residue) motifs that can be phosphorylated at the serine/threonine residues creating a binding site for Axin and leading to the recruitment of DVL and the Axin/GSK3 complex to the plasma membrane (Joiner et al., 2013; Niehrs, 2012).

Although there is multiple evidence of Wnt binding to LRPs, there are no reported structures for the Wnt/LRP complex. Nevertheless, the Wnt/FZD structures show an extensive surface between the two separate FZD binding domains on Wnt (see Wnt structure, page 38), which would easily accommodate coreceptor binding (Nusse & Clevers, 2017). Some studies have proposed there are two distinct binding sites for Wnts in LRP6, each located in its β-propellers 1-2 (E1-E2) and β-propellers 3-4 (E3-E4) (Bourhis et al., 2010; Gong et al., 2010; J. S. Lee et al., 2012).

5.4.3. ROR/RYK coreceptors and others

Receptor tyrosine-protein kinases of the RYK and ROR families are single-pass transmembrane receptors that were first classified as orphan receptors but are now known to interact and transduce Wnt signals (Green et al., 2014). The ROR family comprises ROR1 and ROR2, which are evolutionarily conserved across most species. The extracellular portion of the receptors contains a CRD domain that bears close homology with that of the FZDs. In the intracellular region they have tyrosine-kinase-like domains that are most likely pseudokinases with very low or no catalytic activity (Murillo-Garzón & Kypta, 2017). They can function as stand-alone Wnt receptors, or as coreceptors in combination with FZDs (Green et al., 2014) and they likely signal through DVL-dependent mechanisms (Nishita et al., 2010; Voloshanenko et al., 2018).

Tyrosine-protein kinase RYK receptors are also likely catalytically inactive and believed to mainly work in complex with FZDs. RYK contains an extracellular domain resembling the Wnt inhibitory factor (WIF) protein, which differs from the classic CRD domain of FZDs and RORs (Green et al., 2014; Murillo-Garzón & Kypta, 2017).

There are other tyrosine kinase-like proteins that can interact and transduce Wnt signals, such as protein-tyrosine kinase 7 (PTK7) and the ROR-related muscle, skeletal receptor tyrosine-protein kinase (MuSK). MuSK is, among the protein tyrosine kinase here described, the only one thought to be catalytically active (Niehrs, 2012).

Recently, the GPI-anchored glycoprotein RECK (reversion-inducing-cysteine-rich protein with kazal motifs) was reported to be a receptor for Wnt-7a/b, which, in complex with GPR124 (also known as ADGRA2 (adhesion G protein-coupled receptor A2)) recruits DVL to form Wnt-specific signalosomes for signal transduction (Eubelen et al., 2018).

5.4.4. Dishevelled (DVL)

Dishevelled (DVL/DSH) relays Wnt signals from receptors to downstream effectors in β-catenin-dependent and -independent pathways, acting as a hub for Wnt signaling (Boutros & Mlodzik, 1999; Gao & Chen, 2010). DVL is a scaffold protein that can polymerize and bind to a multitude of partners. Its activity is modulated dynamically by phosphorylation, ubiquitination, and degradation.

DVL was originally identified in Drosophila and there are three DVL paralog genes in humans and mice (DVL1, 2 and 3) that display high sequence identity (Sussman et al., 1994). DVL isoforms show overlapping expression patterns and display functional redundancy, which is apparent by phenotypic rescue experiments in knock-out mice (Gao & Chen, 2010).

DVL proteins consist of about 750 amino acids and possess three conserved domains of about 80-90 amino acids each (Figure 10c). DVL has an N-terminal DIX domain that is also found in Axin and mediates polymerization with similar domains in a weak and reversible manner (Gammons, Renko, Johnson, Rutherford, & Bienz, 2016). A central PDZ (postsynaptic density 95, discs large, zonula occludens-1) domain, which allows DVL interaction with several proteins, including FZDs and DVL-associated kinases. Finally, it has a C-terminal DEP (DVL, Egl-10, Pleckstrin) domain, which participates in the interaction with membrane lipids and is also implicated in the interaction with FZDs (Micka & Bryja, 2021). The DEP domain has been reported to undergo a conformational switch to trigger DIX-dependent polymerization, which is key for signalosome assembly (Gammons et al., 2016). DVL proteins have additionally a basic region with scattered serine/threonine-rich stretches between the DIX

and PDZ domains, and a proline-rich region and both help mediate protein-protein interactions (M. Sharma et al., 2018; Wallingford & Habas, 2005).

Several kinases have been reported to phosphorylate DVL, including casein kinase 1 δ/ε and casein kinase 2, which are the ones responsible for the phosphorylated DVL electrophoretic mobility shift observed on SDS polyacrylamide gels. In addition, other kinases have been reported to phosphorylate DVL such as protein kinase C (PKC) (Velázquez, Castañeda-Patlán, & Robles-Flores, 2017). DVL phosphorylation dictates its activation, and it can also increase its stability. In fact, the DVL pool is regulated by proteasomal degradation and has been reported to be the target of multiple ubiquitin ligases (Gao & Chen, 2010). It has been recently proposed that DVL phosphorylation might also control a conformational change, where the PDZ domain binds to the DVL C-terminus resulting in a closed, less active conformation and that phosphorylation promotes the open, more active, conformation (H. J. Lee, Shi, & Zheng, 2015; Micka & Bryja, 2021).

Furthermore, DVL has been shown to shuttle between the cytoplasm and the nucleus. It bears both a nuclear export sequence (NES) and an atypical nuclear localization sequence (NLS) (Gao & Chen, 2010). Disruption of these peptide signals impacts certain Wnt/β-catenin signals and it has further been proposed that DVL nuclear interactions with Jun, β-catenin, TCF4 and forkhead box (FOX) transcription factors FOXK1 and FOXK2 are also important for the promotion of Wnt/β-catenin signaling (Gan et al., 2008; W. Wang et al., 2015).

5.5. Wnt in development and tissue homeostasis

Wnt proteins play a prominent role both in development and adult tissue homeostasis (Steinhart & Angers, 2018). In the development of multicellular organisms, Wnts control stem cell self-renewal, cell fate decisions and coordinate cell migration and tissue organization. For instance, Wnt/β-catenin activation, in combination with BMP signaling, is key for defining the dorsoventral and anteroposterior body axes in multiple animal species (Niehrs, 2010).

After development, Wnts remain important for adult homeostasis in certain tissues by governing the maintenance of stem cell niches, and controlling their capacity for proliferation and self-renewal (Clevers, Loh, & Nusse, 2014). In adult intestinal epithelium turnover, a Wnt signaling gradient emanating from the base of the crypts tightly controls cell proliferation and stem cell renewal. Wnt proteins also play a prominent role in bone, governing osteoblast differentiation and function (Day, Guo, Garrett-Beal, & Yang, 2005). In skin, Wnts regulate

hair follicle stem cells (HFSCs) which impacts the hair follicle cycle (Veltri, Lang, & Lien, 2018). Wnt/β-catenin signaling activation has been shown to be important for maintaining the naive pluripotent state in embryonic stem cells (ESC) by controlling the transition between naive and primed ESC states (Steinhart & Angers, 2018).

Although the activation of Wnt/β-catenin pathway is the preferred mechanism of Wnt-mediated control of stem cell responses, *in vitro* studies have shown that noncanonical Wnt pathways can also activate stemness properties. For example, both canonical and noncanonical Wnt signaling have been reported to independently promote stem cell proliferation in mammosphere cultures, with Wnt-5a/JNK activation increasing mammosphere formation (Many & Brown, 2014). Wnt-11 has also been shown to promote sphere formation in melanoma cells in a ROCK-dependent manner (Rodriguez-Hernandez et al., 2020) and to stimulate contact-independent growth of IEC6 cells by a β-catenin-independent mechanism (Ouko, Ziegler, Gu, Eisenberg, & Vincent, 2004).

5.6. Wnt in cancer and prostate cancer

Wnt signaling has been associated with cancer ever since the discovery of Wnt-1 upregulation leading to mammary tumors in mice (Nusse & Varmus, 1982). Since then, Wnt signaling has been linked to multiple types of tumors in cancer-type-specific and cancer-stage-specific manners. In particular, aberrant hyperactivation of Wnt signaling can promote tumor initiation, growth, metastasis and drug resistance in certain malignancies (Anastas & Moon, 2013).

The best characterized example of Wnt signaling activation in cancer is loss of APC function in colorectal cancer. This leads to the inappropriate stabilization of β-catenin and the formation of constitutive complexes with TCF4 (Morin et al., 1997). Other Wnt pathway-related mutations include loss-of-function mutations in Axin in hepatocellular carcinomas, CTNNB1 (gene encoding β-catenin) mutations in a wide variety of solid tumors and inactivating mutations in the TCF family member LEF-1 in some skin tumors (Clevers & Nusse, 2012). RNF43 and ZNRF3 Wnt pathway tumor suppressors are found with loss-of-function mutations in multiple cancers, as well as gene fusions involving RSPO2/3 (Nusse & Clevers, 2017).

Although activating pathway mutations are relatively infrequent in prostate cancer, Wnt pathway activation has been reported as a key driver of malignant prostate cancer progression

(Murillo-Garzón & Kypta, 2017). Nevertheless, genomic alterations in the Wnt/β-catenin pathway, mainly loss-of-function mutations in APC and missense mutations in CTNNB1, were found in 10% of prostate tumors in a recent study of 680 primary and 333 metastatic tumors (Armenia et al., 2018). In this study, mutations in genes involved in Wnt/β-catenin signaling were found to be particularly enriched in metastatic tumors. In addition, Wnt signaling mutations appear more frequently in CRPC tumors, with studies reporting APC and CTNNB1 mutations in 18% of samples and RNF43 and ZNRF3 mutations in 6% (Robinson et al., 2015). Furthermore, Wnt signaling activating mutations have been recently associated with increased resistance of CRPC to abiraterone acetate/prednisone and abiraterone and enzalutamide (Isaacson Velho, Wei, Hao, & S. Antonarakis, 2020; L. Wang et al., 2018). In this context, Wnt pathway activation can induce the expression of stem-like genes and Wnt inhibition has been proposed to be beneficial for overcoming enzalutamide resistance (Z. Zhang et al., 2018).

However, Wnt pathway involvement in prostate cancer is thought to be maintained mainly via tissue-specific pathway activators. Thus, alterations in the expression of genes encoding Wnt-5a, Wnt-7b, Wnt-11, sFRP and DKK have been reported (Murillo-Garzón & Kypta, 2017). The expression of several Wnt ligands is upregulated after ADT (Rajan et al., 2014), and the oncogenic TMPRSS2–ERG fusion can drive the expression of some Wnts and FZDs (Gupta et al., 2010; Wu et al., 2013). Other important factors such as FOXB2 have shown to induce the expression of the gene *WNT7B*, which is linked to the promotion of the malignant transformation in prostate cancer (Moparthi, Pizzolato, & Koch, 2019).

In fact, the implication of noncanonical Wnt signaling in prostate cancer progression has recently drawn particular attention, with some of its components being proposed as potential prognostic biomarkers (Fisher, Pleskow, Bedingfield, & Miyamoto, 2020; Murillo-Garzón & Kypta, 2017). A noncanonical Wnt gene signature, termed NCWP-EMT, related with the role of Wnt-5/FZD2 in EMT, has been associated with prostate cancer aggressiveness (Sandsmark et al., 2017). Although, Wnt-5a role in prostate cancer remains ambiguous, it has been shown to promote aggressiveness in some models (H. Yamamoto et al., 2010), whilst other studies point to Wnt-5a/ROR2/SIAH2 signaling axis as a mechanism for maintaining prostate cancer cells dormancy in bone (D. Ren et al., 2018). The role of Wnt-11 in cancer and, particularly, in prostate cancer, is introduced in an independent chapter (see pages 60 and 62).

5.7. Wnt-based therapeutics

Because aberrant Wnt pathway activation is often observed to promote pathogenetic processes, Wnt-based therapies are usually aimed at inhibiting Wnt signaling. These therapies can be subdivided based on the location of their targets within the Wnt signaling pathway. The main agents described here are summarized in Figure 11.

5.7.1. Inhibition of Wnt secretion

Inhibitors of porcupine-mediated palmitoylation of Wnts are likely the most studied class of Wnt-based therapeutics, and their effect is to inhibit secretion and activity of all Wnts. This category includes IWPs (inhibitors of Wnt production), Wnt-C59, ETC-159 and WNT974, also known as LGK974 (Ho & Keller, 2015). The latter molecule's Phase 1 clinical trial has been active since 2011 for the treatment of selected solid tumors. So far, single-agent WNT974 treatment has been generally well-tolerated, with main adverse events being dysgeusia and bone-related disorders (Rodon et al., 2021). The study is ongoing for a combination arm with anti-PD-1 antibodies and is set to be completed by 2023. Other porcupine inhibitors that have reached clinical development for treatment of solid tumors include XNW7201, RXC004 and CGX1321. Recently, CGX1321 was proposed to also attenuate cardiac hypertrophy (Jiang et al., 2018).

5.7.2. β-catenin interaction, stability, and activity modulators

The regulation of the interaction of β-catenin with its partners is the mechanism of action of several therapeutic agents (Krishnamurthy & Kurzrock, 2018). For example, PRI-724 inhibits the interaction between β-catenin and its transcriptional coactivator CBP and is in clinical trials for the treatment of solid tumors. ICG-001 is a similar inhibitor that has not reached clinical development.

There are also strategies that aim to modulate β-catenin stability. CWP23229 is a peptidomimetic that induces tumor-selective apoptosis by promoting β-catenin degradation and is currently being tested for treatment in hematological cancers (Kuek, Hughes, Kotecha, & Cheung, 2021). Recently, this inhibitor was shown to block the growth of castration-resistant prostate cancer by activating the endoplasmic reticulum stress pathway (Pak et al., 2019).

Tankyrase (TNKS1/2) inhibitors limit Axin proteasomal degradation, stabilizing the destruction complex and promoting β-catenin degradation. Tankyrase inhibitors include IWR-1, which was discovered in the same screen that identified IWPs (B. Chen et al., 2009; Haikarainen, Krauss, & Lehtio, 2014), and E7449 (also known as 2X-121). The latter has shown promising results in a Phase 1 trial for solid malignancies (Plummer et al., 2020). However, it should be noted that E7449 can also act as an inhibitor of PARP1 and PARP2 (Plummer et al., 2020) and other TNKS1/2-specific inhibitors (i.e., G007-LK) block additional signaling pathways, such as YAP and PI3K/AKT (Mygland et al., 2021).

SM04755 and SM04690 are small-molecules that were identified as Wnt inhibitors through high-throughput screening and are being developed as a treatment for tendinopathy and osteoarthritis respectively (Deshmukh et al., 2020; Yazici et al., 2017). Both appear to have CLKs (CDC-like kinases) and DYRK1A (dual-specificity tyrosine phosphorylation-regulated kinase 1A) as their main targets, kinases that are proposed to regulate canonical Wnt signaling downstream of β-catenin by controlling alternative splicing of Wnt target genes.

5.7.3. Targeting Wnt pathway regulators

Ipafricept (OMP-54F28) is a recombinant fusion protein with the extracellular part of human FZD8 fused to a human IgG1 Fc fragment that binds Wnt ligands and acts as a decoy receptor (Jimeno et al., 2017). In patient-derived ovarian cancer xenografts, this compound was shown to reduce the frequency of stem cells, inhibit tumor formation and promote cell differentiation, and it also displays synergy with taxane-based therapies (Krishnamurthy & Kurzrock, 2018).

OMP131R10 is an anti-RSPO3 antibody that has been tested in a Phase 1 trial for advanced tumors, displaying an overall manageable profile. It is also proposed to be beneficial for the treatment of fibrosis in multiple organs (M. Zhang et al., 2020).

MCLA-158 is a bispecific antibody targeting EGFR and LGR5. The latter molecule is a receptor associated with Wnt signaling in the intestine. MCLA-158 is in Phase 1 clinical trials for treatment of metastatic colorectal cancer (Argiles et al., 2021).

An adenovirus expressing DKK3 (also known as REIC), which can indirectly inhibit Wnt signaling, entered Phase 1/2 clinical trials in patients with localized prostate cancer that have reported some promising results (Kumon et al., 2016).

Although DKK1 is an inhibitor of Wnt/β-catenin signaling, it is upregulated in some cancers and its inhibition has been postulated to have an immuno-modulatory effect (Wall, Klempner, & Arend, 2020). DKN-01 is a humanized monoclonal antibody targeting DKK1 that is being tested for treatment of several malignancies, such as advanced liver cancer and gastric cancer. It has been described to have a safe profile in combination with gemcitabine and cisplatin, however it has failed to show improved efficacy (Goyal et al., 2020). Currently there is a Phase 1b/2a study of DKN-01 for the treatment of advanced prostate cancer with elevated DKK1 (Wise et al., 2020).

5.7.4. Wnt/receptor interaction modulators

Targeting the Wnt/receptor complex formation can lead to higher specificity for modulating Wnt signaling. This class consists mainly, but not only, of therapeutic antibodies.

Vantictumab (OMP-18R5) is a monoclonal antibody that targets FZD1, 2, 5, 7 and 8. Phase 1 clinical trials in metastatic breast cancer showed good tolerability with promising efficacy in combination with paclitaxel; however, there has also been a high incidence of fractures that has hindered future clinical development (Diamond et al., 2020).

Cirmtuzumab (UC-961) is a humanized monoclonal antibody that binds the extracellular domain of ROR1 (M. Y. Choi et al., 2016). It has been tested in clinical trials for blood malignancies, such as chronic lymphocytic leukemia (CLL). Phase 1b clinical trials in combination with paclitaxel are ongoing in patients with HER2 negative metastatic/advanced breast cancer (S. Zhang et al., 2019).

OTSA101-DTPA-90Y is a radiolabeled (Yttrium 90) monoclonal antibody targeting FZD10 that is currently being evaluated in Phase 1 for the treatment of relapsed or refractory synovial sarcoma (Giraudet et al., 2018).

BI 905677 is a bi-paratopic antibody that binds to two distinct epitopes of LRP5 or LRP6 and potently blocks Wnt signaling, displaying anti-tumor activity in Wnt-driven cancer models, such as those with RNF43 mutations or RSPO fusions. A Phase I clinical trial is underway in patients with advanced solid tumors (Zinzalla et al., 2019).

Foxy-5 is a formylated hexapeptide that functions as a Wnt-5a peptidomimetic that activates its signaling and has been shown to inhibit breast cancer metastasis (Säfholm et al., 2008). It

has been proposed to be beneficial for the treatment of prostate cancer with low Wnt-5a and in a completed Phase 1 clinical trial has demonstrated to have a safe profile (Canesin et al., 2017). Another clinical trial is ongoing with Foxy-5 as neo-adjuvant therapy in subjects with Wnt-5a low colon cancer.

In the opposite manner, there are both polyclonal and monoclonal anti-Wnt-5a antibodies with neutralizing properties that inhibit metastasis of gastric cancer cells *in vivo*. The mechanism of action was described to be the inhibition of receptor-mediated endocytosis of the Wnt-5a receptor, ROR2, without impairing Wnt-5a/ROR2 binding (Hanaki et al., 2012; Shojima et al., 2015).

There is also an anti-Wnt-1 antibody that has been reported to induce apoptosis in Wnt-1 expressing non-small cell lung cancer, breast cancer, mesothelioma, and sarcoma cells (B. He et al., 2004; Mikami et al., 2005). However, no Wnt-targeted antibody has yet reached clinical development.

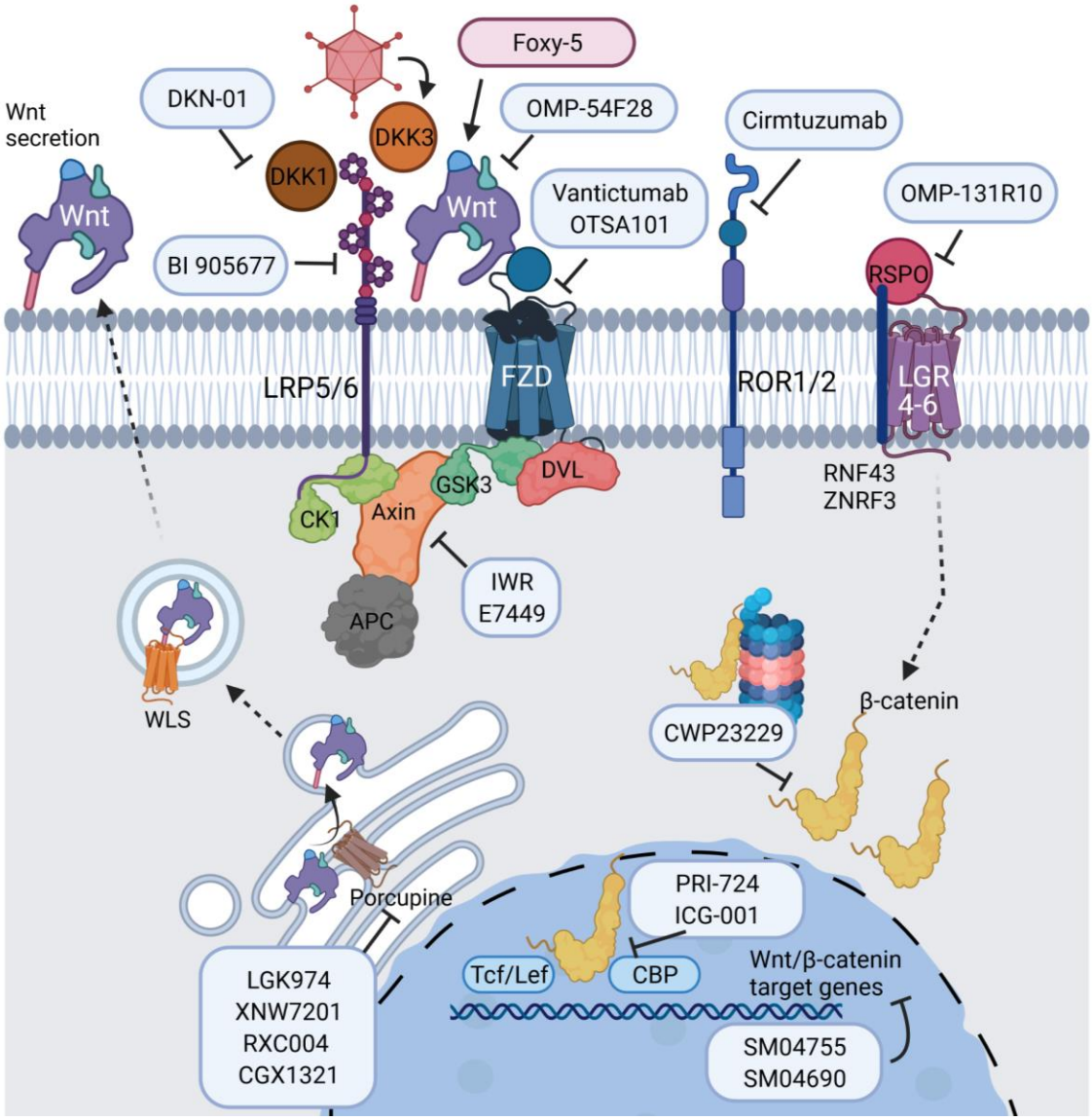

Figure 11. Summary of selected Wnt-based therapeutic agents. Porcupine inhibitors target Wnt secretion, agents highlighted: LGK974, XNW7201, RXC004 and CGX1321. Drugs that target Wnt pathway regulators and Wnt/receptor modulators can be found in the extracellular region and the following are highlighted: DKN-01 targeting DKK1, DKK3 adenovirus, OMP-54F28 decoy receptor, Vantictumab and OTSA101 for FZDs, Cirmtuzumab targeting ROR1/2 and OMP-131R10 anti-RSPO antibody. β-catenin interaction, stability, and activity modulators are located in the intracellular region, acting downstream of Wnt receptors, and are: IWR and E7449 tankyrase inhibitors, CWP23229 inductor of β-catenin degradation, PRI-724 and ICG-001 modulators of β-catenin binding partners and SM04755 and SM04690 regulators of alternative splicing of Wnt target genes.

6. Wnt-11

Wnt-11 is one of the members of the human Wnt family. Molecular cloning and characterization of human *WNT11* was carried out independently in 1998 and 2001, and its expression was already associated with certain malignancies (Kirikoshi, Sekihara, & Katoh, 2001; Lako et al., 1998). The human *WNT11* gene is located at chromosome 11q13.5, comprising 5 coding exons and with a transcript length of 1 900 bp. This is translated to a protein of 354 residues, with a predicted 24 amino acid signal peptide and the 22 core cysteine residues found in all Wnt family members (Uysal-Onganer & Kypta, 2012).

Wnt-11 has been extensively associated with the noncanonical PCP and Ca^{2+} pathways (Ouko et al., 2004; Railo, Nagy, Kilpeläinen, & Vainio, 2008; Uysal-Onganer & Kypta, 2012). Nevertheless, one of the two Wnt-11 proteins present in Xenopus, which is not the human ortholog, but bears high sequence similarity (Hardy et al., 2008), has been identified as the ligand mediating the activation of LRP6/β-catenin-dependent signaling in dorsal axis induction in embryos (Kofron et al., 2007; Steinhart & Angers, 2018; Tao et al., 2005). However, in other contexts Wnt-11 functions as a repressor of Wnt/β-catenin signaling, which has been proposed to happen through multiple mechanisms, including via competition with other Wnts for receptor binding (Maye et al., 2004; Railo et al., 2008; Toyama, Lee, Koga, Wands, & Kim, 2010; Uysal-Onganer & Kypta, 2012). In addition, Wnt-11 has also been reported to inhibit JNK/AP-1 and NF-κB pathways in Chinese hamster ovary (CHO-K1) cells (Railo et al., 2008). These examples illustrate the cell-context dependency and intricacy of Wnt-11 signaling.

6.1. Wnt-11 in development and adult homeostasis

In zebrafish embryos, Wnt-11 regulates gastrulation by mediating convergence and extension movements through the PCP pathway (Heisenberg, Tada, & Wilson, 2000). It plays an important role in cell cohesion and cell-cell contact persistence in a DVL-dependent manner (Ulrich et al., 2005; Witzel, Zimyanin, Carreira-Barbosa, Tada, & Heisenberg, 2006). Together with Wnt-5a, Wnt-11 can regulate mammalian anterior-posterior axis elongation, activating p38 and RhoA (Andre, Song, Kim, Kispert, & Yang, 2015).

Wnt-11 is implicated in kidney development both during embryogenesis and during adult homeostasis. *Wnt11* null mice have smaller kidneys and bear ureteric branching defects (Majumdar, Vainio, Kispert, McMahon, & McMahon, 2003). To coordinate ureteric

branching, Wnt-11 can cooperate with the genes encoding glial cell-derived neurotrophic factor (Gdnf) and Ret tyrosine kinase receptor, in a positive autoregulatory feedback loop. Recently, this feedback mechanism has been modeled computationally with a Turing-type model where the authors further provided experimental confirmation that positive feedback between Wnt-11 and GDNF facilitates dense packing of ureteric tips (Menshykau et al., 2019). Wnt-11 determines cell polarization and movement in nephron progenitor differentiation in embryonic mouse kidney, where it may continue to play a role in the adult (O'Brien et al., 2018).

The importance of Wnt-11 in heart development and function has been also extensively studied (Flaherty, Kamerzell, & Dawn, 2012). Wnt-11 plays a prominent role in differentiation of bone marrow-derived mesenchymal stem cells (MSCs) into cardiac phenotypes, and it has been reported to confer protection to ischemic injury by promoting survival, an effect that could be reversed by Wnt-11 neutralizing antibodies (Zuo et al., 2012). The Wnt-11-induced responses could be exploited for acute myocardial infarction therapy, as has been proposed by transplantation of MSCs overexpressing Wnt-11 in combination AKT (B. Chen et al., 2018). Here, Wnt-11 has been proposed to act via noncanonical Wnt-PKC-JNK pathways (Jingcai Wang et al., 2020) and through the promotion of vascular endothelial growth factor (VEGF) release, which helps to preserve mitochondrial membrane integrity and function (H. X. Li, Lin, Jiang, & Yang, 2020). In this context, Wnt-11 effects may be regulated through Sfrp2, acting in competition with Wnt-3a (Hsueh, Hodgkinson, Pratt, & Dzau, 2020).

Wnt-11 has also been found to be involved in osteoblast differentiation from MSCs (Boyan, Olivares-Navarrete, Berger, Hyzy, & Schwartz, 2018). It has the capacity to enhance the osteogenic potential of bone morphogenetic protein 9 (BMP9) in MSCs, through Smad and p38 MAPK signaling (J. H. Zhu et al., 2018). However, there are contradictory reports showing Wnt-11 downregulation leading to an increase in osteoblasts (Yin et al., 2019). In human umbilical cord-derived mesenchymal stem cells (hucMSCs), Wnt-11 has been reported to enhance stemness properties by activating Wnt/β-catenin signaling (Shi et al., 2017). Finally, fibronectin may promote Wnt-11/FZD7 interaction to facilitate self-renewal in rabbit limbal epithelial stem cells (Zheng, Tian, Fan, & Xu, 2019).

6.2. Wnt-11 in cancer and disease

Early reports using cell lines showed that Wnt-11 can promote malignant transformation of mouse mammary epithelial cells (Christiansen, Monkley, & Wainwright, 1996). Later, Wnt-11 was reported to promote proliferation, migration and malignant transformation of intestinal

cells in a β-catenin independent manner by induction of E-cadherin internalization (Ouko et al., 2004).

In colorectal cancer (CRC) *WNT11* mRNA expression is found higher in tumors compared to healthy tissue and its high expression is associated with recurrence and death after surgery (Nishioka et al., 2013). Recently, immunohistochemical analysis of Wnt-11 protein expression in a cohort of 357 CRC patients found significantly higher levels in tumors compared to paired benign tissue (Gorroño-Etxebarria et al., 2019). In this study, reduced invasion of colorectal cancer cell lines expressing high Wnt-11 is reported upon anti-Wnt-11 antibody-mediated inhibition, using the antibodies that are the focus of this thesis. Wnt-11 enhanced expression in CRC has been proposed to be the result of long noncoding RNA (lncRNA) ABHD11-AS1 and miR-1254-mediated regulation (D. He et al., 2019). In addition, the anterior gradient-2 (AGR2) effect on the promotion of cell migration and metastasis has been reported to take place through the induction of Wnt-11 (Tian et al., 2018).

In other cancer models, Wnt-11 expression has also been associated with tumor cell aggressiveness. For example, Wnt-11 increases breast cancer cell migration, acting downstream of ERRα and β-catenin activation (Dwyer et al., 2010). In pancreatic ductal adenocarcinoma, increased Wnt-11 expression promotes tumor cell invasion (Dart et al., 2019). In cervical cancer, Wnt-11 expression was found associated with high-risk human papilloma virus (HR-HPV) E6 oncoprotein, leading to increased cell proliferation and invasion in a JNK-dependent manner (Wei et al., 2016).

In addition, Wnt-11 signaling has been proposed to display crosstalk with the transforming growth factor beta (TGF-β) pathway, which is a key regulator of EMT. Wnt-11 promotes mesenchymal gene expression in renal cells when activated by TGF-β (P. Zhang, Cai, Soofi, & Dressler, 2012). In squamous cell lung carcinoma, Wnt-11 has been described to promote EMT and decrease cell-cell adhesion (Bartis et al., 2013). In small-cell lung cancer, Wnt-11 can regulate not only EMT, but also neuroendocrine differentiation and proliferation acting as a target of Achaete-scute complex 1 (ASCL1) (Tenjin et al., 2019). Similarly, Wnt-11 has been reported to induce amoeboid invasion in melanoma through FZD7 and disheveled-associated activator of morphogenesis 1 (DAAM1) (Rodriguez-Hernandez et al., 2020). This leads to the activation of Rho-ROCK1/2-Myosin II and regulates tumor-initiating potential, local invasion, and distant metastasis formation.

Wnt-11 has been found to be induced by hypoxia, and is a direct target of HIF-1α in many cancer types, including breast, glioma and cervical cancers, where it leads to increased cell migration and invasion (Mori et al., 2016). Wnt-11 can also be a target of the early growth response 1 (EGR1), acting downstream of tumor necrosis factor-alpha (TNF-α) in breast cancer cells (Kim et al., 2020).

However, in other settings, Wnt-11 has been found to have opposite effects. In hepatocellular carcinoma it inhibits cell proliferation and migration (Toyama et al., 2010). In this context, Wnt-11 promotes PKC and ROCK activation, which counter-acts both the proliferative effect of β-catenin-dependent signaling and the pro-migratory effect of Rac1. Similarly, in ovarian cancer, Wnt-11 has been reported to inhibit tumorigenesis and metastasis by altering integrin and cadherin expression in sphere cultures (Azimian-Zavareh, Hossein, Ebrahimi, & Dehghani-Ghobadi, 2018).

Interestingly, Wnt-11 and Wnt-5a have been studied as potential biomarkers of acute respiratory distress syndrome for severe acute respiratory syndrome coronavirus 2 (SARS-CoV-2) patients (E. Y. Choi et al., 2020). This study found elevated Wnt-11 levels in plasma from COVID-19 patients and indicated that Wnt-11 might be a good indicator for disease survival, likely through the regulation of the inflammatory response. In fact, other studies have pointed to a role of noncanonical Wnt in the function of certain blood cells, with circulating Wnt ligands secreted by leukocytes promoting erythrocyte survival (Siman-Tov et al., 2021). Manipulation of the Wnt pathway has been proposed to improve *ex vivo* storage and transfusion of red blood cells (RBC) (Terenzi, Verma, & Hess, 2021).

6.2.1. Wnt-11 in prostate cancer

In the context of prostate cancer, Wnt-11 is known to promote neuroendocrine-like differentiation, survival and migration of prostate cancer cells (Uysal-Onganer et al., 2010). Wnt-11 has been reported to be elevated in high grade prostate tumors and metastases, and its expression is also activated upon androgen depletion in prostate cancer cell lines *in vitro* (H. Zhu et al., 2004). In patients, *WNT11* mRNA expression is also found increased after ADT (Volante et al., 2016) (Figure 12b). Wnt-11 has been reported to be upregulated by the transcription factor ERG in prostate tumors bearing TMPRSS2-ERG gene fusions (Wu et al., 2013), which was also reported before to occur in certain leukemia models that overexpress ERG (Mochmann et al., 2011). Noncanonical Wnt signaling has been implicated in antiandrogen resistance following analysis of RNA-Seq data from single prostate circulating

tumor cells (CTCs) (Miyamoto et al., 2015). In this study it was further shown that exogenous expression of noncanonical Wnt ligands, including Wnt-5a and Wnt-11, enhanced survival of LNCaP cells in the presence of enzalutamide.

Wnt-11 has been reported to signal through FZD8 in prostate cancer, where FZD8 potentiates Wnt-11-mediated activation of ATF2-dependent transcription (Murillo-Garzón et al., 2018). The expression levels of FZD8 correlate with those of Wnt-11 in prostate cancer patient samples (Figure 12a shows Wnt-11 increased expression in prostate cancer compared to benign prostate). This study also found that *FZD8* gene silencing reduces prostate cancer cell migration, invasion, three-dimensional (3D) organotypic cell growth, expression of EMT-related genes, and TGF-β/Smad-dependent signaling. FZD8 was therefore proposed to integrate Wnt-11 and TGF-β signals to promote EMT, where mechanistically FZD8 forms a TGF-β-regulated complex with TGF-β receptors 1 and 2. In addition, high *WNT11* gene expression was shown to correlate with biochemical recurrence (Figure 12c), which agrees with an independent database analysis that shows an association with poorer disease-free survival (Figure 12d). Recently, miR-21 was proposed to act in coordination with Wnt-11 in the regulation of EMT processes in prostate cancer cells (Arisan et al., 2020).

Taken together, these studies support the case for investigating Wnt-11 as a potential therapeutic target in advanced prostate cancer and for examining Wnt-11-specific inhibitors that could be of use in the treatment of this disease as, currently, none are available.

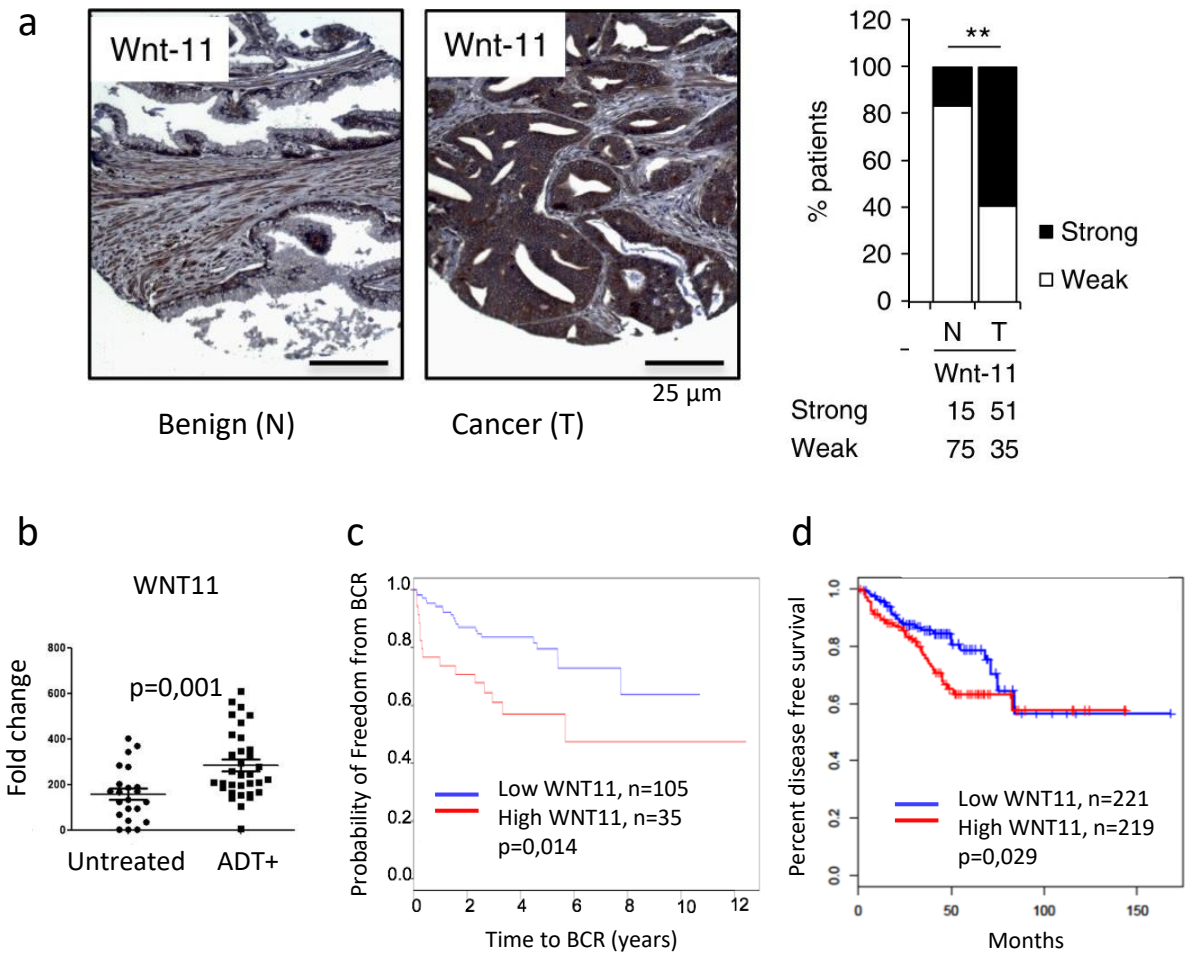

Figure 12. Wnt-11 in prostate cancer. A) Immunohistochemical staining of Wnt-11 in adjacent sections of prostate cancer (Gleason 4+ 3) and matched benign prostate (left) and stratification of Wnt-11 expression in cancer (T) and benign (N) specimens in epithelia (right, **p < 0.001 by Pearson Chi-square test with correction); adapted from Murillo-Garzón et al., 2018. B) WNT11 mRNA expression levels in prostate cancer tissue from untreated patients and from patients treated with ADT before prostatectomy (ADT+), adapted from Volante et al., 2016. C) Biochemical recurrence (BCR) analysis based on *WNT11* expression in the MSKCC dataset, determined using CamcAPP (by Recursive partitioning); adapted from Murillo-Garzón et al., 2018 **(**Suppl. Fig. 8b). D) Disease free survival analysis based on *WNT11* expression using Gepia webtool survival analysis, in PRAD dataset, high cut-off=55%, low cut-off=45%, p(Logrank) indicated (Tang et al., 2017).

Hypothesis and aims

The hypothesis for conceiving this study was based on previous work carried out in Dr. Kypta's laboratory, which indicated that Wnt-11 may be a suitable therapeutic target in advanced prostate cancer and that anti-Wnt-11 antibodies generated *in house* could be of use in blocking aberrant Wnt-11 signaling. In addition, we hypothesized that these Wnt-11 antibodies conjugated to magnetic nanoparticles would retain function-blocking capacity and improve their characteristics for potential use in therapy.

For these purposes, the following aims were enunciated:

1. Determine the effects of anti-Wnt-11 antibodies and magnetic nanoparticle conjugates in prostate cancer cell models *in vitro* and *in vivo*

2. Explore the mechanism of action by which the anti-Wnt-11 antibodies block Wnt-11 signaling and function

Materials and methods

1. Reagents

1.1. Anti-Wnt antibodies, recombinant proteins, peptides, and drugs

Monoclonal anti-Wnt-11 antibodies E8 and F10 were generated by immunizing rats with a mixture of peptides derived from human Wnt-11. After preliminary screening, anti-Wnt-11-E8 (E8) and anti-Wnt-11-F10 (F10) antibodies were selected (Figure 13a). The antibodies were produced in bulk and purified from respective hybridoma cells by Davids Biotechnology GmbH and provided in PBS at a concentration of 0.7 mg/ml. Isotypes of antibodies were determined to be IgG2a for E8 and IgG2c for F10. As control, purified rat IgG (Sigma I4131) in PBS at 0.7 mg/ml concentration was used. Antibodies were tested *in vitro* at a final concentration 2-20 µg/ml. Wnt-11 peptides for the immunization, selection and testing of the anti-Wnt-11 antibodies were purchased from Genescript. Dot blot analysis identified the same peptide as being the epitope for both antibodies, located within Wnt-11 amino acids L101-A112 (LLDLERGTRESA, Figure 13b). E8 recognition of the Wnt-11 epitope in peptide-ELISA assay is shown in Figure 13c.

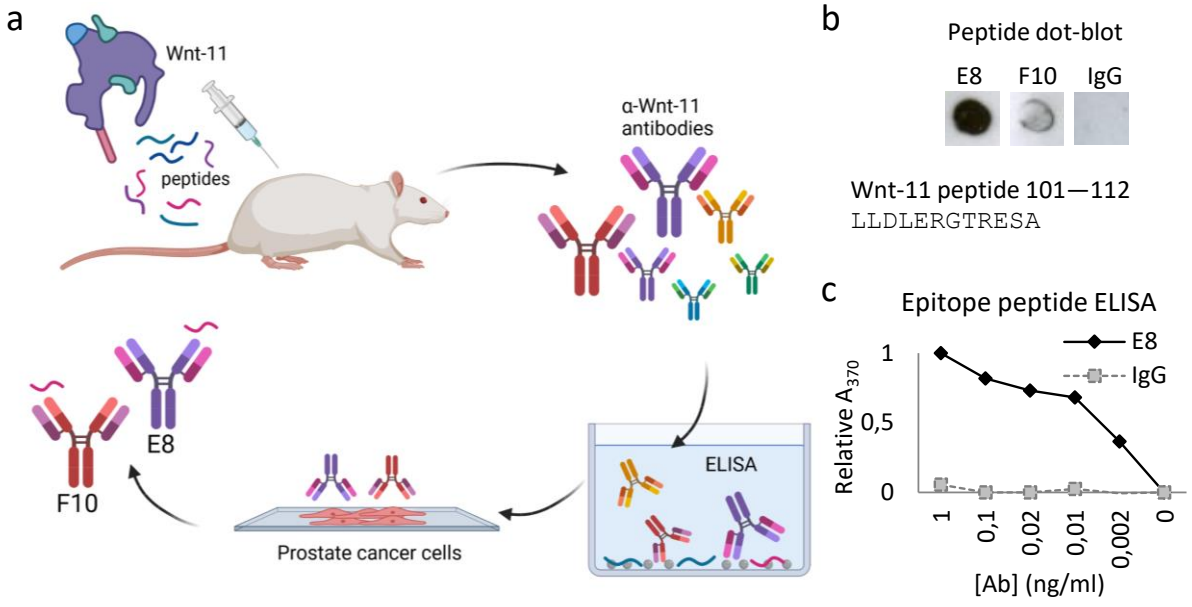

Figure 13. Generation of anti-Wnt-11 antibodies E8 and F10. A) Scheme for the generation of anti-Wnt-11 antibodies E8 and F10 in rat, screened against peptides by ELISA and selected based on recognition of prostate cancer cells. B) Peptide dot blot showing the recognition by E8 and F10 of Wnt-11 peptide L101-A112, sequence indicated in figure. C) Peptide ELISA of E8 recognition above background of non-targeting control rat IgG, at the different concentrations tested. A_{370} – Absorbance 370 nm, ELISA – Enzyme Linked ImmunoSorbent Assay. See Peptide ELISA, page 89 for experimental details.

Human Wnt recombinant proteins were purchased from R&D systems, Biotechne (Wnt-11: 6179-WN-010, Wnt-3a: 5036-WN-010). Porcupine inhibitor Wnt-C59 was purchased from Millipore Merck (Porcn Inhibitor II, Wnt-C59 - CAS 1243243-89-1, Calbiochem) and was used at 100 nM. Dimethyloxaloylglycine, DMOG (CalbioChem, 400091) was used at 1 mM – 0.2 mM. When applicable carrier controls (i.e., Dimethyl sulfoxide (DMSO)) were added at the same dilution in parallel.

1.2. MNP functionalization

Magnetic nanoparticles (MNPs) used in this study were superparamagnetic iron oxide nanoparticles (SPIONs) nanomag®-D-spio with the following surface functionalities COOH (Micromod, 79-02-201) or (Polyethylene glycol) PEG-COOH (Micromod, 79-56-201). Functionalization of MNPs was carried out at CIC biomaGUNE assisted by Antonio Aires, PhD, following two different methods for covalent immobilization.

For the conjugation using the sulfo-SMCC linker (ProteoChem c1109), 5 ml of MNPs at 2.5 mg Fe/ml were pre-activated by incubating overnight at 37 °C with 50 µmol of cysteamine hydrochloride per g Fe (previously neutralized by 1 molar equivalent of sodium hydroxide (NaOH)), 150 µmol/g Fe of 1-Ethyl-3-(3-dimethylaminopropyl) carbodiimide (EDC) and 100 µmol/g Fe of n-hydroxysuccinimide (NHS). After 16 h, the sample was washed by centrifugation and redispersion in Milli-Q water 3 times. For the conjugation, 150 µg of anti-Wnt-11 antibodies E8, F10, and rat IgG control per ml of MNP were used at 0.7 mg/ml in PBS. Antibodies were incubated with a 40 molar equivalents solution of Sulfosuccinimidyl-4-(N-maleimidomethyl) cyclohexane-1-carboxylate (Sulfo-SMCC) linker (ProteoChem c1109) for 30-40 min at room temperature (RT). After that, the modified antibody was purified by gel filtration through a desalting resin PD-10 (Sephadex G-25, Sigma). Activated MNPs were concentrated by centrifugation through 10 kDa cut-off Amicon filters (Merck-Millipore) and correspondent amounts were incubated with the SMCC modified antibodies at RT overnight.

For the thiol-maleimide immobilization, 5 ml of MNPs at 2.5 mg Fe/ml were pre-activated by incubating 4 h at 37 °C with 250 µmol/g Fe of N-(2-Aminoethyl) maleimide, 500 µmol/g Fe of EDC and 500 µmol/g Fe of NHS. Antibodies diluted in HEPES (4-(2-hydroxyethyl)-1-piperazineethanesulfonic acid) buffer pH 8.3 were activated with 50 molar equivalents solution of 2-Iminothiolane, also known as Traut's reagent, for 2 h at RT. After removal of excess reactants, activated antibodies and MNPs were incubated together for 2 h at room temperature

and further incubated overnight at 10°C. Free maleimide groups were blocked with 250 µmol/g Fe of cysteine for 2 h at RT.

After both conjugation procedures, the MNP-antibody conjugates were purified by gel filtration through a sephacryl S200HR (Sigma) column by elution in PBS. Finally, MNPs were washed several times with PBS and stored at 4 °C. They were tested within 1-month of conjugation, which is the estimated time the nanoformulations remain stable. A graphic scheme of the sulfo-SMCC conjugation is presented in Figure 14.

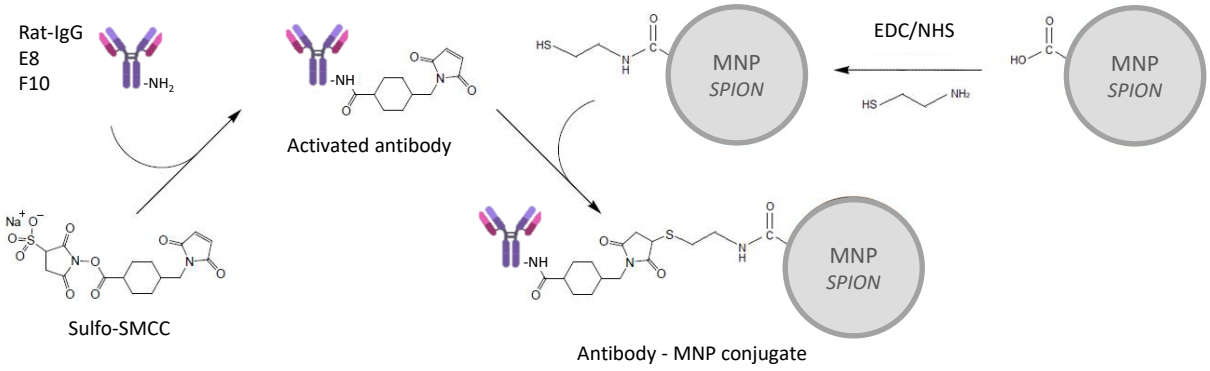

Figure 14. Scheme for MNP functionalization of anti-Wnt-11 antibodies E8, F10 and rat IgG control using sulfo-SMCC. Sulfo-SMCC was used to covalently link antibodies to ECD/NHS-activated SPIONs to obtain the antibody-MNP conjugates. 1-Ethyl-3-(3-dimethylaminopropyl) carbodiimide (EDC); n-hydroxysuccinimide (NHS); Sulfosuccinimidyl-4-(N-maleimidomethyl) cyclohexane-1-carboxylate (Sulfo-SMCC). Modified from (Trabulo et al., 2017).

For estimating the conjugation efficiency the absorbance of consecutive elution fractions was measured at 280 nm in a NanoDrop ND-1000 spectrophotometer using the extinction coefficient estimated for the Ab sequence (210 000 M^{-1} cm^{-1}). MNP sterilization was carried out by filtration through 0.22 µm Millex-GP filters (Merck-Millipore) and it was followed by sonication for 1 min for redispersion. The final concentration of iron as determined by inductively coupled plasma mass spectrometry (ICP-MS) to be of 2.5 mg Fe/ml in a total of 1-2 ml with approximately 40 µg Ab per mg Fe. A concentration of 0.15-0.2 mg Fe/ml was used in functional assays. Hydrodynamic diameter and zeta potential were determined by dynamic light scattering (DLS) using a Zetasizer Nano-ZS device (Malvern Instruments) from dilute sample suspensions (0.1 mg Fe per ml) in water at pH 7.4. Throughout the course of this work, three independent formulations were generated, with different MNP synthesis batches and slightly different conjugation processes and efficiencies. Their respective characteristics are summarized in Table 1.

Table 1. Characteristics of the MNP-Ab conjugation batches generated. Sulfo-SMCC - Sulfosuccinimidyl-4-(N-maleimidomethyl) cyclohexane-1-carboxylate, SPION - Superparamagnetic iron oxide nanoparticles. PEG - Polyethylene glycol. Cat. No. – Catalog number.

Conjugation			SPIONs	
Batch year	Antibody concentration (µg Ab/ml)	Linker	PEG	Cat. No.
2018	88 -105	Thiol-maleimide	Yes	79-56-201
2020	85 -120	Sulfo-SMCC	No	79-02-201
2021	119 -127	Sulfo-SMCC	Yes	79-56-201

2. Cell culture

2.1. Cell lines

The following cell lines were purchased from the American Type Culture Collection (ATCC): PC3, DU145, VCaP and HEK 293 cells. The following cell lines were kindly received from colleagues: C4-2B from Charlotte Bevan (Imperial College London); PC3M cells from Scott Fraser and Mustafa Djamgoz (Imperial College London). HEK 293T LRP5/6$^{-/-}$ knock-out cells were kindly provided by Benoit Vanhollebeke's laboratory (Eubelen et al., 2018). L-Wnt-3a and control parental cells were purchased from ATCC for conditioned media (CM) production, which was collected according to manufacture's instructions. CM was then centrifuged for 5 min at 400 g and subsequently filtered through 0.22 µm Millex-GP filters (Merck-Millipore), then stored at 4 °C for up to 1 month. For stimulation, CM was used in a 1:1 ratio with fresh media. The parental cell line was used for retrieving control CM in a parallel manner.

Cell lines were cultured from low-passage stocks for up to 6 months, monthly tested for mycoplasma and authenticated by DNA profiling (Eurofins Genomics, Germany). Culture conditions were the standard 37 °C, 5% CO2 in corresponding culture media (Table 2) supplemented with 10% fetal bovine serum (FBS, Gibco) and Pen/Strep antibiotics (100 units/mL penicillin, 100 µg/mL streptomycin, Gibco), this may be referred to as *complete media*. For passaging and seeding, cells were detached using Trypsin (0.25% Gibco), centrifuged (400 g, 5 min) and counted for seeding the pertinent experiments or for stock maintenance. For experiments, HEK 293 cells were plated on 0.01% poly-L-lysine (Sigma) coated plates. For some assays the concentration of the FBS was reduced to 0.5%. For experiments requiring transfection, cells were maintained in OptiMEM (Gibco) for 3-5 h during transfection and then it was changed to complete media. C4-2B cells overexpressing Wnt-11 (C4-2B-WNT11) were produced by transfection with Wnt-11 plasmid and control cells

(C4-2B-V) with pcDNA empty plasmid (see Table 4 for plasmids details) and selection with G418 (Sigma 10131-027), which was kept in culture at 0.4 mg/ml.

Table 2. Cell lines characteristics and culture conditions. Culture media: RPMI (Roswell Park Memorial Institute), DMEM (Dulbecco's modified Eagle's medium) and DMEM F12 (DMEM mixed 1:1 with Ham's F-12). AR - androgen receptor, p53 - cellular tumor antigen p53, PTEN - phosphatase and tensin homolog.

		Prostate cancer cells characteristics	
Cell line	Culture media	Mutations	Androgen dependency
PC3	RPMI	Prostate cancer. AR-; p53 del; PTEN -	No
PC3M	RPMI	Prostate cancer. AR-; p53 del; PTEN -	No
DU145	RPMI	Prostate cancer. AR-; p53 del; PTEN +	No
C4-2B	RPMI	Prostate cancer. AR+; p53 low; PTEN -	No
VCaP	DMEM F12	Prostate cancer. AR+; p53 low; PTEN +; TMPRSS2-ERG fusion +	Yes
HEK 293	DMEM	Embryonic kidney	-

2.2. Cell transfection

Cells were plated in 6, 12 or 24-well plates in complete media to be 60-80% confluent at the time of transfection, see Table 3 for cell density and plasmid transfection conditions per experiment type. Before transfecting, cells were washed in PBS and culture media was changed to OptiMEM (Gibco). After that, DNA/transfection reagent mixture diluted in OptiMEM were added on top for the pertinent duration and then changed back to complete media. The transfection procedures for gene silencing and plasmid transfection are described below.

2.2.1. Gene silencing

Cells were plated to be 60% confluent at the time of transfection, washed in PBS and changed to OptiMEM (Gibco). RNAiMAX (Invitrogen) was used according to manufacturer's instructions. Briefly, both RNAiMAX and siRNA (small interfering RNA), were prediluted in OptiMEM for the subsequent incubation of 5 min 1:1 siRNA: RNAiMAX. siRNAs for *WNT11* silencing (Wnt-11 SMARTpool, Dharmacon L009474-00-0005; sequences 3'-5': GCGCUAUGUCUGCAAGUGA, AACAAGACAUCCAACGGAA, UCAAGUGGCUGGCGCUGUC, CCAAUAAACUGAUGCGUCU) as well as non-targeting siRNA pool control (Dharmacon D-001810-10-20) were used at a final concentration of 50 nM. The mixture was added to the cells for 3-5 h and then complete media was added on top in a 1:1 ratio. Next day media were renewed, and transfected cells were used for experiments. Generally, the extent of silencing was evaluated 48 h after transfection.

2.2.2. Plasmid transfection

For plasmid transfection, Lipofectamine LTX with PLUS reagent (LifeTechnologies) were used following the procedures instructed by the manufacturer. Plasmids were diluted in OptiMEM and mixed with Plus reagent and left incubating for 10 min, see Table 3 for quantities used per type of plate and experiment. LTX reagent was diluted in OptiMEM in a different tube for 5 min. Then, diluted LTX was placed in the Plasmid/Plus tube by mixing in a 1:1 volume ratio and left to incubate for 15 min. The mixture was then placed on top of OptiMEM containing wells for 3-5 h. Transfection agents were subsequently removed, and cells were allowed to recover in complete media for 24-72 h in the case of transient transfections. For stable transfections, the adequate selection antibiotic was added to culture media appropriately 2 days post-transfection until death of the non-transfected control cells and then kept in culture at a lower dose.

Table 3. LTX/Plus plasmid transfection volume and concentrations.

Plate	Experiment type	Cell number ($x10^3$/well)	OptiMEM (ml/well)	DNA (ng/well)	LTX (µl/well)	Plus (µl/well)	Vol (µl/well)
6-well	Immunoprecipitation	200-300	1	1000	3	1	1000
12-well	Gene Reporter	70-100	0.5	500	1.5	0.5	500
24-well	Immunofluorescence	40-60	0.25	250	0.75	0.25	250

The plasmids used in this work are summarized in respective tables containing exogenous expression plasmids (Table 4), table for information on protein tags carried by some exogenous expression plasmids (Table 5) and plasmids used for gene reporter assays (Table 6).

2.2.3. Plasmid mutagenesis

For generation of the antibody epitope deletion mutant (AE) plasmid of Wnt-11 a mutagenesis kit (NE Biolabs, E0554S) was used following manufacturer's instructions. The mutation generated was a deletion of part of the peptide contained in the antibody epitope, shown here underlined and with flanking sequences: APNY/LLDLERGT/RESA and the primers used for the mutation were the following: forward primer 3'-CGGGAGTCGGCCTTCGTG-5'; reverse primer 3'-ATAGTTGGGGGCGAGCTC-5'. After mutagenesis, plasmids were purified, and Sanger sequenced (STABVIDA) prior to their use.

Table 4. Plasmids used for ectopic expression. (h) – human, (m) - mouse. *Tag details are described in Table 5. **AE – Wnt-11 Antibody Epitope mutant (deletion). (FZD8) CRD – cysteine-rich domain, (LRP6)N - N-terminal extracellular domain.

#	Plasmid name	Backbone	Insert	Tag*	Source / Reference
1	pcDNA 3.1	pcDNA	-	-	-
2	Wnt-11	pcDNA	Wnt-11 (h)	-	(Uysal-Onganer et al., 2010)
3	Wnt-3a-PA	pcDNA	Wnt-3a (h)	-	Junichi Takagi (Mihara et al., 2016)
4	Wnt-11-PA	pcDNA	Wnt-11 (h)	PA	Junichi Takagi (Mihara et al., 2016)
5	Wnt-11-V5	pcDNA	Wnt-11 (h)	V5	Marian Waterman, Addgene #35941 (Najdi et al., 2012)
6	AE**	pcDNA	Mutated Wnt-11 (h) from *plasmid 1*	-	*Homemade*, see Plasmid mutagenesis page 76
7	AE-PA	pcDNA	Mutated Wnt-11 (h) from *plasmid 2*	PA	*Homemade*, see Plasmid mutagenesis page 76
8	AE-V5	pcDNA	Mutated Wnt-11 (h) from *plasmid 3*	V5	*Homemade*, see Plasmid mutagenesis page 76
9	pCS2	pCS2	-	-	-
10	LRP6-VSV-G	pCS2	VSV-G	VSV-G	Xi He, Addgene #27282 (Tamai et al., 2004)
11	LRP6N-IgG	pCS2	LRP6N	Fc	Xi He, Addgene #27279 (Tamai et al., 2000)
12	pRK5	pRK5	-	-	-
13	mFZD8-CRD-IgG	pRK5	FZD8-CRD (m)	Fc	Xi He, Addgene #16689 (Semënov et al., 2001)

Table 5. Details of the protein tags carried in some of the exogenous expression plasmids shown in Table 4. Sequence is provided N-terminal to C-terminal in one-letter notation. kDa – kilodalton.

Tag	Protein origin	Sequence	Location
PA	Podoplanin	GVAMPGAEDDVV	Wnt-11; N-terminal
V5	SV5 paramyxovirus	GKPIPNPLLGLDST	Wnt-11; C-terminal
VSV-G	Vesicular Stomatitis Virus (VSV) G	YTDIEMNRLGK	LRP6; N-terminal
Fc	Immunoglobulin constant region of heavy chain	25 kDa	LRP6N; C-terminal mFZD8-CRD; C-terminal

Table 6. Plasmids specific for gene reporter assays. Promoter is provided 5' – 3'. 1x refers to a different plasmid to measure ATF2-dependent transcription that contains 1 copy of the ATF2 promoter instead of the 2 presented in the ATF2-luc. mt5 – mutant 5; luc – luciferase.

Plasmid	Backbone	Transcription factors	Promoter	Source / Reference
ATF2-luc/ 1x	TATATK-LUC	ATF2	ATTGCATCA	Christof Niehrs (Van Der Sanden, Meems, Houweling, Helms, & Vaandrager, 2004)
mt5-luc	TATATK-LUC	Mutated ATF2	ATT---TCA	Pierre Fafournoux (Bruhat et al., 2000)
Super 8XTOP/FOPFlash	pTA-LUC	TCF/LEF; β-catenin	CCTTTGATC	Randall Moon, Addgene #12456 (Veeman et al., 2003)
Renilla tk	pRL-Tk	-	-	Promega

2.2.4. E. coli transformation for plasmid amplification

For plasmid amplification, 50 µl of DH5α competent cells (Life Technologies, 18265017) were transformed with 5-50 ng of plasmid DNA (see plasmids in Table 4 and Table 6) by incubation for 30 min on ice, followed by a heat-shock at 42 °C for 45 sec and subsequent incubation of 2 min on ice. Cells were recovered by adding 450 µl of S.O.C. medium (Invitrogen) and shaken at 225 rpm for 1 h at 37 °C. Bacteria suspension (50 µl) was plated on LB agar plates containing selection antibiotic (e. g., ampicillin at 50 µg/ml) and incubated overnight at 37 °C. Colonies were picked using a pipette tip, placed into a conical flask with 400 ml LB media with antibiotic and grown overnight at 37 °C, 225 rpm. Plasmid DNA was purified using a PureLink™ HiPure Plasmid Maxiprep Kit (Invitrogen) according to manufacturer's instructions. Final DNA was resuspended in TE buffer (10 mM Tris·Cl, pH 8.0 1 mM EDTA), the concentration was determined using a NanoDrop ND-1000 spectrophotometer, aliquoted and stored frozen at -20 °C.

2.3. Lentiviral transduction

For the generation of PC3-GFP (green fluorescent protein) expressing cells, PC3 cells (referred to as target cells here) were transduced with lentiviral particles produced according to the following protocol performed in a Biosafety level 2 laboratory (BSL2). A 10 cm plate with 2 million HEK 293FT packaging cells per condition were transfected overnight using the calcium phosphate method. Briefly: a premix with 3rd generation lentiviral plasmids (Table 7) diluted with 50 µl of 2.5 M calcium chloride ($CaCl_2$) in a final volume of 500 µl of H_2O, was mixed with 500 µl of 2X HEPES-buffered solution (HBS; 50 mM HEPES, 280 mM NaCl, 10 mM KCl, 1.5 mM $Na_2HPO_4.2H_2O$, 12 mM dextrose, pH 7.05). The mixture was incubated for 30 min air-exposed, to favor the formation of the oxygen-dependent calcium phosphate crystals, before addition to the cells. 16 h later, the medium was changed to that of the target cells medium. 24 h later, the conditioned media from HEK 293FT cells containing lentiviral particles was filtered through a 0.45 µm filter and added to target cells in a 4:1 ratio with fresh complete media. Protamine sulfate was added at a final concentration of 1 µg/mL to increase transduction efficiency. HEK 293FT media were renewed and the next day the same operation was performed (2 rounds of transduction). Target cells were then cultured for 5-7 days with daily washing in PBS and passaging when appropriate (for lentiviral particle clearance) before FACS-sorting cells positive/high for the expression of GFP. Cells were then replated and

cultured in a BSL2 for a minimum of 1 additional week, before transfer to a Biosafety level 1 laboratory for experiments.

Table 7. Plasmids used for lentiviral transduction. Plasmid amounts are provided for calcium phosphate transfection of a 10 cm plate of HEK 293FT cells.

Plasmid	Function (genes)	Plasmid (µg)	Source
pREE	Packaging (Gag and Pol)	8	James D. Sutherland, Addgene #12251 (Dull et al., 1998)
pRSV-Rev	Packaging (Rev)	4	James D. Sutherland, Addgene #12253 (Dull et al., 1998)
VSV-G	Envelope	2	James D. Sutherland, Addgene #1733
pCLX-UBI-GFP	Transfer plasmid	4	Patrick Salmon, Addgene #27245

2.4. Proliferation assay

For proliferation assays, cells were seeded in quadruplicate in 24-well plates at 1 000-5 000 cells/well and cultured for 5-7 days, feeding every 2-3 days with treatments where relevant. Antibodies tested (see page 71) were used at 5-20 µg/ml and MNP conjugates at 0.2 mg Fe/ml. At endpoint, cells were washed in PBS and fixed/stained for 10-20 min with crystal violet solution (PBS containing 0.1% methyl violet 10B (Sigma C6158), 20% methanol, 0.36% paraformaldehyde (PFA)). Then, cells were washed repeatedly in PBS until the solutions were running clear. Plates were dried at room temperature overnight. Crystal violet stain was solubilized using 10% acetic acid for 10-30 min. 50-100 µl of the solution was then transferred to a 96-well transparent plate for absorbance measurement at 595 nm. Absorbance values are presented relative to the internal control condition.

2.5. Sphere assay

Cells were detached using TrypLE (1x, Gibco) and then seeded in either ultra-low attachment 24-well (Corning) in quadruplicate at 500 – 1 000 cells/well for sphere counting assays or on poly (2-hydroxyethyl methacrylate) (pHEMA)-coated (Sigma) T75 flasks (Corning) at 10 000 cells/ml for protein and RNA analyses. Sphere medium consisted of serum-free DMEM: F12 supplemented with B27 (Invitrogen), 20 ng/mL EGF (Epithelial Growth Factor, Life Technologies), 20 ng/mL bFGF (basic fibroblast growth factor, BD Biosciences) and 1% Pen/Strep (100 units/mL penicillin, 100 µg/mL streptomycin, Invitrogen, UK). Antibodies tested (see page 71) were used at 20 µg/ml. Cells were cultured undisturbed for 5-7 days. At endpoint spheres were either retrieved for protein and RNA extractions or counted

manually under a microscope using a 10X magnification lens and sphere numbers are presented relative to the control condition.

2.6. Transwell cell migration and invasion

Cells were detached with TrypLE (1x, Gibco) and resuspended in corresponding growth media containing 0.5% FBS. 10 000-50 000 cells were seeded in a volume of 500 µl/well in the upper chamber of an insert with an 8 µm pore polycarbonate membrane (Falcon Corning 353097) for migration assays and a Matrigel-coated membrane for invasion assays (Corning 354480). Antibodies tested (see page 71) were used at 2-20 µg/ml and added to the upper chamber, only considering its volume. Inserts were placed each into a well of a 24-well plate filled with 600 µl of 20% FBS containing media (bottom chamber) for producing an FBS gradient for cells to migrate or invade toward. A proliferation control was seeded in parallel with the suspension of cells prepared for the upper chamber in triplicate in 24-well plates. Migration and invasion assays were carried out in triplicate and left to migrate or invade for 24 or 48 h, respectively.

At endpoint, inserts were processed for counting the migrating/invading cells located at the bottom of the inserts. Non-migrating/invading cells on top of the filters were removed by rubbing with a cotton swab. After PBS washes, inserts were placed in crystal violet containing vessels to fix and stain remaining cells. After repeated PBS washes, migrating/invading cells were imaged under a microscope using a 10X magnification lens by taking 5 pictures in predetermined fields for manual or automated cell counting. The control plate was processed at the same time following the proliferation assay protocol described in page 79. Cell counts per well were then averaged for each replicate and relative numbers to the control condition are presented. Migrating/invading cell numbers were normalized for proliferation or presented with the proliferation control numbers in a parallel graph. For automated counting ImageJ was used, see page 97 for details.

For migration assays of cells in hypoxic condition, a similar protocol to that described in Mori et al., 2016 was used. Cells were pretreated for 24 h with 0.2 mM DMOG (dimethyloxaloylglycine), then detached and plated in migration inserts with media containing the tested antibodies (see page 71) at 2-20 µg/ml. The plate was then transferred to a humidified hypoxia workstation (InvivO2 400, Ruskin) at 1% O_2 and 5% CO_2, balanced with nitrogen, and the cells were then allowed to migrate for 16 h.

2.7. Wound healing assay (Cell migration)

Cells were plated in 6-well plates at high-density in complete media. Once attached, >80% confluent cells were partially starved overnight in medium containing 2-5% FBS. Confluent cells were then scratched twice per well using a 200 µl pipette tip and media were subsequently renewed with 2-5% FBS media containing treatments where relevant, antibodies at 10 µg/ml and MNP conjugates at 0.2 mg Fe/ml (see page 71). For gene silencing experiments, cells were transfected with siRNA 48 h prior to scratching. Wounds were imaged at time 0 h in 6 predetermined marked locations and then allowed to migrate to close the wound, which was surveyed for 8-30 h. When appropriate (mid- or endpoint), wounds were imaged in the same predetermined locations. Images were processed using ImageJ for determination of wound closure (see page 97 for ImageJ method). Data are presented relative to the control condition or relative to complete closure.

2.8. Gene reporter assay

Cells were plated in 12-well plates in triplicate and subjected to transfection (see page 75 for method), generally using 250 ng luciferase containing plasmid, 100 ng overexpression plasmids and 10 ng of renilla plasmid (see Table 6). When using various exogenous expression plasmids, they were added in equivalent ratios (adding up to 100 ng), unless stated otherwise. For the experiments presented in Figure 56, page 158) the amounts of plasmids transfected per well was the following: 10 ng renilla, 50 ng ATF2-luc, 100 ng FZD8 (1D4, full length), 100 ng LRP6 (VSV-G, full length), 200 ng of Wnt-11 or AE (untag). Treatments, where pertinent, were added 3-5 h post-transfection at the time of the change to complete media. For Wnt-3a stimulation, the conditioned media (CM) collected from L-Wnt-3a cells and control parental cells (see page 74 for details) were added 3-5 h post-transfection at the time of the media change, in a 1:1 dilution with fresh complete media.

Gene reporter experiments were analyzed 24 h post transfection. Cells were washed in PBS and lysed using 130 µl/well of Passive Lysis Buffer (Promega). Plates were shaken for 10 min at RT followed by incubation at -80 °C for a minimum of 20 min for improved lysis. Lysates were collected in Eppendorf tubes and centrifuged 5 min at 15 000 g. The Dual Glo Luciferase Assay System (Promega) was used for weak luciferase signal, and the Luciferase Assay Kit (PJK, Germany) was used when higher signal was expected; both kits were used according to manufacturer's instructions. Briefly, for Dual Glo assays, 50 µl/well of lysate was transferred

to white luminometer plates (PerkinElmer), mixed with 50 µl/well of luciferase reagent and incubated for 10 min prior to light measurement (luciferase signal) using a Veritas microplate luminometer (Turner biosystems). Measurements were saved and 50 µl/well of renilla substrate diluted 1:100 in corresponding buffer was added on top and left to incubate for 10 min before re-measuring light (renilla signal). Similarly, for the PJK kit, 30µl of lysate was mixed with 80 µl of PJK luciferase reagent and, independently, 25 µl of lysate was mixed with 25 µl of 1:50 diluted renilla substrate; plates were incubated at RT for 10 min and light intensity measured. In both cases, gene reporter activities were calculated as the luciferase:renilla ratio, triplicates were averaged and normalized to the internal control condition. Data correspond to at least 3 independent experiments.

3. mRNA analysis

3.1. RNA extraction

For analysis of gene expression, messenger RNA (mRNA) was evaluated 48 h post-treatment unless stated otherwise. Total RNA purification from 6-well or 12-well plated cells was performed using the NucleoSpin RNA (Macherey-Nagel GmbH, 740955-250) following the manufacturer's instructions. Briefly, cells were lysed in RA-1 buffer containing 1% β-mercapthoethanol (Sigma). Lysates were pass through a column to reduce viscosity, the flow-through was mixed 1:1 with EtOH 70% and transferred to RNA purification columns. On column DNAse treatment was performed for degradation of interfering genomic DNA. Several washes with EtOH-containing buffers were performed prior to the final elution of RNA from the column with 25-35 µl RNAse free H_2O. Samples were thereafter maintained on ice. RNA concentration and quality parameters were measured using a NanoDrop ND-1000 spectrophotometer, by absorbance determination at 230/260/280nm. Purified RNA samples were immediately stored at -80 °C or subjected to retro-transcription reaction.

3.2. Retro-transcription reaction

Equal amounts of total RNA from experimental samples (generally 2 µg), were retro-transcribed into complementary DNA (cDNA) using the reagents and concentrations shown in Table 8. The retro-transcription reaction was then carried out in a thermocycler for 1 h at 37 °C followed by 5 min at 95 °C for inactivation of the enzyme. cDNA was then immediately used for Real-Time Quantitative PCR (RT-PCR) or stored at -20 °C.

Table 8. Volumes and concentrations of reagents for retro-transcription reactions. A mix was prepared for each RNA sample to be retro-transcribed with the reagents indicated.

		Concentration		
Reagent	Company	Stock	Final	Volume (µl)
Random Primers	Life Technologies	100 ng/µl	5 ng/µl	2
dNTP mix	Bioline	10 mM (2.5 mM each)	1 mM (0.25 mM each)	4
5X First strand buffer	Invitrogen	5X	1X	8
DTT	Invitrogen	100 mM	5 mM	2
M-MLV	Life Technologies	200 U/µl	5 U/µl	1
RNAseOUT	Life Technologies	400 U/µl	1 U/µl	1
RNA (diluted in H_20)	-		2 µg	22
Total				40

3.3. Real-Time quantitative PCR (RT-PCR)

Real time (RT) quantitative, polymerase chain reaction (PCR) was performed using a mixture of PerfeCTa SYBR® Green Supermix, Low Rox (Quanta, Spain), primers (Table 9 for sequences and concentrations) and the corresponding cDNA (1 µl/well) in experimental triplicates in 384-well RT-PCR plates (LifeTechnologies, 4309849) in a total volume of 6 µl/well. RT-PCR reactions were carried out in a Viia7 Real-Time PCR System (Applied Biosystems, Madrid, Spain) with the following protocol: 95 °C for 3 min (Taq polymerase activation), 40 cycles of 95 °C for 15 sec (denaturation cDNA) and 62 °C for 1 min (annealing of primers and extension); with standard melting curve step added at the end. Amplification curves were visualized using Viia7 software to verify the quality of the data (the absence of primer dimers and/or genomic DNA contamination) and data were exported for analysis. Relative levels of mRNA were determined using the ΔΔCT quantification method (Livak & Schmittgen, 2001), relative to the expression of *36B4* (a housekeeping gene).

3.4. Primer design and sequences

The design of forward and reverse primers for RT-PCR was performed with the help of the Primer-BLAST tool (https://www.ncbi.nlm.nih.gov/tools/primer-blast/). For obtaining highly efficient RT-PCR primers for each gene, the search parameters were set as follows: length of 80-150 base-pairs (bp), when possible primers located in different exons (to avoid genomic DNA amplification), melting temperature of 60-63 °C (with the lowest possible difference in between *forward* and *reverse* primers), Guanine-cytosine content (GC) of 30-55% and minimum self-complementarity. Obtained primers were ordered from Life Technologies and subjected to optimization for the determination of the appropriate concentration to be used for

RT-PCR (300, 600 or 900 nM final concentration) with a serial-diluted set of cDNA samples. The list of primer sequences and concentrations is provided in Table 9.

Table 9. Details of primers used for RT-PCR. F - forward primer, R - reverse primer; concentration refers to final in the RT-PCR reaction mix. Note: for *WNT11* no-CDS (located in the non-coding sequence) primers were used for detection of endogenous *WNT11* and CDS (located in the coding sequence) primers for detection of both endogenous and exogenous *WNT11*.

Gene	F/R	Sequence	Concentration	Amplicon size
36B4	F	GTGTTCGACAATGGCAGCAT	300	103
36B4	R	AGACACTGGCAACATTGCGGA	300	
LRP6	F	TGAGGGTCTGCGTGAAATCC	300	120
LRP6	R	TGGGAACAACCCCCATTGTC	300	
FZD8	F	GCTCTACAACCGCGTCAAGA	900	70
FZD8	R	GCTGAAAAAGGGGTTGTGGC	900	
WNT11 CDS	F	TGAAGGACTCGGAACTCGTC	600	119
WNT11 CDS	R	GTCGCTTCCGTTGGATGTCT	600	
WNT11 no-CDS	F	CTCCTCCTGGGTGTGACC	600	175
WNT11 no-CDS	R	CAGTGTTGCGTCTGGTTCAG	600	
AXIN2	F	AAGTGCAAACTTTCGCCAAC	300	122
AXIN2	R	ACAGGATCGCTCCTCTTGAA	300	
NKD1	F	ACTTCCAGCCGAAAGTCGT	900	90
NKD1	R	CACCATAGGCCGAAGCAC	900	
LEF1	F	AGCACGGAAAGAAAGACAGC	300	92
LEF1	R	TCGTTTTCCACCTGATGCAGA	300	
DKK1	F	ATGCGTCACGCTATGTGCT	900	147
DKK1	R	TCTGGAATACCCATCCAAGG	900	
ATF2	F	GATGTGGGCTGTGCAGTTTG	300	72
ATF2	R	AGTCCTTTACCTCACCCAGAGT	300	
HIF2A	F	GTCACCAGAACTTGTGC	600	249
HIF2A	R	CAAAGATGCTGTTCATGG	900	
DVL2	F	GCCCACTTTCTCCTACCAATACC	600	129
DVL2	R	CTCCGGCTGCCCTCACT	600	
SOX2	F	TGCTGCGAGTAGGACATGCTGTAGG	900	207
SOX2	R	GCACATGAACGGCTGGAGCAACG	900	

4. Fluorescence activated cell sorting (FACS)

For experiments involving protein analysis after FACS sorting, HEK 293 cells were transfected with Wnt-11 and antibody epitope mutant (AE) plasmids. 24 h later, cells were detached with TrypLE (1x, Gibco) and pipetted onto 96-well V-shaped bottom plates for in-well staining. Cells were fixed in PBS/4% PFA (Santa Cruz) for 15 min, washed in PBS and permeabilized for 10 min at room temperature in 0.3% saponin (Sigma, 57900-25G). After 3 PBS washes, cells were blocked in 40% FBS in PBS for 30 min. Cells were then incubated with primary antibodies (E8 and rat anti-Wnt-11 (R&D MAB3746), see Table 11) diluted in 1% bovine serum albumin (BSA, Sigma)/PBS for 30 min at 4 °C. After 3 PBS washes, cells were incubated for 30 min in the dark with secondary antibodies diluted 1:5 000 in 1% BSA/PBS (anti-rat AlexaFluor647, Life Technologies). Cells were washed 3 times in PBS and transferred to 5 ml tubes prior to FACS sorting in a FACSAria cytometer with FACSDiva software. Gates for the top and bottom 10-20% staining intensities were set and those cells presenting high and low (+/-) staining were collected. Approximately 100 000-200 000 cells were retrieved for each condition and were then processed for protein analysis by western blot by directly lysing in preheated Laemmli buffer followed by incubation at 95 °C for 5 min (see page 87). Bulk, unsorted cells were also retrieved and processed in parallel as control for the transient overexpression. A scheme of the experiment is presented in Figure 15.

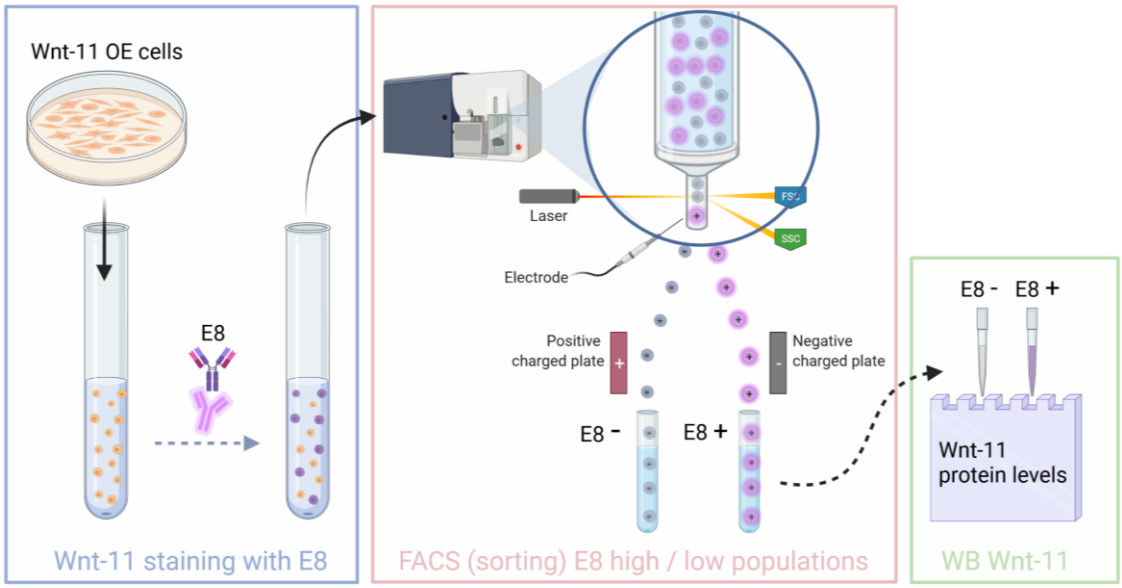

Figure 15. Scheme of protein analysis of FACS sorted cells. HEK 293 cells transfected for the expression of Wnt-11 (or AE, mutant) were stained for E8 (and R&D rat anti-Wnt-11) and sorted for high (+) and low (-) intensity signal. Cells were then lysed, and total protein was analyzed by western blot (WB) to evaluate Wnt-11 expression levels. OE -Overexpression, FACS - Fluorescence activated cell sorting.

5. Protein analysis

5.1. Protein extraction

Total cell extracts were retrieved using the following procedure. Cell lysis was performed on ice for 10-15 min using RIPA buffer (50 mM Tris-HCl pH 7.4, 150 mM NaCl, 0.25% deoxycholic acid, 1% NP-40, 1 mM Ethylenediaminetetraacetic acid (EDTA, Millipore)) supplemented with 0.1% sodium dodecyl sulfate (SDS) (Life Technologies), 1x cOmplete™ Mini EDTA-free Protease Inhibitor Cocktail (Roche) and 1x PhosSTOP Phosphatase Inhibitor Cocktail Tablets (Roche). Lysates were transferred to chilled Eppendorf tubes for centrifugation at 15 000 g for 10-15 min at 4 °C. Pellets were discarded and supernatants collected for storage at -80 °C or directly mixed 1:1 with 2x Laemmli buffer (Sigma). Laemmli containing protein extracts were incubated at 95 °C for 5-10 min in a Thermomixer compact (Eppendorf) and loaded on SDS-polyacrylamide gels for western blots. For experiments involving protein analysis, extracts were generally obtained 2-48 h post-treatment.

For recombinant protein western blot, 200 ng of protein per lane was added diluted in PBS and mixed directly with 2x Laemmli. Mixtures were incubated at 95 °C for 3 min and loaded on SDS-polyacrylamide gels.

5.2. Western blot (WB)

SDS-PAGE (sodium dodecyl sulfate-polyacrylamide gel electrophoresis) was performed by loading the protein extracts onto homemade SDS-polyacrylamide gels, using 6% or 8% resolving solution topped with a 5% stacking solution (Table 10). 6% polyacrylamide gels were specifically used for DVL shift assays. In a parallel lane, protein marker (PageRulerTM Plus Prestained Protein Ladder, Thermo Scientific, 250-10 kDa) was loaded and gels were run using a Mini Protean System (BioRad) at 15 mA/gel for 1.5-2 h. In some cases, the protein content of the polyacrylamide gel was stained using Coomassie Brilliant blue G 250 (Sigma) 0.25% (w/v) diluted in 50% EtOH and 10% acetic acid for 1 h at RT, followed by destaining in 30% EtOH, 10% acetic acid, 60% H_2O until protein bands were clear.

Table 10. SDS-polyacrylamide gel information. Numbers indicate the volume (ml) needed for a 1 mm thickness gel. ddH_2O – double distilled water. Tris – Tris (hydro methyl) aminomethane.

		Volume for 1 mm polyacrylamide gel (ml)		
Reagent	Company	Resolving 8%	Resolving 6%	Stacking 5%
ddH_2O	Gibco	2.3	2.6	1.7
30% Acrylamide Bisacrylamide	Sigma	1.3	1	0.42
1.5M Tris HCl (pH 8.8)	Homemade	1.3	1.3	
1.5M Tris HCl (pH 6.8)	Homemade			0.32
Sodium dodecyl sulfate (SDS) 10%	Gibco	0.05	0.05	0.02
Ammonium persulfate (APS) 10%	Sigma	0.05	0.05	0.01
Tetramethylethylenediamine (TEMED)	Sigma	0.003	0.004	0.003

The protein content of the polyacrylamide gels was then transferred to 0.22 μm pore nitrocellulose membranes (Millipore) using a Semi-Dry Transfer Cell (10 V for 30-40 min) or a Trans-Blot® Turbo™ Transfer System (Bio-Rad, Turbo or High Molecular weight setting: 1.3 A constant, up to 25 V per gel during 7-10 min) with Bio-Rad transfer buffer containing 20% EtOH. If pertinent, protein loading was confirmed by Ponceau-S staining (0.01% Ponceau-S Sigma P3504; 0.1% acetic acid) of the membranes for 2 min followed by repeated washings in TBS-T (Tris (hydro methyl) aminomethane-buffered saline 0.05% Tween20) until the membrane was cleared.

Membranes were blocked for 30-60 min in TBS-T containing 3% BSA (Bovine serum albumin, Sigma) buffer. For blotting, membranes were incubated overnight at 4 °C with primary antibodies diluted in blocking buffer (see Table 11). After 5 washes of 5-10 min in TBS-T, membranes were incubated with HRP-conjugated secondary antibodies diluted in blocking buffer (1:20 000; Jackson ImmunoResearch: α-rat 712-035-153, α-rabbit 711-036-152, α-mouse 715-035-151, α-goat 705-035-147). Membranes were washed 5 times for 5-10 min in TBS-T, before developing using Immobilon Forte (Millipore WBLUF0100) in a developer (AGFA, Curix 60) or imaged using an iBright™ FL1500 Imaging System (Thermo).

5.3. Primary antibodies

For protein analysis assays the following antibodies were used at the concentrations indicated for each type of assay (Table 11). HSP60, GAPDH or Vinculin were used as protein loading controls.

Table 11. List of primary antibodies and experimental details. Working final dilutions are provided for each assay: WB – western blot; IF – Immunofluorescence; FACS - Fluorescence activated cell sorting; IHC – Immunohistochemistry. *Fc - detection of Fc-tagged proteins was done by direct incubation with a secondary anti-human antibody.

				Working dilutions			
Antibody	Company	Reference	Species	WB	IF	FACS	IHC
DVL2	Santa Cruz	SC-13974	Rabbit	1:1000			
DVL3	Santa Cruz	SC-8027	Mouse	1:500			
Fc* (secondary anti-human)	GenScript	A00166	Goat	1:10000			
GAPDH	Santa Cruz	SC-47724	Mouse	1:5000			
HIF-1α	Novus Biological	NB100-479	Rabbit	1:1000			
HIF-2α	Novus Biological	NB100-122	Rabbit	1:1000			
HSP60	Santa Cruz	sc-13966	Rabbit	1:1000			
Ki67	GenomeMe (GeneAb™)	IHC067	Mouse				1:100
LRP6	Santa Cruz	SC-25317	Mouse	1:1000	1:50		
PA (tag)	Novus Biological	NBP-03952	Rat	1:1000			
V5 (tag)	Invitrogen	R960-25	Mouse	1:1000	1:50		
Vinculin	Cell Signaling	13901	Rabbit	1:2000			
VSV-G (tag)	Biomol (Bethyl Laboratories)	A190-131A	Rabbit	1:1000			
Wnt-11	R&D systems	AF2647	Goat	1:1000	1:100		1:100
Wnt-11	R&D systems	MAB3746	Rat	1:500		1:50	
Rat-Igg (non-targeting)	Sigma	I4131	Rat	1:1000			
E8 (Wnt-11)	Homemade		Rat	1:1000	1:30	1:30	
F10 (Wnt-11)	Homemade		Rat	1:1000			

5.4. Peptide ELISA

Clear polystyrene enzyme linked immunosorbent assay (ELISA) microplates (R&D systems, DY990) were coated with Wnt-11 peptides at 1 μg/ml (see Anti-Wnt antibodies, recombinant proteins, peptides, and drugs; page 71) by overnight incubation at 4 °C. Next day, several TBS washes were performed, and the plate was blocked overnight with TBS containing 0.1% Tween 1% BSA. Antibodies (E8 and rat IgG control) were tested by serial dilution (1 μg/ml, starting dilution 1:1 000 to 1:50 0000) and incubated for 1.5-2 h at RT. Plates were washed twice with TBS containing 0.1% Tween 1% BSA. Anti-rat HRP-conjugated secondary antibody (1: 2 000; Jackson ImmunoResearch) was incubated for 1 h at RT. Plates were washed three times with TBS containing 0.1% Tween 1% BSA. Signal was developed with 3,3′,5,5′-Tetramethylbenzidine (TMB) ELISA high sensitivity kit (Abcam ab171523), and absorbance measured at 370 nm. Data regarding this section is presented in Figure 13, page 71.

5.5. Dot blot

5.5.1. Peptide dot blot

1 µg of peptide was dot blotted on nitrocellulose membranes and left to dry. The membranes were blocked in TBS-T containing 3% BSA. The subsequent steps were as for western blotting, starting from the blocking step (see page 87) and incubation was done with E8 and F10 antibodies from hybridoma cells conditioned media (see Anti-Wnt antibodies, recombinant proteins, peptides, and drugs; page 71). Data regarding this section is presented in Figure 13, page 71.

5.5.2. Cell supernatant dot blot

HEK 293 cells were transfected and cultured in 5% FBS containing media for 48 h prior to cell supernatant or conditioned media (CM) collection. CM was centrifuged at 500 g for 10 min to remove any cell debris. From a total of 1 ml cleared CM, 100 µl was blotted on a nitrocellulose 0.22 µm membrane using a concentrator manifold system (Minifold^{TM}). After complete drying of the membrane (1-2 h), the nitrocellulose was blocked in TBS-T buffer containing 3% BSA and analyzed by western blotting starting from the blocking step (see page 87).

5.6. Immunoprecipitation (IP) and pull-down

For immunoprecipitation (IP) and pull-down assays, PC3 or HEK 293 cells were plated in 6-well plates and transfected with a total of 1 µg of plasmids (when co-transfected with multiple plasmids, equal amounts of each were used unless stated otherwise) by following the procedure described on page 75. After 24-48 h, plates were placed on ice and cells washed in PBS and lysed for 5-10 min in 1 mL IP buffer (50 mM Tris-HCl, pH 8, 150 mM NaCl, 1% Triton X-100, 1 mM EDTA, supplemented with 1x cOmplete™ EDTA-free Protease Inhibitor Cocktail and 1x PhosSTOP Phosphatase Inhibitor Cocktail Tablets). Samples were then centrifuged at 15 000 g for 12 min at 4 °C, pellets were discarded, and supernatants collected. Part of the supernatant was immediately processed for western blotting by mixing 40-50 µl of total protein extract 1:1 with 2x Laemmli Buffer (Sigma) in order to have an expression control (input). Inputs were stored on ice during the immunoprecipitation procedure.

For immunoprecipitation (for direct fc tag pull-down this step was skipped), the remaining lysates were incubated on ice for 90 min with 1 µg of immunoprecipitating primary antibody

(PA or VSV-G see Table 11 for antibodies details and Figure 16 for IP/pull-down scheme). Immunoprecipitating antibodies or fc-tagged proteins were pulled down with 15-20 µl of Protein A/G PLUS-Agarose beads (Santa Cruz) by incubation for 30-60 min at 4 °C on a rotating wheel. Agarose beads were pelleted by gentle centrifugation for 30 sec at 500 g. Supernatants were removed (containing non-interacting proteins) and agarose pellets washed in IP buffer and centrifuged again. The washing procedure by centrifugation rounds was performed 3-5 times. An additional final wash in ice-cold TBS (Tris-buffered saline) buffer was performed prior to resuspension of the agarose pellet in 15-20 µl 2x Laemmli Buffer (Sigma). Immunoprecipitated samples (IPs) and inputs (non-immunoprecipitated, total cell extracts) were incubated at 95 °C in a Thermomixer compact (Eppendorf) for 5 min. After that, the samples were subjected to SDS-PAGE electrophoresis for western blotting.

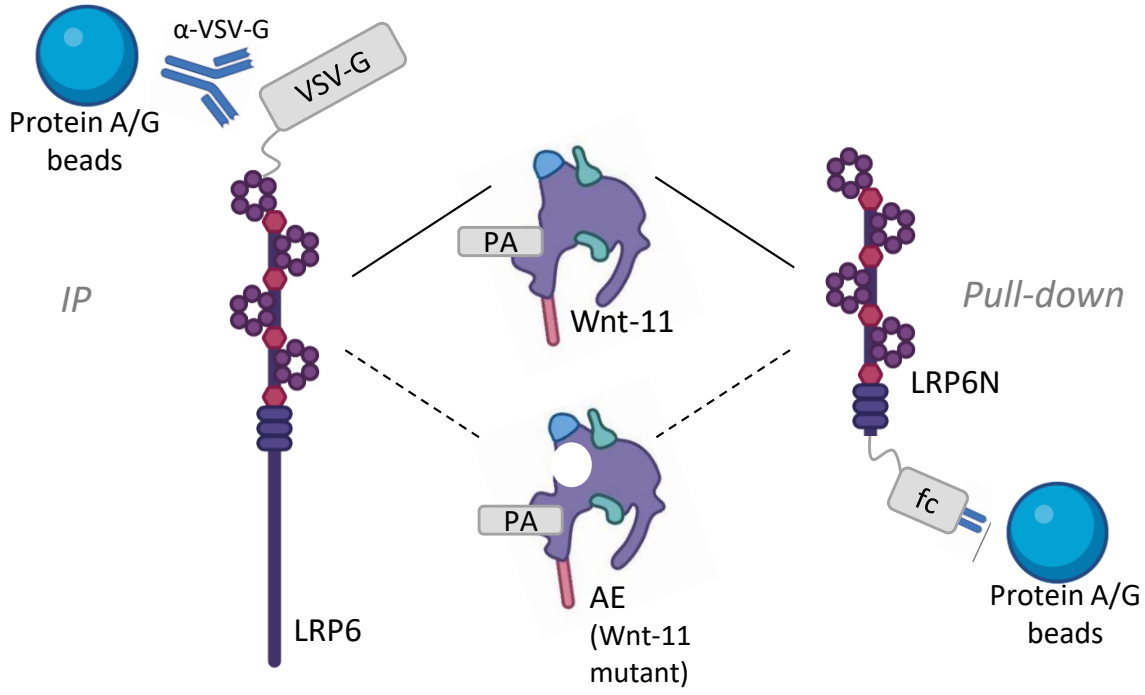

Figure 16. Experimental designs for PA-tagged Wnt-11 (W11) or antibody epitope mutant (AE) immunoprecipitation (IP) or pull-down with VSV-G or Fc tagged LRP6. IP of VSV-G tagged LRP6 is presented in the left and pull-down of fc-tagged LRP6N is depicted in the right. PA, VSV-G and fc tags are highlighted in grey squares, details are provided in Table 5, page 77. Lines indicate putative interaction detected in the experiments (dashed lines denote a weaker interaction). LRP6N – extracellular domain only or ectodomain of LRP6.

5.7. Immunofluorescence (IF)

Cells were plated on 12 mm sterile coverslips (VWR, 0111250) in 24-well or 12-well plates. If appropriate, cells were transfected by following the procedure described on page 75. For immunofluorescence (IF) staining, cells were washed in PBS and fixed at RT in PBS containing 4% PFA (Santa Cruz) for 15 min followed by 3 washes in PBS. Permeabilization was done for 10 min at RT in PBS containing 0.1% Triton X-100 (this step was skipped for cell surface staining of antigens). Samples were blocked for 30-60 min in 2% BSA, 50 mM glycine, 0.01% NaN_3 in PBS (IF blocking buffer). After that, coverslips were incubated overnight at 4 °C with primary antibodies diluted in IF blocking buffer (see Table 11 for dilutions). Coverslips were then washed 3 times in PBS and incubated with secondary antibodies diluted 1:500 in IF blocking buffer for 40 min at RT (AlexaFluor488, AlexaFluor594, AlexaFluor647, Life Technologies). Coverslips were washed in PBS for 3-5 times before a final wash in ddH_2O. Mounting the coverslips onto slides (Thermo 20 mm frosted) was performed by placing them cell-side down on a drop of 5-10 µl Vectashield mounting medium with DAPI (Vector Labs), leaving them to dry for 1 h and then stored at 4 °C. Immunofluorescence was visualized using an upright fluorescent microscope (Axioimager D1) and a confocal microscope (Leica TCS SP8) with a 20x objective and a 63x oil immersion objective. Co-localization analyses of LRP6 and Wnt-11/AE were performed using Fiji (see page 97) from the indicated numbers of cells corresponding to 2 independent experiments.

5.8. Immunohistochemistry (IHC)

Formalin/EtOH fixed specimens were paraffin-embedded and 5 µm sections were cut, placed onto slides and dried at least overnight. Histo-Clear II (National Diagnosis, USA) was used for de-paraffinization, followed by four changes of 100%, 96%, 70% EtOH and H_2O. Antigen retrieval was conducted for 30 min in a vapor cooker filled with Tris EDTA buffer at pH 9.0 for Ki67 staining and with citrate buffer pH 6.0 for Wnt-11 staining. Endogenous peroxidase activity was quenched by incubation for 10 min in 3% H_2O_2. Then, avidin/biotin were blocked for 15 min each (avidin/biotin blocking kit (Vector Labs)). After PBS washes, specimens were blocked in 5% horse serum for 30 min at RT. Primary antibody (see Table 11) to Ki67 (R&D, 1:100) was incubated 1 h RT and additionally overnight at 4 °C and primary antibody to Wnt-11 (R&D, Goat, 1:100) was incubated overnight at 4 °C. After PBS washes, sections were incubated for 30 min with biotinylated secondary antibodiy (anti-mouse/rabbit/goat IgG Antibody (H+L), Universal Pan-Specific biotinylated BA-1300, Vector

Labs) followed by Vectastain® Elite ABC reagent (Vector Labs) for 30 min. Liquid 3,3'-diaminobenzidine (DAB) (DAKO) was used as a chromogenic agent for 1-2 min and sections were counterstained with Mayer's hematoxylin. Samples were then dehydrated through ascending alcohols to xylene and mounted with dibutylphthalate polystyrene xylene (DPX) mounting media (Sigma). Specimens were imaged on an AxioImager D1 light microscope. QuPath software was used for quantitation of intensity of nuclear Ki67 (see page 97 for method). For hematoxylin/eosin (H&E) staining, specimens were only deparaffinized and rehydrated, then stained with consecutive Mayer's hematoxylin and eosin solutions followed by dehydration and DPX-mounting.

5.8.1. Prussian blue

Prussian blue histochemical reaction for the demonstration of iron was performed using a kit (Polyscience, 24199) and according to manufacturer's instructions. Samples were incubated with a 1:1 mixture of 4% potassium ferrocyanide and 4% hydrochloric acid (Prussian blue staining solution) for 20 min at RT, renewing the Prussian blue staining solution once after the first 10 min. They were then washed with PBS three times. Counterstaining was done with Nuclear Fast Red for 2 min at RT to stain the cytoplasm, followed by washing thoroughly in PBS. After that, samples were mounted accordingly and imaged using an AxioImager D1 light microscope. IHC tumor tissue specimens were processed for Prussian Blue staining after the fixed specimens had been paraffin-embedded, sectioned, placed onto slides and de-paraffinized as described in the section above. After Prussian blue reaction, specimens were dehydrated through ascending alcohols to xylene and mounted with DPX mounting media (Sigma). For the MNP cell-staining assays, a modified IF protocol was followed. Briefly, cells were seeded on coverslips placed into 24-well plates. MNP conjugates were incubated at 0.2 mg Fe/ml for 2-4 h at 37 °C or at 4 °C (control). Cells were then washed twice with PBS and fixed with 4% PFA for 10 min at RT. Cells were then washed again twice with PBS and subjected to the Prussian Blue histochemical reaction described above. Samples were mounted with Vectashield without DAPI (Vector Labs).

6. Chick chorioallantoic membrane (CAM) model

The chick chorioallantoic membrane (CAM) assay is a unique *in vivo* model that allows the xenografting of cells on the highly vascularized CAM, facilitating the study of tumor growth and metastasis in the short time frame of days (Crespo & Casar, 2016). It has been utilized in cancer research for more than 30 years and has recently received renewed interest (J. J. Harris, 1958; Hu, Ishihara, Chin, & Wu, 2019; Kobayashia et al., 1998; Ribatti, 2016). It has the potential to deliver reliable results in a rapid and cost-effective manner. It is viewed as a promising alternative to help reduce experimentation in rodents and other animal models. Also, CAM assays are exempt from ethical approval.

For experiments, fertilized chicken eggs were purchased from Gibert (Tarragona). Upon arrival, the surfaces of the eggs were cleaned superficially with 70% ethanol. Eggs were then placed into a wine refrigerator and maintained at 12 °C usually for 2 days, but up to 1 week, depending on the timeline of the experiment. A scheme of the CAM assay is presented in Figure 17. At embryo development day (EDD) 0 the eggs were placed with the pointed end facing down in the rotary incubator set at 37 °C, 60% humidity and with rotation of 100 degrees every 20 min. On EDD 4 a hole was made with the help of a Dremel tool and a syringe (Braun Sterican) in the pointed end of the eggs to induce the dropping of the developing CAM and its separation from the outer shell (referred to as *dropped* CAM). Holes were covered with tape and eggs placed in a stationary incubator (37 °C, humidity 60-80%). On EDD 7, holes were enlarged with the help of forceps to a ~ 1 cm diameter window to expose the CAM. Plastic rings cut from plastic Pasteur pipettes of 5-6 mm diameter were placed on the CAMs. For the implantation of cells, they were detached with TrypLE (1x, Gibco), counted, and resuspended at a density of 500 000 PC3 cells/egg in a volume of 12.5 µl/egg of media 0% FBS and 1% Pen/Strep antibiotics (Gibco). Treatments were added where pertinent, and the suspension was mixed 1:1 (12.5 µl/egg) with Matrigel matrix growth factor reduced (BD Biosciences, 356230). Then, the 25 µl/egg of the cell: Matrigel mixture was implanted by placing it drop-wise into the plastic ring. Tumors were allowed to form and grow for 5-7 days.

Antibodies were added to the cell: Matrigel implantation mixture at 3 µg/egg and then tumors received topical reminder doses every 2-3 days with 3 µg antibody/egg. MNP conjugate treatments of the tumors at the day of implantation was performed by either adding 2 µl/egg of MNPs to the cell:Matrigel implantation mixture (MNP final concentration of 0.1 mg Fe/ml, corresponding to approximately 0.2-0.3 µg Ab/egg) or by addition of 18-20 µl/egg of MNPs

topically 4 h after the cell implantation (at a final concentration of 1 mg Fe/ml in PBS, corresponding to approximately 2-3 µg Ab /egg). MNP treatments were then renewed topically every 2 days at the same dose (18-20 µl/egg).

On endpoint (EDD 12-14), holes were enlarged for imaging tumors *in ovo* and excised for weight determination in a precision balance (Sartorius TE1245). Tumor area was established as a ratio of tumor area to ring using in ImageJ (see page 97). When tumor specimens were processed for IHC (see page 92), they were fixed overnight in 10% formalin solution (Merck, HT5012) and subsequently changed to EtOH 50% for up to two weeks. Specimens were then paraffin embedded and the procedure described in page 92 was followed for IHC analysis. 5-10 eggs were used per condition in each experiment and data were normalized to the IgG-treated condition for combining at least 3 independent experiments.

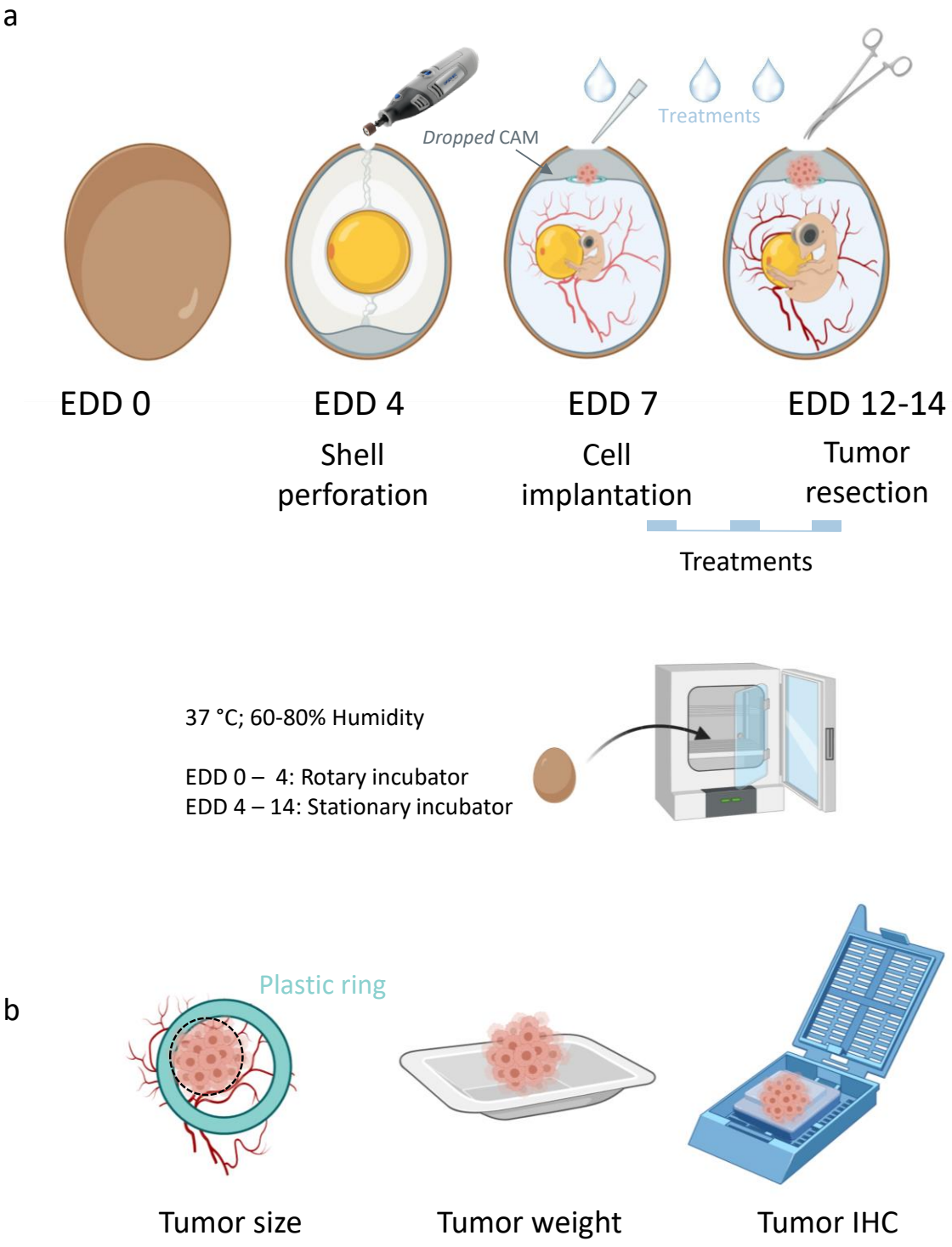

Figure 17. Scheme of chick chorioallantoic membrane (CAM) assay of tumor growth. A) *In ovo* process for CAM assay: opening and dropping of the CAM on EDD 4 with the help of a Dremel tool, tumor cell implantation on EDD 7 and tumor resection at day 5-7 post-implantation, corresponding to EDD 12 - 14. Treatments were added every 2-3 days topically, on top of the tumors in the course of the assay. Fertilized eggs were kept in a 37 °C incubator at 60-80% humidity with (EDD 0 - 4) and without (EDD 4 - 14) rotation. B) Harvesting process at endpoint: imaging of tumors for measurement of tumor size/area compared to plastic rings, weight determination of the resected tumors and processing for IHC analysis. EDD – Embryo development day, IHC – Immunohistochemistry.

7. Bioinformatics resources

7.1. Databases

Protein sequences were retrieved from the Uniprot database (Bateman et al., 2021), alignments were performed using MUSCLE (Edgar, 2004) with default parameters and visualized with Jalview (Waterhouse, Procter, Martin, Clamp, & Barton, 2009). The conservation score provided in the alignment is given as a numerical index reflecting the conservation of physico-chemical properties and is visualized as a histogram giving the score for each column. Conserved columns (score of 11 with default amino acid property grouping) are indicated by '*', and columns with mutations where all properties are conserved are marked with a '+' (score of 10). Protein structures were retrieved from the RCSB Protein Data Bank (PDB; http://www.rcsb.org/pdb/; PBD IDs: 6AHY, 4F0A, 4QCI, 1IGT) and analysis and molecular graphics were done using UCSF Chimera (Pettersen et al., 2004). Biorender webtool (biorender.com) was used to make some of the illustrations. Tools used to evaluate the gene expression, co-expression and its correlation with patient survival in prostate cancer datasets included CANCERTOOL (Cortazar et al., 2018) and GEPIA (Tang et al., 2017).

7.2. Image analysis

Basic image analysis was carried out using ImageJ's (NIH, Bethesda, MD, USA) Fiji distribution (Schindelin et al., 2012). Homemade macros were used for automated cell number quantification (Table 12 and Figure 18), area determination and fluorescence image mounting.

Densitometries of western blot images were performed after background subtraction using the default commands for gel analysis: *select lanes* and *plot lanes*, followed by the area measurements corresponding to the intensity values of the bands. Densitometry values were normalized to those of the loading control and then to the internal control condition. For the semi-quantification of the turbidity produced by the MNP aggregation, the *Find Maxima* command was used with a threshold set at 10. Prussian Blue cell staining blue color deconvolution was performed using Fiji's *Color deconvolution* command for *Brilliant Blue*. The deconvoluted blue signal intensity was measured in the images for each replicate and the average value is presented.

Wound healing analysis was done using the *MRI Wound Healing Tool* (https://github.com/MontpellierRessourcesImagerie/imagej_macros_and_scripts/wiki/Wound-Healing-Tool). Area measurements at endpoint were made relative to the same area at time 0 h (x) and was recalculated relative to closure (1-x). Relative closure values of the six replicates were then averaged and relativized to the internal control. Co-localization tests were done using the coloc2 plugin (https://imagej.net/Coloc2).

Table 12. Example ImageJ macro used for automated cell counting of migrating cells. In Figure 18 example images before and after processing with the ImageJ macro are shown.

```
run("8-bit");
run("Subtract Background...", "rolling=30 light");
setThreshold(0, 240);
setOption("BlackBackground", false);
run("Convert to Mask");
run("Watershed");
run("Analyze Particles...", "size=60-Infinity show=Outlines display summarize add");
```

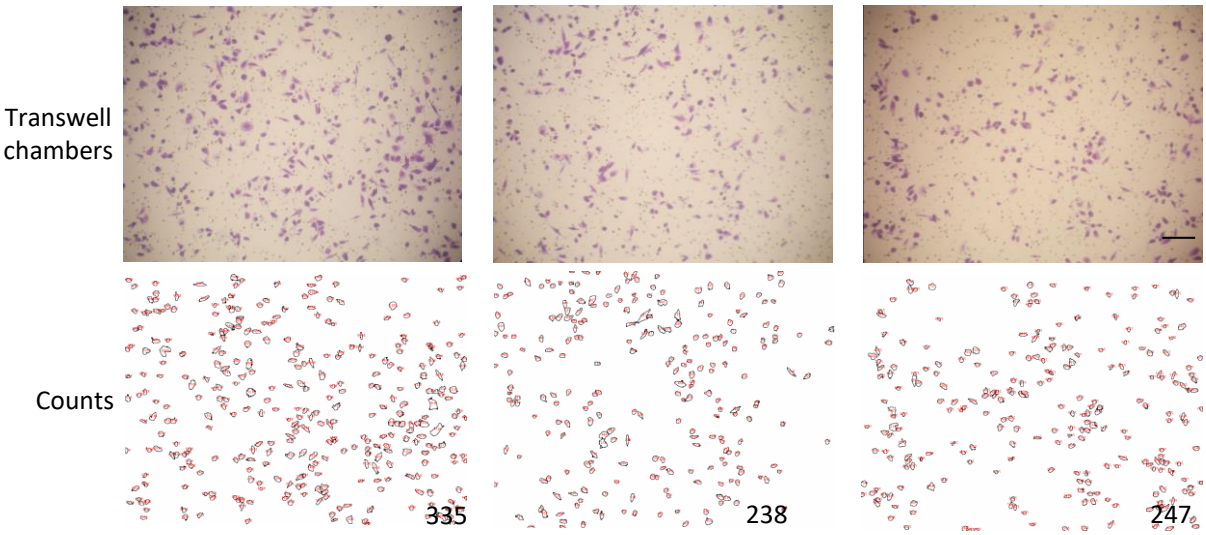

Figure 18. Example images obtained for automated cell counting of migrating cells using the ImageJ macro shown in Table 12. Representative images of transwell chambers (upper panel) and macro-output (lower panel) with numbers obtained indicated at the bottom right. Scale bar 100 µm.

Qupath software (Bankhead et al., 2017) was used for the analysis of IHC images. For Ki67 nuclear intensity quantification the following method was used. Briefly: images were imported to a Qupath project and tumor area was selected, automated cell segmentation tool based on hematoxylin staining was used with manual supervision and DAB mean intensity was obtained for each of the segmented nuclei. Data of the nuclei from each picture were averaged and statistically analyzed as independent as described below.

8. Statistical analysis

Data presented are the result of 3 independent experiments, unless stated otherwise and are represented as the mean ± standard error of the mean (SEM) indicated by error bars. For most experiments data are presented as the fold-change relative to the internal control. Data were handled on Microsoft Office Excel spreadsheets, aided by the use of GraphPad Prism 5.0 (GraphPad, La Jolla, CA, USA) and PlotssOfData webtool (Postma & Goedhart, 2019) (https://huygens.science.uva.nl/PlotsOfData/). Using the latter tool, data are presented as boxplots and tables containing the statistical associated information are presented indicating: 95CI, 95% confidence interval; IQR, interquartile range; MAD, median absolute deviation; Q1, quartile 1; Q3, quartile 3; SD, standard deviation; SEM, standard error of the mean.

For determination of statistically significant differences, pairwise comparisons were analyzed using two-tailed Student's t tests. For normalized data unequal variances were assumed, and heteroscedastic t-tests were calculated; for paired observations, paired t tests were performed. Large group comparisons (>6) were analyzed using one-way analysis of variance (ANOVA) and p-values were then obtained as post-hoc Tukey corrected p-values. A p-value<0.05 was considered statistically significant: * is indicative of $p<0.05$; ** of $p<0.01$; *** of $p<0.001$; and n.s. notation was used to indicate non-significant differences; sometimes specific p-values are noted on the graph or in the figure legend.

Results

Chapter I: Characterization of anti-Wnt-11 antibodies and functionalized nanoparticles

I.1. Characterization of anti-Wnt-11 antibodies' recognition of Wnt-11

The importance of Wnt-11 in advanced prostate cancer progression has been studied extensively in Dr. Kypta's lab (Murillo-Garzón et al., 2018; Uysal-Onganer et al., 2010; Uysal-Onganer & Kypta, 2012; H. Zhu et al., 2004). Increased expression of Wnt-11 is found in prostate tumors and in metastatic lesions. Moreover, high *WNT11* mRNA expression correlates with poor prognosis in patients (see Figure 12, page 64).

With the aim of selectively blocking Wnt-11 function, rat anti-Wnt-11 antibodies were generated *in house* to human Wnt-11 peptides (see Figure 13, page 71). Two antibodies, named E8 and F10, were selected for studies. Dot blot analysis identified the same peptide as being recognized by both antibodies, comprising Wnt-11 amino acids 101-112 (LLDLERGTRESA), constituting the antibodies epitope. E8 further recognized this Wnt-11 peptide by ELISA and the recognition of Wnt-11 full length protein was confirmed as follows.

As cellular models, the next prostate cancer cell lines were used: VCaP, androgen dependent cells that express moderate to high levels of *WNT11* mRNA; PC3, androgen independent cells that also express moderate to high levels of *WNT11* mRNA; DU145, androgen independent cells that express moderate levels of *WNT11* mRNA; and C4-2B, androgen independent cells derived as a bone metastatic subline from LNCaP (Lymph Node Carcinoma of the Prostate) cells, which express low levels of *WNT11* mRNA. In Table 13 *WNT11* mRNA levels and androgen dependency for each cell line are presented and further information of their characteristics can be found in Table 2 (page 75).

Table 13. *WNT11* mRNA expression in the prostate cancer cell lines used. The levels of mRNA were determined using the ΔΔCT method, relative to the expression of *36B4* housekeeping gene (Livak & Schmittgen, 2001). Relative values are calculated to those of VCaP cells. Primers no-CDS (located in the non-coding sequence) for detecion of endogenous *WNT11* and primers CDS (coding sequence) for detection of both endogenous and ectopic *WNT11*. For DU145 cells only relative values (for primers no-CDS) are presented because data corresponds to an independent set of experiments.

		WNT11 mRNA		
WNT11 mRNA	Prostate cancer cell line	ΔΔCT	Relative	Androgen dependency
Primers CDS	VCaP	11.055	1.000	Yes
	PC3	10.835	1.165	No
	DU145	-	-	No
	C4-2B-V	14.488	0.093	No
	C4-2B-WNT11	3.419	199.020	No
Primers no-CDS	VCaP	11.743	1.000	Yes
	PC3	11.752	0.993	No
	DU145	-	0.564	No
	C4-2B-V	15.031	0.102	No
	C4-2B-WNT11	15.628	0.068	No

First, Wnt-3a and Wnt-11 recombinant proteins were used to demonstrate that E8 specifically recognized Wnt-11 by western blot but not Wnt-3a, which only contains the latest part of the antibodies epitope sequence (TRESA). As controls, commercial goat-α-Wnt-11 and rat-α-Wnt-3a antibodies were used to confirm the presence of each protein. Additionally, Coomassie staining of the gel was carried out, which revealed the presence of comparable amounts of the BSA used as carrier for these recombinant proteins as an indicator of loading. E8 recognized Wnt-11 recombinant protein, as did the commercial anti-Wnt-11 antibody, and did not show cross-reaction with Wnt-3a (Figure 19a).

An important requirement for function-blocking antibodies is the ability to recognize its antigen in a cellular context. For that, C4-2B prostate cancer cells that express low levels of Wnt-11 were used for stable overexpression of either empty vector (pcDNA) as control (C4-2B-V cells) or pcDNA-Wnt-11 (C4-2B-WNT11 cells). The overexpression of ectopic WNT11 was confirmed by RT-PCR (Table 13). Also, by western blot, a much-enhanced expression of Wnt-11 in the latter cells was detected (Figure 19b). Immunofluorescence signal intensity was low for both E8 and commercial goat-R&D-Wnt-11 antibodies in C4-2B-V control cells. Meanwhile, the staining intensity was high in C4-2B-WNT11 cells for both antibodies and they showed relatively optimal co-localization in Wnt-11 high-expressing cells (Figure 19c).

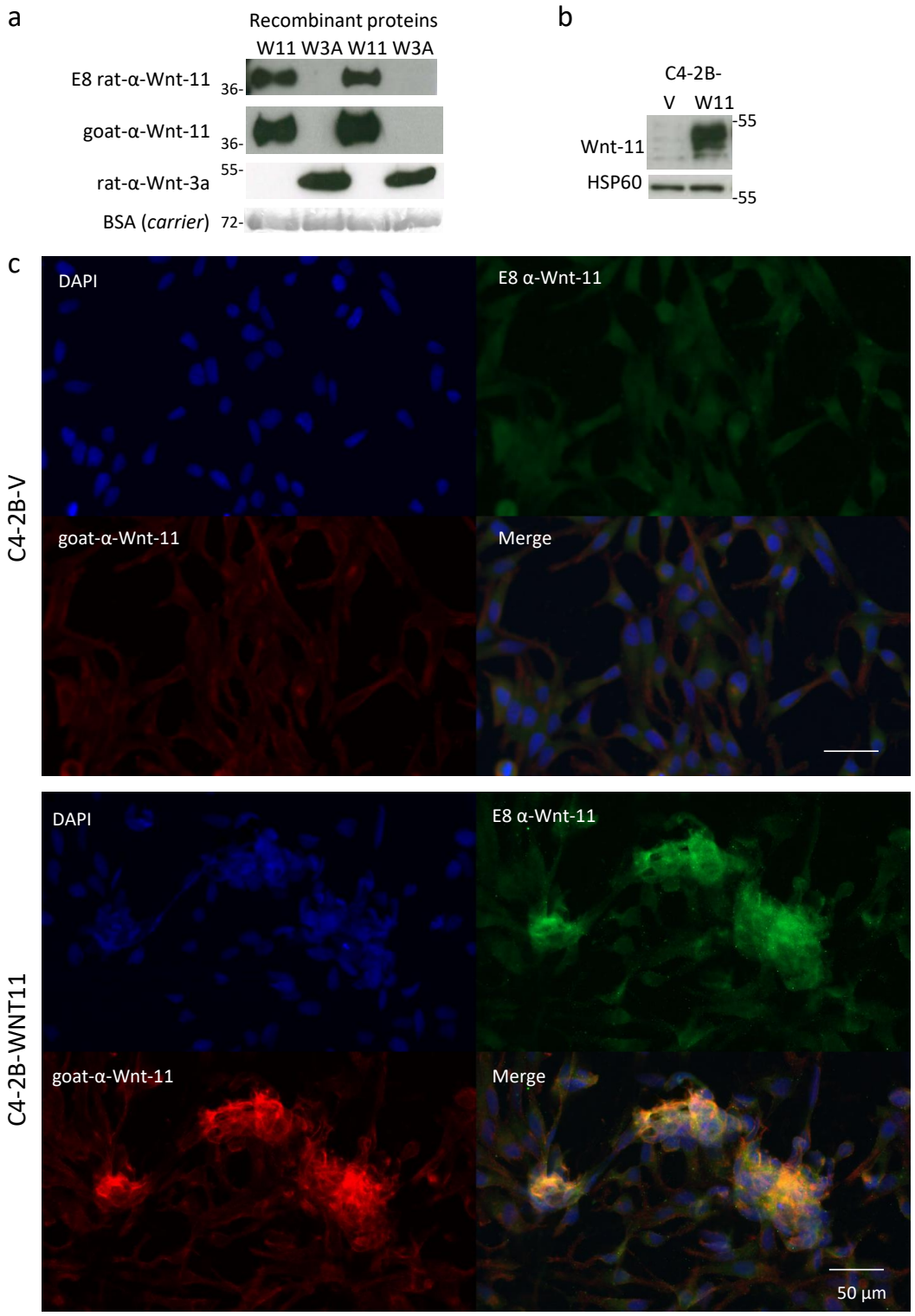

Figure 19. Detection of recombinant Wnt-11 protein and ectopic Wnt-11 in C4-2B cells with E8 antibody. A) 200 ng of recombinant protein for Wnt-11 (W11) and Wnt-3a (W3A) were blotted with E8 and control antibodies goat-α-Wnt-11 and rat-α-Wnt-3a; as loading control, the BSA used as carrier for the recombinant proteins, was analyzed by Coomassie staining of the polyacrylamide gel. Recombinant proteins were loaded in duplicate. B) Western blot showing Wnt-11 overexpression in C4-2B-WNT11 cells compared to C4-2B-V control cells. C) Immunofluorescence of the C4-2B-V/WNT11 cells using E8 α-Wnt-11 (green), goat-α-Wnt-11 (red) and DAPI (blue, nuclei) and a merge of the 3 channels.

To further prove E8 recognition in a cellular context, HEK 293 cells transfected for the transient expression of Wnt-11 were used. The cells were stained with E8 and the populations showing high (+) and low (-) intensity for the staining were sorted by Fluorescence-activated cell sorting (FACS, see Figure 15 in page 86 for the experiment scheme). Sorted cells were then processed for protein extraction and probed for Wnt-11 by western blot with a commercial anti-Wnt-11 antibody. First, E8 stained cells showed higher signal intensity compared to controls of unstained and only secondary α-rat-stained cells (AlexaFluor-647, APC) (Figure 20a). The western blot results indicated that the E8 high/positive sorted cells were enriched for Wnt-11 protein expression (Figure 20b), with the confirmation of Wnt-11 overexpression in total protein extracts compared to vector-transfected cells (Figure 20c). A pilot experiment carried out in parallel using a commercial (R&D) rat anti-Wnt-11 antibody found that cells sorted using this antibody were not enriched for Wnt-11 expression (Figure 20d), suggesting E8 was able to recognize native Wnt-11 on the cell surface, in contrast to R&D rat anti-Wnt-11 antibody.

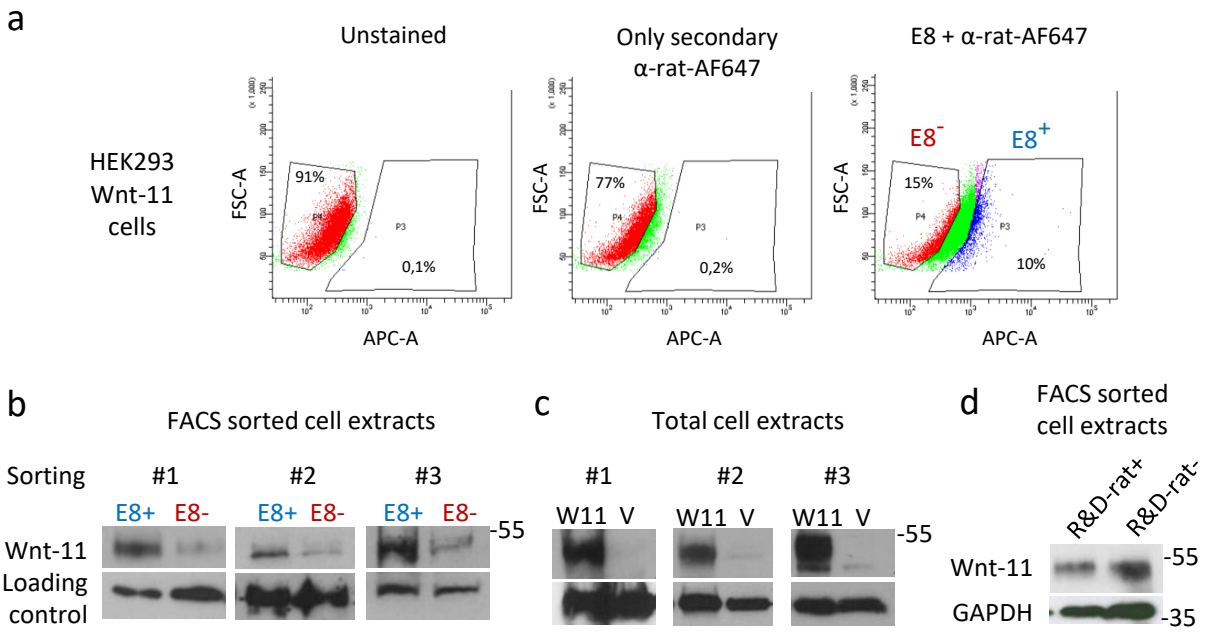

Figure 20. Detection of Wnt-11 protein levels of FACS-sorted HEK 293 cells overexpressing Wnt-11 transiently. A) Example FACS plots of Wnt-11 expressing HEK 293 cells unstained, stained for only secondary α-rat-AF647 and E8 stained, showing the gates for E8 high (+) and E8 low (-) populations for FACS-sorting. B) Western blots of E8+ and E8- sorted cells for detection of Wnt-11 and loading control (HSP60, GAPDH). 3 independent experiments shown. C) Western blots showing Wnt-11 protein expression of bulk/unsorted HEK 293 cells transfected for the transient expression of Wnt-11 with a Wnt-11 plasmid compared to vector (V, pcDNA)-transfected cells. 3 independent experiments carried out in parallel to the sorted cell extracts presented in (B) are shown. D) Western blots of R&D rat-anti-Wnt-11+ and R&D rat-anti-Wnt-11- sorted Wnt-11 expressing HEK 293 cells for detection of Wnt-11 and loading control (GAPDH); n=1, pilot experiment. For detection of Wnt-11 expression by western blot a commercial antibody (R&D goat) was used. AF647-AlexaFluor-647 secondary antibody was detected with the APC (Allophycocyanin) filter by FACS.

These results together with previous findings reported in Dr. Kypta's lab, indicated that the *in house* generated anti-Wnt-11 antibodies were able to recognize Wnt-11 in different assays. Next, the hypothesis that these antibodies might function as function-blocking antibodies for Wnt-11 in prostate cancer models was studied. For testing this, *in vitro* and *in vivo* functional assays were carried out using these antibodies, which are presented in the following chapters.

I.2. Functionalization of MNPs with anti-Wnt-11 antibodies

To improve the properties of the anti-Wnt-11 antibodies in the context of *in vivo* delivery and imaging, functionalization of superparamagnetic iron oxide nanoparticles (SPIONs), here referred to as magnetic nanoparticles (MNPs), was carried out with the anti-Wnt-11 antibodies. The conjugation was performed following previously described methods (see page 72 and Figure 14).

Anti-Wnt-11 antibodies conjugates (MNP-E8 and MNP-F10) were produced, as well as two control nanoformulations, unconjugated nanoparticles (MNP-C) and antibody control rat-IgG conjugated MNPs (MNP-IgG). After functionalization, a characterization of a sample from each conjugate was carried out using dynamic light scattering (DLS). Table 14 shows representative DLS measurements corresponding to the MNP batch of 2020 (see Table 1, page 74). The antibody conjugation produced a slight increase in size compared to activated MNPs (MNP-SH). Charge was also found altered, as activated MNPs showed a decrease in the negative charge compared to the unmodified MNPs (COOH, from -12.3 to -6.6 mV) and the conjugation of antibodies increased back the negative charge (to approximately -10 mV).

Table 14. Dynamic light scattering (DLS) measurements of the MNP nanoformulations, 2020 batch. MNP-COOH corresponds to MNP-C unconjugated nanoparticles; MNP-SH corresponds to activated MNP, an intermediate compound of the conjugation process; MNP-IgG, E8 and F10 correspond to the rat antibodies conjugates; and IgG antibody alone is also presented that was used as a reference. PDI - Polydispersity index.

Sample	Hydrodynamic diameter (nm)	Zeta potential (mV)	PDI
MNP-COOH	69.2 ± 5.0	-12.3 ± 2.0	0.21
MNP-SH	59.0 ± 0.8	-6.6 ± 1.6	0.15
MNP-IgG	62.2 ± 0.6	-10.3 ± 1.1	0.18
MNP-E8	76.4 ± 1.2	-9.6 ± 0.6	0.21
MNP-F10	61.2 ± 0.6	-9.9 ± 0.8	0.19
IgG antibody	--	-10.6 ± 0.5	--

Although the MNP-Ab conjugates were soluble in PBS, for their use in *in vitro* assays their dilution in cell culture media RPMI and DMEM F12 was required. In media containing low levels of fetal bovine serum (FBS), the aggregation of MNP-Ab nanoformulations was noted. This was dependent on the concentration of FBS, with MNP precipitates observed in the media at below 5% FBS (Figure 21). These conditions were not adequate for the exposure of the antibodies' paratopes and therefore low serum conditions were not used for functional assays. Also, experiments involving MNPs were thoroughly surveyed for MNP aggregation and those in which they were visibly aggregating were not considered.

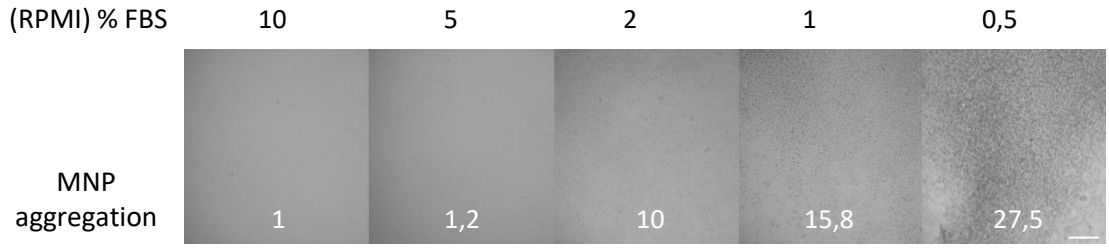

Figure 21. MNP aggregation under low fetal bovine serum (FBS) conditions in RPMI media. Pictures (in black and white) of RPMI containing 10, 5, 2, 1, 0.5% FBS with MNP at 0.2 mg Fe/ml showing visible precipitates at conditions below 5% FBS. MNP aggregation semi-quantification score based on granularity of the picture, as estimated using ImageJ. The images correspond to a representative example of MNP-Ab conjugates. Scale bar 500 µm.

I.2.1. Recognition of prostate cancer cells by anti-Wnt-11-functionalized MNPs

The anti-Wnt-11-MNP conjugates were tested for their capacity to recognize Wnt-11 in a cellular context, using the prostate cancer cell line VCaP which expresses high levels of endogenous *WNT11* (see Table 13) and Prussian Blue staining for the detection of the iron containing nanoparticles. Incubation of the MNPs for 2 h at 37 °C showed certain MNPs attached to the surface of VCaP cells (representative pictures and quantification of surface

binding is shown in Figure 22a). The MNP-cell interactions were abolished when the MNPs were incubated at 4 °C (Figure 22b), indicating the specificity of the recognition. MNP-E8 showed enhanced membrane staining, compatible with Wnt-11 binding on the cell surface compared to MNP-IgG and MNP-C controls. However, in the case of MNP-F10 conjugates Prussian blue staining intensity was not stronger than that of the MNP-IgG control. This preliminary characterization allowed the testing of the nanoformulations in a parallel setting to the naked anti-Wnt-11 antibodies.

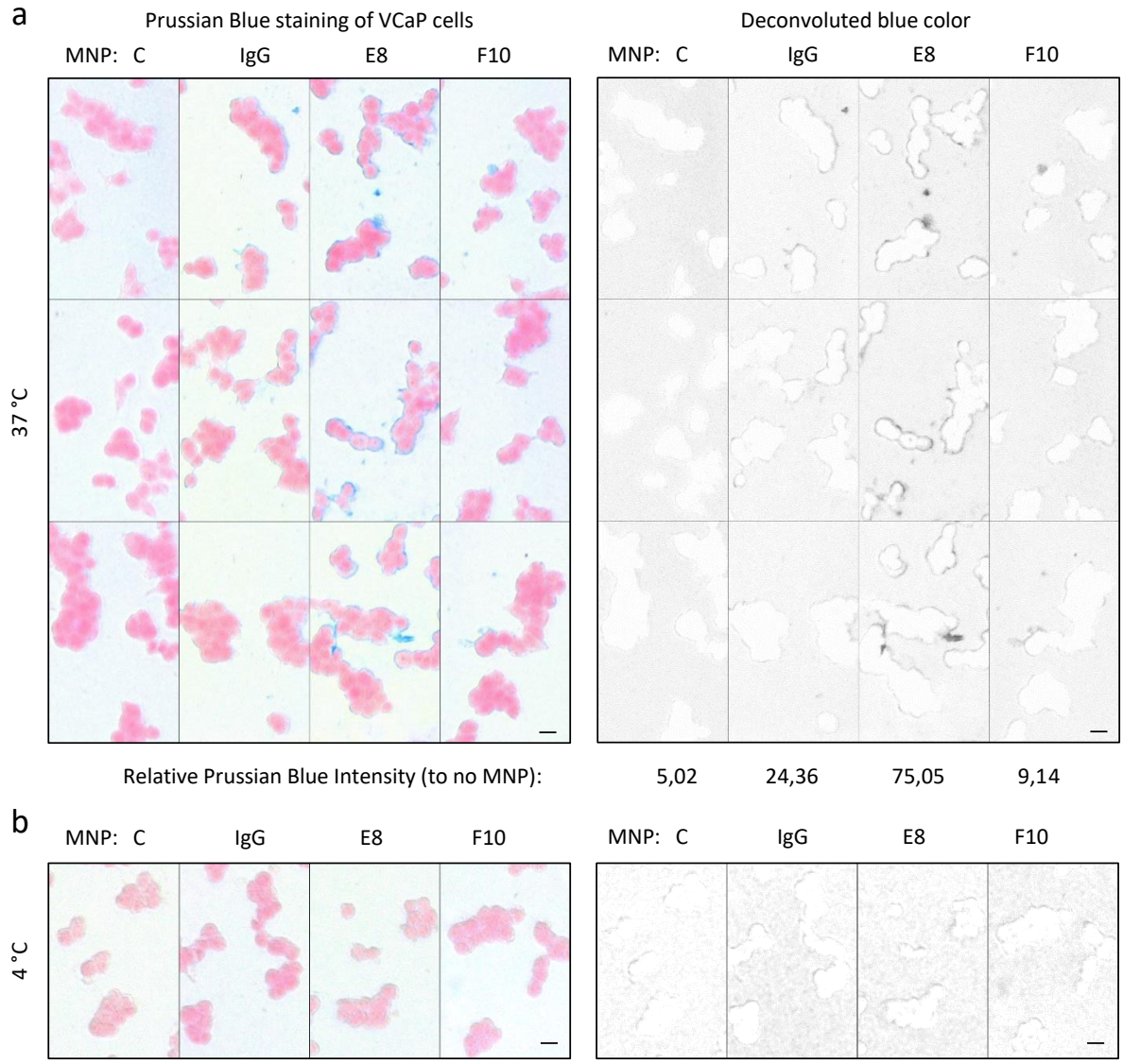

Figure 22. Prussian Blue staining of VCaP cells incubated with MNP conjugates for 2 h at 37 °C and 4 °C. MNP unconjugated (MNP-C, control) and conjugated with rat antibodies (MNP-IgG for rat-IgG, MNP-E8 and MNP-F10 for anti-Wnt-11 antibodies) were incubated at 37 °C (A) and 4 °C (B) with VCaP cells for 2 h and then fixed and subjected to Prussian Blue staining for the detection of the iron contained in the MNPs (blue precipitate). Right panel shows deconvoluted blue color from pictures for improved visualization and semi-quantitation of the blue color intensity. Scale bar 50 µm.

Chapter II: Effects of anti-Wnt-11 monoclonal antibodies and MNP conjugates on prostate cancer cells *in vitro*

II.1. Anti-Wnt-11 monoclonal antibodies inhibit proliferation and sphere formation of prostate cancer cells

Wnt-11 has been reported to play a role in cancer cell proliferation and survival (Mori et al., 2016; Ouko et al., 2004; Tenjin et al., 2019), including in the context of prostate cancer (Uysal-Onganer et al., 2010). However it has also been reported that Wnt-11 can have the opposite effect (Toyama et al., 2010) and its role appears to be context dependent.

In order to characterize the effect of anti-Wnt-11 antibodies, E8 and F10, on prostate cancer cells, proliferation of adherent cells (2D) cultured for 7 days was determined. A significant concentration-dependent reduction in PC3 cell proliferation using both antibodies, E8 and F10, was detected at the highest dose tested (20 μg/ml), but not at a lower dose (5 μg/ml; Figure 23a). In DU145 cells, this was significant only for E8 (Figure 23b), although a trend for a reduction could be observed also for the F10 antibody. However, the effects of both antibodies on proliferation at lower concentrations and at earlier timepoints were generally small (see Figure 27, page 116).

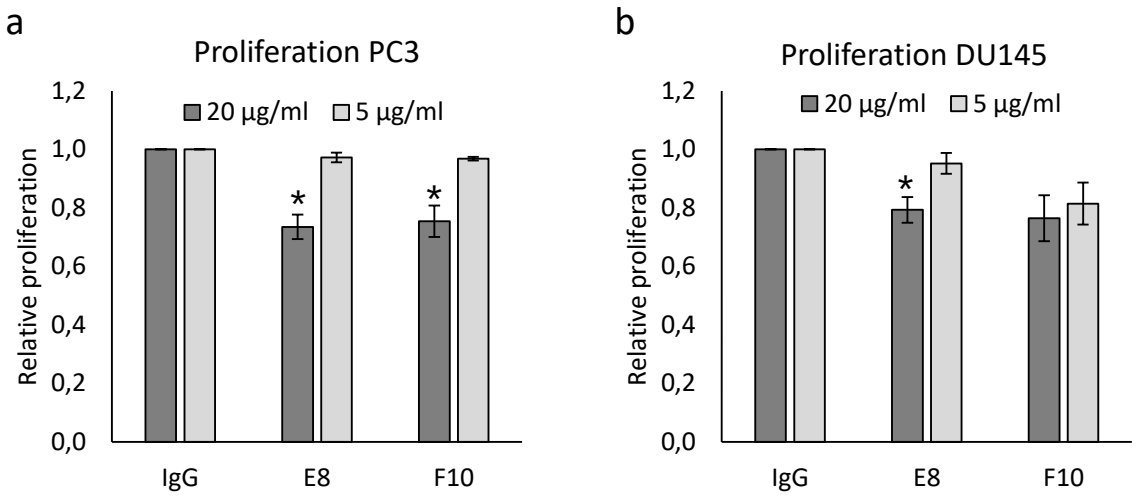

Figure 23. Proliferation assays of PC3 (a) and DU145 (b) cells treated with E8 and F10. Cells were treated for 7 days with renewal of media and antibodies every 2-3 days. Plots represent the effect of the antibodies at a high dose (20 μg/ml) and a low dose (5 μg/ml) normalized to the rat IgG controls. Statistical differences are calculated comparing to the IgG-treated control condition.

Wnts, particularly those mediating β-catenin activation, are proteins with prominent roles in stemness and differentiation processes (Katoh, 2017; Many & Brown, 2014). Here, the role of Wnt-11 in prostate cancer stem cell-like features was studied using sphere formation assays. For this, cells were cultured in defined media in adherence-independent conditions, which was termed as "3D" condition.

In this assays, RNA and protein extracts from 3D spheres was compared to cells cultured attached in normal growth media, 2D condition. In PC3 cells, *WNT11* mRNA level was found upregulated in spheres (Figure 24b) and even more markedly so at the protein level (Figure 24a). In C4-2B-WNT11 (C4-2B cells stably overexpressing Wnt-11) spheres compared to control C4-2B-V spheres, increased levels of *SOX2* mRNA were detected, a well-known factor of stemness (Takahashi et al., 2007) (Figure 24c). This evidence pointed to a correlation of *WNT11* with *SOX2* expression levels and suggested Wnt-11 might be playing a role in prostate cancer cell stemness.

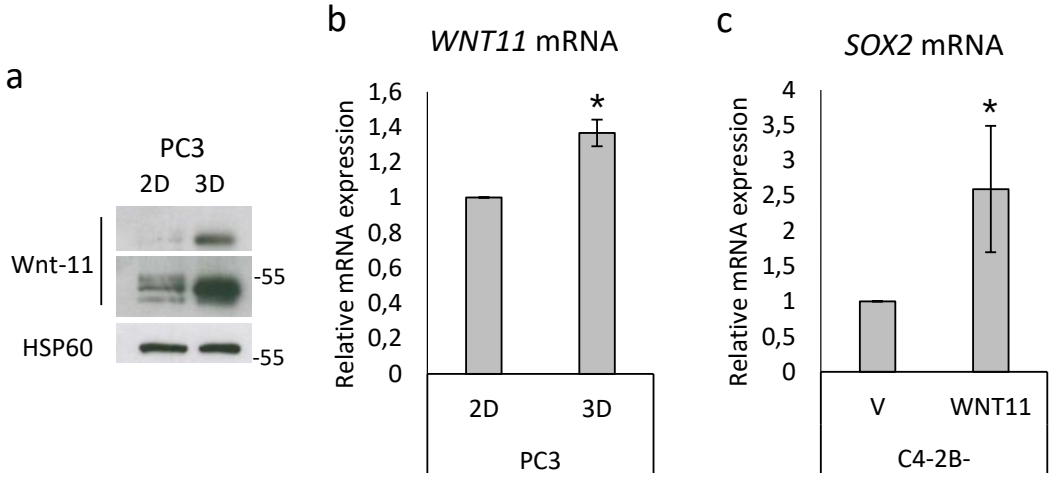

Figure 24. Potential role of Wnt-11 in prostate cancer cell stemness. A) Western blot of 3D and 2D cultured PC3 cells showing a Wnt-11 upregulation in 3D at the protein level, low (upper) and high (bottom) exposures shown. B) RT-PCR of 3D and 2D cultured PC3 cells showing a *WNT11* mRNA upregulation in 3D. C) RT-PCR of Wnt-11 overexpressing C4-2B-WNT11 cells compared to control vector (V) cells cultured as spheres (3D), showing higher expression of *SOX2* mRNA levels in C4-2B-WNT11 cells.

Therefore, the effects of the anti-Wnt-11 antibodies on prostate cancer cell sphere formation were determined. Treatment with the anti-Wnt-11 antibodies reduced the number of spheres formed by PC3 (Figure 25a) and DU145 (Figure 25b) cells, without impairing sphere morphology (Figure 25c, d; respectively). These results indicate that antibody-mediated inhibition of Wnt-11 partially disrupts the ability of prostate cancer cells to grow as spheres, possibly interfering with their stem cell-like properties.

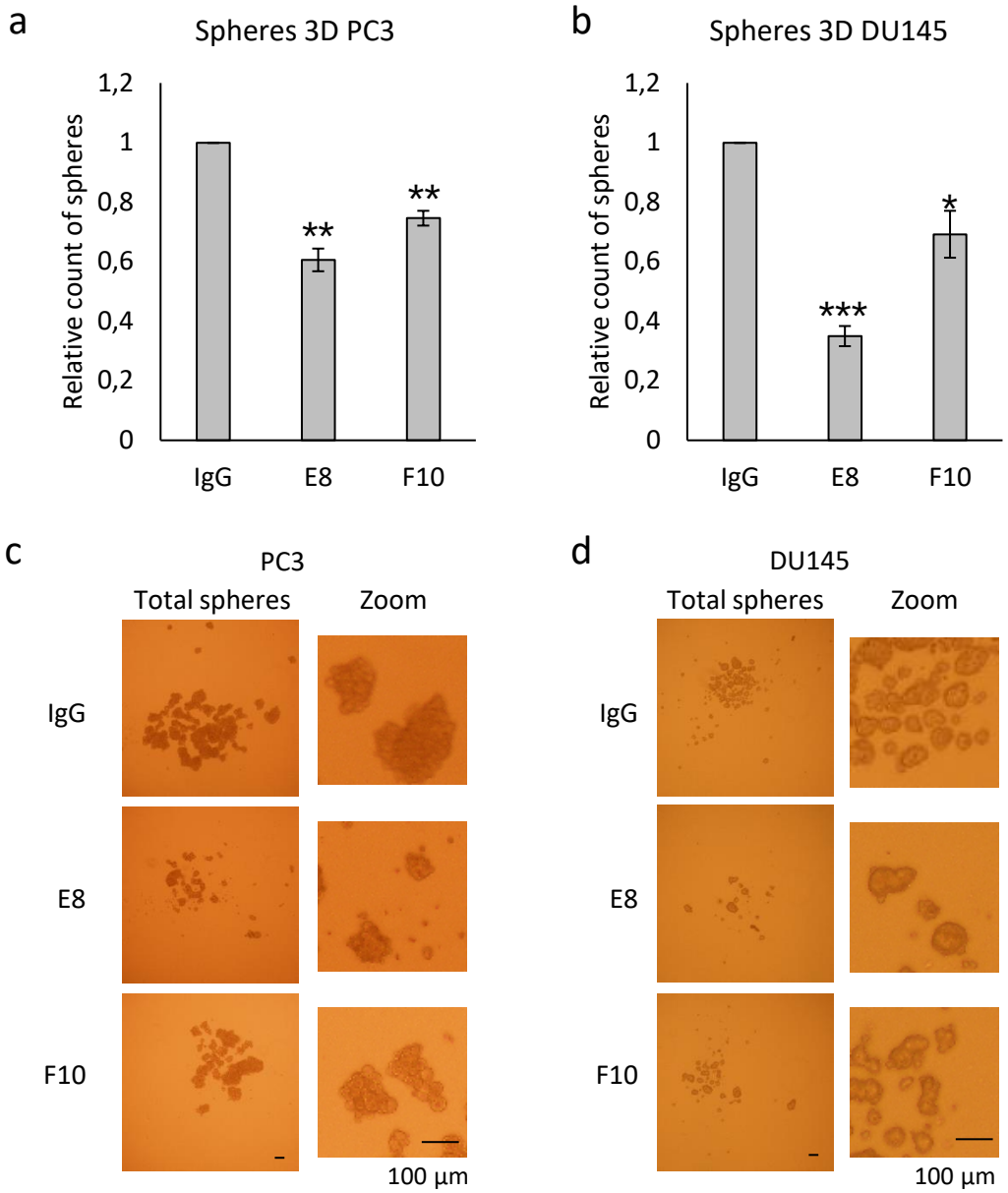

Figure 25. Sphere formation assays for PC3 and DU145 cells treated with E8 and F10. Top panels show counts of number of spheres for PC3 (A) and DU145 (B), respectively, normalized to IgG control. Bottom panels show representative images of PC3 (C) and DU145 (D) spheres, respectively, for total spheres and zoom for a more detailed view of morphology. Counts were obtained from 4 independent experiments for each cell line. Sphere formation assays were performed using 20 µg/ml of antibody. Statistical differences are calculated comparing to the IgG-treated control condition.

In conclusion, the anti-Wnt-11 antibodies elicited a modest reduction in 2D proliferation of prostate cancer cells and had an enhanced impact on cells in sphere 3D cultures, in which Wnt-11 expression was found to be upregulated and correlating with *SOX2* mRNA expression.

II.2. Anti-Wnt-11 monoclonal antibodies inhibit prostate cancer cell migration and invasion

Previous studies report that Wnt-11 has an important role in cell cohesion and migration (Mori et al., 2016; Ouko et al., 2004; Ulrich et al., 2005; Witzel et al., 2006) and also in the context of prostate cancer (Uysal-Onganer et al., 2010).

To confirm previous observations in the PC3 cell system, the effects of *WNT11* gene silencing were determined using wound healing assays. The results showed that *WNT11* gene silencing reduced PC3 cell migration measured by the relative closure of the wound to control siRNA transfected cells (Figure 26a, c). The *WNT11* mRNA expression was confirmed to be effectively reduced upon *WNT11* gene silencing by RT-PCR at the experiment endpoint (Figure 26b). In parallel, treatments with E8 and F10 were found to reduce PC3 cell migration into the wounded area compared to IgG-treated cells (Figure 26d, e). Anti-Wnt-11 antibodies reduced PC3 wound closure to a similar extent to that of the *WNT11* gene silencing.

The reduction in migration of PC3 cells upon antibody treatment was confirmed using transwell migration assays. Here, anti-Wnt-11 antibodies showed a similar effect to the described above, reducing migration (Figure 27a, c). These treatments did not affect proliferation during the course of the assays (24 h), which was measured as a control (Figure 27b).

These effects were validated in other cell model, using DU145 cells, in which E8 treatment elicited a comparable reduction in migration, without affecting proliferation (Figure 27d, e, f). However, F10 antibody treatment only showed a non-significant trend for reduction.

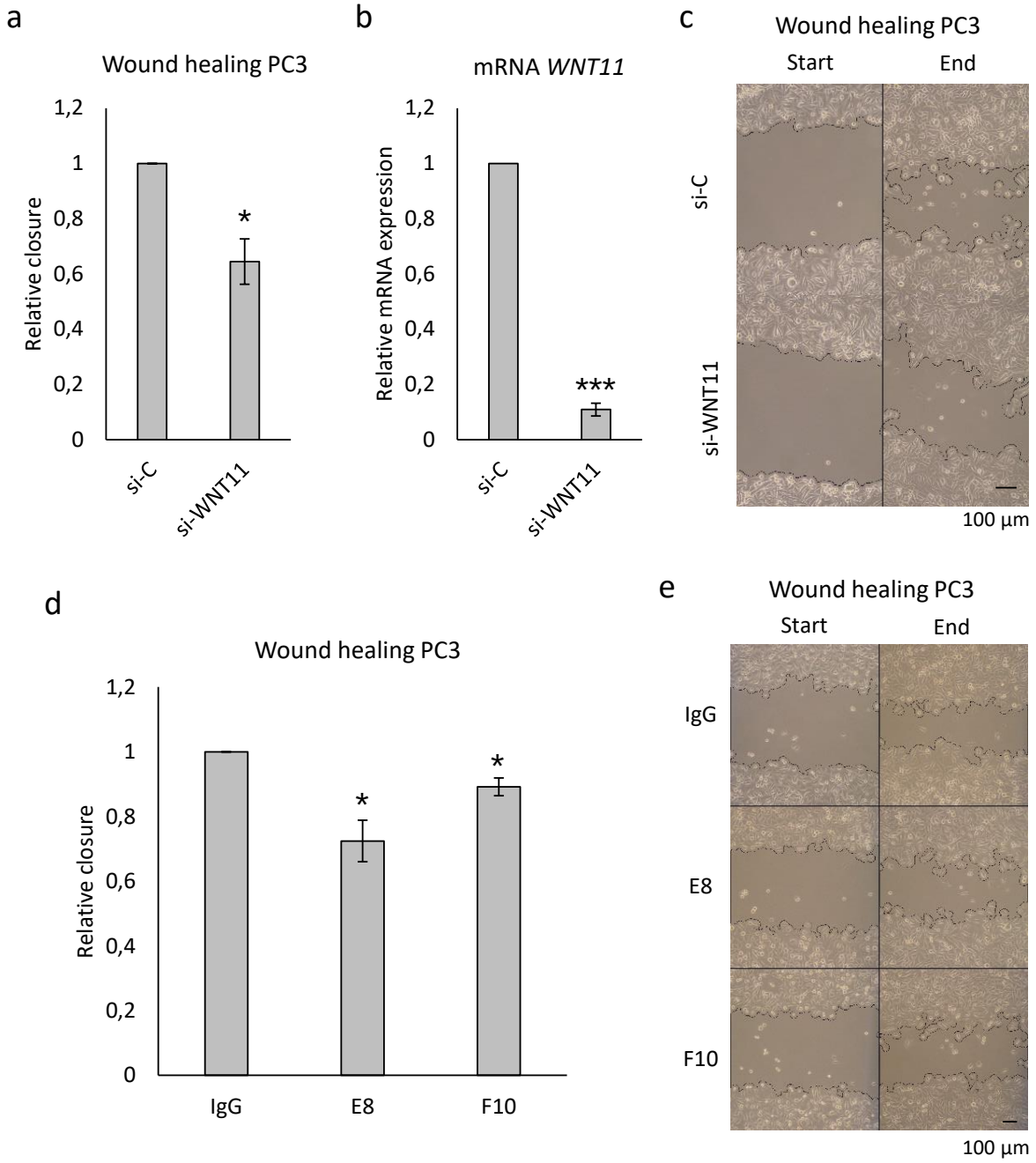

Figure 26. Wound healing assays for *WNT11* gene silencing and anti-Wnt-11 antibody treatment in PC3 cells. A) Plot showing the relative effect on wound closure of *WNT11* gene silencing (si-WNT11) compared to control siRNA (si-C) transfected PC3 cells, performed in 2% FBS RPMI. B) RT-PCR of *WNT11* gene silenced (si-WNT11) PC3 cells compared to control (si-C) showing *WNT11* mRNA downregulation. C) Representative images of the si-C (53% closure) and si-WNT11 (39% closure) cells in the wounded area at start and endpoint of the experiment. D) Plot showing relative effect on wound closure of treatments with E8 and F10 antibodies, relative to control IgG in PC3 cells, performed in 5% FBS RPMI, n=4. E) Representative images of the wounded area for E8 (38% closure) and F10 (36% closure) and IgG control (47% closure) treatments at start and endpoint of the experiment. Statistical differences are calculated comparing to the IgG-treated control condition. Wound healing assays were performed overnight or for 24 h, using 10 µg/ml of antibody.

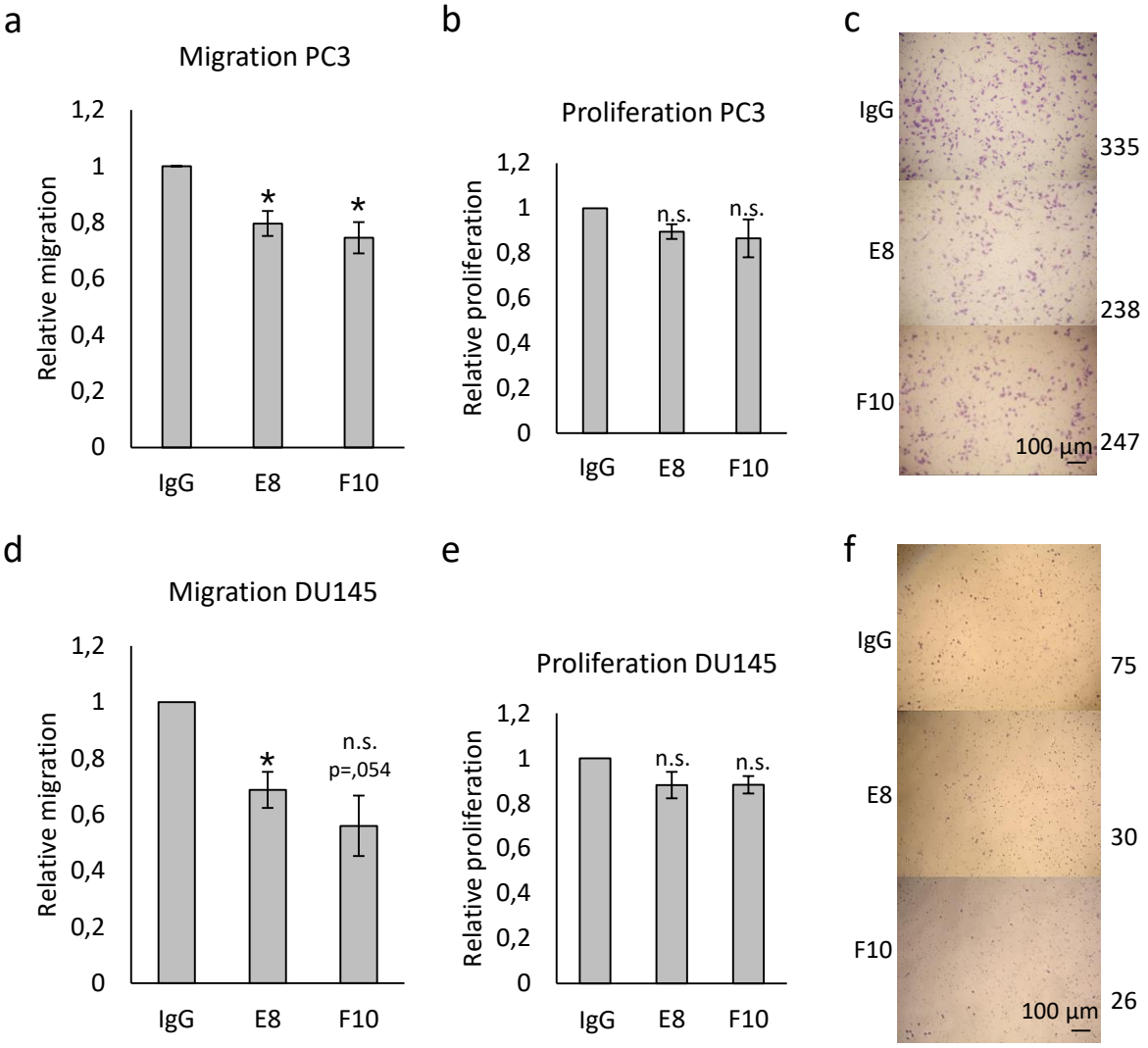

Figure 27. Transwell migration assays for prostate cancer cells treated with E8 and F10. A, D) Plots showing relative number of migrating cells treated with E8 and F10 relative to the IgG control for PC3 and DU145 cells, respectively. B, E) Plots showing effect of the treatments on proliferation as control for the migration, measured in parallel to the migration assay for PC3 and DU145 cells, respectively. C, F) Representative pictures of the membrane of the inserts with number of migrated cells for each treatment for PC3 and DU145 cells, respectively. Migration assays were performed for 24 h using 10 µg/ml of antibody. Statistical differences are calculated comparing to the IgG-treated control condition.

In addition, Matrigel-coated transwell invasion assays were carried out with C4-2B-WNT11 Wnt-11 overexpressing cells. Wnt-11 high expressing cells, when compared to control (C4-2B-V), showed a greater invasion capacity (Figure 28). Moreover, this Wnt-11-driven increase in invasion, could be abolished upon E8 and F10 treatments.

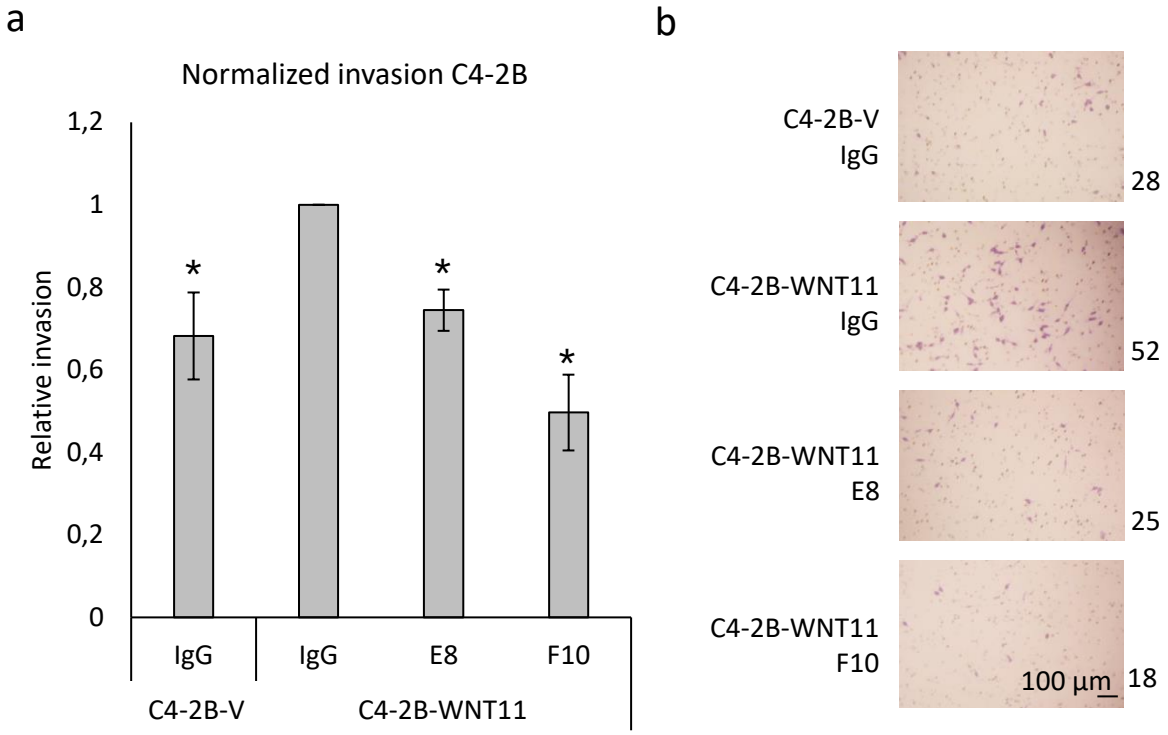

Figure 28. Transwell invasion assays of C4-2B-V and C4-2B-WNT11 cells treated with E8 and F10. A) Plot showing number of invading C4-2B-V and C4-2B-WNT11 cells treated with E8 and F10 relative to the IgG-treated cells and normalized to the proliferation control. B) Representative pictures of the invasion inserts with number of invading cells for each treatment. Invasion assays were performed for 48 h using 10 µg/ml of antibody. Statistical differences are calculated comparing to the C4-2B-WNT11 IgG-treated control condition.

II.3. Anti-Wnt-11 monoclonal antibodies inhibit hypoxia-induced migration of prostate cancer cells

Based on previous reports of Wnt-11 expression being upregulated in cells cultured under hypoxic conditions and that this drives migration in several cancer cell types (Mori et al., 2016), the investigation into the role of Wnt-11 in hypoxia-conditioned PC3 cells was pertinent. First, a marked Wnt-11 upregulation at the protein level was detected upon treatment with the hypoxia mimetic DMOG (dimethyloxaloylglycine) both at the standard dose of 1 mM and at the lower dose of 0.2 mM (Figure 29a). As controls, the expression levels of known hypoxia-related genes (HIF-1α, HIF-2α) were determined and found to be similarly upregulated (Figure 29b). To prove the specificity of Wnt-11 induction, gene silencing of *WNT11* in DMOG treated cells was performed and abolished Wnt-11 upregulation, as expected (Figure 29c). Notably, silencing prior to DMOG treatment was important for Wnt-11 levels to be reduced effectively.

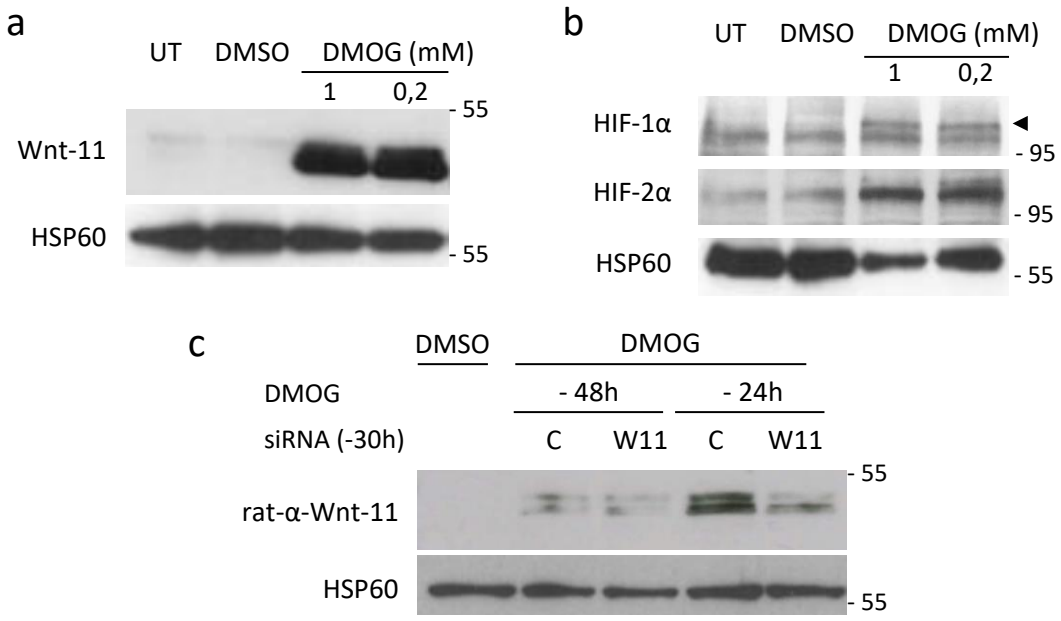

Figure 29. Analysis of Wnt-11 protein expression upon treatment with the hypoxia mimetic DMOG. A) Representative western blot of PC3 cells treated with DMOG at 1 mM and 0.2 mM final concentrations, control (DMSO) and untreated (UT) probed with a goat anti-Wnt-11 antibody and loading control HSP60. B) Western blot for HIF-1α (indicated by black arrowhead), HIF-2α and loading control HSP60 in same protein extracts of PC3 cells shown in (A). C) Western blot of PC3 cells silenced for *WNT11* (si-WNT11) or control (si-C) treated with DMOG at 0.2 mM or vehicle control (DMSO) at the indicated times probed with a rat anti-Wnt-11 antibody and loading control HSP60. DMOG and siRNA were added at the times indicated in the figure relative to harvesting (the 0 h timepoint). DMOG - dimethyloxaloylglycine.

In a further inquiry, the expression levels of other noncanonical Wnt signaling components were measured by RT-PCR in DMOG-treated PC3 cells (Figure 30a). In accordance with the protein levels being increased, *WNT11* mRNA was upregulated upon DMOG treatment. *FZD8*, which has been identified as a major receptor for Wnt-11 in prostate cancer (Murillo-Garzón et al., 2018), was found to be also upregulated,. Although not statistically significant, *ATF2* expression, a component and target of Wnt-11/ATF2 signaling, showed a trend for a modest upregulation. *HIF2A* mRNA also showed a trend for upregulation, but this was not statistically significant.

For a wider view into the status of overall Wnt signaling, expression of a selected gene set of canonical Wnt signaling components and target genes was also determined (Figure 30b, c). Here, some genes showed a clear upregulation (*AXIN2*), while others trended down (*LEF1*, *DKK1*, *NKD1*, *LRP6*). However, the latter effects were not always significant nor dose dependent. Overall, these results suggested that Wnt/β-catenin signaling is not generally altered, whereas Wnt-11/FZD8/ATF2 signaling could be elevated, being Wnt-11 and its pathway partners the main players among Wnt signaling components under hypoxia conditions. This analysis highlights the complexity and intricacy of Wnt signaling in the prostate cancer hypoxic response.

Given that hypoxia-induced Wnt-11 has been reported to impact cell migration in other cancer cell models (Mori et al., 2016), transwell migration assays were carried out to determine its role in hypoxic PC3 cells. First, culture of PC3 cells under hypoxic conditions enhanced cell migration compared to migration in normoxia (Figure 31a; cells were pretreated with DMOG 0.2 mM for 24 h and transwell migration was performed overnight at 1% O_2, see page 80 for further information). The activity of the anti-Wnt-11 antibody E8 was tested in this context. Treatment of hypoxia-conditioned PC3 cells with E8 partially reversed hypoxia-induced migration, resulting in a fold change of inhibition greater than that observed in migration assays carried out in normoxia (Figure 31a, b, e; see Figure 27a-c, page 116). The dose of E8 treatment was increased to 20 μg/ml to take into account the increased levels of Wnt-11 expression. A limited number of experiments were carried out at lower doses, which showed a trend for dose-dependency: at 10 μg/ml of antibody the treatment elicited an inhibition similar to that of 20 μg/ml and at 2 μg/ml there was no clear effect (n=2, Figure 31c). Proliferation controls of cells cultured under the same conditions of hypoxia and antibody treatment found no significant effects (Figure 31b, d).

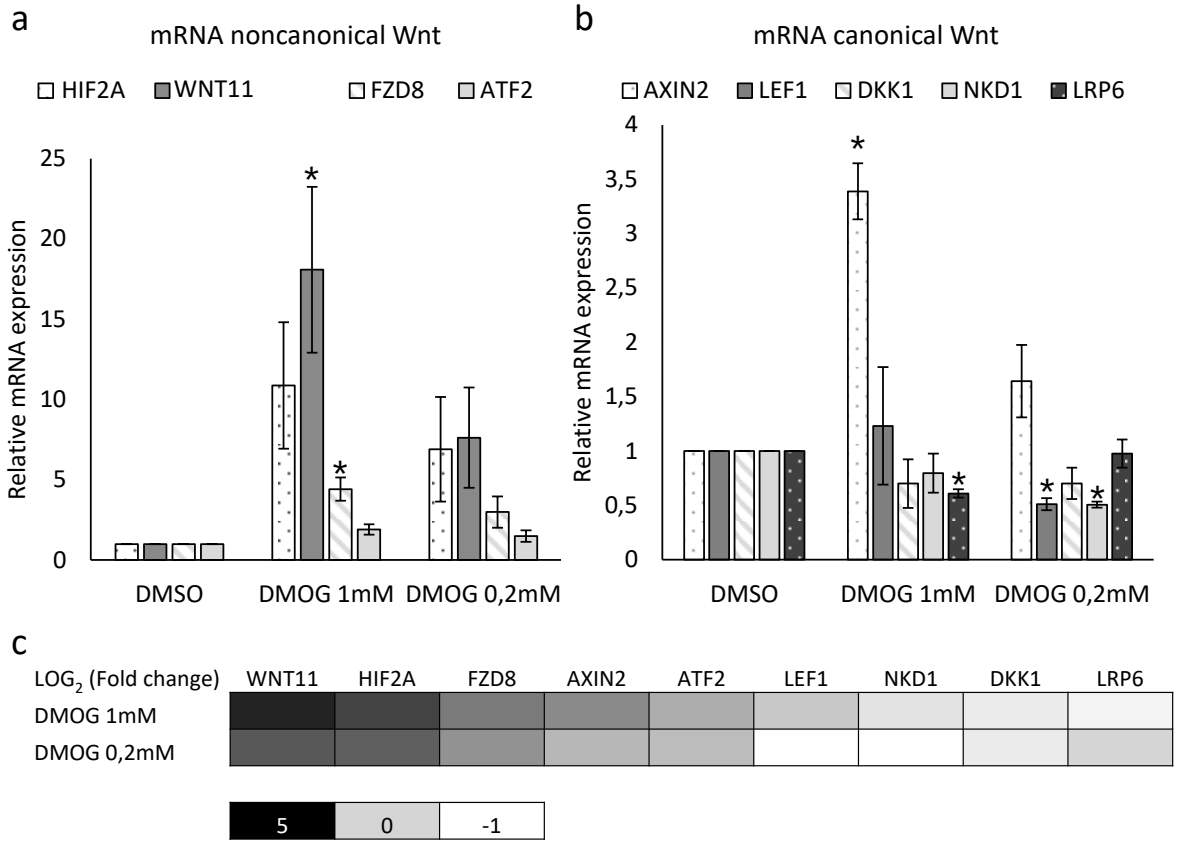

Figure 30. mRNA expression analysis of selected Wnt signaling components upon treatment with the hypoxia mimetic DMOG. A) mRNA expression in PC3 cells treated with DMOG at 1 mM and 0.2 mM relative to DMSO-treated cells of noncanonical Wnt components: *WNT11* (no-CDS primers used for RT-PCR), *FZD8* and *ATF2*, together with hypoxia target gene *HIF2A*. B) mRNA expression in PC3 cells treated with DMOG at 1 mM and 0.2 mM relative to DMSO-treated cells of canonical Wnt components: *AXIN2*, *LEF1, DKK1, NKD1* and *LRP6*. C) Heatmap showing LOG_2 of fold change values presented in (A) and (B) with noncanonical and canonical components combined and relative to vehicle control, DMSO-treated cells. mRNA was analyzed by RT-PCR 48 h post-treatments and statistical differences are calculated compared to DMSO-treated cells. DMOG - dimethyloxaloylglycine.

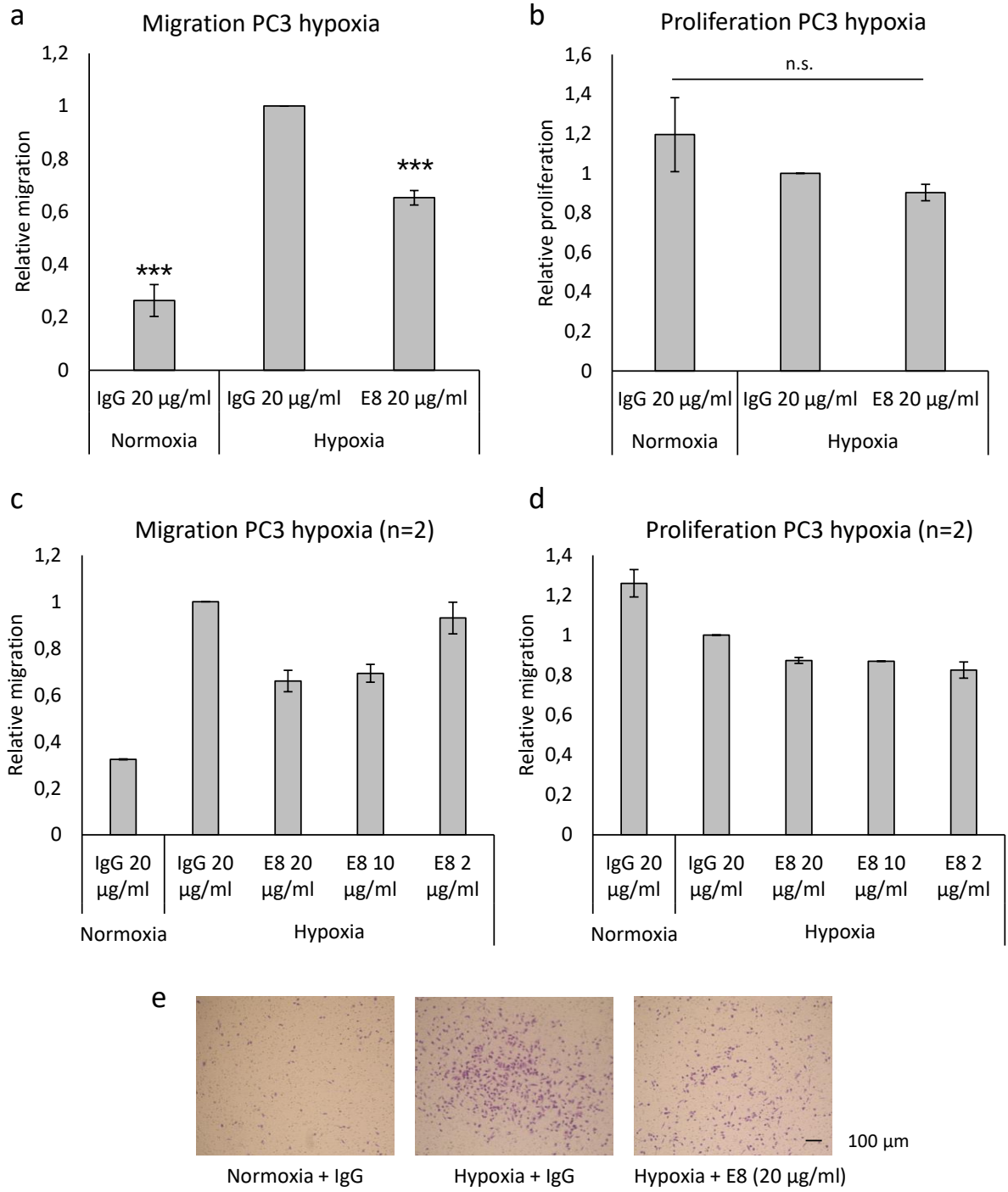

Figure 31. Transwell migration assays of PC3 cells carried out under hypoxic conditions with E8 antibody treatment. A, C) Plots showing number of migrating PC3 cells treated as indicated and relative to IgG-treated hypoxic cells, n=3 (A) and n=2 (C). B, D) Plots showing the proliferation effect of the treatments measured in parallel to the migration assay as control, n=3 (B) and n=2 (D). E) Representative pictures of the insert membranes with migrating cells treated as indicated, corresponding to the graph shown in (A). Statistical differences are calculated compared to normoxia IgG-treated cells only for n=3 experiments.

II.4. Anti-Wnt-11 functionalized magnetic nanoparticles inhibit migration of prostate cancer cells

In a parallel testing to that of the anti-Wnt-11 antibodies, the anti-Wnt-11 MNP conjugates were characterized for their effects on PC3 cell proliferation and migration. A limited number of experiments were carried out owing to the relatively short half-life of the nanoformulations and batch variability (see page 72 and Table 1 for further information). Conjugation, even when efficient, resulted in the dilution of the active antibodies. This was accounted for by increasing the concentration of the conjugated-antibody treatments for the assays, without exceeding the maximum tolerated dose of iron of 0.2 mg Fe/ml (Aires, Cadenas, Guantes, & Cortajarena, 2017; Aires et al., 2016), which was the concentration used for experiments (corresponding to approximately 7 μg/ml of antibody).

As previously reported for other cell models (Aires et al., 2016; Trabulo et al., 2017), the iron oxide nanoparticles alone (MNP-C) did not have an effect on PC3 cell proliferation in 5-7 day assays (Figure 32a). This was also the case for IgG, E8 and F10 conjugates in accordance with previous results using naked antibodies, where proliferation was only affected at high doses (20 μg/ml, see Figure 23, page 111).

To measure the effects of the antibody conjugates in migration assays, experiments were carried out in media containing 5% FBS to avoid the aggregation of the nanoparticles observed in low serum conditions (see page 108, Figure 21). Because these conditions could be incompatible with migration and invasion assays, which are performed in media containing 0.5% FBS, wound healing assays were carried out instead. A range of timepoints (24 h, 48 h) were used with the first batch of MNPs (2018), but only a pilot experiment could be performed (Figure 32b, n=1). Later, a short timepoint (8 h) was decided as optimal for testing the latest MNP batch (2021) to avoid confounding variables (e.g., possible reduced cell proliferation). A consistent reduction in the migration of cells treated with MNP-E8 compared to MNP-IgG control was determined (Figure 32b, c, d). In addition, MNP-F10 conjugates showed a non-significant trend for a similar inhibitory effect.

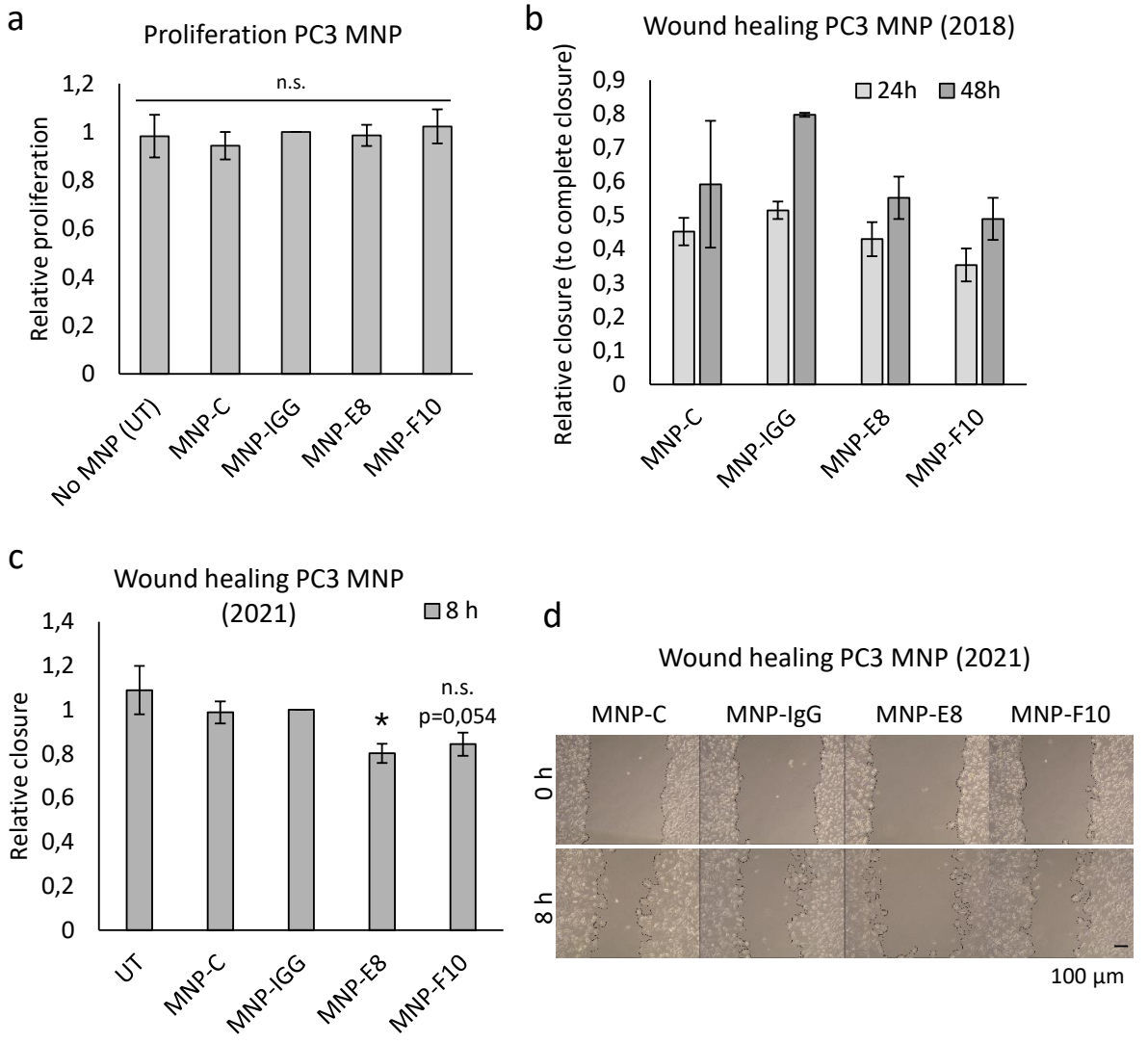

Figure 32. Proliferation and wound healing assays of PC3 cells treated with MNP nanoformulations. A) Proliferation assay in PC3 cells untreated and treated with the MNPs relative to MNP-IgG. B) Wound healing assay performed for 24 and 48 h, n=1 pilot experiment, error bars indicate SEM of the six technical replicates used in the assay. C) Wound healing assay performed during 8 h, error bars indicate SEM of the 5 independent experiments. D) Representative pictures of the wounded area at 0 h and 8 h, corresponding to data presented in (C). UT – untreated; MNP conjugates are the following: MNP-C unconjugated; MNP-IgG, -E8 and -F10 conjugates for each of the rat antibodies. MNPs were used at 0.2 mg Fe/ml. Statistical differences are calculated comparing to the MNP-IgG control condition.

Chapter III: Effects of anti-Wnt-11 monoclonal antibodies and MNP-antibody conjugates on prostate cancer cells *in vivo*

III.1. Anti-Wnt-11 antibody E8 inhibits PC3 cell tumor growth in CAM assays

To explore the effect of antibody treatment in tumor growth in an *in vivo* model, the CAM (chick chorioallantoic membrane) system was used. For preliminary characterization, the tumors formed on the CAM upon PC3 cell engraftment, from now on called PC3 CAM tumors, were analyzed by IHC hematoxylin-eosin (H&E) staining. PC3 CAM tumors were found to be distinguishable from the CAM tissue, e.g., bigger nuclei, compacted cells (Figure 33a).

The expression of Wnt-11 in PC3 CAM tumors was also apparent by immunohistochemistry (IHC) staining (Figure 33b). It should be noted here that the *WNT11* gene in chick (*Gallus gallus*) shows a high sequence identity to human *WNT11* (>80%), and by IHC some chick CAM cells showed WNT11 positive staining, likely corresponding to the endogenous WNT11 expressed by those cells. This observation prompted the delivery of the treatment of E8 antibody locally, in a topical manner on the PC3 tumors, to minimize the quenching of the antibody by the chick WNT11.

A series of five independent experiments using a total of 26 and 25 eggs for IgG and E8 treatments, respectively, were carried out. The results indicated that, compared to treatment with IgG, E8 significantly reduced PC3 tumor growth on the CAM, as measured by tumor weight (Figure 34a) and tumor area (Figure 34b). *In ovo* images of the tumors from a representative experiment are shown in Figure 34c. Statistical analysis is shown independently for tumor weight (Table 15) and for tumor area (Table 16).

No significant change in the viability of the chick embryos was detected upon IgG or E8 treatments. For F10 treatments, an insufficient number of experiments were carried out to draw consistent conclusions. In general, F10 treatments showed a weaker effect in *in vitro* assays, so *in vivo* experiments were focused on determining the effect elicited by the E8 antibody.

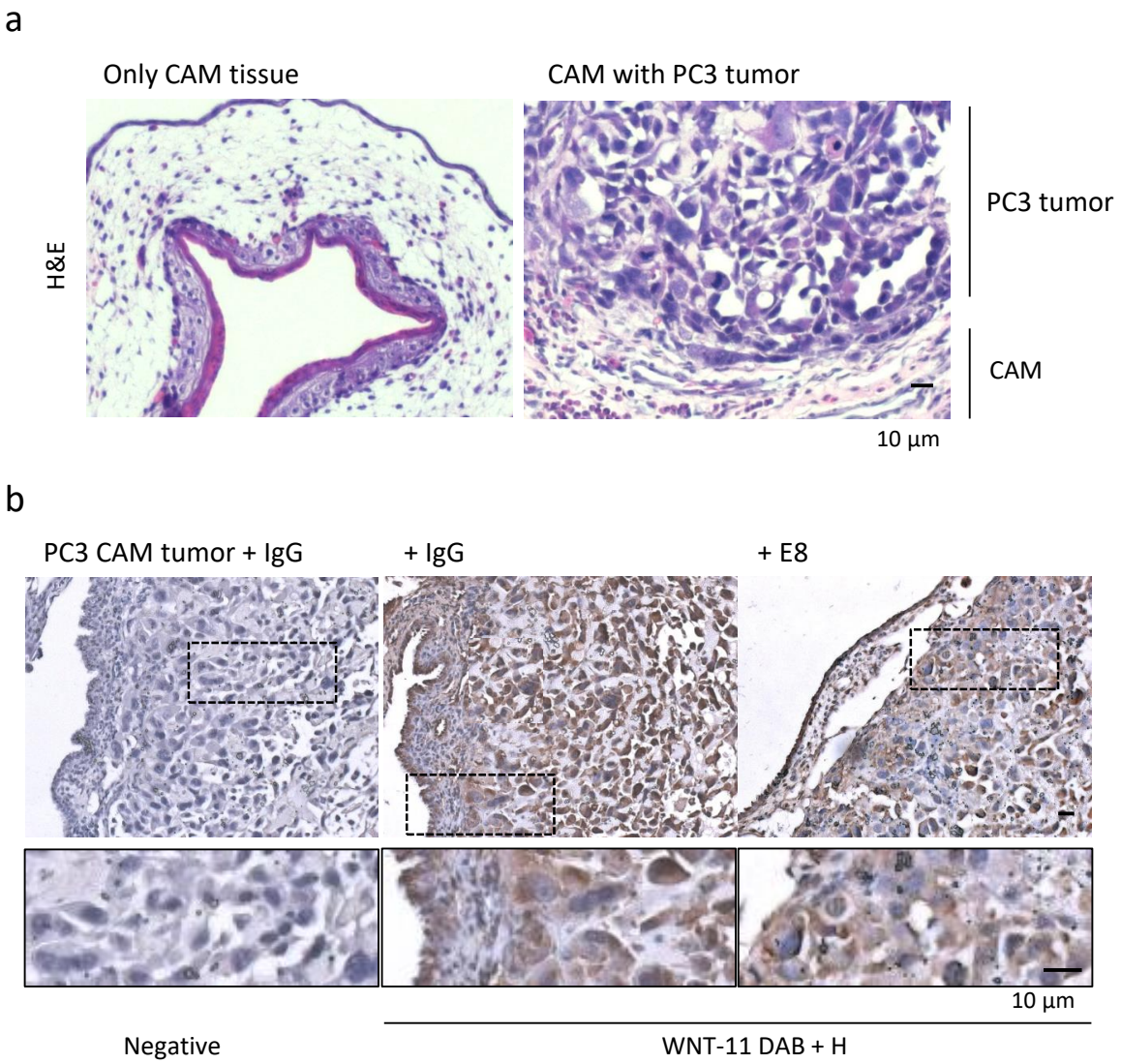

Figure 33. Histology and Wnt-11 immunohistochemistry of PC3 CAM tumors. A) Hematoxylin-eosin (H&E) staining of PC3 cell CAM engrafted tumors (right) compared to only CAM tissue (left). B) IHC staining for Wnt-11 detection (DAB + Hematoxylin) in PC3 tumors treated with IgG (middle) and E8 (right) performed with a commercial goat-anti-Wnt-11 antibody, including negative (only secondary antibody) control (left). DAB – 3,3'-Diaminobenzidine developing reagent (brown staining). H – Hematoxylin (blue/purple staining).

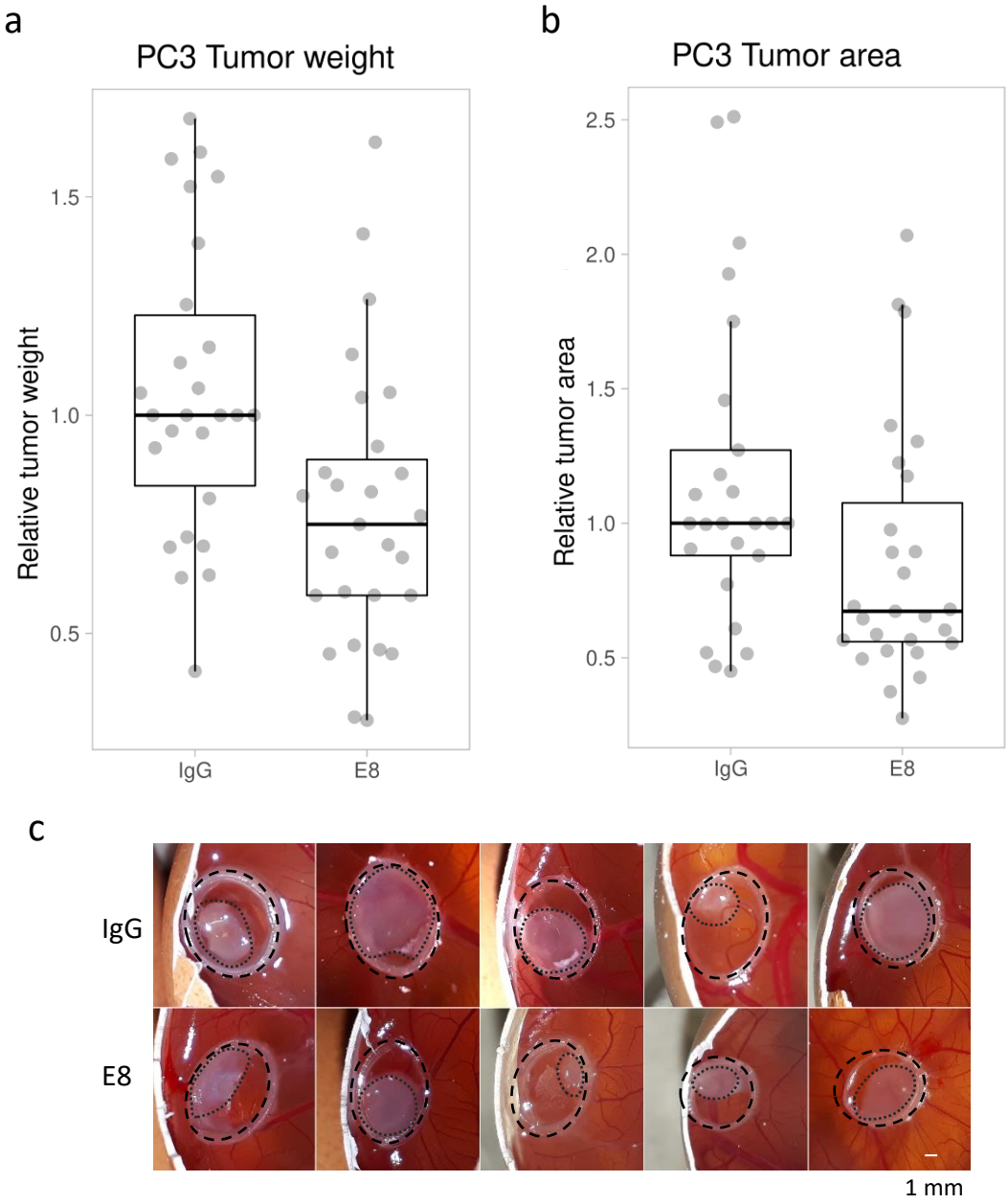

Figure 34. Effect of E8 and IgG control antibodies in PC3 tumor growth on the CAM. A) Relative normalized PC3 tumor weight boxplots for E8 treatment relative to IgG, p<.05 for the combined data, further statistical information is provided in Table 15. B) Relative PC3 tumor area boxplots for E8 treatment relative to IgG, p<.05 for the combined data, further statistical information is provided in Table 16. C) *In ovo* PC3 CAM tumor pictures at end timepoint (highlighted by a dotted line) enclosed in a plastic ring (dashed line) of approximately 6 mm diameter, from one representative CAM experiment.

Table 15. Statistical analysis of PC3 CAM tumor weight upon treatment with E8 and IgG control antibodies. Associated with Figure 34a. 95CI, 95% confidence interval; IQR, interquartile range; MAD, median absolute deviation; Q1, quartile 1; Q3, quartile 3; SD, standard deviation; SEM, standard error of the mean.

Condition	n	mean	SD	SEM	95CI mean	median	MAD	IQR	Q1	Q3	95CI median
IgG	26	1.06	0.34	0.07	0.92 - 1.19	1	0.22	0.39	0.84	1.23	0.96 - 1.12
E8	27	0.78	0.32	0.06	0.65 - 0.91	0.75	0.16	0.31	0.59	0.90	0.59 - 0.87

Table 16. Statistical analysis of PC3 CAM tumor area upon treatment with E8 and IgG control antibodies. Associated with Figure 34b. 95CI, 95% confidence interval; IQR, interquartile range; MAD, median absolute deviation; Q1, quartile 1; Q3, quartile 3; SD, standard deviation; SEM, standard error of the mean. n=25 for IgG is presented (compared to tumor weight n=26) due having lost one tumor image for technical reasons.

Condition	n	mean	SD	SEM	95CI mean	median	MAD	IQR	Q1	Q3	95CI median
IgG	25	1.16	0.58	0.12	0.91 - 1.40	1	0.23	0.39	0.88	1.27	0.90 - 1.18
E8	27	0.86	0.47	0.09	0.67 - 1.05	0.67	0.18	0.52	0.56	1.08	0.57 - 0.89

To further validate the reduction in PC3 CAM tumor growth upon E8 treatment, tumors were resected from the CAM and IHC-stained for detection of the proliferation marker Ki67. After imaging of the stained specimens, an automated measurement of nuclear Ki67 intensities were performed using Qupath (Figure 35a shows representative images). Measurements of 42-55 sections from 7-8 tumors for IgG and E8 treatments, respectively, from 2 independent CAM experiments were analyzed. E8-treated tumors were found to have reduced nuclear Ki67 intensity score, compared to control IgG-treated tumors (Figure 35b). Statistical analysis is shown independently (Table 17).

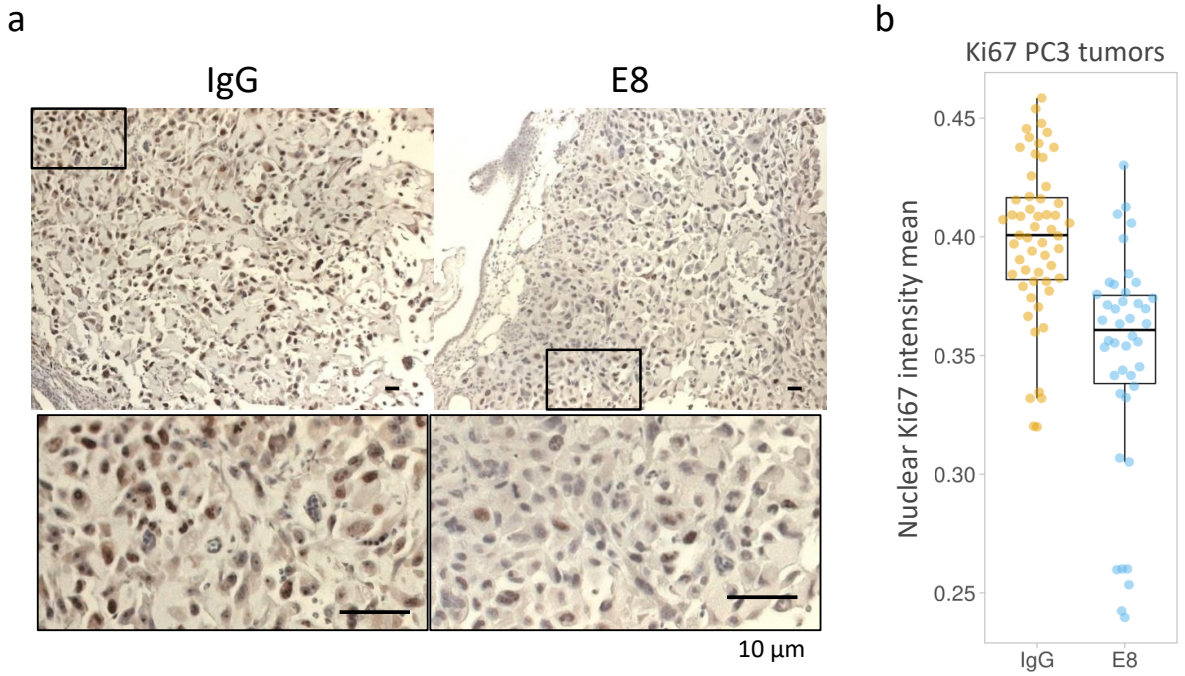

Figure 35. Proliferation marker Ki67 IHC staining of PC3 CAM tumors treated with E8 and IgG control antibodies. A) Example images of Ki67 stained specimens of PC3 CAM tumors treated with E8 or IgG. B) Boxplots showing Qupath automated quantification of nuclear Ki67-DAB intensities using 42-55 sections from 7-8 tumors from 2 independent experiments, for IgG and E8 respectively. Further statistical information is provided in Table 17.

Table 17. Statistical analysis of Ki67 IHC staining of PC3 CAM tumors treated with E8 and IgG control. Associated with Figure 35. Qupath automated quantification of nuclear Ki67-DAB intensities using 42-55 sections from 7-8 tumors from 2 independent experiments, for IgG and E8 respectively. 95CI, 95% confidence interval; IQR, interquartile range; MAD, median absolute deviation; Q1, quartile 1; Q3, quartile 3; SD, standard deviation; SEM, standard error of the mean.

Condition	n	mean	SD	SEM	95CI mean	median	MAD	IQR	Q1	Q3	95CI median
IgG	55	0.399	0.033	0.005	0.390 - 0.408	0.401	0.018	0.035	0.382	0.417	0.392 - 0.409
E8	42	0.349	0.047	0.007	0.334 - 0.364	0.361	0.019	0.037	0.338	0.375	0.349 - 0.371

III.2. Anti-Wnt-11 functionalized magnetic nanoparticles partially inhibit PC3 cell tumor growth in CAM assays

To test the activity of the anti-Wnt-11 magnetic nanoparticle (MNP) formulations *in vivo*, CAM experiments were also performed. For these experiments, with the aim of visualizing tumors more effectively, PC3-GFP expressing cells were generated and used. Tumors were imaged for GFP at the endpoint of the assay.

MNP treatments were performed as similarly as possible to those of the naked antibodies. However, the use of lower equivalent amounts of conjugated antibodies compared to naked antibodies was required (see page 94). No difference in the viability of the chick embryos was detected upon treatment with either nanoformulation, indicating they were not toxic at the doses used.

Combining 3 independent CAM experiments (one experiment with the 2020 MNP batch, two experiments with the 2021 MNP batch, see Table 1 page 74), PC3-GFP CAM tumor weight and size were examined upon treatment with the nanoformulations. There were no significant differences in between tumor growth of the controls used for the assay, with tumors treated with MNP-C and MNP-IgG being similar to each other and similar to the untreated tumors (Figure 36, statistical analyses on Table 18 and Table 19). For the anti-Wnt-11 antibody nanoformulations, MNP-E8 and MNP-F10, there was a trend for a reduction in tumor growth, with a stronger effect of MNP-E8. Pairwise comparisons determined the only significant difference was between MNP-IgG and MNP-E8 on tumor area ($p=.03$) and only when MNP-E8-treated tumors were compared to untreated tumors, a strong significant reduction was achieved for both tumor weight and tumor area ($p<.01$).

Figure 36. Effect of MNP nanoformulations on PC3-GFP tumor growth on the CAM. A) PC3-GFP tumor area boxplots for MNP treatments relative to untreated (UT), statistical information is provided in Table 18. B) PC3-GFP tumor weight boxplots for MNP treatments relative to untreated (UT), statistical information is provided in Table 19. C) *In ovo* images from a representative CAM experiment showing MNP treated PC3-GFP tumors at end timepoint. MNP conjugates are the following: MNP-C unconjugated; MNP-IgG, -E8 and -F10 conjugates for each of the antibodies. See page 94 for details on the MNP treatments.

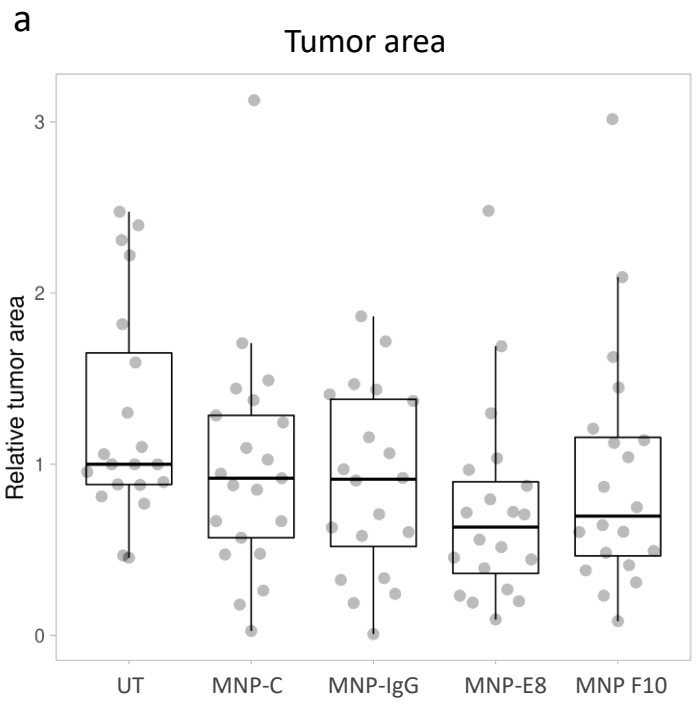
a
Tumor area
Relative tumor area
3
2
1
0
UT
MNP-C
MNP-IgG
MNP-E8
MNP F10

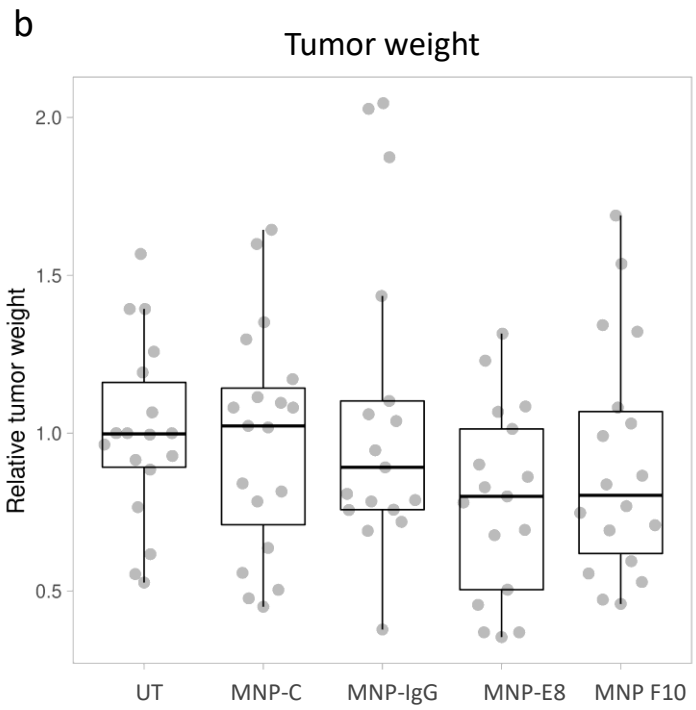
b
Tumor weight
Relative tumor weight
2.0
1.5
1.0
0.5
UT
MNP-C
MNP-IgG
MNP-E8
MNP F10

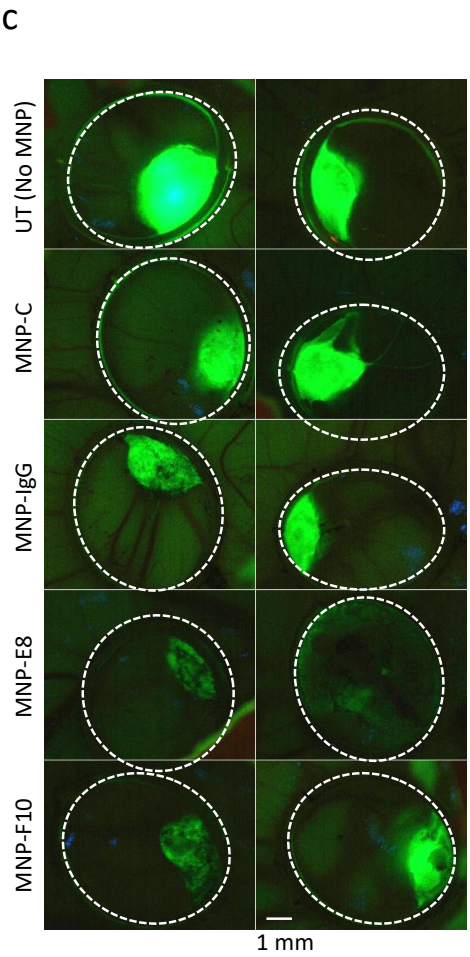
c
UT (No MNP)
MNP-C
MNP-IgG
MNP-E8
MNP-F10
1 mm

Table 18. Statistical analysis of PC3-GFP CAM tumor area upon treatments with MNP nanoformulations. Associated with Figure 36a. 95CI, 95% confidence interval; IQR, interquartile range; MAD, median absolute deviation; Q1, quartile 1; Q3, quartile 3; SD, standard deviation; SEM, standard error of the mean. UT – untreated. The slightly different number of eggs presented per condition compared to tumor weight (Table 19) is due to having lost some tumor images for technical reasons.

Condition	n	mean	SD	SEM	95CI mean	median	MAD	IQR	Q1	Q3	95CI median
UT	17	1.18	0.51	0.13	0.91 - 1.45	1	0.12	0.42	0.88	1.3	0.88 - 1.3
MNP-C	17	0.92	0.37	0.09	0.73 - 1.12	0.92	0.33	0.58	0.67	1.24	0.67 - 1.24
MNP-IgG	17	0.93	0.45	0.11	0.69 - 1.17	0.92	0.34	0.77	0.6	1.37	0.60 - 1.37
MNP-E8	16	0.64	0.31	0.08	0.47 - 0.81	0.63	0.21	0.38	0.43	0.82	0.42 - 0.8
MNP-F10	16	0.82	0.40	0.10	0.60 - 1.04	0.70	0.30	0.64	0.50	1.13	0.49 - 1.12

Table 19. Statistical analysis of PC3-GFP CAM tumor weight upon treatments with MNP nanoformulations. Associated with Figure 36b. 95CI, 95% confidence interval; IQR, interquartile range; MAD, median absolute deviation; Q1, quartile 1; Q3, quartile 3; SD, standard deviation; SEM, standard error of the mean. UT – untreated.

Condition	n	mean	SD	SEM	95CI mean	median	MAD	IQR	Q1	Q3	95CI median
UT	18	1	0.29	0.07	0.86 - 1.15	1	0.15	0.27	0.89	1.16	0.91 - 1.13
MNP-C	19	0.98	0.36	0.08	0.80 - 1.15	1.02	0.24	0.43	0.71	1.14	0.78 - 1.11
MNP-IgG	17	1.07	0.49	0.12	0.80 - 1.33	0.89	0.17	0.34	0.76	1.1	0.76 - 1.10
MNP-E8	17	0.78	0.3	0.08	0.62 - 0.94	0.80	0.27	0.51	0.50	1.01	0.51 - 1.01
MNP-F10	18	0.90	0.37	0.09	0.71 - 1.09	0.80	0.24	0.44	0.62	1.07	0.67 - 1.04

In a preliminary IHC analysis with a limited number of MNP-treated tumor sections, a significant trend was observed for a reduction in nuclear Ki67 staining in MNP-E8-treated tumors compared to MNP-IgG-treated (Figure 37b, c), validating the previous results on tumor growth (Figure 36). The MNPs were partially visible as a light brown stain in non-DAB-stained sections, due to their iron content, and this could be also distinguished in Ki67 (DAB) stained sections (Figure 37a, b). However, to demonstrate the presence of the MNPs in the tumors more clearly, Prussian Blue staining was carried out. This analysis showed accumulation of the MNPs at the site of the tumors apparently not in contact with the CAM tissue. This is likely because the MNPs were applied topically and corresponds to the apical side of the tumors. Nevertheless, some penetration of the nanoformulations further into the bulk of the PC3 tumors could also be observed (Figure 37d).

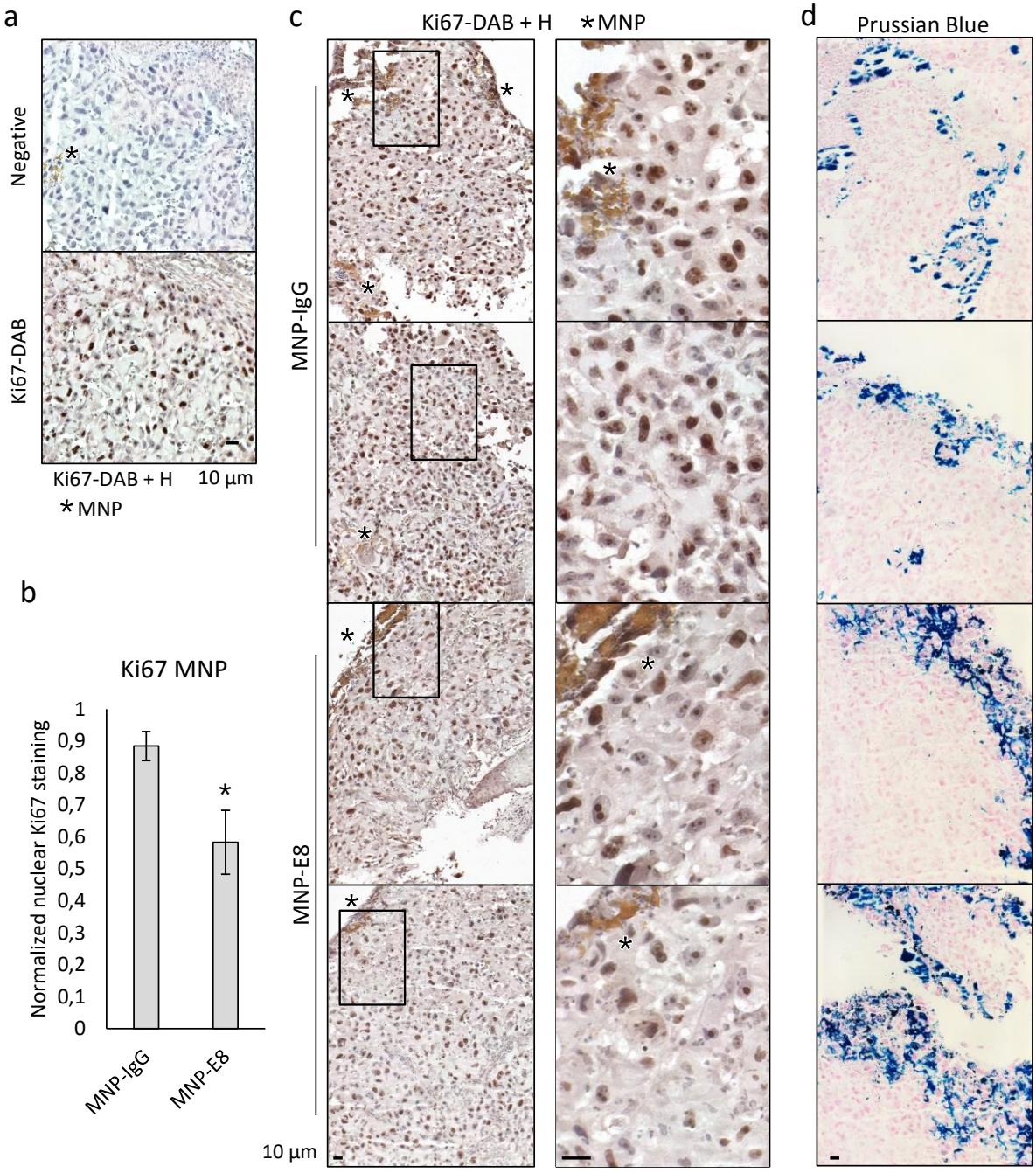

Figure 37. IHC of Ki67 and Prussian Blue stainings in PC3-GFP CAM tumors treated with MNP-IgG and MNP-E8. A) Example images of Ki67 stained MNP-treated PC3-GFP CAM tumor sections and negative (only secondary) control, which shows weak brown staining owing to the presence of MNPs highlighted by *. B) Plot showing Qupath automated quantification of nuclear Ki67 intensity from 4 sections corresponding to 2 tumors from one CAM experiment. C) Images at low (left) and high magnification (right) of Ki67 stained specimens of PC3-GFP CAM tumors treated with MNP-IgG control (top two rows) or MNP-E8 (bottom two rows), MNPs are highlighted by *. D) Prussian Blue histochemical staining to detect iron contained in the MNPs in the PC3-GFP CAM tumors treated with MNP-IgG control (upper two rows) or MNP-E8 (bottom two rows).

Chapter IV: Mechanism of action of anti-Wnt-11 monoclonal antibodies

IV.1. Anti-Wnt-11 antibodies interfere with Wnt-11 signaling through DVL and ATF2

Given the inhibitory effects the anti-Wnt-11 antibody treatments had on prostate cancer cell sphere formation, migration, invasion, and CAM tumor growth, it was pertinent to investigate the impact of antibody treatment on Wnt-11 signaling.

To this end, western blotting was used to examine the phosphorylation status of DVL. Phosphorylation of DVL is regarded as an indication of Wnt signaling activation, for canonical and noncanonical pathways (Gonzalez-Sancho, Brennan, Castelo-Soccio, & Brown, 2004). When DVL is phosphorylated, it migrates as a doublet in SDS-PAGE, in which the upper or shifted band, that presents reduced mobility is predicted to correspond to the phosphorylated form (p-DVL).

Treatment of PC3 cells with anti-Wnt-11 monoclonal antibodies significantly reduced the levels of the upper bands of DVL2 and DVL3, compared to the IgG-treated control (Figure 38 a, b, d). PC3 cells treated with Wnt-C59, which blocks Wnt secretion and signaling, abolished the DVL shift, suggesting that the basal level of shifted DVL was the result of endogenous Wnt signaling activity (Figure 38c). Given that *WNT11* knock-down has been reported to alter *DVL2* mRNA levels (Nagy et al., 2016), *DVL2* mRNA expression was measured upon *WNT11* gene silencing and E8 antibody treatment in PC3 cells. This was not altered by either condition (Figure 38 e, f). These results suggest that the effect of Wnt-11 antibodies is not mediated through changes in *DVL*2 mRNA, with the regulation rather taking place at the protein level.

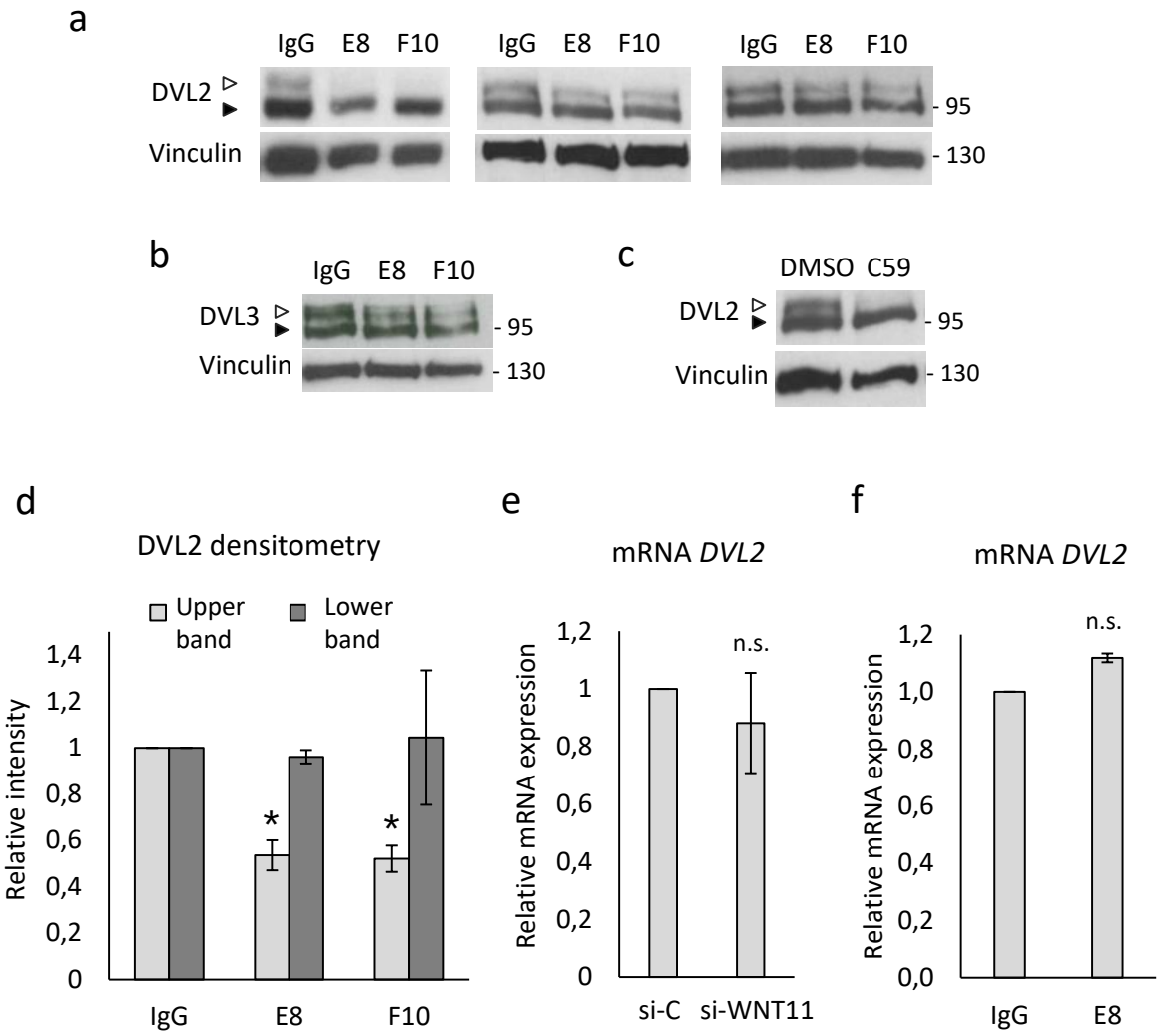

Figure 38. DVL status upon anti-Wnt-11 antibodies treatment in PC3 cells. A) Western blots for DVL2 mobility shift in antibody treated PC3 protein extracts, 3 independent experiments shown. B) Representative western blot for DVL3 mobility shift in antibody treated PC3 protein extracts. C) Representative western blot for DVL2 mobility shift in Wnt-C59 treated PC3 cell protein extracts. D) Densitometry values from DVL2 western blots shown in (A) for upper and lower DVL bands, statistical differences are calculated comparing to IgG-treated control. E) mRNA analysis of *DVL2* upon *WNT11* gene silencing (si-WNT11) for 48 h compared to control siRNA (si-C) transfected PC3 cells. F) mRNA analysis of *DVL2* upon E8 treatment for 24 h compared to IgG-treated PC3 cells. Antibody treatments were performed overnight at 10 µg/ml and Wnt-C59 treatment was done overnight at 100 nM. Black arrowheads indicate lower DVL bands, predicted to correspond to the non-phosphorylated-DVL and white arrowheads indicate upper DVL bands, predicted to correspond to the phosphorylated-DVL.

To asses downstream signaling, an ATF2-dependent luciferase (ATF2-luc) reporter was used (Ohkawara & Niehrs, 2011) (see Luciferase-based Wnt gene reporters, page 45). A similar ATF2-based reporter (1x), which contains only one copy of the ATF2 responsive sequences (vs. ATF2-luc which contains 2), was also used to allow for the correction of the signal using a control reporter containing mutations in the ATF2 binding site (mt5) (Bruhat et al., 2000).

Wnt-11 overexpression in PC3 cells induced an increase in ATF2-luc activity (1x/mt5; Figure 39a). However, the reduction of the basal activity of the reporter in these cells upon antibody-mediated inhibition of Wnt-11 was more difficult to achieve, with E8 only reducing slightly this activity (Figure 39b).

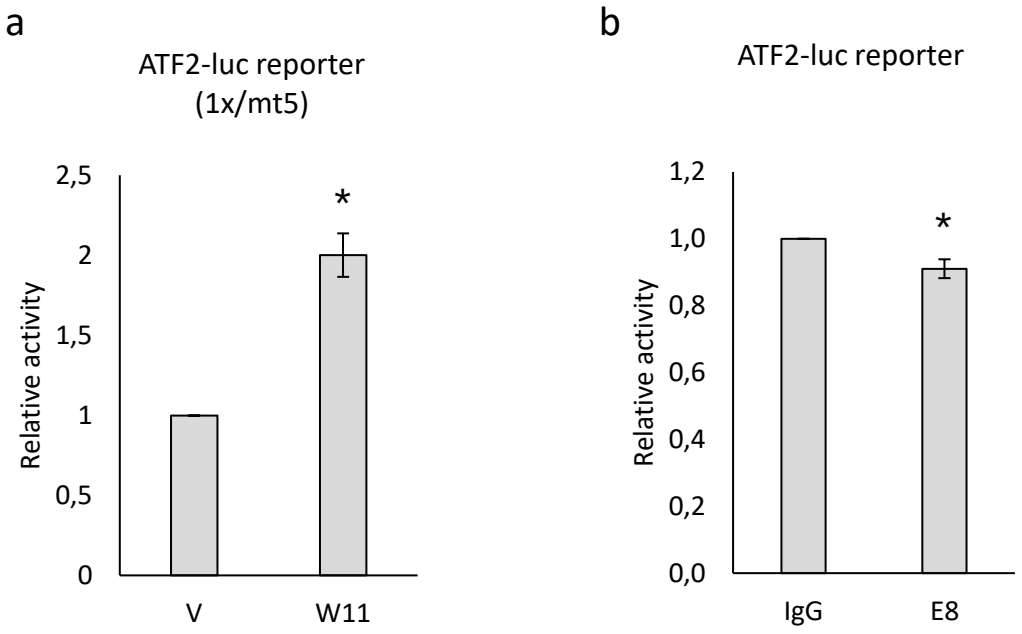

Figure 39. Effect of Wnt-11 ectopic expression and E8 treatment on ATF2-luc reporter activity in PC3 cells. A) 1x/mt5 reporter activity (corrected ATF2-luc signal) in Wnt-11 (W11) transfected PC3 cells relative to vector (V) transfected cells measured 24 h post-transfection. B) ATF2-luc reporter activity in PC3 cells after 16 h of E8 treatment (10 µg/ml) relative to IgG-treated control, 14 independent experiments combined.

IV.2. The antibody epitope is required for Wnt-11 mediated migration and signaling

IV.2.1. Molecular characterization of the antibody epitope deletion mutant

Taken together, the results so far indicate that blocking Wnt-11 using the antibodies E8 and F10 had an impact on Wnt-11 function and signaling. Because both antibodies target the same known epitope in Wnt-11, it was pertinent to assess the role of this region in its function. To this end, site-directed mutagenesis of the *WNT11* gene encoded in the plasmids used for ectopic expression (see Table 4, page 77) was carried out to partially delete the antibody epitope region, thus generating the antibody epitope deletion mutant Wnt-11Δ L101-T108 (referred to as *AE* from now on).

Locating the epitope in a protein sequence alignment of human Wnts, revealed that it laid in a region with relatively low sequence similarity among the Wnt family members (Figure 40a). Based on sequence conservation, the epitope may be divided into two parts, a first part less conserved (Figure 40a, red colored, `LLDLERT`) and a second part that is more similar in all Wnts (Figure 40a, orange colored, `RESA`).

The alignment also facilitated locating the epitope in a structural context, based on the alignment to human Wnt-3, for which there is a crystal structure (Hirai et al., 2019). The epitope is in the apical region of the "palm" of the Wnt, far from FZD interacting domains (Figure 40b, "thumb" and "index finger" regions, see also Figure 7 on page 39). The second more conserved region was engaged in secondary helix structure in the equivalent region of Wnt-3. Therefore, deletion of only the first, non-conserved region was carried out to try not to alter protein stability (Figure 40b, c, red colored sequence was mutated). V5, and PA-tagged *WNT11* containing plasmids were also mutated, which enabled some of the studies described hereafter (Figure 40d).

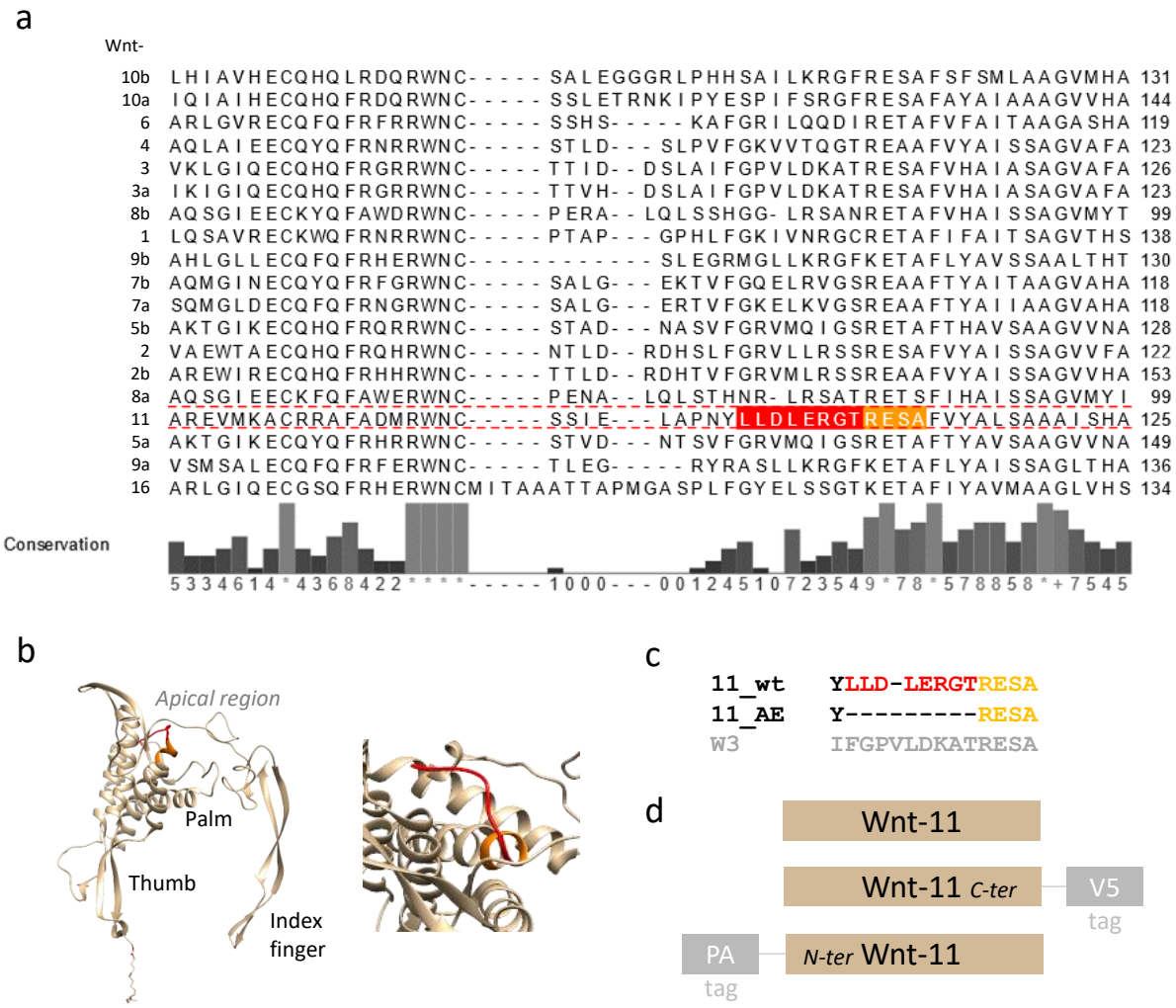

Figure 40. Antibody epitope location in Wnt sequence and structure. A) Alignment of human Wnt protein sequences showed as a partial view centered in the antibody epitope region (red, mutated; orange, not mutated in the AE). Conservation scores are provided with the alignment, showing the conservation of physico-chemical properties: conserved columns are indicated by '*' and columns with property conserving mutations are marked with a '+', see page 97. B) Location of the antibody epitope is highlighted in the equivalent region of Wnt-3 structure (beige Wnt; red, mutated; orange, not mutated), with the thumb, palm, apical region and index fingers indicated. C) Sequence of the antibody epitope deletion mutant (11_AE) compared to wild-type Wnt-11 (11_wt) and aligned to Wnt-3 (W3) for modeling of the structure shown in (B). D) Depiction of Wnt-11 protein with PA and V5 tags location. Structure retrieved from PDB: 6HAY (Hirai et al., 2019). AE - antibody epitope deletion mutant, N-ter – N-terminal, C-ter – C-terminal.

In a first molecular characterization of the Wnt-11 mutant AE, the expression at the protein level of the untagged, V5 and PA-tagged constructs was analyzed, showing a comparable expression to that of the wild-type (Figure 41a, b, c). The presence of PA-tagged Wnt-11 and AE in the conditioned media (CM) of transiently transfected HEK 293 cells was confirmed, showing similar levels of secreted protein (Figure 41d). To exclude the possibility of contaminating cells in the CM, this was also analyzed after filtration through a 0.2 µm membrane prior to being blotted.

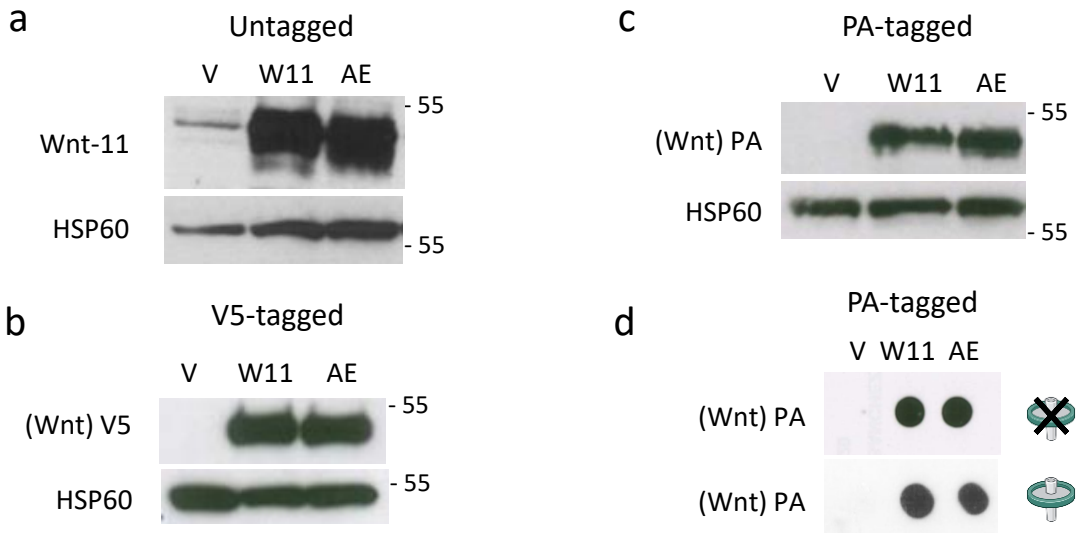

Figure 41. Antibody epitope mutant (AE) expression and secretion. A) Western blot of protein extracts from HEK 293 cells transfected with plasmids expressing untagged Wnt-11 (W11) and AE. B) Western blot of protein extracts from HEK 293 cells transfected with plasmids expressing V5-tagged Wnt-11 and AE. C) Western blot for overexpression in HEK 293 cells of PA-tagged Wnt-11 and AE. D) Dot blot of CM collected from HEK 293 cells transfected with plasmids expressing PA-tagged Wnt-11 and AE, unfiltered (upper dot blot) and filtered through a 0.2 µm membrane (lower dot blot) indicated with an illustration on the right. Dot blot of 100 µl of concentrated conditioned media. See page 90 for more details.

By cell surface immunofluorescence staining of HEK 293 cells transfected with plasmids expressing V5-tagged Wnt-11 and AE, the AE protein was observed to reach the surface of the cells, in a similar manner to wild-type Wnt-11. This indicated that the transport and localization of the AE to the cell membrane was not grossly altered (Figure 42).

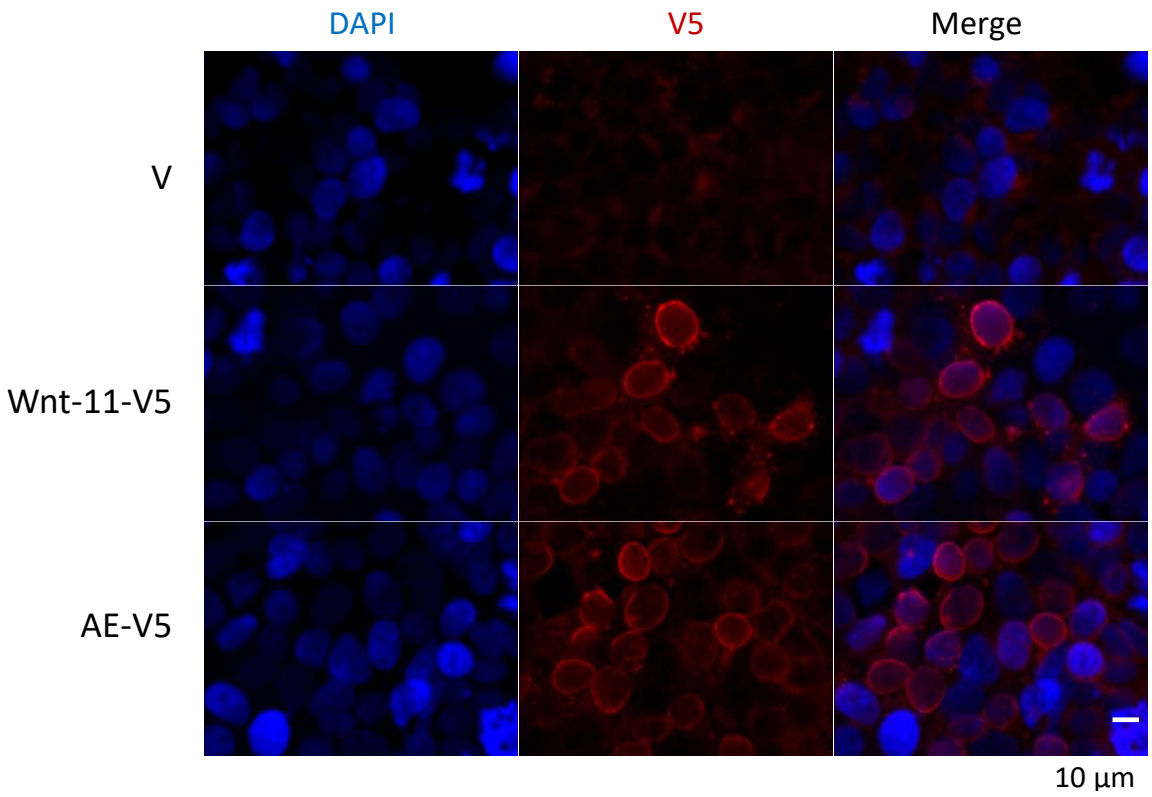

Figure 42. Cell surface immunofluorescence staining of Wnt-11 and antibody epitope mutant (AE). HEK 293 cells transfected with plasmids expressing V5-tagged Wnt-11 and AE subjected to unpermeabilized immunofluorescence staining with an anti-V5 antibody. Images show independent channels for DAPI (blue) and V5 (red) and merge.

The evidence of the AE being comparably expressed, secreted and detectable on the surface of HEK 293 cells transfected with the respective ectopic expression plasmids, indicated that the AE mutation was likely not impairing Wnt-11 overall folding, transport and release. Hence, the Wnt-11 mutant AE was used as a tool for investigating the importance of the antibody epitope for Wnt-11 signaling and function, aiding in the study of the mechanism of action of the antibodies.

To test whether the partial deletion of the epitope in the AE was sufficient to hamper recognition by E8, similar FACS experiments to those described in Figure 20 (page 106) were carried out. By these means, FACS sorting for high vs low E8 (+/-) stained populations of HEK 293 cells expressing the AE, did not produce protein cell extracts enriched for Wnt-11 protein in the E8+ sorted cells, in clear contrast with the cells expressing wild-type Wnt-11. This indicated that E8 recognition of Wnt-11 was likely impaired after deletion of this part of the epitope (Figure 43).

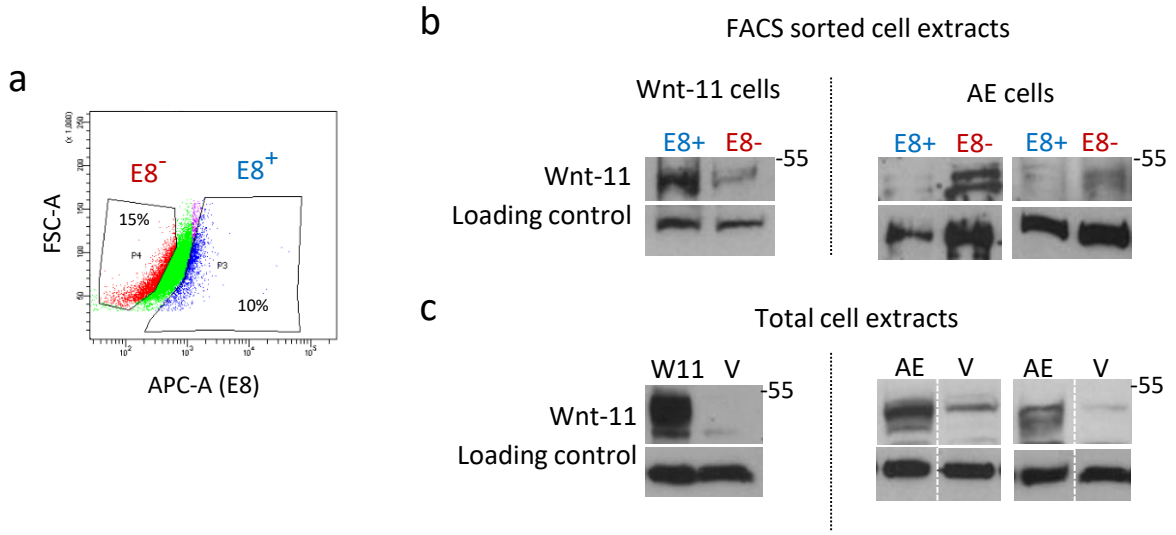

Figure 43. Detection of Wnt-11 protein levels of FACS-sorted HEK 293 cells transfected with plasmids for Wnt-11 and antibody epitope mutant (AE) expression. A) Example FACS plot for E8 staining and sorting gates of E8 high (+) and E8 low (-) cell populations for subsequent protein analysis. B) Western blots for detection of Wnt-11 protein levels in E8+ and E8- sorted HEK 293 cells expressing Wnt-11, a representative experiment shown on the left, or AE, two independent experiments shown on the right. C) Western blots of bulk/unsorted Wnt-11 or AE expressing HEK 293 cells compared to vector (V) transfected cells, corresponding to the cells of the experiments shown in (B). Western blot detection of Wnt-11 was carried out using a commercial (R&D goat) antibody and loading control corresponds to either HSP60 or GAPDH. APC (Allophycocyanin) filter was used in the FACS for the detection of E8-AlexaFluor-647. See Figure 20 (page 106) for the Wnt-11 experiment replicates.

IV.2.2. Functional role of the antibody epitope for Wnt-11-mediated prostate cancer cell migration

To analyze the functional impact of the antibody epitope mutation, PC3M cell migration assays were carried out. In concordance with previous results, showing antibody treatment reduced cell migration (see Figure 27), overexpression of Wnt-11 was found to significantly enhance PC3M cell migration (Figure 44a). In contrast, the antibody epitope deletion mutant (AE), lacking part of the region mediating the antibody interaction, did not affect migration compared to vector (V)-transfected cells. Neither overexpression of Wnt-11 nor AE significantly changed the proliferation controls carried out in parallel to the migration assay (Figure 44b). Protein extracts tested in parallel to these assays confirmed similar expression levels of Wnt-11 and AE (Figure 44c).

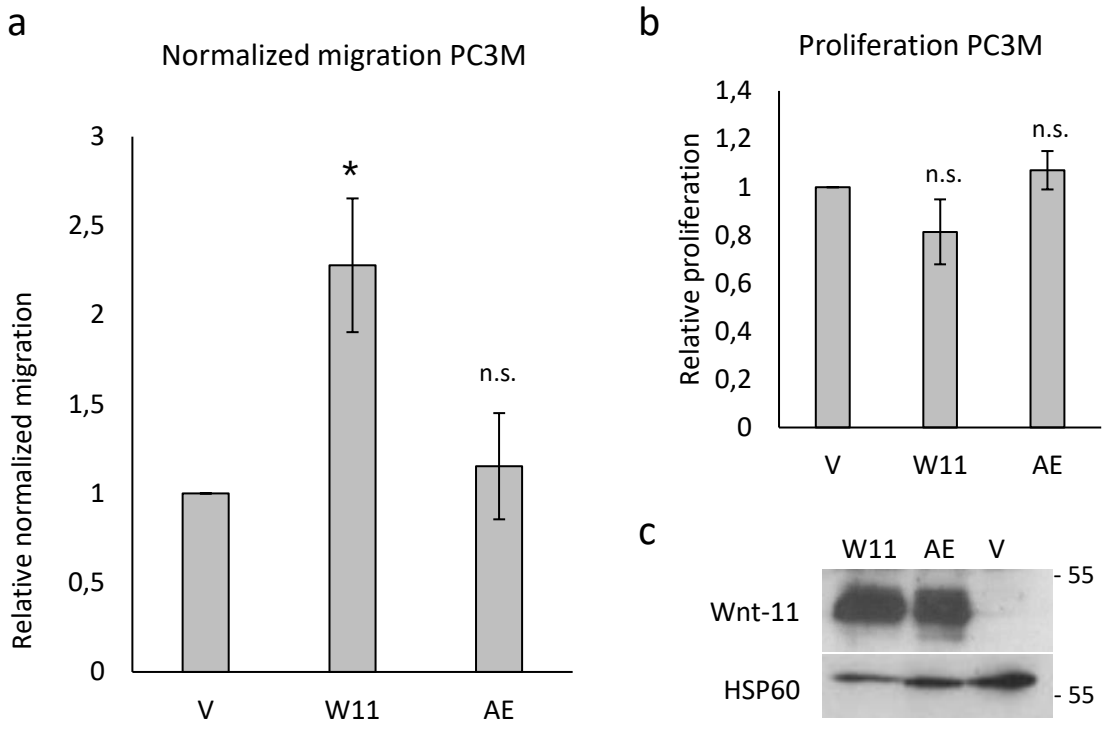

Figure 44. Transwell migration assays of PC3M cells transfected for the expression of Wnt-11 (W11) and antibody epitope mutant (AE). Migration of PC3M cells transfected with the indicated plasmids relative to vector (V) transfected cells and normalized for the proliferation controls, n=4. B) Plot showing proliferation data used to normalize migration shown in (A). C) Representative western blot for the detection of Wnt-11 and AE protein expression in extracts from cells transfected in parallel and analyzed at the experiment endpoint. Statistical differences are calculated comparing to the V-transfected condition.

IV.2.3. The potential role of the antibody epitope in Wnt-11-mediated signaling

Because the antibody epitope mutant (AE) showed a distinct phenotype from that of Wnt-11 in its capacity to induce PC3M cell migration, it was important to determine if Wnt-11 signaling was impaired by the antibody epitope mutation. This was first tested by examining the phosphorylation of DVL by mobility shift assay, which was previously found to be inhibited by anti-Wnt-11 antibody treatment (Figure 38, page 136).

Exogenous expression of Wnt-11 in HEK 293 cells increased the intensity of the DVL3 upper band, predicted to be the phosphorylated form (Figure 45a, c). In contrast, the AE was unable to induce a comparable DVL3 shift. To corroborate the Wnt-11-mediated induction of shifted DVL3, treatment of Wnt-11 transfected cells with porcupine inhibitor Wnt-C59 was carried out in combination, blocking Wnt secretion, and the shifted DVL3 was found to be abolished (Figure 45b).

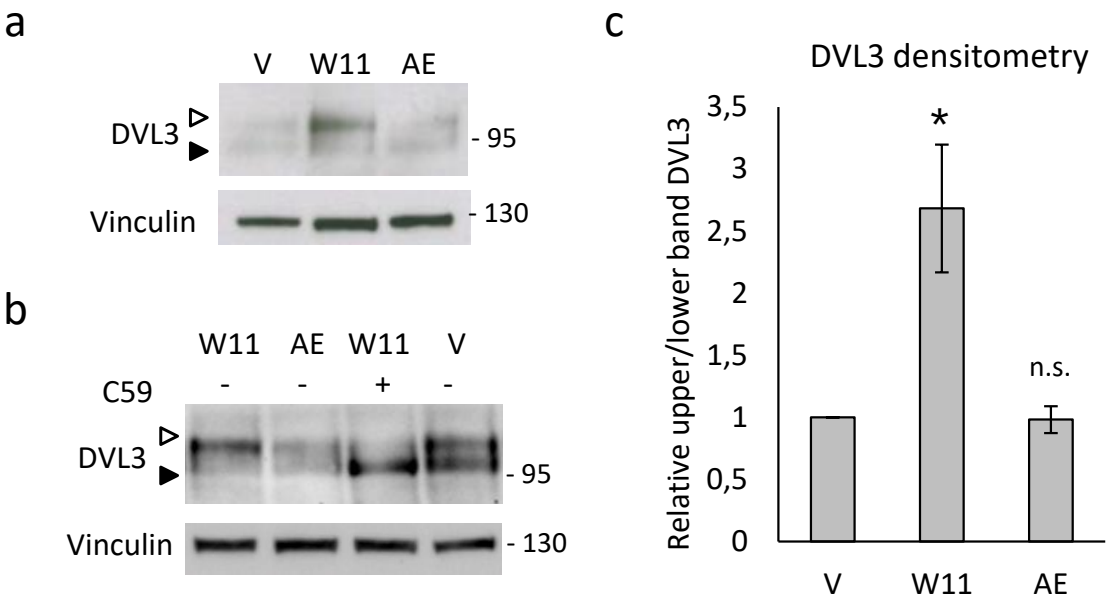

Figure 45. Effect of Wnt-11 (W11) and antibody epitope mutant (AE) ectopic expression on DVL status. A) Representative western blot for DVL3 mobility shift in HEK 293 cells transfected with plasmids for the ectopic expression of Wnt-11 (W11) and AE. B) Western blot for DVL3 mobility shift in HEK 293 transfected cells as indicated in combination with Wnt-C59 treatment. C) Densitometry values combining 4 independent experiments in PC3 and HEK 293 cells expressing Wnt-11 and AE, showing the ratio of upper to lower DVL3 bands. Protein was harvested 24 h post-transfection and Wnt-C59 treatment was performed overnight at 100 nM. Black arrowheads indicate lower DVL bands, predicted to correspond to the non-phosphorylated-DVL and white arrowheads indicate upper DVL bands, predicted to correspond to the phosphorylated-DVL. Statistical differences are calculated comparing to the V-transfected control condition.

To investigate further the role of the antibody epitope in Wnt-11 signaling, gene reporter assays were carried out. In these, the repression mediated by Wnt-11 and antibody epitope mutant (AE) of Wnt/β-catenin TCF-dependent activity was assessed. Wnt-11 expression in HEK 293 cells significantly inhibited Wnt-3a conditioned media (CM) stimulation of β-catenin/TCF-dependent gene reporter (TOP-luc, Figure 46a). In contrast, the expression of the AE was unable to repress Wnt-3a CM-induced β-catenin/TCF-dependent signaling, indicating it lacked the capacity previously shown for wild-type Wnt-11. Protein expression analysis carried out in parallel to the gene reporters showed that both Wnt-11 and AE were similarly expressed (Figure 46b).

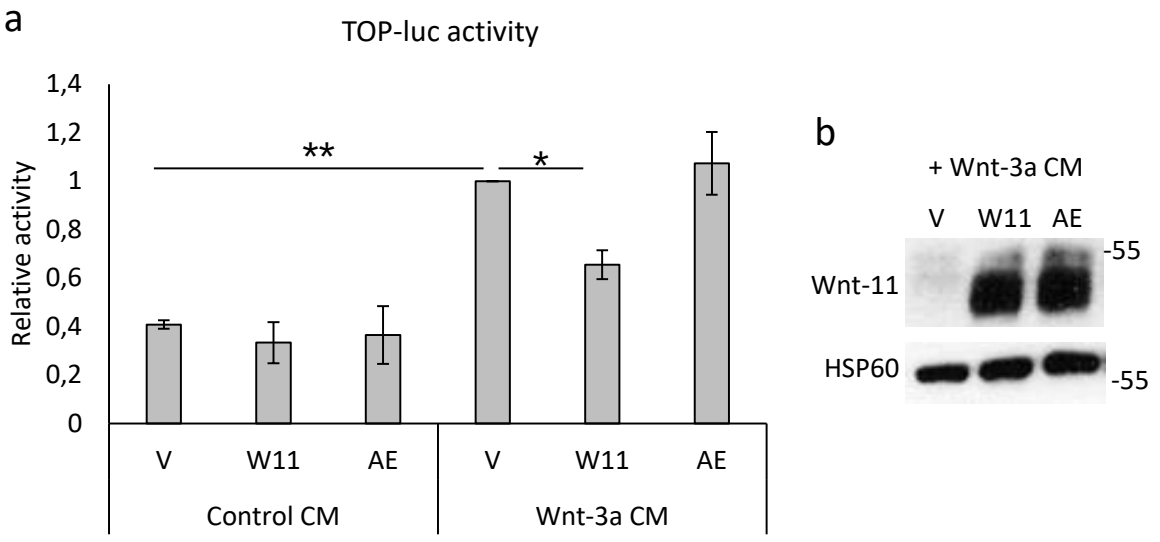

Figure 46. Effect of Wnt-11 (W11) and antibody epitope mutant (AE) ectopic expression on TOP-luc reporter activity stimulated with Wnt-3a conditioned media (CM). A) HEK 293 cells were simultaneously transfected with gene reporter plasmids, Wnt-11 (W11) and AE and 4 h later media was changed to control or Wnt-3a CM. Reporter activity was measured 24 h later. B) Western blot for Wnt-11 (W11) and AE expression analyzed in parallel to the gene reporter assays, for the Wnt-3a CM stimulated condition. Statistical differences are calculated comparing to the V-transfected +Wnt-3a CM condition as indicated, if not shown the comparison is n.s.

IV.3. The role of the antibody epitope in Wnt receptor and coreceptor binding

IV.3.1. Structural context

Given that the antibody epitope region is located outside of known Wnt receptor binding sites and has not been implicated in mediating Wnt function (see pages 38 and 46), it was pertinent to further analyze the potential implications of the epitope mutation in this context.

For this, the location of the epitope in structural context regarding Wnt receptor and coreceptor binding was studied. To this end, the human Wnt-3 protein sequence was aligned with Wnt-11 and the equivalent regions of interest were highlighted in the sequences (Figure 47a) and in the structure (Figure 47b). The epitope appears to be far from the FZD interacting regions (FZD highlighted in pale pink, interacting regions in Wnt indicated in brown), localizing to the apical region of the Wnt, which has been proposed to be involved in Wnt ternary interactions with coreceptors (Janda et al., 2012).

To extend this analysis, the predicted location of the Wnt coreceptor LRP6 interacting region is also highlighted in the structure (dark blue for linker regions, light blue for interface motifs), which several studies have proposed binds to the apical part of the Wnt (Chu et al., 2013; Hirai et al., 2019), proximal to the antibody epitope. However, there is presently no solved protein structure for a Wnt-LRP6 complex.

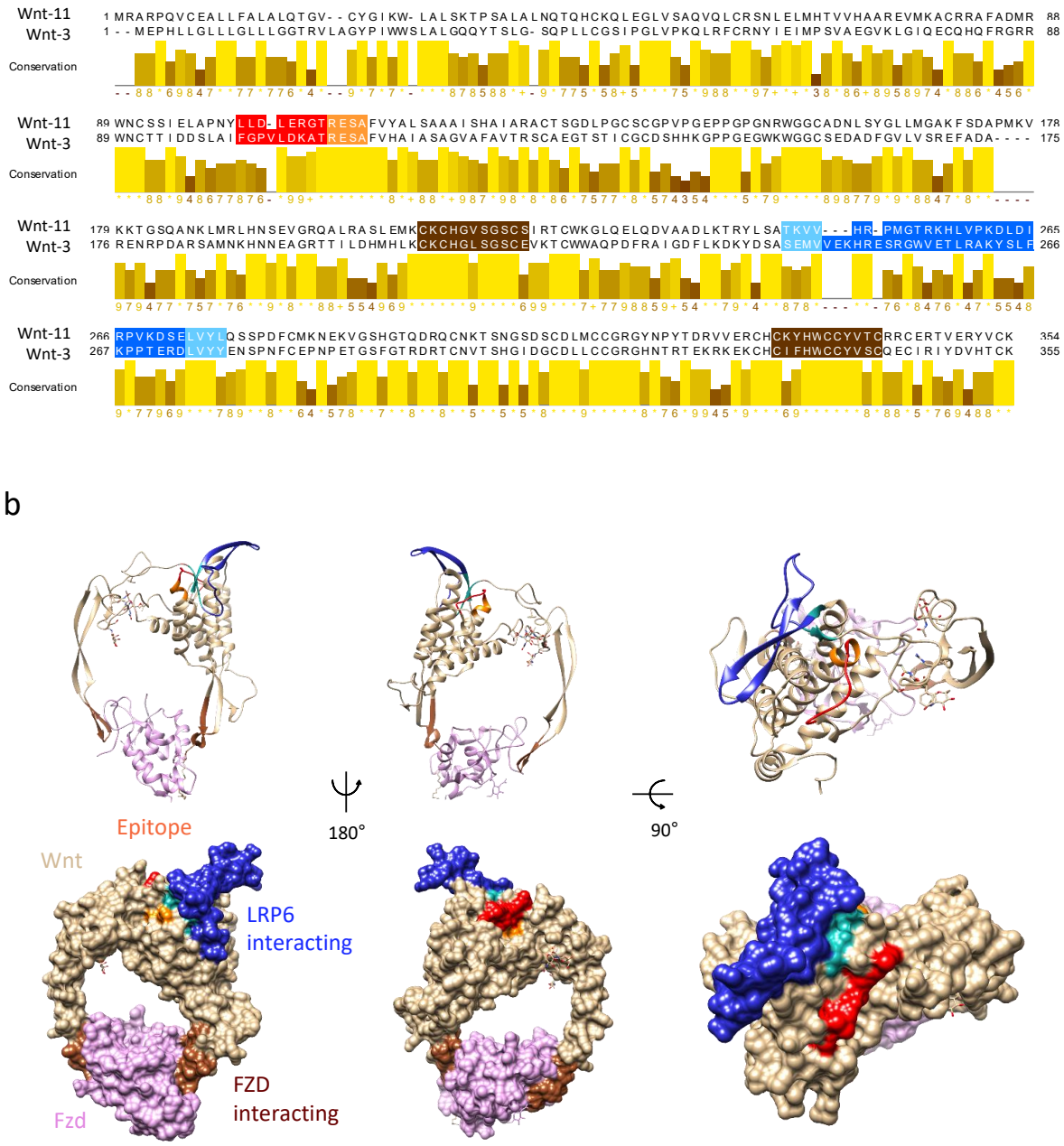

Figure 47. Structure of Wnt-3 in complex with FZD8-CRD highlighting the Wnt-11 antibody epitope region. A) Protein sequence alignment of human Wnt-11 and Wnt-3 with the antibody epitope region highlighted in red (mutated in AE) and orange (not mutated), FZD interacting regions in brown and putative LRP6 interacting region in blue (light blue for interface motifs and dark blue for linker region). Conservation scores are provided with the alignment, showing the conservation of physico-chemical properties: conserved columns are indicated by '*' and columns with property conserving mutations are marked with a '+', see page 97. B) Structure of Wnt-3 (beige) in complex with Fz8-CRD (pale pink) with the features described above highlighted. Upper panel, ribbon; bottom, surface filling structures. Structure retrieved from PDB: 6HAY (Hirai et al., 2019).

To visualize the scale and sizes of an antibody's Fab to the Wnt, a model was generated (Figure 48). For this model, the Fab was retrieved from the structure of the anti-platelet-derived growth factor (PDGF)-B monoclonal antibody (MOR8457; PDB: 4QCI, Kuai et al., 2015). The putative location and size of the antibody Fab relative to the antibody epitope in Wnt shows that the interaction might sterically hinder binding of Wnt-11 to LRP6, thus providing grounds for exploring LRP6 implication for the observed effects mediated by the anti-Wnt-11 antibodies.

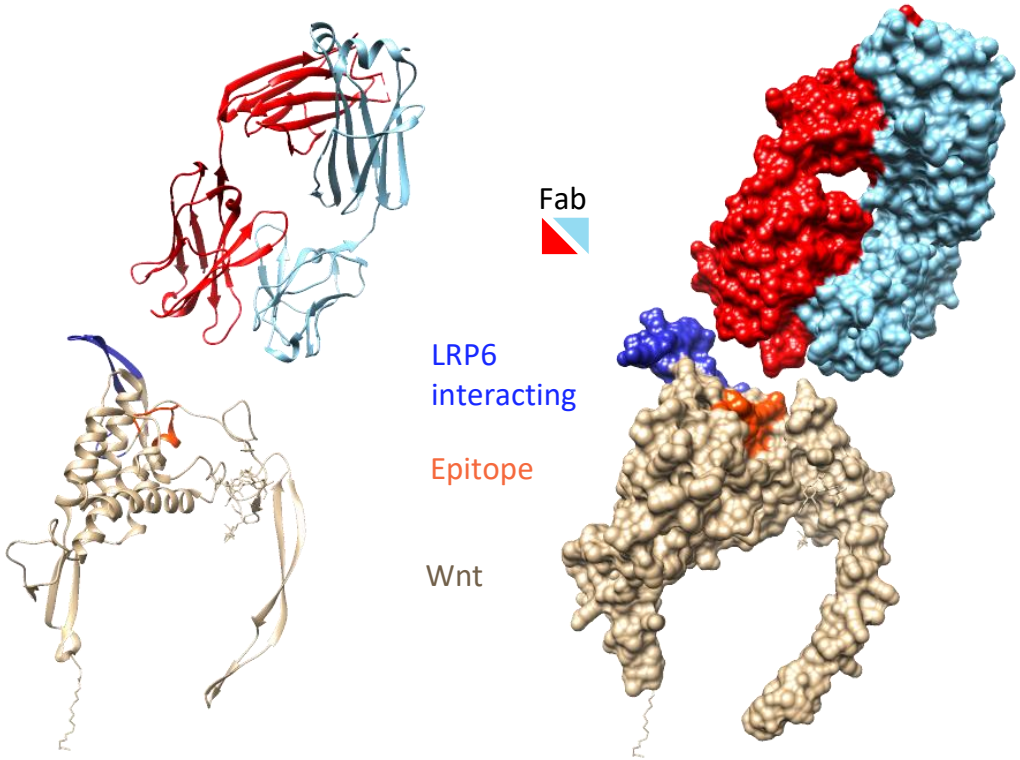

Figure 48. Juxtaposition of Wnt-3 with Fab structures. The region in Wnt-3 equivalent of the Wnt-11 antibody epitope is highlighted in orange in the Wnt-3 (beige) and the Fab is depicted in red and light blue. Ribbon (left) and surface filling (right) structures. Structures retrieved from PDB: 4QCI (Kuai et al., 2015) for the Fab of the anti-platelet-derived growth factor (PDGF)-B monoclonal antibody (MOR8457) and 6HAY (Hirai et al., 2019) for Wnt-3.

IV.3.2. Interaction of Wnt-11 and the antibody epitope mutant with FZD8

Cell-based immunoprecipitation (IP) assays were used to study the possible involvement of the antibody epitope region in Wnt-11 interaction with receptors and coreceptors. The interaction with FZD8, a known Wnt-11 receptor in prostate cancer (Murillo-Garzón et al., 2018) was assessed.

First, as expected, interaction between the FZD8 cysteine-rich domain (CRD) and Wnt-11 (PA-tagged) was readily detected (Figure 49a). However, there was no significant difference in binding of the FZD8-CRD to the antibody epitope mutant (AE), indicating that binding was of a similar magnitude to that of Wnt-11 wild-type (Figure 49b).

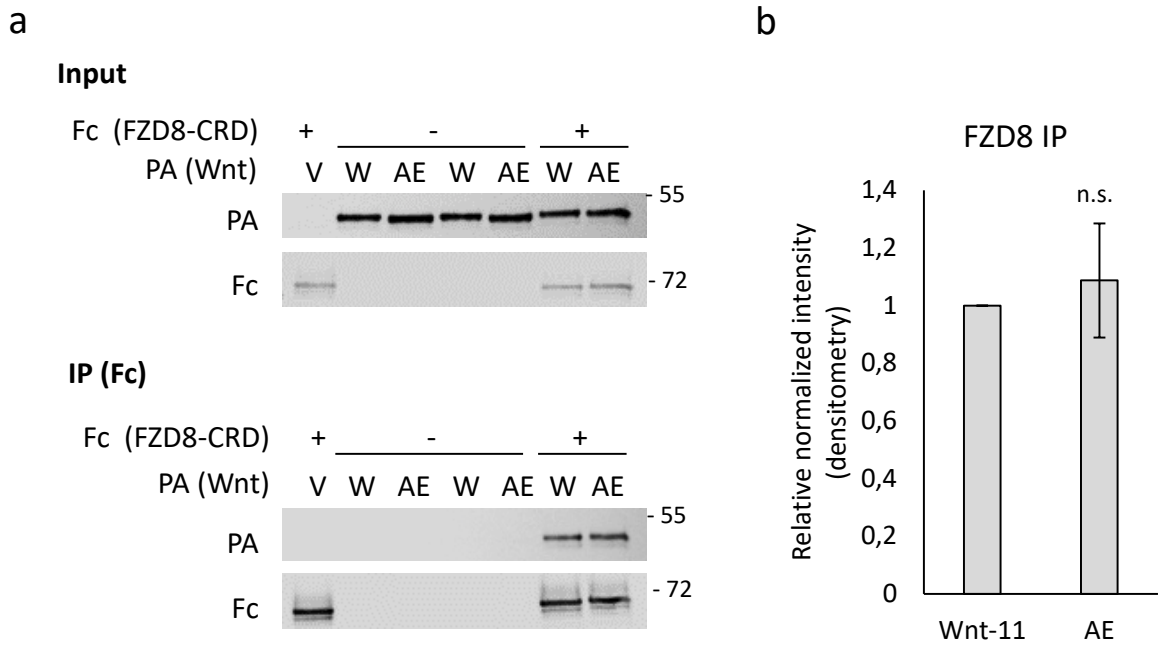

Figure 49. Immunoprecipitation of Wnt-11 (W) and antibody epitope mutant (AE) with FZD8-CRD in PC3 cells. A) Representative immunoprecipitation experiment for co-expression of Fc-tagged FZD8-CRD and PA-tagged Wnt-11 or AE, IP or pull-down of Fc; western blot for Fc and PA antibodies in inputs (total protein extracts) and IPs samples. B) Plot showing relative binding normalized for expression in inputs, as determined by western blot densitometry using data from 5 independent experiments.

IV.3.3. Interaction of Wnt-11 and the antibody epitope mutant with LRP6

Based on the proximity of the antibody epitope region to the LRP6 coreceptor putative interacting region with Wnt (page 148, Figure 47) it was pertinent to analyze its binding to Wnt-11, although LRP6 is best known for its implication in Wnt/β-catenin signaling (Joiner et al., 2013).

Immunoprecipitation experiments with an anti-PA antibody in HEK 293 cells co-expressing VSV-G-tagged full length LRP6 and PA-tagged Wnt-11 or Wnt-3a, showed that Wnt-11 co-immunoprecipitated with LRP6 (Figure 50a). This interaction was comparable to that of Wnt-3a. In a separate series of experiments, it was noted that gene silencing of *WNT11* in PC3 cells resulted in a reduction in *LRP6* gene expression (Figure 50b). This suggests that *WNT11* and *LRP6* might be co-regulated in these prostate cancer cells.

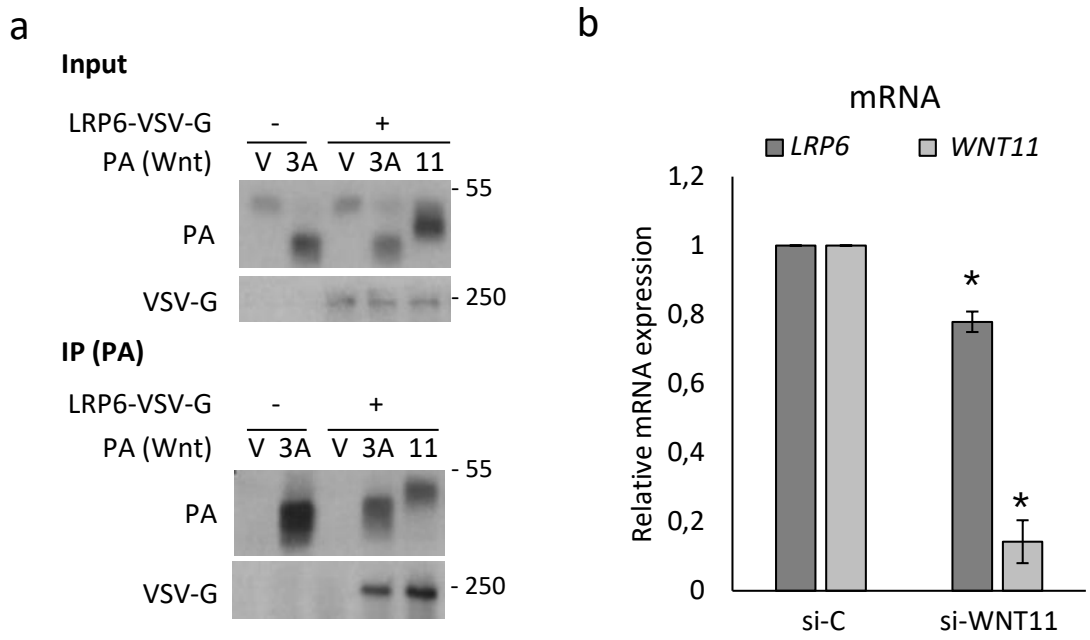

Figure 50. Analysis of Wnt-11 and LRP6 interaction and co-expression. A) Representative immunoprecipitation experiment for co-expression of VSV-G-tagged LRP6 and PA-tagged Wnt-11 (11) or Wnt-3a (3A); IP of PA, western blot with VSV-G and PA antibodies in extracts from inputs and IPs. B) Relative mRNA expression of *LRP6* and *WNT11* upon gene silencing of *WNT11* (si-WNT11) normalized to control siRNA (si-C) in PC3 cells. V - vector (pcDNA).

Similarly, immunoprecipitation experiments were carried out in HEK 293 cells transfected with plasmids for the expression of full length VSV-G tagged LRP6 in combination with PA-tagged Wnt-11 or AE. In reciprocal IP experiments to the described above, immunoprecipitation of LRP6 using an anti-VSV-G antibody also showed Wnt-11 binding (Figure 51a). The AE co-immunoprecipitated also with LRP6, however the interaction appeared weaker (Figure 51b). The extent of binding of Wnt-11 and AE to LRP6 was quantitated by densitometry from multiple immunoprecipitation assays and, after normalization to input controls (total cell extracts), AE/LRP6 interaction was found to be 47-66% weaker (based on 95CI; Figure 51b).

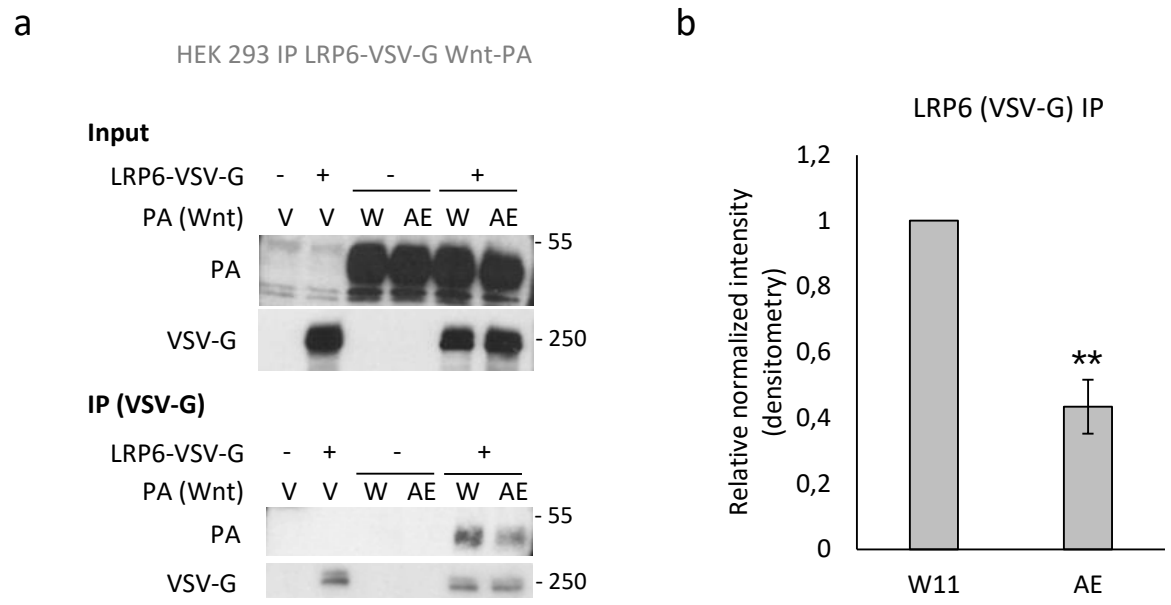

Figure 51. Immunoprecipitation of Wnt-11 (W) and the antibody epitope mutant (AE) with VSV-G tagged LRP6 in HEK 293 cells. A) Representative immunoprecipitation experiment for co-expression of VSV-G-tagged LRP6 and PA-tagged Wnt-11 (W, W11) or AE; IP of VSV-G, western blot with VSV-G and PA antibodies in extracts from inputs and IPs. B) Plot showing relative binding normalized for expression in inputs (total cell extracts), as determined by western blot densitometry, using data from 3 independent experiments. V - vector (pcDNA).

Then, given that the Wnt binding domains of LRP6 are in the extracellular region, analogous experiments were carried out using the Fc-tagged extracellular domain of LRP6 (LRP6N). There was a similar reduction in binding of the antibody epitope mutant (AE) to LRP6 compared to wild-type Wnt-11 (Figure 52a). These results were confirmed using PC3 prostate cancer cells with the untagged Wnt-11 and AE proteins (Figure 52b).

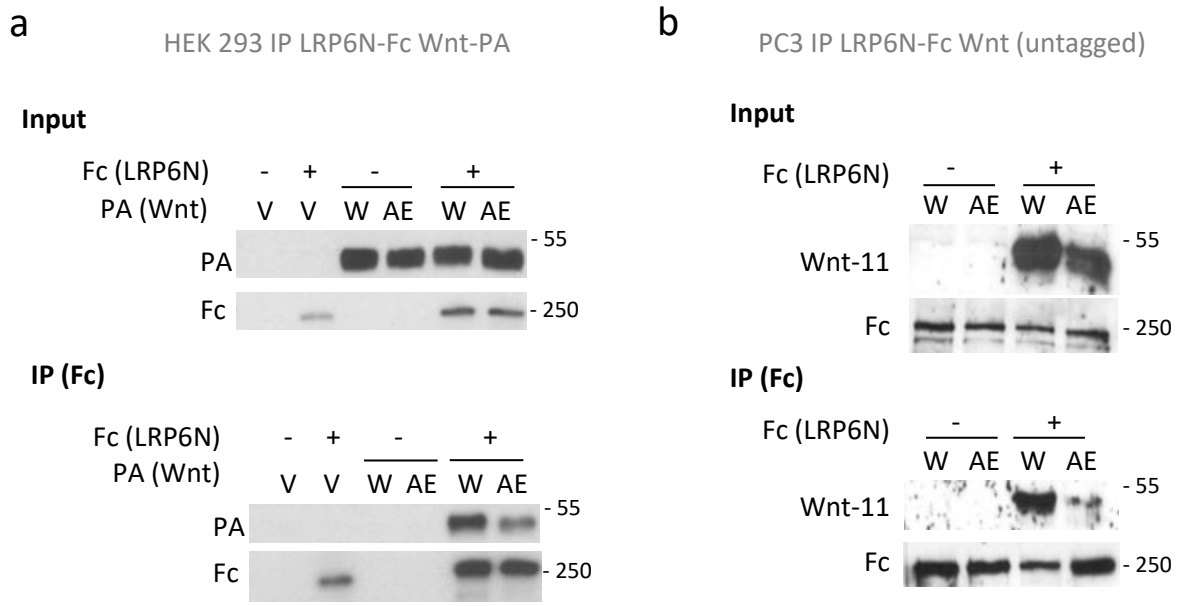

Figure 52. Immunoprecipitation of Wnt-11 (W) and the antibody epitope mutant (AE) with the Fc-tagged extracellular domain of LRP6 (LRP6N) in HEK 293 and PC3 cells. A) Representative immunoprecipitation experiment in HEK 293 cells co-expressing Fc-tagged LRP6N and PA-tagged Wnt-11 (W) or AE; pull-down of Fc (LRP6N), western blot with Fc and PA antibodies in extracts from inputs and IPs. B) Representative immunoprecipitation experiment in PC3 cells co-expressing Fc-tagged LRP6N and untagged Wnt-11 or AE; pull-down of Fc (LRP6N), western blot with Fc and Wnt-11 antibodies (using a commercial R&D goat antibody) in extracts from inputs and IPs. V - vector (pcDNA).

These results were followed up by immunofluorescence staining of PC3 cells transfected with LRP6 (VSV-G) and untagged Wnt-11 and AE. Co-localization analysis of co-expressing cells found that Wnt-11 and LRP6 co-localized (Pearson co-localization value of 0.6; Spearman 0.67) and the extent of co-localization was lower for the AE (Pearson 0.4; Spearman 0.46); a difference that was statistically significant (Figure 53).

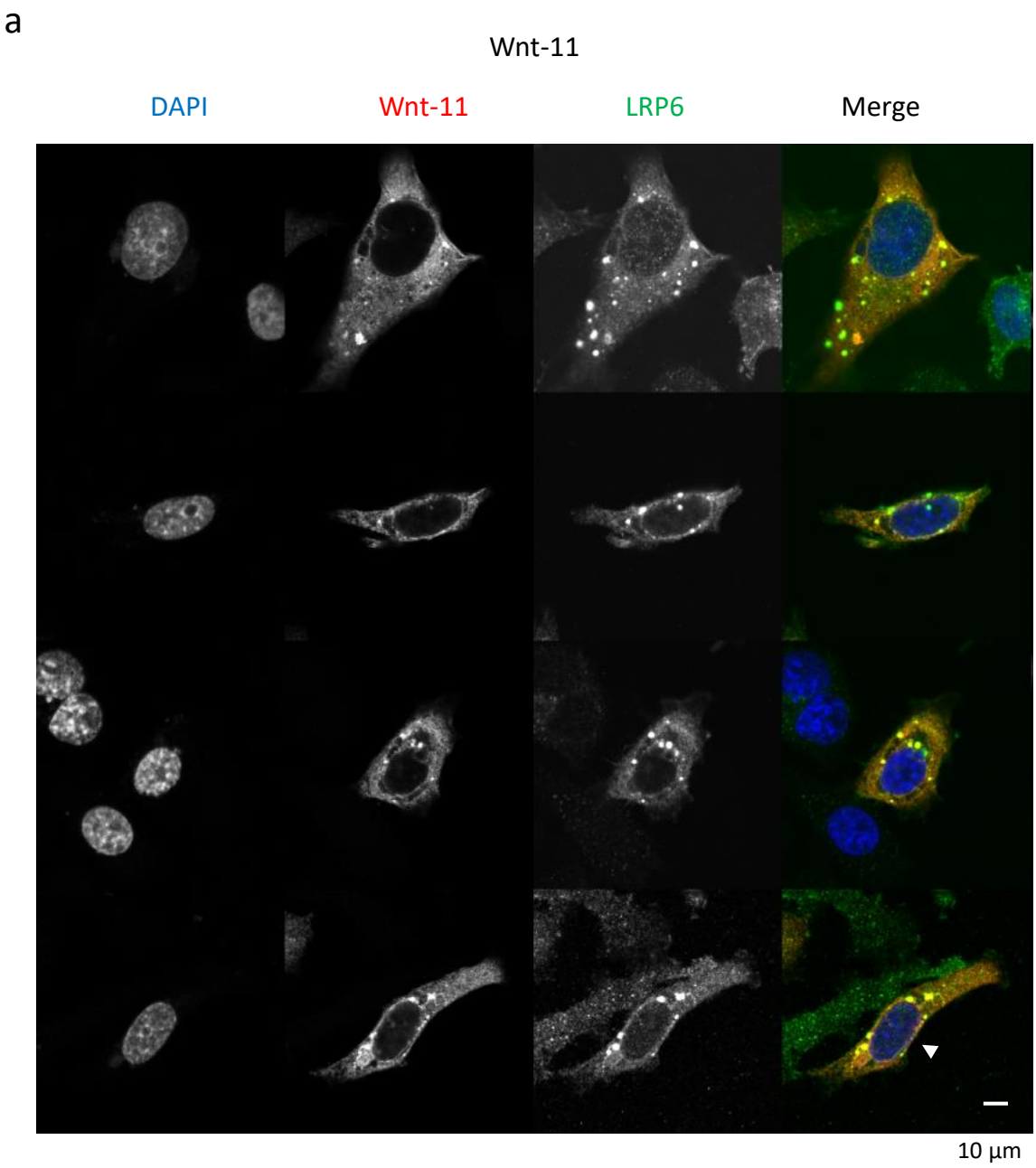

Figure 53. Imunofluorescence co-localization of Wnt-11 and antibody epitope mutant (AE) with VSV-G-tagged full length LRP6 in PC3 cells. A, B) Representative images of cells showing co-expression of Wnt-11 (A) or AE (B) (red channel), and LRP6 (green channel). Cells used for the quantification are indicated by white arrowheads when multiple cells are present in the field. C) Co-localization Pearson and Spearman scores were calculated from 25 cells co-expressing LRP6/Wnt-11, and 16 cells co-expressing LRP6/AE, from 2 independent experiments. Calculated using Coloc2 plug-in in Fiji distribution of ImageJ. Figure continues in the next page.

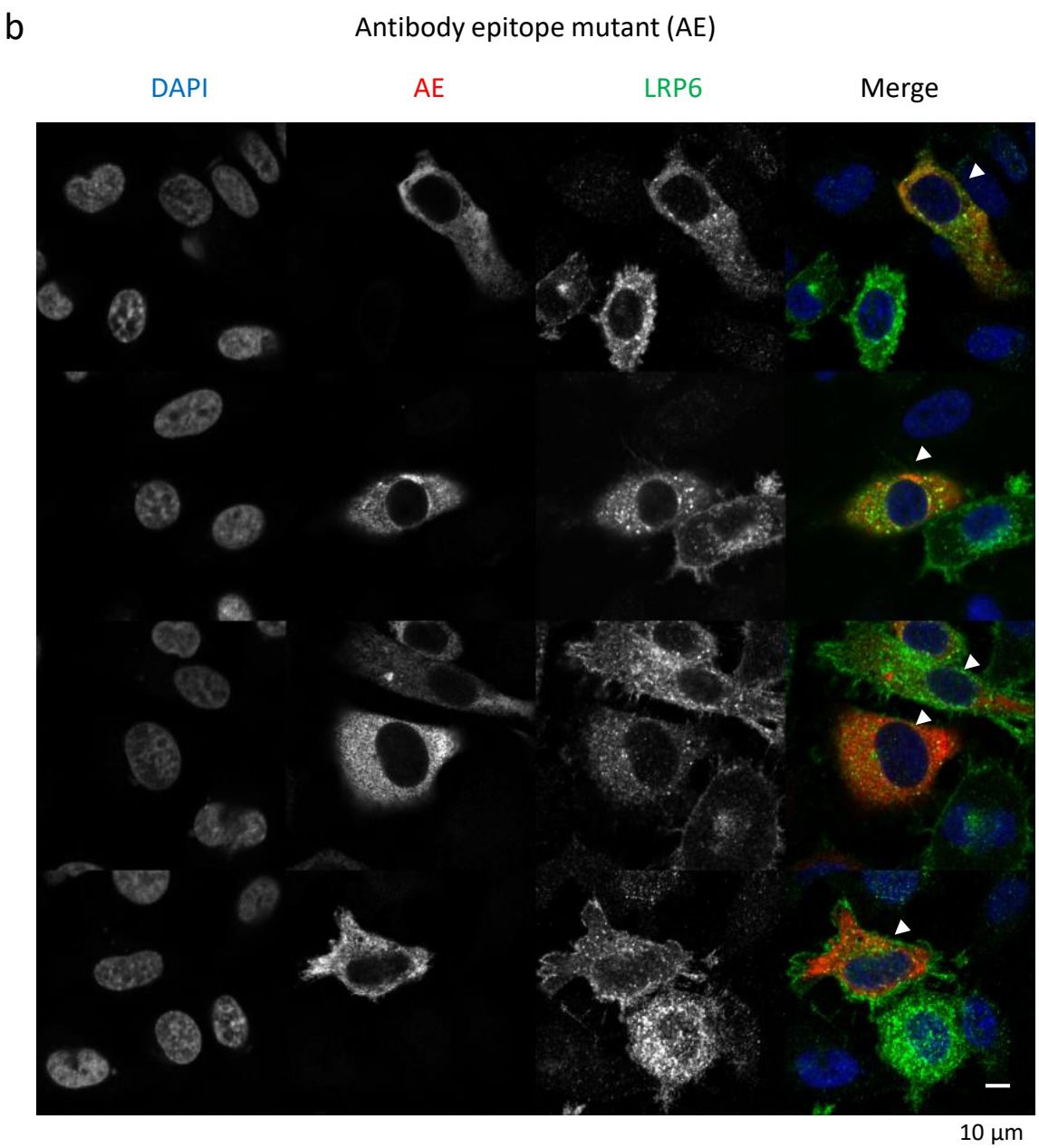

Figure 53. Continuation

IV.4. Effect of the Wnt-11 antibody epitope mutation on signaling by Wnt receptors and coreceptors

To measure the impact of the antibody epitope deletion in the context of Wnt-11 signaling in combination with Wnt co/receptors, gene reporter assays were carried out to measure β-catenin/TCF-mediated signaling (TOP-luc/FOP-luc) and noncanonical ATF2-dependent transcription (ATF2-luc).

First, Wnt-11 repression of β-catenin/TCF-mediated signaling was assessed, as done previously for Wnt-3a-mediated activation (Figure 46, page 145). In HEK 293 cells LRP6 transfection induced TOP/FOP luciferase reporter activity, and this was inhibited by co-expression of Wnt-11 (Figure 54). In contrast, the AE co-expression was unable to repress LRP6-mediated TOP/FOP-luc activation.

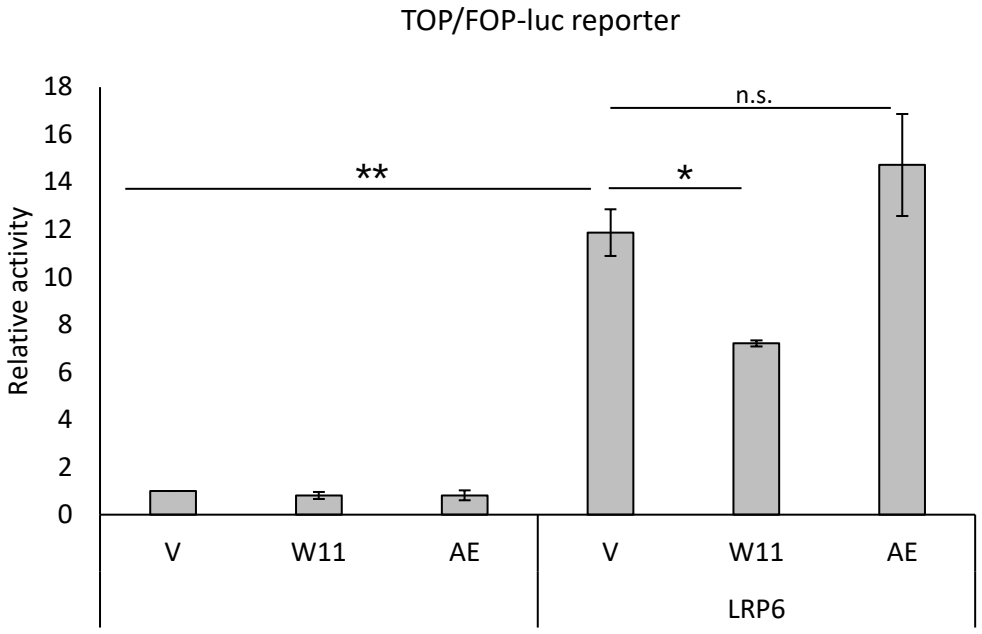

Figure 54. Effects of Wnt-11 (W11) and antibody epitope mutant (AE) on LRP6-mediated activation of β-catenin/TCF-mediated signaling. HEK 293 cells were co-transfected with plasmids for the expression of Wnt-11 or AE in combination with LRP6 for TOP/FOP-luc gene reporter assays. Plot showing the ratio of TOP-luc over FOP-luc (mutated control reporter) activity relative to vector (V) transfected cells, data from 3 independent experiments. V – empty vector (pcDNA for Wnts, pCS2 for LRP6).

Next, ATF2-luc reporter assays were carried out to investigate the role LRP6 coreceptor has in transducing Wnt-11/ATF2-mediated signaling in PC3 cells. Ectopic expression of LRP6 by itself did not result in increased ATF2-dependent gene reporter activity (1x/mt5, corrected ATF2-luc activity, see page 126), nor did it have an additive effect when co-expressed with Wnt-11 (Figure 55). However, PC3 cells already express high levels of endogenous LRP6 (21-22 *LRP6* CTs; 15-16 *36B4* CTs, housekeeping gene, measured by RT-PCR).

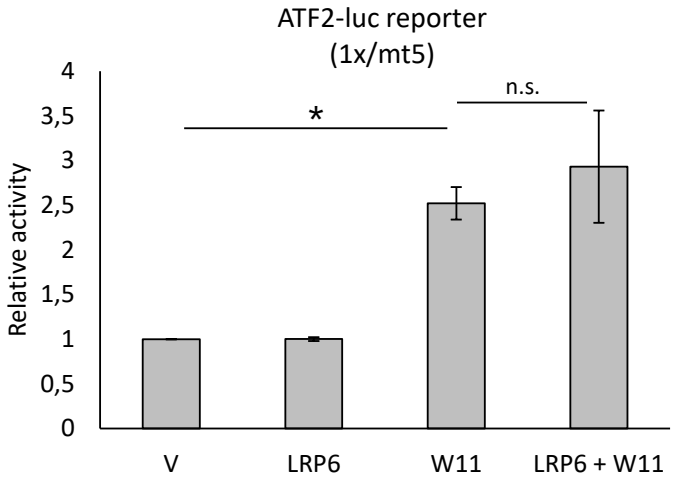

Figure 55. Effects of Wnt-11 (W11) and LRP6 expression in ATF2-depedent transcription. PC3 cells were co-transfected with plasmids for the expression of Wnt-11 and LRP6 for ATF2-dependent gene reporter assays measured by the ratio of 1x/mt5 (see page 137). Plot showing relative ATF2-dependent activity to vector (V) transfected cells, data from 3 independent experiments. V – empty vector (pcDNA for Wnt-11, pCS2 for LRP6).

In order to analyze in more detail the putative role of LRP6 in Wnt-11/ATF2 signaling, HEK 293 LRP5/6$^{-/-}$ knock-out cells were used (Figure 56, statistical analysis is provided also in Table 20). This facilitated the study of ectopic LRP6 expression in a null background model. Restoration of LRP6 expression in these cells slightly increased ATF2-dependent reporter activity (ATF2-luc), and this increase was only significant when LRP6 was co-expressed with FZD8 (V vs. LRP6+FZD8). Combined expression of Wnt-11 or the AE and FZD8 activated the reporter to a similar extent (V vs. FZD8+W11/AE). However, when LRP6 expression was restored in combination with Wnt-11/FZD8, the reporter activity was further increased (FZD8+W11 vs. LRP6+FZD8+W11, p=.03) and this did not occur using the AE/FZD8 (FZD8+AE vs. LRP6+FZD8+AE, n.s.).

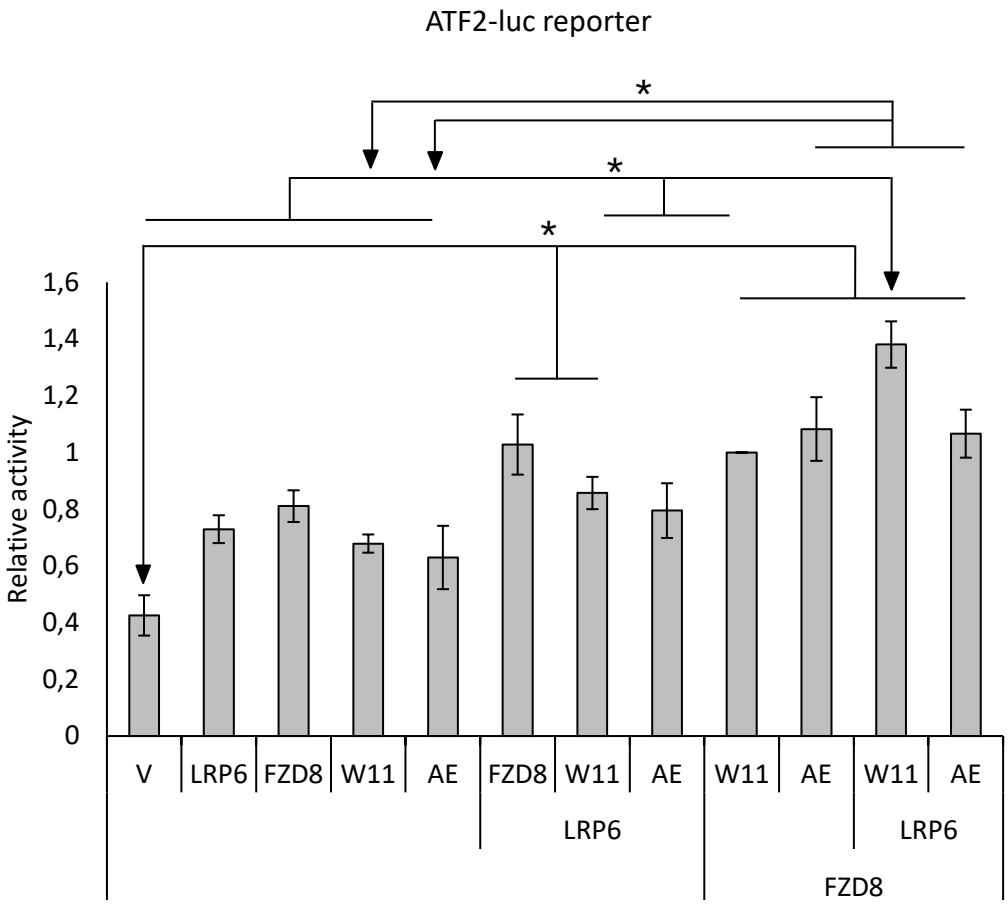

Figure 56. Effects of Wnt-11 (W11) and antibody epitope mutant (AE) in combination with FZD8 and LRP6 in ATF2-dependent transcription in HEK 293 LRP5/6 $^{-/-}$ knock-out cells. Cells were co-transfected with plasmids for the expression of LRP6, FZD8 and W11 or AE as indicated. Plot showing relative ATF2-luc gene reporter activity to W11/FZD8 transfected cells. In these experiments the amount of plasmids transfected was the following: 10 ng renilla, 50 ng ATF2-luc, 100 ng FZD8 (1D4, full length), 100 ng LRP6 (VSV-G, full length), 200 ng of Wnt-11 or AE (untag), see Gene reporter assay, page 81 for further method details. Data from 5 independent experiments. Statistical significance is calculated as post-hoc Tukey corrected p-values and are indicated by lines with arrowheads pointing towards which condition the pertinent comparisons are calculated. Statistical analysis is also presented independently in Table 20. V – empty vector (pcDNA for Wnt-11, pCS2 for LRP6, pRK5 for FZD8).

Table 20. Statistical analysis of data presented in Figure 56. Post-hoc Tukey corrected p-values are indicated as * for p<.05; ** for p<.01; *** for p<.001. If not indicated, the difference was not significant (n.s.). The comparisons referenced in the text are underlined.

	V	LRP6	FZD8	W11	AE	LRP6+FZD8	LRP6+W11	LRP6+AE	FZD8+W11	FZD8+AE	LRP6+FZD8+W11	LRP6+FZD8+AE
V						***	*		***	***	***	***
LRP6											***	
FZD8											***	
W11										*	***	*
AE										*	***	*
LRP6+FZD8												
LRP6+W11											**	
LRP6+AE											***	
FZD8+W11											*	
FZD8+AE												n.s.
LRP6+FZD8+W11												
LRP6+FZD8+AE												

These results point to a putative role of LRP6 in the Wnt-11-mediated regulation of ATF2-dependent transcription and that the antibody epitope mutation impacts this activity. Nonetheless, the expression of FZD8 appeared to be important for the signaling in this context, suggesting it may play a role in receptor-coreceptor complex formation and signal transduction.

Discussion

Prostate cancer is the second most diagnosed cancer in the male population worldwide as of 2020. Prostate cancer growth is usually androgen-dependent and therefore, androgen deprivation therapy (ADT) constitutes a main line of therapy (Attard et al., 2016). Many patients develop progressive disease after castration, stage known as castration-resistant prostate cancer (CRPC), which is accompanied by increased aggressiveness and higher probability of metastatic spread. Therapeutic targets outside the androgen-related pathway are needed and lacking in the clinic.

The reactivation of developmental signaling pathways has been highlighted to be relevant for prostate cancer progression (Shen & Abate-Shen, 2010). Although activating Wnt pathway mutations are not commonly found in prostate cancer, nongenomic alterations in the expression of tissue-specific pathway activators have been found at different stages of the disease and have been associated with disease progression (Fisher et al., 2020; Murillo-Garzón & Kypta, 2017; L. Wang et al., 2018). In addition, Wnt pathway components have been identified altered in many cancers and have been proposed to constitute therapeutic targets, and because of this, several drugs that target Wnt signaling are in development (Anastas & Moon, 2013). Some Wnt-targeting therapeutic agents being studied in clinical trials include porcupine inhibitors (e.g., WNT974), β-catenin modulators (e.g., PRI-724) and monoclonal antibodies targeting Wnt receptors and coreceptors (e.g., vantictumab, cirmtuzumab and BI 905677).

Among the Wnt signaling components found altered in prostate cancer, Wnt-11 is found upregulated in prostate cancer, particularly in metastatic disease, and it has been proposed to promote malignant progression by increasing neuroendocrine-like differentiation and cancer cell migration and invasion (Uysal-Onganer et al., 2010; H. Zhu et al., 2004). FZD8 has been reported as one of the main Wnt-11 receptors in prostate cancer, where it is required for crosstalk with the TGF-β signaling pathway, activating EMT features that promote the aggressiveness of the disease (Murillo-Garzón et al., 2018). Furthermore, Wnt-11 and FZD8 high expression is found correlated with poor prognosis in patients. These previous studies provide a basis for the exploration of Wnt-11 as a therapeutic target in advanced prostate cancer. Hence, selective inhibitors for Wnt-11 could be of use for the treatment of prostate cancer and other cancers. Although some studies have reported the use of commercial anti-Wnt-11 antibodies as neutralizing or function-blocking, none have been explored further as therapeutic agents (Dwyer et al., 2010; Hsueh et al., 2020; Ouko et al., 2004; Jingcai Wang et al., 2020; Zuo et al., 2012). In a therapeutic context, the functionalization of antibodies to

magnetic nanoparticles (MNP) can improve their stability, tumor selectivity delivery and imaging without affecting the targeting their properties (Dulińska-Litewka et al., 2019; Sousa et al., 2017). Here, the characterization of putative function-blocking anti-Wnt-11 antibodies and their conjugates to superparamagnetic iron oxide nanoparticles (SPIONs) has been carried out, investigating their effects in prostate cancer cell models.

Chapter I: Characterization of anti-Wnt-11 antibodies and functionalized nanoparticles

Two rat anti-Wnt-11 monoclonal antibodies named E8 and F10 were pre-selected for studies, with both having the same peptide epitope located within L101-A112 (LLDLERGTRESA). The recognition of Wnt-11 by E8 and, in some instances, F10, was determined using a variety of assays, including in a cellular context. Immunofluorescence staining of C4-2B prostate cancer cells that stably overexpress Wnt-11 (C4-2B-WNT11) using the E8 antibody, showed increased staining intensity compared to vector transfected cells and the signal co-localized with that obtained using a commercial anti-Wnt-11 antibody. Moreover, using an indirect assay, extracts from E8-positive cells collected by FACS were found to be enriched in Wnt-11 protein expression. Although E8 and F10 only recognized Wnt-11 from cell extracts and conditioned media poorly by western blotting, they did recognize recombinant Wnt-11 protein. This facilitated confirmation of their specificity for Wnt-11 as compared to other Wnt family members, such as Wnt-3a, that share sequence homology in part of the peptide injected into rats for the antibodies generation. Western blotting of recombinant Wnt-11 and Wnt-3a showed that the common sequence (TRESA) is alone insufficient for recognition, as E8 only recognized Wnt-11 and not Wnt-3a. This result also suggests that the E8 epitope in Wnt-11 mainly resides in the first part of the peptide (LLDLERG).

Other anti-Wnt antibodies that have been proposed to block function have undergone a similar characterization for their recognition of the target Wnt protein prior to functional assays. Polyclonal anti-Wnt-5a antibodies were shown to recognize Wnt-5a-containing CM without cross-reacting with Wnt-3a (Hanaki et al., 2012). Similar monoclonal anti-Wnt-5a antibodies were later characterized by ELISA and dot blot (Shojima et al., 2015). Function-blocking anti-Wnt-1 antibodies were characterized by western blotting and immunoprecipitation (B. He et al., 2004). Another study has reported the use of commercial anti-Wnt-3a antibodies to block function, but cross-reactivity with other Wnts was not examined (Pacella et al., 2018).

Many studies have proposed the conjugation of antibodies to MNPs as a way to improve their stability and delivery *in vivo* (Dulińska-Litewka et al., 2019; Sousa et al., 2017), which can be beneficial in the context of cancer therapy (Farzin et al., 2020). MNPs has been extensively explored also in prostate cancer theranostics, however their current use is mainly

limited to imaging purposes (Chowdhury et al., 2017). The use of prostate-specific membrane antigen (PSMA) antibodies conjugated MNP is of particular relevance for the diagnosis of prostate cancer and this antigen has also served to improve tumor-selective delivery of docetaxel-loaded MNPs (Nagesh et al., 2016; Tse et al., 2015). In the context of antibodies interfering with the Wnt pathway, conjugation to nanomaterials has also been employed for improving potency and delivery. For instance, antibody-nanoshell conjugates (FZD7-NS) have been reported to be more effective at inhibiting Wnt signaling than naked FZD7 antibodies in breast cancer cells (Riley & Day, 2017). Additionally, anti-FZD7 antibodies have been used for targeted delivery of zinc oxide nanoparticles to selectively induce cancer cell apoptosis in drug-resistant breast cancer cells (Ruenraroengsak et al., 2019). In this thesis, superparamagnetic iron oxide nanoparticles (SPIONs) have been used for the bioconjugation of E8 and F10 antibodies, as these have been successfully employed for targeting CD44 in breast cancer cells (Aires et al., 2016).

In a first characterization of the conjugated SPIONs, DLS measurements were carried out. The size and charge changes detected upon the conjugation were in the expected trend and range. MNP aggregation was observed only in culture media with low FBS (<5%). It is well established that the interaction of nanoparticles with the proteins contained in cell culture media can induce the formation of the so-called protein corona, which affects the MNP properties leading to the collapse or stabilization of colloidal systems (Moore et al., 2015). In this case, conditions that induced aggregation were avoided by changing the experimental design. However, the basis of the observed aggregation could not be unraveled, and further studies will be needed to clarify this.

Prussian Blue staining is commonly employed to demonstrate binding of SPIONs to cells (Aires et al., 2016; Trabulo et al., 2017). Prussian Blue staining of VCaP cells incubated with the E8 functionalized SPIONs (MNP-E8) produced a membrane staining compatible with Wnt-11 recognition. Nevertheless, these assays presented difficulties, as Prussian Blue staining with the control rat IgG-MNP conjugates was more intense than expected and MNP-F10 nanoformulation showed only weak staining. The latter might reflect the fact that F10 showed lower apparent affinity for Wnt-11 than E8 in other assays (e.g., peptide dot blot). Optimized binding conditions might be needed to further favor anti-Wnt-11 conjugate-specific binding.

Chapter II: Effects of anti-Wnt-11 monoclonal antibodies and MNP conjugates on prostate cancer cells *in vitro*

The effects of the anti-Wnt-11 antibodies were investigated in functional *in vitro* assays using prostate cancer cell lines. Proliferation of PC3 and DU145 cells was only impaired in 7-day assays at the highest dose tested (20 µg/ml) and not at lower doses or shorter times. This is consistent with Wnt-11 being more involved in prostate cancer cell survival under stress conditions than in cell proliferation (Uysal-Onganer et al., 2010).

Next, the role of Wnt-11 in sphere formation assays was studied. Sphere formation assay are commonly used in cancer research to measure stemness and tumor initiating properties, and both canonical and noncanonical Wnt pathways have been shown to be implicated (Many & Brown, 2014). However, the role of Wnt-11 is not well established. Recently, *WNT11* gene silencing in melanoma cells was reported to reduce melanosphere formation (Rodriguez-Hernandez et al., 2020). In PC3 cells, *WNT11* mRNA and protein levels were found upregulated in spheres when compared to cells grown as a monolayer. Also, *SOX2* mRNA was found increased in spheres of C4-2B-WNT11 cells, compared to vector control C4-2B-V cells; *SOX2* is a stem cell marker associated with cancer progression in several malignancies (Piva et al., 2014; Takahashi et al., 2007). Furthermore, *SOX2* has been implicated in neuroendocrine-like differentiation of C4-2B cells (Metz, Wilder, Dong, Datta, & Rizzino, 2020). These observations suggest that Wnt-11 may play a relevant role in the survival or proliferation of prostate cancer cells when cultured as spheres, although further studies are required to provide a full characterization of the role of Wnt-11 in this setting. Consistent with these results and further supporting a role for Wnt-11 in this context, both E8 and F10 antibodies reduced PC3 and DU145 cell sphere number.

The role of Wnt-11 in cell migration and invasion is better established than its role in proliferation and has been demonstrated in several models, with functions during tissue morphogenesis and cancer (Mori et al., 2016; Ouko et al., 2004; Ulrich et al., 2005; Witzel et al., 2006). In PC3 cells, *WNT11* silencing has been reported to reduce cell migration in transwell assays and, in turn, its overexpression in LNCaP cells increases invasion (Uysal-Onganer et al., 2010). Here, PC3 cell migration upon *WNT11* gene silencing was also found to be reduced in wound healing assays. Similarly, treatment with anti-Wnt-11 antibodies resulted in inhibition of cell migration measured by wound healing assays. E8 and F10 also reduced

PC3 and DU145 cell migration in transwell assays, although the effect was weaker in DU145 cells. One possible reason for this is that DU145 cells express lower *WNT11* levels than PC3 cells. C4-2B-WNT11 cells were found to display higher invasion capacity, compared to control vector-expressing cells, and this increase was abolished by treatment with either E8 or F10. Nevertheless, a Wnt-11 null model would be needed to confirm the specificity of these effects. Importantly, a similar assay was already performed with these antibodies in colorectal cancer cells, where Wnt-11 has been proposed as a prognostic marker and E8 and F10 antibodies (there called Ab1 and Ab2, respectively) inhibit colorectal cancer cell invasion (Gorroño-Etxebarria et al., 2019). Gorroño-Etxebarria et al. reported that there were no additive effects when combining *WNT11* gene silencing with E8 or F10 antibody treatment, providing support for the inhibition of migration and invasion by E8 and F10 being specific.

These Wnt-11 antibodies can be contextualized with other function-blocking anti-Wnt antibodies that have been proposed for cancer treatment. An anti-Wnt-1 antibody was proposed to induce apoptosis in a variety of human cancer cell lines with high Wnt-1 levels, including non-small cell lung cancer, breast cancer, mesothelioma, and sarcoma (B. He et al., 2004; Mikami et al., 2005). B. He et al. reported achieving similar results with *WNT1* gene silencing, a strategy that was also used in this thesis for Wnt-11 in some experiments. Polyclonal and monoclonal anti-Wnt-5a antibodies were reported to inhibit migration and invasion of gastric cancer cell lines (KKLS, MKN-1, MKN-45 and TMK-1) and of HeLaS3 and A549 cells (Hanaki et al., 2012; Shojima et al., 2015), using similar approaches to those presented here with prostate cancer cell lines.

Furthermore, Wnt-11 has been shown to be upregulated by hypoxia, as a direct target of HIF-1α, and this upregulation was found responsible for increased migration and invasion in several cancer cell models (Mori et al., 2016). In PC3 cells treated with the hypoxia mimetic DMOG, similar results were observed, with a specific upregulation of Wnt-11 protein levels. Although demonstration of increases in HIF-1α and HIF-2α protein levels upon DMOG treatment strongly suggest induction of hypoxia, DMOG effects are not restricted to the hypoxia pathway and it can have direct effects on metabolism and on mitochondrial function independently of PHD/HIF (Nguyen & Durán, 2016). Some of its effects on Wnt-11 expression should therefore be verified by culturing cells in a low oxygen environment, as was later performed for migration assays. PC3 cells pretreated with DMOG and subjected to hypoxia (1% O_2) for the duration of the experiment were found to display increased cell migration compared to cells cultured in normoxia. Importantly, the increase in cell migration driven by

the hypoxic response could be partially reversed by treatment with the E8 antibody in a dose-dependent manner. The Mori et al., 2016 study reported that Wnt-11 only affected migration of MDA-MB-231 breast cancer cells under hypoxia, contradicting other previous reports (Dwyer et al., 2010). In prostate cancer cells, Wnt-11 was found to be important for cell migration both under hypoxia and normoxia, albeit the inhibitory effect of E8 was enhanced in hypoxia suggesting Wnt-11 plays a more prominent role.

In this context, the expression of selected Wnt pathway genes was investigated in hypoxic PC3 cells. *WNT11* mRNA levels were found consistently upregulated in DMOG-treated cells, as expected, and there was also an upregulation in the mRNA expression of its receptor *FZD8*. An analysis of canonical Wnt components and target genes was also carried out. Among them, only the expression of *AXIN2* was significantly increased, while other genes (*LEF1*, *DKK1*, *NKD1*) showed non-significant or non-consistent reductions in the expression. Downregulation of the canonical Wnt pathway in response to hypoxia has been previously reported (Öztürk, Hobiger, Despot-Slade, Pichler, & Zenobi-Wong, 2017; Scholten et al., 2014). Öztürk et al. showed that *AXIN2* expression under hypoxia can be either up- or down-regulated in a microenvironment-dependent manner in chondrocytes cultured in 3D hydrogels. It is also worth noting that under hypoxia, *LRP6* was slightly downregulated. This contrasts with the increased expression of both *WNT11* and *FZD8*, which suggests that these two genes may be co-regulated in the context of hypoxia, unlike *LRP6*.

Hypoxia is relevant to prostate cancer, as the prostate gland itself is often hypoxic and it has been associated with disease progression and poorer prognosis (Dehm & Tindall, 2019, p 165; Movsas et al., 1999). Hypoxia in prostate cancers has been found associated with genomic instability, mutant TP53, allelic loss of PTEN, chromothripsis and shorter telomeres; with these features correlating with higher probability of metastasis (C. Q. Yao et al., 2019). Given that high expression of *WNT11* also correlates with disease progression (Murillo-Garzón et al., 2018; Uysal-Onganer et al., 2010; H. Zhu et al., 2004) and that it is upregulated in prostate cancer cells under hypoxia, it could therefore be interesting to study the correlation of Wnt-11 expression and that of hypoxic markers in prostate tumors.

Hypoxia is only one of the factors driving Wnt-11 expression, as it has also been reported to be a target of ERRα and β-catenin (Dwyer et al., 2010), contains TCF/LEF sites in its promoter (Uysal-Onganer & Kypta, 2012) and is negatively regulated by androgens (H. Zhu et

al., 2004). These may partially explain how Wnt-11 expression is upregulated in prostate tumors in advanced stages without showing activating mutations or copy number variations. However, the upstream factors that initiate the aberrant expression of Wnt-11 have not been further studied here.

Antibody-functionalized MNPs were tested in parallel to the naked antibodies in proliferation and migration assays. Unconjugated and control (IgG-conjugated) MNPs did not produce any effects on PC3 cell viability at the dose used for functional assays (0.2 mg Fe/ml), as has been previously observed in other cell models with this class of MNPs (Aires et al., 2017, 2016; Singh, Jenkins, Asadi, & Doak, 2010; Tse et al., 2015). Neither MNP-E8 nor MNP-F10 nanoformulations affected proliferation at the dose employed in these experiments, which was lower than the doses used for naked antibodies.

For measuring migration, only wound healing assays could be performed, owing to the limitation of MNP aggregation in media containing low amounts of FBS. No significant effects on PC3 cell migration were detected among the various control conditions (untreated, MNP-C and MNP-IgG). Some studies have reported intrinsic anti-migratory effects of SPIONs, with serum levels influencing the amount of inhibition (Diana, Bossolasco, Moscatelli, Silani, & Cova, 2013), while studies in other models have not detected these effects (Matuszak et al., 2015). MNP-E8 elicited a reduction in PC3 cell migration, compared to MNP-IgG, and this was comparable to the effect of naked E8 antibody. MNP-F10 showed a similar trend, but this was not significant, consistent with the weaker effects of naked F10 antibody. These results indicate that conjugation of MNPs to anti-Wnt-11 antibodies does not affect their ability to inhibit PC3 cell migration.

The exclusive use of cell lines as prostate cancer models is a clear limitation of most of this work and these results need further validation using additional, more physiologically relevant systems, such as 3D spheroids (Härmä et al., 2010), primary cells and/or patient-derived xenograft (PDX) models. While prostate PDX models have been shown to serve as a useful tool to better reflect the heterogeneity found in patient tumors, they have only recently become available (Faugeroux et al., 2020; Hu et al., 2019; Lange et al., 2018). In fact, a prostate PDX model has been used during this work, but the results have not yet generated conclusive results.

Chapter III: Effects of anti-Wnt-11 monoclonal antibodies and MNP-antibody conjugates on prostate cancer cells *in vivo*

The CAM model was used to test the effects of the anti-Wnt-11 antibody MNP conjugates *in vivo*. This model has been used extensively for the study of PC3 cell tumor growth and metastasis (Ateeq et al., 2011; Bekes et al., 2011; Chakravarthi et al., 2017; Jefferies et al., 2017; Murillo-Garzón et al., 2018; Stoletov et al., 2018). Moreover, it has also been used to determine the effects of therapeutic antibodies, with different modes of administration and a wide range of concentrations being reported: antibody administration in the cell:Matrigel implantation mix (Lokman, Elder, Ricciardelli, & Oehler, 2012), topical treatment on tumor cells (Bekes et al., 2011; Conn et al., 2009), and using filter disks (Yan et al., 2003), with doses ranging from 0.6 μg/egg to 25 μg/egg. Intravenous delivery of antibodies is also an option, but requires the use of higher quantities (100 μg/egg) (Zijlstra, Lewis, DeGryse, Stuhlmann, & Quigley, 2008). This, together with the possibility that embryonic chick WNT11, which shares the same sequence as human Wnt-11 in the region of the antibody epitope, might affect the efficacy of the antibodies, prompted treatment delivery in the implantation mixture with the cells and later topically at a dose of 3 μg/egg. E8 was given priority, as it showed stronger effects in *in vitro* assays, and, although F10 was used in some assays, an insufficient number of experiments were carried out, rendering those results inconclusive.

Tumor growth was determined by measurement of tumor area and by weighing the resected tumors. Treatment with E8 antibody was found to reduce PC3 cell tumor growth in the CAM compared to IgG-treated tumors in a consistent and significant manner. Immunohistochemical analysis of the resected PC3 tumors revealed that these could be clearly distinguished from CAM tissue and that the expression of Wnt-11 could be readily detected. Because tumor growth was found to be reduced, staining of the proliferation marker Ki67 was performed, as previously reported in this system (Swadi et al., 2019). Although measurement of the percentage of Ki67-positive cells has been traditionally used as the output of these analyses, it was recently shown that Ki67 is a graded rather than a binary marker of proliferation (Miller et al., 2018). Therefore, the analysis of Ki67 nuclear intensity instead of the percentage of positive cells was carried out in an automated manner, using Qupath. This analysis revealed that E8-treated tumors had a consistent and significant reduction in Ki67 nuclear staining, compared to IgG-treated tumors.

Wnt-11 has previously been linked to Ki67 expression in melanoma cells, where both these proteins colocalized at the invasive front of human primary melanoma specimens (Rodriguez-Hernandez et al., 2020). As noted in chapter II, E8 treatment had minimal effects on PC3 cell proliferation in monolayer cultures but had a stronger effect in sphere cultures. These *in vivo* results are more consistent with the latter. They are also consistent with results obtained in studies with the Wnt-11 receptor FZD8, where *FZD8* gene silencing did not affect proliferation *in vitro* but was proven to reduce to PC3 tumor growth in the CAM system (Murillo-Garzón et al., 2018).

The CAM model also allows analysis of capacity for metastasis, with the determination of the presence of human cells based on the detection of human Alu repeat sequences by quantitative PCR in the distal CAM being one very sensitive assay that has been used by several groups (Crespo & Casar, 2016; Rasheed, Efferth, Asangani, & Allgayer, 2010; Zijlstra et al., 2002). Some experiments have been performed using this approach, but to date not enough replicates have been analyzed to reach conclusive results. In addition, technical limitations were encountered using this technique. The most important was the relatively low rate of spontaneous metastasis of PC3 cells in the CAM model. PC3 cells are metastatic in mouse xenograft assays, but even then, more metastatic variants are generally used, and the site of implantation is important (Y. Zhang et al., 2016). Some studies have used the CAM model to develop more metastatic variants of PC3 cells that exhibit enhanced dissemination capacities in both chick embryo and mouse spontaneous metastasis models (Conn et al., 2009), which could be of use for pursuing this aspect.

The use of MNPs in the CAM has also been reported in different cancer models (Predoi et al., 2020; Vu et al., 2018). Here, administration of the MNPs was done as similarly as possible to that for naked antibodies, i.e., topical delivery to tumor cells on the CAM. MNP-E8 and MNP-F10 treatments were analyzed in comparison to multiple controls, (MNP-IgG, MNP-C) and untreated (UT), which made the analysis more complex but was important to rule out potential effects unrelated to targeting Wnt-11. A trend in the reduction of PC3 tumor growth was detected for the anti-Wnt-11 antibody conjugates, but it was only significant for MNP-E8 when compared to MNP-IgG by pairwise comparison ($p<.05$) and to UT after post-hoc Tukey HDS correction ($p<.01$). Additional experiments will be needed to clarify the MNP-F10 results.

Only a limited number of samples of MNP-treated tumors were analyzed for Ki67 intensity, but the results showed a promising reducing trend in MNP-E8-treated tumors compared to

MNP-IgG-treated. Prussian blue staining permitted the visualization of the MNPs, which were readily detected on and around the tumors, with accumulation at what is likely to be the site of antibody-MNP administration. The use of topical delivery of MNPs to the tumors precluded analysis of whether Wnt-11 antibody conjugation to MNPs improved delivery to tumor cells. There was no evident benefit of MNP conjugation for the antibodies, with respect to effects on tumor growth. However, this is a difficult comparison to make, as less antibody was used when delivered as MNP-conjugated. Future studies should include intravenous injection of antibody-conjugated MNPs in order to measure tumor-selective delivery, as has been reported by others (Vu et al., 2018). Nonetheless, the Ab functionalized MNPs were shown to retain the capacity of E8 antibody to inhibit PC3 CAM tumor growth. This, combined with their previously shown capacity to limit PC3 cell migration and their advantageous properties for imaging and delivery, indicate that MNP functionalization is a promising strategy for the *in vivo* applications of these neutralizing Abs in prostate cancer models.

Topically applied drugs to the CAM can reach the systemic circulation, affecting the development of the chick embryo. Thus, CAM assays have been employed to evaluate the activity or toxicity of drugs (Ribatti, 2016). Although Wnt-11 is a protein expressed during development, no reduction in the viability of the chick embryos was detected upon treatment with the antibody-conjugated MNPs or with the naked antibodies, suggesting low/null toxicity in the system at the doses used. However, even if no toxicity is observed in the chick embryo, potential antibody toxicity, as well as antibody treatment efficacy, will also need to be investigated in adult mammalian models. Wnt-11 expression has been detected by immunohistochemistry in the smooth muscle of the small intestine and colon (Ouko et al., 2004), and it is also present in specific regions of adult mouse kidney, where knock-out studies have suggested it plays a role both in the embryonic and adult kidney (Nagy et al., 2016). Loss of Wnt-11 leads to a significant reduction in nephron endowment, impacting nephron progenitor polarity and motile behavior (O'Brien et al., 2018). Wnt-11 has also been reported to play an important role in cardiomyocyte survival under hypoxia, where it appears to help preserve mitochondrial membrane integrity and function (H. X. Li et al., 2020). Finally,Wnt-11-induced responses have been proposed to be beneficial for acute myocardial infarction therapy (B. Chen et al., 2018). Therefore, these are the sites where possible toxicity of the anti-Wnt-11 antibodies and MNP conjugates might be anticipated.

The role of Wnt-11 in prostate cancer may be limited to more advanced stages of the disease (Uysal-Onganer et al., 2010; Volante et al., 2016). Thus, anti-Wnt-11 targeted therapy would likely be most beneficial after or in combination with ADT, preferably with stratification of patients for those with high Wnt-11 expressing tumors or those positive for hypoxic markers. While there is evidence that high Wnt-11 is indicative of poor prognosis in CRC patients (Gorroño-Etxebarria et al., 2019), the prognostic value of Wnt-11 expression levels in patients with advanced, treatment-resistant prostate cancer requires further investigation.

Chapter IV: Mechanism of action of anti-Wnt-11 monoclonal antibodies

It was deemed pertinent to explore the mechanism by which the antibodies block Wnt-11 effects in prostate cancer cells. First, the hypothesis that antibody treatment was able to impair Wnt-11 signaling was tested by analyzing DVL phosphorylation. This was measured by detection of DVL reduced mobility in western blots, where the appearance of an upper band is predicted to correspond to the phosphorylated form of these proteins. The phosphorylation of DVL is regarded as an indicator of Wnt signaling initiation that is independent of β-catenin activation (Gonzalez-Sancho et al., 2004). DVL is already partially phosphorylated in PC3 cells and treatment with Wnt-C59, which blocks endogenous Wnt secretion, abolishes the appearance of the upper DVL band, indicating that basal DVL phosphorylation is a result of endogenous Wnt signaling activity. Treatment of PC3 cells with E8 and F10 antibodies also produces a significant reduction in the intensity of the upper band of DVL2 and DVL3 consistent with inhibition of Wnt signaling. Nonetheless, *DVL2* mRNA expression has been reported downregulated upon Wnt-11 deficiency in kidney (Nagy et al., 2016). Therefore, analysis of *DVL2* mRNA was also carried out. Neither E8 treatment nor *WNT11* gene silencing in PC3 cells reduced *DVL2* mRNA, indicating that the effects of the anti-Wnt-11 antibodies are not mediated by changes in *DVL2* mRNA expression. Although DVL phosphorylation has been classically assessed as a mobility shift, anti-phosphorylated DVL antibodies are available that could be useful to corroborate the phosphorylation status directly (K. H. Lee et al., 2012).

As an additional readout of Wnt-11 signaling, gene reporter assays measuring ATF2-dependent transcriptional activity were used, as these have been reported in the lab in prostate cancer cells (Murillo-Garzón et al., 2018), as well as by other groups in other cell types (Boitard et al., 2015; C. Chen et al., 2018; Veronika et al., 2014). Here, a reporter (mt5) (Bruhat et al., 2000) containing mutations in the ATF2 binding site was also used as a control. While Wnt-11 ectopic expression in PC3 cells elicited an increase in ATF2-dependent gene reporter activity, E8 treatment resulted only in a limited reduction, that was found statistically significant but so small that it is unlikely to be physiologically relevant. ATF2 is a transcription factor not exclusive to Wnt signaling that be activated by diverse stimuli, such as growth factors, cytokines and stress (e.g., UV radiation) (Watson, Ronai, & Lau, 2017). The results using E8 suggest that most of the basal ATF2-dependent activity measured is not related to activation of

endogenous noncanonical Wnt signaling. Further investigation of this issue is complicated by Wnt-11 being mostly insoluble, which hampers the use of recombinant protein or cell-conditioned media for gene reporter assays.

There is very limited knowledge of Wnt-11 signaling mediators that might contribute to the effects of Wnt-11 in prostate cancer cells. There is evidence that Wnt-11 affects Jun and JNK phosphorylation and RhoA activation in other contexts (Andre et al., 2015; Nishioka et al., 2013; Rodriguez-Hernandez et al., 2020; Witzel et al., 2006). However, it has also been found to inhibit JNK phosphorylation in some cell types (Railo et al., 2008). Similarly, Wnt-11-dependent transcription factors and target genes relevant to prostate cancer have not been identified. Perturbation-based high throughput gene expression analyses have been useful in determining β-catenin-independent target genes in colorectal cancer cells, where noncanonical responses were found to be regulated via DVL2 and ATF2, among other factors (Voloshanenko et al., 2018). High throughput screens might be a useful approach in unravelling Wnt-11 mediators and target genes in prostate cancer cells. However, it is possible that Wnt-11 does not have such a direct effect on gene expression, in contrast to β-catenin signaling.

To explore the relevance of the region that contains the E8 and F10 antibodies epitope in Wnt-11, a partial deletion mutant was generated, Wnt-11ΔL101-T108 (`LLDLERT`), which was termed AE. The AE lacks a short peptide sequence that likely constitutes the main part of the epitope, as the deleted sequence corresponds to the part that does not share identity with Wnt-3a and E8 does not recognize recombinant Wnt-3a protein. The mutation in AE might be considered to mimic the state of Wnt-11 when it is bound to E8 antibody. However, it is not known if the effects of E8 on Wnt-11 activity are a result of direct steric impedance of Wnt-11 binding to protein partners, or if they are due to allosteric effects which the AE mutation would likely fail to mimic. To clarify this, structural studies will be required, as has been reported for function-blocking antibodies that target other proteins (Kuai et al., 2015; Sun et al., 2021).

Another limitation is that the deletion mutation may affect Wnt-11 tertiary structure. The equivalent region for the Wnt-11 epitope in Wnt-3, does not have secondary structure, hence its absence in Wnt-11 was not expected to blatantly disrupt the tertiary structure. To explore this further, modeling of the structure of Wnt-11 and of the AE deletion mutant was performed using AlphaFold (Jumper et al., 2021; Senior et al., 2020). No overt structural differences between Wnt-11 and AE were observed (Figure 57). However, these predictions are highly based on the homology between Wnt-11 and Wnt-3, and homology-based modeling is not

completely accurate in predicting the effects of mutations (AlphaFold Protein Structure Database, 2021). Interestingly, meanwhile the equivalent region in Wnt-3 does not form secondary structure (see Figure 40, page 139), in the Wnt-11 modeled structure a short alpha-helix is predicted. Nonetheless, the AE mutation removes this alpha-helix entirely and no other major differences in the structures could be observed. Although these results are encouraging, a more robust strategy will be to generate point mutants in the region of the deleted epitope to identify those amino acids that are essential for the antibody interaction and for Wnt-11 activity. Nevertheless, several lines of experimental evidence support the conclusion that the deletion in AE does not grossly alter Wnt-11 folding and structure: the AE protein is expressed, secreted, and can be readily detected on the surface of expressing cells at levels comparable to those of wild-type Wnt-11.

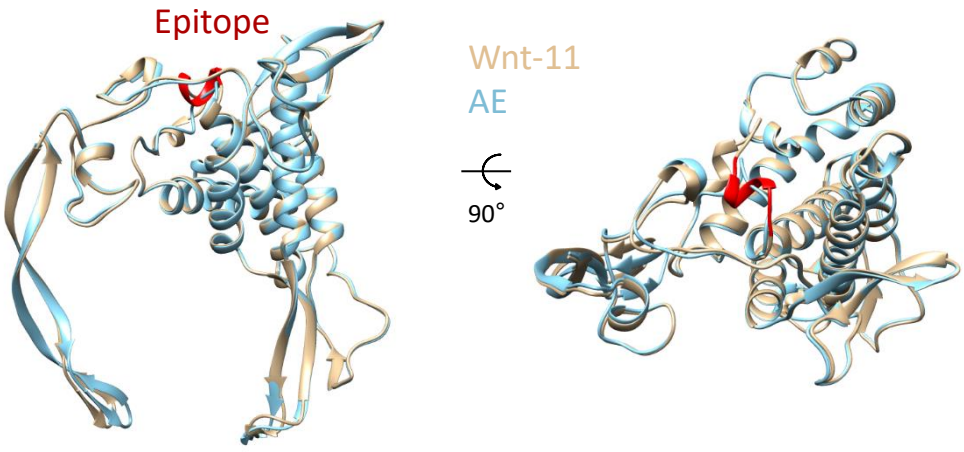

Figure 57. Modeled Wnt-11 and antibody epitope mutant (AE) structures using AlphaFold. Ribbon depiction of predicted structures: Wnt-11 in beige and AE in blue. Epitope is highlighted in red. Left: side view, right: top view. Note a short alpha-helix is predicted in the epitope. These structures were modeled with the assistance of Gonzalo Jiménez-Osés (CIC bioGUNE) based on the protein sequences using AlphaFold (Senior et al., 2020).

FACS experiments were carried out to show that the E8 antibody does not recognize the AE: when cells expressing the AE were FACS-sorted using the E8 antibody, there was no enrichment for Wnt-11 protein levels, in clear contrast to experiments performed using cells expressing wild-type Wnt-11. However, this result requires further validation as it was only performed in duplicate. Ideally, the Wnt-11 and the AE should be expressed and purified and directly compared for binding to E8 *in vitro*. However, given the Wnt-11 solubility issues noted above, this is not a trivial approach.

The AE was found to recapitulate some effects shown upon E8 antibody treatment. The Wnt-11 mutant AE was found to have lost the capacity displayed by Wnt-11 to increase PC3M cell migration upon being exogenously expressed, implicating the epitope as being required for this function of Wnt-11. The ability of Wnt-11 to increase migration in this context is consistent with the inhibition of migration observed upon *WNT11* gene silencing and when Wnt-11 is inhibited using antibodies. However, these were the only experiments aimed at determining the functional implications of the AE mutation and other effects, such as those on tumor cell survival, stemness and apoptosis remain to be studied. With respect to signaling, exogenous expression of the AE protein was unable to alter DVL3 mobility, in clear contrast to wild-type Wnt-11, which increased the DVL3 shift (predicted phosphorylation) in a Wnt-C59-dependent manner. These results are consistent with the effect of the E8 antibody on reducing DVL shift.

The capacity of Wnt-11 for inhibiting β-catenin/TCF signaling was analyzed by luciferase-based gene reporter assays (TOP-luc), as has been analyzed in the past (Elizalde et al., 2011; Hua et al., 2018; Maye et al., 2004; Toyama et al., 2010; van Amerongen, 2012; H. Zhu et al., 2004). While Wnt-11 expression reduced the TOP-luc activation induced by Wnt-3a CM, AE expression was unable to do so. There are multiple mechanisms by which Wnt-11 can inhibit canonical Wnt signaling, among them is by competing for binding to Wnt receptors (Grumolato et al., 2010; Maye et al., 2004). The effects of Wnt-11 on canonical signaling in PC3 cells were restricted to when exogenously activated with Wnt-3a CM and E8 antibody treatment of PC3 cells did not appear to increase canonical Wnt activity in basal conditions (data not shown). This is consistent with the idea that additional Wnt ligand stimuli are required for an effect to be observed. Hence in cells where mutations in APC or CTNNB1 constitutively activate canonical Wnt signaling, anti-Wnt-11 antibody treatment is not expected to further increase activity, but should inhibit the effects of Wnt-11 induced by canonical signaling, as *WNT11* can be a canonical target gene (Uysal-Onganer & Kypta, 2012). However, this aspect requires further investigation.

The antibody epitope region is outside of known Wnt receptor binding sites identified on other Wnts. This region of the Wnt-11 protein is highly conserved in evolution but shares little sequence similarity with the same region in other Wnt family members, consistent with the observed specificity of the antibodies. In context of receptor and coreceptor binding, the epitope is located far from the predicted FZD-interacting regions but is adjacent to a region that has been proposed to be involved in binding of Wnt-3 to LRP6 (Hirai et al., 2019). Although the antibody epitope *per se* has not been described as mediating binding, it was

considered that being adjacent in the structure could affect binding affinity. Furthermore, a model in which the crystal structure of an antibody Fab fragment is juxtaposed to that of Wnt-3 was generated and suggested that antibody binding to Wnt-11 at the site of the epitope could sterically hinder binding of LRP6 to Wnt-11 at the predicted LRP6 binding site.

The following observations also prompted further study of LRP6. First, *WNT11* gene silencing reduced *LRP6* mRNA levels in PC3 cells, suggesting they might be co-regulated. Second, IP experiments demonstrated that Wnt-11 interacted with LRP6 in a comparable manner to Wnt-3a. Accordingly, LRP6 interaction with the AE protein was found to be reduced, compared to binding to wild type Wnt-11, and this contrasted with the binding detected with FZD8, which showed to be equal for both Wnt-11 and AE in IP assays. Reduced interaction of the AE was observed with full length LRP6 and with the LRP6 extracellular region (ectodomain), using different tagged constructs (VSV-G, Fc) and in different cell models (PC3, HEK 293). The reduced LRP6/AE interaction was further confirmed by co-localization immunofluorescence assays of LRP6 and Wnt-11 or AE in co-expressing PC3 cells. However, an important question is whether the Wnt-11 antibodies are able to directly inhibit the interaction between Wnt-11 and LRP6. Unfortunately, this could not be addressed for technical reasons related to the difficulties carrying out immunoprecipitation assays in the presence of both blocking antibody and immunoprecipitating antibody, and the difficulties in the assessment of the Wnt-11/LRP6 interaction in an extracellular environment.

Therefore, given the alteration in binding of the AE to LRP6, the implications of LRP6 in Wnt-11 signaling and *vice versa* were examined by comparing wild-type Wnt-11 and the AE in gene reporter assays. LRP6 is a potent activator of β-catenin/TCF signaling (Cong, Schweizer, & Varmus, 2004) and Wnt-11 was able to inhibit LRP6-induced activation of TOP-luc in gene reporter assays, as was also observed for stimulation with Wnt-3a CM. In contrast, AE expression was not able to repress LRP6-induced activity. As LRP6 overexpression alone activated canonical Wnt signaling further experiments are required to determine if the Wnt-11 effects involves Wnt receptor competition or other mechanisms in this matter.

The role of LRP6 was also examined in the context of Wnt-11/ATF2 signaling. In PC3 cells, transfection of LRP6 did not increase ATF2-dependent reporter activity and did not potentiate the activation by Wnt-11. However, PC3 cells express high levels of endogenous *LRP6*, with a ΔΔCT of 6, which is about 16-fold higher than for *WNT11* (see Table 13, page 104).

Therefore, the role of LRP6 was further analyzed using HEK 293 LRP5/6$^{-/-}$ mutant cells (Eubelen et al., 2018). As FZD8 is a known Wnt-11 receptor, the effects of LRP6 were examined in combination with both Wnt-11/AE and FZD8. Co-expression of LRP6 and FZD8 increased ATF2-dependent activity to a greater extent than either alone, and when co-expressed with Wnt-11, there was a further increase in ATF2-dependent transcription. Comparing Wnt-11 and AE, both elicited a comparable activation by themselves and when co-expressed with FZD8 (in the absence of LRP6), suggesting that FZD8/AE interaction is not impaired and is able to activate an ATF2-dependent signal. However, in this context, the restoration of LRP6 led to a further increase in ATF2-dependent activity for wild-type Wnt-11 and not for the Wnt-11 mutant AE. These results suggest that the difference in ATF2-dependent transcription observed between Wnt-11 and the AE in this setting results from differential interactions with LRP6.

However, several limitations are acknowledged regarding the use of ATF2-luc gene reporter assays. First, HEK 293 cells are known to express adenovirus early region 1A protein that directly binds and regulates ATF2 (X.-Y. Li & Green, 1996), which likely drives the high basal ATF2-dependent transcriptional activity these cells show, rendering the effects of FZD8/LRP6/Wnt-11 on gene reporter activity modest. Another, is that ATF2 is not a transcription factor dedicated to noncanonical Wnt signaling activity, as acknowledged above (van Amerongen, 2012). Finally, the transfection of multiple plasmids for expression required the use of lower quantities of each, rendering lower expression levels and the possibility that not all cells received all expression plasmids and reporters.

Nonetheless, LRP6 is far from being an obvious coreceptor for Wnt-11. Although Wnt-11 and Wnt-5a have been found to activate some of the same noncanonical signals, they show differences in many instances. For example, fusion receptors of Wnt to LRP6 or ROR1/2 have been useful in the study of Wnt-3a and Wnt-5a signaling, but for Wnt-11, this strategy was found unable to trigger a response (Grumolato et al., 2010). LRP6 is a well-known component of β-catenin-dependent Wnt signaling (Pinson et al., 2000; Tamai et al., 2000; Wehrli et al., 2000). Oligomerization of FZD and LRP5/6 is regarded as an early event leading to intracellular β-catenin-dependent signaling, and this can also happen Wnt-independently (Cong et al., 2004; Hua et al., 2018). Moreover, LRP6 has been shown to interact with several different Wnts, and with multiple binding sites. Specifically, two distinct binding sites have been proposed for Wnts in LRP6, one comprising the extracellular domains E1-E2, which can bind

Wnt-1 and Wnt-9, and the other E3-E4, which binds Wnt-3/Wnt-3a (Bourhis et al., 2010; S. Chen et al., 2011; Gong et al., 2010). It remains unclear which domains of LRP6 bind Wnt-11.

The role of LRP6 in noncanonical Wnt signaling is controversial. LRP6 has been reported to bind to Wnt-5a, but this interaction leads to repression of noncanonical signaling in Xenopus and mouse embryos (Bryja et al., 2009). It has also been reported that mutations linked to neural tube defects in humans lead to increased PCP pathway signaling during mouse embryo development, suggesting LRP6 acts as an inhibitor, rather than an activator of noncanonical Wnt signaling (Allache et al., 2013). In contrast to the model of oligomerization of FZD with LRP5/6 being an initiator of canonical Wnt signaling, it has been proposed that this interaction in a basal state represses both canonical and noncanonical pathways (D. N. Ren et al., 2015). Consistent with this, the same group reported that soluble recombinant LRP6 ectodomain inhibits mouse and human breast cancer cell migration and metastasis by inhibiting FZD-dependent noncanonical signaling. Another LRP6 construct comprising only a part of the extracellular domain (E1, E2) has also been reported to inhibit not only canonical Wnt signaling, but also EMT, and its expression was shown to induce apoptosis in lung cancer cells (J. S. Lee et al., 2012).

However, there are some instances in which LRP6 has been found to interact with noncanonical Wnt ligands and/or potentiate noncanonical Wnt signaling. LRP6 has been reported to enhance noncanonical Wnt signaling through RhoA-dependent mechanisms by association with disheveled-associated activator of morphogenesis 1 (DAAM1); and Wnt-5a stimulation of RhoA activity was found to be impaired in LRP6-null mouse embryonic fibroblast cells (Gray et al., 2013). LRP6 can associate with one of the two *WNT11* paralogs present in Xenopus oocytes to mediate β-catenin-dependent signaling. However, although both paralogs display high sequence similarity, *xWnt11* is not the human *WNT11* ortholog, which is rather *xWnt11b* (Hardy et al., 2008; Kofron et al., 2007). LRP6 was recently reported to interact indirectly with Wnt-11, impacting cardiac fibrosis (X. Wang et al., 2021). The interaction was described to take place intracellularly and resulted in degradation of Wnt-11 and Wnt-5a through cathepsin D (CTSD) protease.

The methods used here for detection of the interaction LRP6/Wnt-11, i.e., co-immunoprecipitation and immunofluorescence can also report indirect interactions, and the use of direct binding assays, such as surface plasmon resonance, could be explored. The status of

LRP6 phosphorylation in the context of Wnt-11 activation/inhibition was explored by stimulation with Wnt-11 in combination with Wnt-C59 treatment, as well as with E8 and F10 antibody treatment, but the results were inconclusive. Therefore, although LRP6 appears to be important for the effects of the antibody epitope deletion, the exact role of LRP6 in Wnt-11 signaling remains to be explored, and further studies will be required to determine which of the cellular responses to Wnt-11 in prostate cancer involve LRP6.

As for LRP6 role in cancer, it has been described to be important in colorectal, liver, breast and pancreatic cancers (Raisch, Côté-Biron, & Rivard, 2019; Roslan, Muhamad, Selvaratnam, & Ab-Rahim, 2019). LRP6 can promote invasion and metastasis of colorectal cancer, inducing microtubule dynamics and actin remodeling, probably through regulation of RhoA and Rac1, which are hallmarks of noncanonical Wnt signaling (Q. Yao et al., 2017). Wnt-11 is also known to play a role in colorectal cancer (Gorroño-Etxebarria et al., 2019). LRP6 has been found upregulated in a subpopulation of human breast cancers where it promotes cell proliferation and tumor growth (C. C. Liu, Prior, Piwnica-Worms, & Bu, 2010). LRP6 was also found to promote migration and invasion of triple negative breast cancer cells through β-catenin signaling-mediated regulation of S100A4 (Ma, Lu, Chen, Xu, & Li, 2017). LRP6 has also been implicated in prostate cancer: LRP6 induced-degradation by the antihelminthic drug niclosamide and by the antibiotic salinomycin has been reported to reduce prostate cancer cell growth and to promote apoptosis (W. Lu & Li, 2014; W. Lu et al., 2011). Similarly, another drug, silibinin, the major active constituent of silymarin, a standardized extract of milk thistle, reduces prostate cancer cell growth by reducing LRP6 levels (W. Lu et al., 2012). However, these effects might not be specific to LRP6. MESD, a specialized chaperone for LRP5 and LRP6, can also act as their inhibitor, and was shown to inhibit the growth of prostate tumors in xenograft assays (C. Lin et al., 2011; W. Lu, Liu, Thottassery, Bu, & Li, 2010).

Multiple studies have been focused on developing specific LRP6 inhibitors, some using neutralizing antibodies (N. K. Lee et al., 2018) and single-domain antibody fragments (VHH) against a specific region of LRP6, which strongly inhibits Wnt-3a-induced β-catenin-mediated transcription (Fenderico et al., 2019). Importantly there is a Phase I clinical trial with a bi-paratopic anti-LRP6 antibody, BI 905677, which is being investigated for therapy in Wnt-driven tumors (Zinzalla et al., 2019).

It is also important to highlight that the predicted LRP6 binding site on Wnt-3 has been shown to mediate binding to other coreceptors on other Wnts, for example, RECK (reversion

inducing cysteine-rich protein with kazal motifs) (Eubelen et al., 2018). While RECK binding appears to be unique to Wnt-7a/b, the possibility that Wnt-11 binds RECK or the associated receptor GPR124 has not been tested. Alternatively, a Wnt-11-specific partner may bind this region in Wnt-11. In the context of prostate cancer, ROR1 is also a good candidate co-receptor, since it has been linked to prostate cancer progression (Murillo-Garzón et al., 2018; S. Zhang et al., 2012). In addition to understanding which receptors are involved, it will be important to explore the potential implications of the equivalent region of the Wnt-11 antibody epitope in the function of other Wnts.

Together, the results in this thesis suggest that antibodies targeting amino acids within the sequence L101-A112 in Wnt-11 impair its ability to signal and function. The anti-Wnt-11 antibodies inhibit prostate cancer cell sphere proliferation, invasion, and migration. E8 antibody and its nanoformulation (MNP-E8) reduce PC3 tumor growth in the CAM, which is accompanied by a reduction in the intensity of the Ki67 proliferation marker. The region containing the antibody epitope has been shown to be important in mediating DVL activation and Wnt-11/FZD8-induced ATF2-dependent transcription, which could be the result of reduced binding of Wnt-11 to LRP6. These observations, which are summarized in a model (Figure 58), lend support for further investigation of Wnt-11 as a therapeutic target in prostate cancer. Also, these antibodies and their nanoformulations provide the means to block Wnt-11 function, which may be beneficial for treatment of patients in the future.

Figure 58. Working model of anti-Wnt-11 antibodies and MNP nanoformulations strategy in the treatment of advanced prostate cancer. In advanced prostate cancer ADT, TMPRSS2-ERG fusion and hypoxia among other factors increase Wnt-11 expression levels (upper panel). Wnt-11 (represented by yellow spheres) then signals via increased phosphorylation of DVL and activation of FZD8/LRP6/ATF2-dependent signaling (Wnt-11 on, bottom left panel). These effectors of Wnt-11, and possibly others that remain to be identified, result in the promotion of prostate cancer cell migration, invasion, tumor growth and stemness. Delivery of anti-Wnt-11 antibodies and their MNP nanoformulations to prostate tumors impairs Wnt-11 signaling by diminishing DVL phosphorylation, reducing Wnt-11/LRP6 coreceptor binding, and limiting FZD8/LRP6/ATF2-dependent signaling (Wnt-11 inhibition, bottom right panel). This results in reduced migration, invasion, tumor growth and stemness.

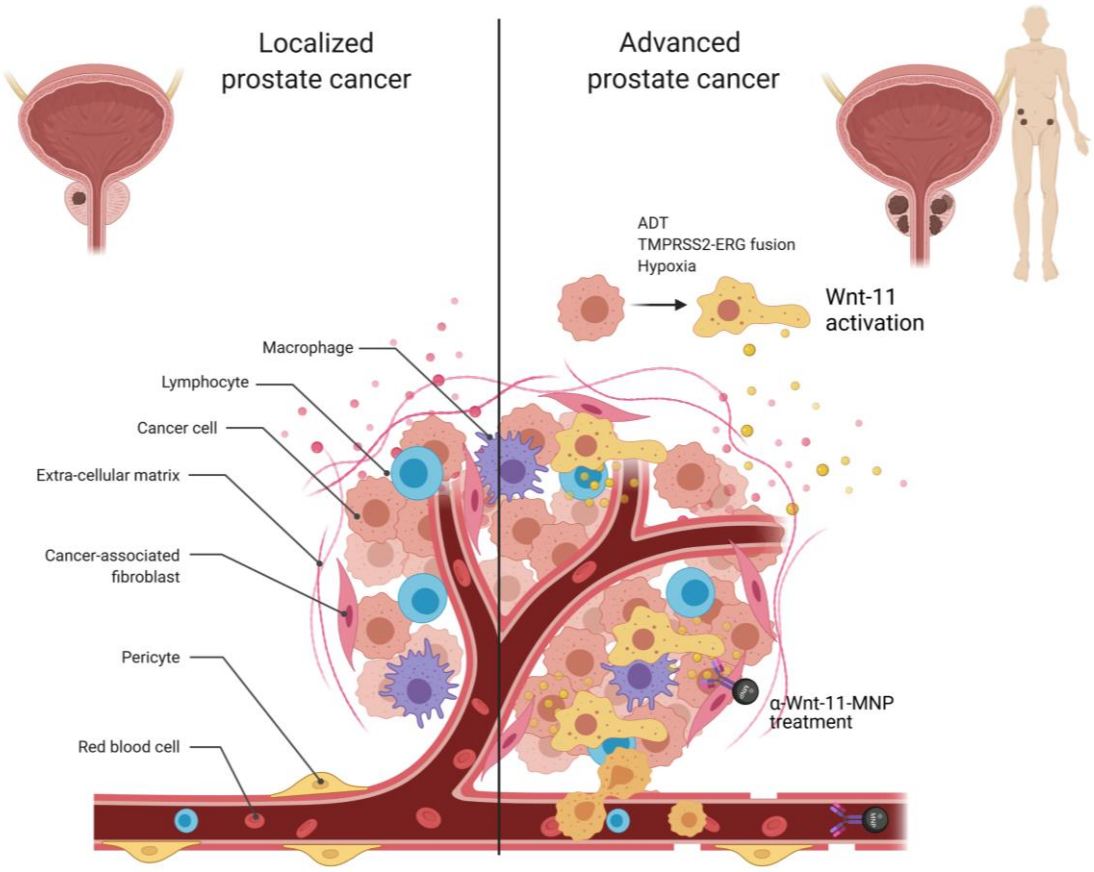
Localized
prostate cancer
Advanced
prostate cancer
ADT
TMPRSS2-ERG fusion
Hypoxia
Wnt-11
activation
Macrophage
Lymphocyte
Cancer cell
Extra-cellular matrix
Cancer-associated
fibroblast
Pericyte
Red blood cell
α-Wnt-11-MNP
treatment

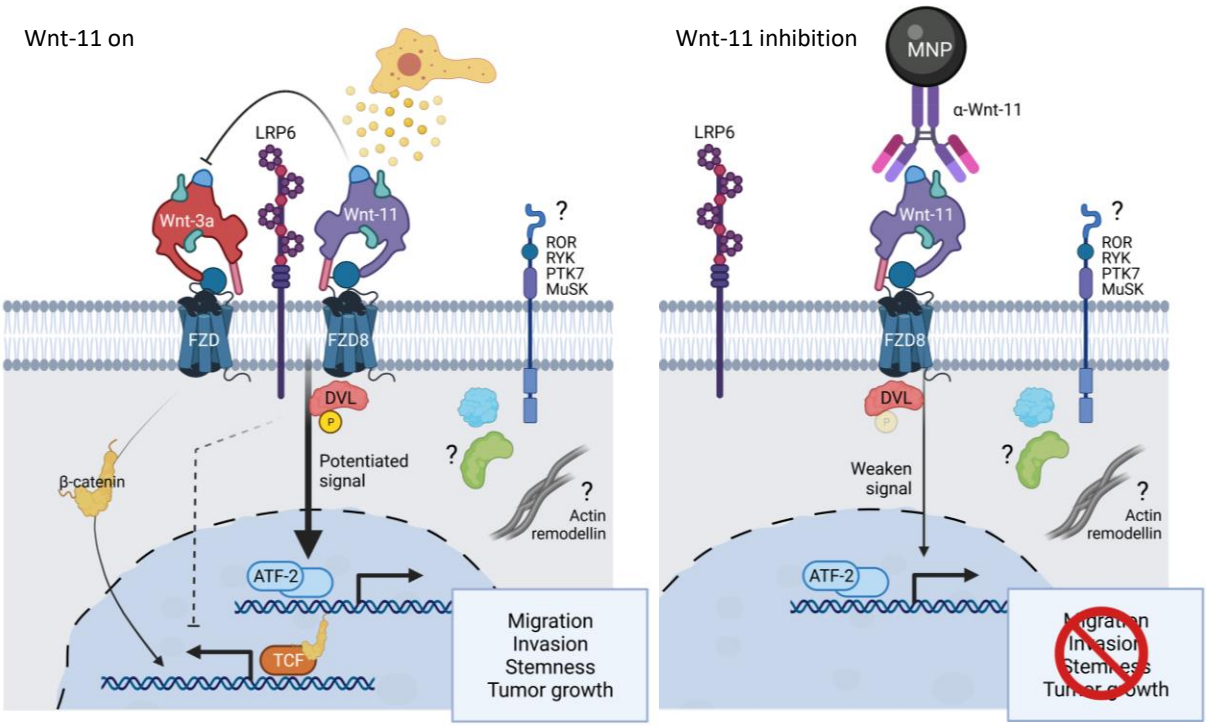
Wnt-11 on
LRP6
Wnt-3a
Wnt-11
FZD
FZD8
ROR
RYK
PTK7
MuSK
DVL
P
β-catenin
Potentiated
signal
Actin
remodellin
ATF-2
TCF
Migration
Invasion
Stemness
Tumor growth
Wnt-11 inhibition
MNP
α-Wnt-11
LRP6
Wnt-11
FZD8
ROR
RYK
PTK7
MuSK
DVL
Weaken
signal
Actin
remodellin
ATF-2

Conclusions

The results obtained in this thesis lead to the following conclusions:

1. Two rat monoclonal antibodies, E8 and F10, bind to the same unique Wnt-11 peptide and inhibit Wnt-11 mediated processes, namely DVL phosphorylation, prostate cancer cell sphere formation, cell migration under normoxia and hypoxia, and cell invasion.
2. Iron oxide magnetic nanoparticles functionalized with anti-Wnt-11 neutralizing antibodies inhibit prostate cancer cell migration without affecting viability.
3. Antibody E8 and MNP-E8 nanoconjugates reduce PC3 cell tumor growth *in vivo* in the chick chorioallantoic membrane (CAM) model.
4. The Wnt-11 antibody epitope is required for Wnt-11 induction of DVL phosphorylation and of PC3M cell migration.
5. The Wnt-11 antibody epitope deletion reduces binding of Wnt-11 to the Wnt coreceptor LRP6 and limits Wnt-11 inhibition of β-catenin/TCF-dependent transcription and potentiation of FZD8/LRP6/ATF2 signaling.
6. Wnt-11 neutralizing antibodies and nanoconjugates have the potential to be further explored as therapeutic agents to treat patients with advanced prostate cancer.

References

Acebron, S. P., & Niehrs, C. (2016). β-Catenin-Independent Roles of Wnt/LRP6 Signaling. *Trends in Cell Biology*, *26*(12), 956–967. https://doi.org/10.1016/j.tcb.2016.07.009

Aires, A., Cadenas, J. F., Guantes, R., & Cortajarena, A. L. (2017). An experimental and computational framework for engineering multifunctional nanoparticles: designing selective anticancer therapies. *Nanoscale*, *9*(36), 13760–13771. https://doi.org/10.1039/C7NR04475E

Aires, A., Ocampo, S. M., Simões, B. M., Josefa Rodríguez, M., Cadenas, J. F., Couleaud, P., … Cortajarena, A. L. (2016). Multifunctionalized iron oxide nanoparticles for selective drug delivery to CD44-positive cancer cells. *Nanotechnology*, *27*(6). https://doi.org/10.1088/0957-4484/27/6/065103

Allache, R., Lachance, S., Guyot, M. C. laud., De Marco, P., Merello, E., Justice, M. J., … Kibar, Z. (2013). Novel mutations in Lrp6 orthologs in mouse and human neural tube defects affect a highly dosage-sensitive Wnt non-canonical planar cell polarity pathway. *Human Molecular Genetics*, *23*(7), 1687–1699. https://doi.org/10.1093/hmg/ddt558

AlphaFold Protein Structure Database. (2021). AlphaFold FAQs. Retrieved October 5, 2021, from https://alphafold.ebi.ac.uk/faq

American cancer society. (2021). Cancer (ACS). Retrieved May 17, 2021, from https://www.cancer.org/cancer/cancer-basics/what-is-cancer.html

Anastas, J. N., & Moon, R. T. (2013). WNT signalling pathways as therapeutic targets in cancer. *Nature Reviews Cancer*, *13*(1), 11–26. https://doi.org/10.1038/nrc3419

Andre, P., Song, H., Kim, W., Kispert, A., & Yang, Y. (2015). Wnt5a and Wnt11 regulate mammalian anterior-posterior axis elongation. *Development*, *142*(8), 1516–1527. https://doi.org/10.1242/dev.119065

Antonarakis, E. S., Piulats, J. M., Gross-Goupil, M., Goh, J., Ojamaa, K., Hoimes, C. J., … de Bono, J. S. (2020). Pembrolizumab for Treatment-Refractory Metastatic Castration-Resistant Prostate Cancer: Multicohort, Open-Label Phase II KEYNOTE-199 Study. *Journal of Clinical Oncology*, *38*(5), 395–405. https://doi.org/10.1200/JCO.19.01638

Arap, W., Pasqualini, R., & Costello, J. F. (2020). Prostate Cancer Progression and the Epigenome. *Clinical Implications of Basic Research, NEJM*, 2287–2290.

Argiles, G., Jungels, C., Garcia-Carbonero, R., Diez Garcia, M., Bendell, J. C., Tabernero, J., … Hollebecque, A. (2021). Phase I dose-escalation study of MCLA-158, a first-in-class bispecific antibody targeting EGFR and LGR5, in metastatic colorectal cancer (CRC). *Journal of Clinical Oncology*, *39*(3_suppl), 62. https://doi.org/10.1200/JCO.2021.39.3_suppl.62

Arisan, E. D., Rencuzogullari, O., Freitas, I. L., Radzali, S., Keskin, B., Kothari, A., … Uysal-Onganer, P. (2020). Upregulated wnt-11 and mir-21 expression trigger epithelial mesenchymal transition in aggressive prostate cancer cells. *Biology*, *9*(3). https://doi.org/10.3390/biology9030052

Armenia, J., Wankowicz, S. A. M., Liu, D., Gao, J., Kundra, R., Reznik, E., … Van Allen, E. M. (2018). The long tail of oncogenic drivers in prostate cancer. *Nature Genetics*, *50*(5), 645–651. https://doi.org/10.1038/s41588-018-0078-z

Ateeq, B., Tomlins, S. A., Laxman, B., Asangani, I. A., Cao, Q., Cao, X., … Chinnaiyan, A. M. (2011). Therapeutic targeting of SPINK1-positive prostate cancer. *Science Translational Medicine*, *3*(72). https://doi.org/10.1126/scitranslmed.3001498

Attard, G., Parker, C., Eeles, R. A., Schröder, F., Tomlins, S. A., Tannock, I., … De Bono, J. S. (2016). Prostate cancer. *The Lancet*, *387*(10013), 70–82. https://doi.org/10.1016/S0140-6736(14)61947-4

Azimian-Zavareh, V., Hossein, G., Ebrahimi, M., & Dehghani-Ghobadi, Z. (2018). Wnt11 alters integrin and cadherin expression by ovarian cancer spheroids and inhibits tumorigenesis and metastasis. *Experimental Cell Research*, *369*(1), 90–104. https://doi.org/10.1016/j.yexcr.2018.05.010

Azzolin, L., Panciera, T., Soligo, S., Enzo, E., Bicciato, S., Dupont, S., … Piccolo, S. (2014). YAP/TAZ incorporation in the β-catenin destruction complex orchestrates the Wnt response. *Cell*, *158*(1), 157–170. https://doi.org/10.1016/j.cell.2014.06.013

Bankhead, P., Loughrey, M. B., Fernández, J. A., Dombrowski, Y., McArt, D. G., Dunne, P. D., … Hamilton, P. W. (2017). QuPath: Open source software for digital pathology image analysis. *Scientific Reports*, *7*(1), 1–7. https://doi.org/10.1038/s41598-017-17204-5

Bartis, D., Csongei, V., Weich, A., Kiss, E., Barko, S., Kovacs, T., … Pongracz, J. E. (2013). Down-Regulation of Canonical and Up-Regulation of Non-Canonical Wnt Signalling in the Carcinogenic Process of Squamous Cell Lung Carcinoma. *PLoS ONE*, *8*(3). https://doi.org/10.1371/journal.pone.0057393

Bateman, A., Martin, M. J., Orchard, S., Magrane, M., Agivetova, R., Ahmad, S., … Zhang, J. (2021). UniProt: The universal protein knowledgebase in 2021. *Nucleic Acids Research*, *49*(D1), D480–D489. https://doi.org/10.1093/nar/gkaa1100

Bekes, E. M., Deryugina, E. I., Kupriyanova, T. A., Zajac, E., Botkjaer, K. A., Andreasen, P. A., & Quigley, J. P. (2011). Activation of Pro-uPA Is Critical for Initial Escape from the Primary Tumor and Hematogenous Dissemination of

Human. *Neoplasia*, *13*(9), 806–821. https://doi.org/10.1593/neo.11704

Beltran, H., Prandi, D., Mosquera, J. M., Benelli, M., Puca, L., Cyrta, J., … Author, N. M. (2016). Divergent clonal evolution of castration resistant neuroendocrine prostate cancer. *Nat Med*, *22*(3), 298–305. https://doi.org/10.1038/nm.4045.Divergent

Bengoa-Vergniory, N., Gorroño-Etxebarria, I., González-Salazar, I., & Kypta, R. M. (2014). A switch from canonical to noncanonical wnt signaling mediates early differentiation of human neural stem cells. *Stem Cells*, *32*(12), 3196–3208. https://doi.org/10.1002/stem.1807

Bengoa-Vergniory, N., Gorroño-Etxebarria, I., López-Sánchez, I., Marra, M., Di Chiaro, P., & Kypta, R. (2017). Identification of Noncanonical Wnt Receptors Required for Wnt-3a-Induced Early Differentiation of Human Neural Stem Cells. *Molecular Neurobiology*, *54*(8), 6213–6224. https://doi.org/10.1007/s12035-016-0151-5

Boitard, M., Bocchi, R., Egervari, K., Petrenko, V., Viale, B., Gremaud, S., … Kiss, J. Z. (2015). Wnt signaling regulates multipolar-to-bipolar transition of migrating neurons in the cerebral cortex. *Cell Reports*, *10*(8), 1349–1361. https://doi.org/10.1016/j.celrep.2015.01.061

Bourhis, E., Tam, C., Franke, Y., Bazan, J. F., Ernst, J., Hwang, J., … Hannoush, R. N. (2010). Reconstitution of a Frizzled8·Wnt3a·LRP6 signaling complex reveals multiple Wnt and Dkk1 binding sites on LRP6. *Journal of Biological Chemistry*, *285*(12), 9172–9179. https://doi.org/10.1074/jbc.M109.092130

Boutros, M., & Mlodzik, M. (1999). Dishevelled: At the crossroads of divergent intracellular signaling pathways. *Mechanisms of Development*, *83*(1–2), 27–37. https://doi.org/10.1016/S0925-4773(99)00046-5

Boyan, B. D., Olivares-Navarrete, R., Berger, M. B., Hyzy, S. L., & Schwartz, Z. (2018). Role of Wnt11 during Osteogenic Differentiation of Human Mesenchymal Stem Cells on Microstructured Titanium Surfaces. *Scientific Reports*, *8*(1), 1–11. https://doi.org/10.1038/s41598-018-26901-8

Brahimi-Horn, M. C., Chiche, J., & Pouysségur, J. (2007). Hypoxia and cancer. *Journal of Molecular Medicine*, *85*(12), 1301–1307. https://doi.org/10.1007/s00109-007-0281-3

Bruhat, A., Jousse, C., Carraro, V., Reimold, A. M., Ferrara, M., & Fafournoux, P. (2000). Amino acids control mammalian gene transcription: activating transcription factor 2 is essential for the amino acid responsiveness of the CHOP promoter. *Molecular and Cellular Biology*, *20*(19), 7192–7204. Retrieved from http://www.ncbi.nlm.nih.gov/pubmed/10982836%0Ahttp://www.pubmedcentral.nih.gov/articlerender.fcgi?artid=PMC86273

Bryja, V., Andersson, E. R., Alexandra, S., Milan, E., Bryjova, L., Biris, K. K., … Arenas, E. (2009). The Extracellular Domain of Lrp5/6 Inhibits Noncanonical Wnt Signaling In Vivo. *Molecular Biology of the Cell*, *20*(2007), 2673–2683. https://doi.org/10.1091/mbc.E08

Buffa, F. M., Harris, A. L., West, C. M., & Miller, C. J. (2010). Large meta-analysis of multiple cancers reveals a common , compact and highly prognostic hypoxia metagene. *British Journal of Cancer*, *102*(2), 428–435. https://doi.org/10.1038/sj.bjc.6605450

Canesin, G., Evans-Axelsson, S., Hellsten, R., Krzyzanowska, A., Prasad, C. P., Bjartell, A., & Andersson, T. (2017). Treatment with the WNT5A-mimicking peptide Foxy-5 effectively reduces the metastatic spread of WNT5A-low prostate cancer cells in an orthotopic mouse model. *PLoS ONE*, *12*(9), 1–19. https://doi.org/10.1371/journal.pone.0184418

Castelli, M. S., McGonigle, P., & Hornby, P. J. (2019). The pharmacology and therapeutic applications of monoclonal antibodies. *Pharmacology Research & Perspectives*, *7*(6), e00535. https://doi.org/10.1002/prp2.535

Cha, S.-W., Tadjuidje, E., Tao, Q., Wylie, C., & Heasman, J. (2008). Wnt5a and Wnt11 interact in a maternal Dkk1-regulated fashion to activate both canonical and non-canonical signaling in Xenopus axis formation. *Development*, *135*(22), 3719–3729. https://doi.org/10.1242/dev.029025

Chakravarthi, B. V. S. K., Goswami, M. T., Pathi, S. S., Dodson, M., Chandrashekar, D. S., Agarwal, S., … Varambally, S. (2017). Expression and Role of PAICS, a De Novo Purine Biosynthetic Gene in Prostate Cancer. *Prostate*, *77*(1), 10–21. https://doi.org/10.1002/pros.23243

Chang, T. H., Hsieh, F. L., Zebisch, M., Harlos, K., Elegheert, J., & Jones, E. Y. (2015). Structure and functional properties of norrin mimic wnt for signalling with Frizzled4, Lrp5/6, and proteoglycan. *ELife*, *4*(JULY 2015), 1–27. https://doi.org/10.7554/eLife.06554

Chen, B., Chen, X., Liu, C., Li, J., Liu, F., & Huang, Y. (2018). Co-expression of Akt1 and Wnt11 promotes the proliferation and cardiac differentiation of mesenchymal stem cells and attenuates hypoxia/reoxygenation-induced cardiomyocyte apoptosis. *Biomedicine and Pharmacotherapy*, *108*(September), 508–514. https://doi.org/10.1016/j.biopha.2018.09.047

Chen, B., Dodge, M. E., Tang, W., Lu, J., Ma, Z., Fan, C.-W., … Lum, L. (2009). Small molecule-mediated in Tissue Regeneration and Cancer. *Nature Chemical Biology*, *5*(2), 100–107. https://doi.org/10.1038/nchembio.137.Small

Chen, C., Aihemaiti, M., Zhang, X., Qu, H., Sun, Q.-L., He, Q.-S., & Yu, W.-B. (2018). Downregulation of histone

demethylase JMJD1C inhibits colorectal cancer metastasis through targeting ATF2. *American Journal of Cancer Research*, *8*(5), 852–865.

Chen, S., Bubeck, D., MacDonald, B. T., Liang, W. X., Mao, J. H., Malinauskas, T., … Jones, E. Y. (2011). Structural and functional studies of LRP6 ectodomain reveal a platform for Wnt signaling. *Developmental Cell*, *21*(5), 848–861. https://doi.org/10.1016/j.devcel.2011.09.007

Chien, A. J., Conrad, W. H., & Moon, R. T. (2009). A wnt survival guide: From flies to human disease. *Journal of Investigative Dermatology*, *129*(7), 1614–1627. https://doi.org/10.1038/jid.2008.445

Choi, E. Y., Park, H. H., Kim, H., Kim, H. N., Kim, I., Jeon, S., … Lee, W. (2020). Wnt5a and Wnt11 as acute respiratory distress syndrome biomarkers for severe acute respiratory syndrome coronavirus 2 patients. *European Respiratory Journal*, *56*(5). https://doi.org/10.1183/13993003.01531-2020

Choi, M. Y., 2nd, G. F. W., Wu, C. C. N., Cui, B., Lao, F., Sadarangani, A., … Kipps, T. J. (2016). Pre-clinical specificity and safety of UC-961, a first-in-class monoclonal antibody targeting ROR1. *Physiology & Behavior*, *176*(1), 139–148. https://doi.org/10.1016/j.clml.2015.02.010.Pre-clinical

Chowdhury, P., Roberts, A. M., Khan, S., Hafeez, B. B., Chauhan, S. C., Jaggi, M., & Yallapu, M. M. (2017). Magnetic nanoformulations for prostate cancer. *Drug Discovery Today*, *22*(8), 1233–1241. https://doi.org/10.1016/j.drudis.2017.04.018

Christiansen, J. H., Monkley, S. J., & Wainwright, B. J. (1996). Murine WNT11 is a secreted glycoprotein that morphologically transforms mammary epithelial cells. *Oncogene*, *12*(12), 2705—2711. Retrieved from http://europepmc.org/abstract/MED/8700530

Chu, M. L.-H. H., Ahn, V. E., Choi, H.-J. J., Daniels, D. L., Nusse, R., & Weis, W. I. (2013). Structural studies of wnts and identification of an LRP6 binding site. *Structure*, *21*(7), 1235–1242. https://doi.org/10.1016/j.str.2013.05.006.Structural

Clevers, H., Loh, K. M., & Nusse, R. (2014). An integral program for tissue renewal and regeneration: Wnt signaling and stem cell control. *Science*, *346*(6205). https://doi.org/10.1126/science.1248012

Clevers, H., & Nusse, R. (2012). Wnt/β-catenin signaling and disease. *Cell*, *149*(6), 1192–1205. https://doi.org/10.1016/j.cell.2012.05.012

Cong, F., Schweizer, L., & Varmus, H. (2004). Wnt signals across the plasma membrane to activate the β-catenin pathway by forming oligomers containing its receptors, Frizzled and LRP. *Development*, *131*(20), 5103–5115. https://doi.org/10.1242/dev.01318

Conn, E. M., Botkjaer, K. A., Kupriyanova, T. A., Andreasen, P. A., Deryugina, E. I., & Quigley, J. P. (2009). Comparative analysis of metastasis variants derived from human prostate carcinoma cells: Roles in intravasation of VEGF-mediated angiogenesis and uPA-mediated invasion. *American Journal of Pathology*, *175*(4), 1638–1652. https://doi.org/10.2353/ajpath.2009.090384

Cortazar, A. R., Torrano, V., Martín-Martín, N., Caro-Maldonado, A., Camacho, L., Hermanova, I., … Carracedo, A. (2018). Cancertool: A visualization and representation interface to exploit cancer datasets. *Cancer Research*, *78*(21), 6320–6328. https://doi.org/10.1158/0008-5472.CAN-18-1669

Coudreuse, D., & Korswagen, H. C. (2007). The making of Wnt: New insights into Wnt maturation, sorting and secretion. *Development*, *134*(1), 3–12. https://doi.org/10.1242/dev.02699

Craig Venter, J., Adams, M. D., Myers, E. W., Li, P. W., Mural, R. J., Sutton, G. G., … Zhu, X. (2001). The sequence of the human genome. *Science*, *291*(5507), 1304–1351. https://doi.org/10.1126/science.1058040

Crespo, P., & Casar, B. (2016). The Chick Embryo Chorioallantoic Membrane as an in vivo Model to Study Metastasis. *Bio-Protocol*, *6*(20). https://doi.org/10.21769/bioprotoc.1962

Dart, D. A., Arisan, D. E., Owen, S., Hao, C., Jiang, W. G., & Uysal-Onganer, P. (2019). Wnt-11 expression promotes invasiveness and correlates with survival in human pancreatic ductal adeno carcinoma. *Genes*, *10*(11), 1–13. https://doi.org/10.3390/genes10110921

Day, T. F., Guo, X., Garrett-Beal, L., & Yang, Y. (2005). Wnt/β-catenin signaling in mesenchymal progenitors controls osteoblast and chondrocyte differentiation during vertebrate skeletogenesis. *Developmental Cell*, *8*(5), 739–750. https://doi.org/10.1016/j.devcel.2005.03.016

Dehm, S. M., & Tindall, D. J. (2019). *Prostate Cancer Cellular and Genetic Mechanisms of Disease Development and Progression*. (S. M. Dehm & D. J. Tindall, Eds.) (Second). Advances in Experimental Medicine and Biology.

Deshmukh, V., Seo, T., O'Green, A. L., Ibanez, M., Hofilena, B., Sunil, K. C., … Yazici, Y. (2020). SM04755, a small-molecule inhibitor of the Wnt pathway, as a potential topical treatment for tendinopathy. *Journal of Orthopaedic Research*, (May). https://doi.org/10.1002/jor.24898

DeVita, V. T., & Chu, E. (2008). A history of cancer chemotherapy. *Cancer Research*, *68*(21), 8643–8653. https://doi.org/10.1158/0008-5472.CAN-07-6611

Diamond, J. R., Becerra, C., Richards, D., Mita, A., Osborne, C., O'Shaughnessy, J., … Mita, M. (2020). Phase Ib clinical trial of the anti-frizzled antibody vantictumab (OMP-18R5) plus paclitaxel in patients with locally advanced or metastatic HER2-negative breast cancer. *Breast Cancer Research and Treatment*, *184*(1), 53–62. https://doi.org/10.1007/s10549-020-05817-w

Diana, V., Bossolasco, P., Moscatelli, D., Silani, V., & Cova, L. (2013). Dose dependent side effect of superparamagnetic iron oxide nanoparticle labeling on cell motility in two fetal stem cell populations. *PLoS ONE*, *8*(11). https://doi.org/10.1371/journal.pone.0078435

Doumpas, N., Lampart, F., Robinson, M. D., Lentini, A., Nestor, C. E., Cantù, C., & Basler, K. (2019). TCF / LEF dependent and independent transcriptional regulation of Wnt/β-catenin target genes . *The EMBO Journal*, *38*(2), 1–14. https://doi.org/10.15252/embj.201798873

Dulińska-Litewka, J., Łazarczyk, A., Hałubiec, P., Szafrański, O., Karnas, K., & Karewicz, A. (2019). Superparamagnetic iron oxide nanoparticles-current and prospective medical applications. *Materials*, *12*(4). https://doi.org/10.3390/ma12040617

Dull, T., Zufferey, R., Kelly, M., Mandel, R. J., Nguyen, M., Trono, D., & Naldini, L. (1998). A Third-Generation Lentivirus Vector with a Conditional Packaging System. *Journal of Virology*, *72*(11), 8463–8471. https://doi.org/10.1128/jvi.72.11.8463-8471.1998

Dwyer, M. A., Joseph, J. D., Wade, H. E., Eaton, M. L., Kunder, R. S., Kazmin, D., … McDonnell, D. P. (2010). WNT11 expression is induced by estrogen-related receptor α and β-catenin and acts in an autocrine manner to increase cancer cell migration. *Cancer Research*, *70*(22), 9298–9308. https://doi.org/10.1158/0008-5472.CAN-10-0226

Ecker, D. M., Jones, S. D., & Levine, H. L. (2015). The therapeutic monoclonal antibody market. *MAbs*, *7*(1), 9–14. https://doi.org/10.4161/19420862.2015.989042

Edgar, R. C. (2004). MUSCLE: Multiple sequence alignment with high accuracy and high throughput. *Nucleic Acids Research*, *32*(5), 1792–1797. https://doi.org/10.1093/nar/gkh340

Elizalde, C., Campa, V. M., Caro, M., Schlangen, K., Aransay, A. M., Vivanco, M. D. M., & Kypta, R. M. (2011). Distinct roles for Wnt-4 and Wnt-11 during retinoic acid-induced neuronal differentiation. *Stem Cells*, *29*(1), 141–153. https://doi.org/10.1002/stem.562

Eubelen, M., Bostaille, N., Cabochette, P., Gauquier, A., Tebabi, P., Dumitru, A. C., … Vanhollebeke, B. (2018). A molecular mechanism for Wnt ligand-specific signaling. *Science*, *1178*(July), eaat1178. https://doi.org/10.1126/science.aat1178

Farzin, A., Etesami, S. A., Quint, J., Memic, A., & Tamayol, A. (2020). Magnetic nanoparticles in cancer therapy and diagnosis. *Adv Healthc Mater.*, *9*(9). https://doi.org/10.1002/adhm.201901058

Faugeroux, V., Pailler, E., Oulhen, M., Deas, O., Brulle-Soumare, L., Hervieu, C., … Farace, F. (2020). Genetic characterization of a unique neuroendocrine transdifferentiation prostate circulating tumor cell-derived eXplant model. *Nature Communications*, *11*(1), 1–16. https://doi.org/10.1038/s41467-020-15426-2

Fenderico, N., van Scherpenzeel, R. C., Goldflam, M., Proverbio, D., Jordens, I., Kralj, T., … Maurice, M. M. (2019). Anti-LRP5/6 VHHs promote differentiation of Wnt-hypersensitive intestinal stem cells. *Nature Communications*, *10*(1). https://doi.org/10.1038/s41467-018-08172-z

Fisher, R. R., Pleskow, H. M., Bedingfield, K., & Miyamoto, D. T. (2020). Noncanonical Wnt as a prognostic marker in prostate cancer: "you can't always get what you Wnt." *Expert Review of Molecular Diagnostics*, *20*(2), 245–254. https://doi.org/10.1080/14737159.2020.1702522

Fizazi, K., Shore, N., Tammela, T. L., Ulys, A., Vjaters, E., Polyakov, S., … Smith, M. R. (2019). Darolutamide in Nonmetastatic, Castration-Resistant Prostate Cancer. *New England Journal of Medicine*, *380*(13), 1235–1246. https://doi.org/10.1056/NEJMoa1815671

Flaherty, M. P., Kamerzell, T. J., & Dawn, B. (2012). *Wnt signaling and cardiac differentiation*. *Progress in Molecular Biology and Translational Science* (1st ed., Vol. 111). Elsevier Inc. https://doi.org/10.1016/B978-0-12-398459-3.00007-1

Frenzel, A., Schirrmann, T., & Hust, M. (2016). Phage display-derived human antibodies in clinical development and therapy. *MAbs*, *8*(7), 1177–1194. https://doi.org/10.1080/19420862.2016.1212149

Gammons, M. V., Renko, M., Johnson, C. M., Rutherford, T. J., & Bienz, M. (2016). Wnt Signalosome Assembly by DEP Domain Swapping of Dishevelled. *Molecular Cell*, *64*(1), 92–104. https://doi.org/10.1016/j.molcel.2016.08.026

Gan, X. Q., Wang, J. Y., Xi, Y., Wu, Z. L., Li, Y. P., & Li, L. (2008). Nuclear Dvl, c-Jun, β-catenin, and TCF form a complex leading to stabilization of β-catenin-TCF interaction. *Journal of Cell Biology*, *180*(6), 1087–1100. https://doi.org/10.1083/jcb.200710050

Gao, C., & Chen, Y. G. (2010). Dishevelled: The hub of Wnt signaling. *Cellular Signalling*, *22*(5), 717–727. https://doi.org/10.1016/j.cellsig.2009.11.021

Geetha-Loganathan, P., Nimmagadda, S., Fu, K., & Richman, J. M. (2014). Avian facial morphogenesis is regulated by c-Jun N-terminal Kinase/Planar Cell Polarity (JNK/PCP) wingless-related (WNT) signaling. *Journal of Biological Chemistry*,

289(35), 24153–24167. https://doi.org/10.1074/jbc.M113.522003

Gianfaldoni, S., Gianfaldoni, R., Wollina, U., Lotti, J., Tchernev, G., & Lotti, T. (2017). An overview on radiotherapy: From its history to its current applications in dermatology. *Open Access Macedonian Journal of Medical Sciences*, *5*(4 Special Issue GlobalDermatology), 521–525. https://doi.org/10.3889/oamjms.2017.122

Giraudet, A. L., Cassier, P. A., Iwao-Fukukawa, C., Garin, G., Badel, J. N., Kryza, D., … Blay, J. Y. (2018). A first-in-human study investigating biodistribution, safety and recommended dose of a new radiolabeled MAb targeting FZD10 in metastatic synovial sarcoma patients. *BMC Cancer*, *18*(1), 1–13. https://doi.org/10.1186/s12885-018-4544-x

Gleason, D. F. (1992). Histologic grading of prostate cancer: A perspective. *Human Pathology*, *23*(3), 273–279. https://doi.org/10.1016/0046-8177(92)90108-F

Global Cancer Observatory (GCO) IARC. (2021). GloboCancer Prostate 2021. Retrieved May 25, 2021, from https://gco.iarc.fr/today/data/factsheets/populations/900-world-fact-sheets.pdf

Gong, Y., Bourhis, E., Chiu, C., Stawicki, S., Dealmeida, V. I., Liu, B. Y., … Costa, M. (2010). Wnt isoform-specific interactions with coreceptor specify inhibition or potentiation of signaling by LRP6 antibodies. *PLoS ONE*, *5*(9), 1–17. https://doi.org/10.1371/journal.pone.0012682

Gonzalez-Sancho, J. M., Brennan, K. R., Castelo-Soccio, L. A., & Brown, A. M. C. (2004). Wnt Proteins Induce Dishevelled Phosphorylation via an LRP5/6- Independent Mechanism, Irrespective of Their Ability To Stabilize β-Catenin. *Molecular and Cellular Biology*, *24*(11), 4757–4768. https://doi.org/10.1128/mcb.24.11.4757-4768.2004

Gordon, R. D., Tzakis, A. G., Iwatsuki, S., Todo, S., Esquivel, C. O., Marsh, J. W., … Starzl, T. E. (1988). Experience With Orthoclone OKT3 Monoclonal Antibody in Liver Transplantation. *American Journal of Kidney Diseases*, *11*(2), 141–144. https://doi.org/10.1016/S0272-6386(88)80199-9

Gorroño-Etxebarria, I., Aguirre, U., Sanchez, S., González, N., Escobar, A., Zabalza, I., … Kypta, R. M. (2019). Wnt-11 as a potential prognostic biomarker and therapeutic target in colorectal cancer. *Cancers*, *11*(7), 1–19. https://doi.org/10.3390/cancers11070908

Goyal, L., Sirard, C., Schrag, M., Kagey, M. H., Eads, J. R., Stein, S., … Duda, D. G. (2020). Phase I and biomarker study of the wnt pathway modulator dkn-01 in combination with gemcitabine/ cisplatin in advanced biliary tract cancer. *Clinical Cancer Research*, *26*(23), 6158–6167. https://doi.org/10.1158/1078-0432.CCR-20-1310

Gray, J. D., Kholmanskikh, S., Castaldo, B. S., Hansler, A., Chung, H., Klotz, B., … Ross, M. E. (2013). LRP6 exerts non-canonical effects on Wnt signaling during neural tube closure. *Human Molecular Genetics*, *22*(21), 4267–4281. https://doi.org/10.1093/hmg/ddt277

Green, J., Nusse, R., & van Amerongen, R. (2014). The role of Ryk and Ror receptor tyrosine kinases in wnt signal transduction. *Cold Spring Harbor Perspectives in Biology*, *6*(2), 1–12. https://doi.org/10.1101/cshperspect.a009175

Greijer, A. E., & Van Der Wall, E. (2004). The role of hypoxia inducible factor 1 (HIF-1) in hypoxia induced apoptosis. *Journal of Clinical Pathology*, *57*(10), 1009–1014. https://doi.org/10.1136/jcp.2003.015032

Grumolato, L., Liu, G., Mong, P., Mudbhary, R., Biswas, R., Arroyave, R., … Aaronson, S. A. (2010). Canonical and noncanonical Wnts use a common mechanism to activate completely unrelated coreceptors. *Genes and Development*, *24*(22), 2517–2530. https://doi.org/10.1101/gad.1957710

Gujral, T. S., Chan, M., Peshkin, L., Sorger, P. K., Kirschner, M. W., & MacBeath, G. (2014). A Noncanonical Frizzled2 Pathway Regulates Epithelial-Mesenchymal Transition and Metastasis. *Cell*, *159*(4), 844–856. https://doi.org/10.1016/j.cell.2014.10.032

Gupta, S., Iljin, K., Sara, H., Mpindi, J. P., Mirtti, T., Vainio, P., … Kallioniemi, O. (2010). FZD4 as a mediator of ERG oncogene-induced WNT signaling and epithelial-to-mesenchymal transition in human prostate cancer cells. *Cancer Research*, *70*(17), 6735–6745. https://doi.org/10.1158/0008-5472.CAN-10-0244

Haikarainen, T., Krauss, S., & Lehtio, L. (2014). Tankyrases: Structure, Function and Therapeutic Implications in Cancer. *Current Pharmaceutical Design*, *20*(41), 6472–6488. https://doi.org/10.2174/1381612820666140630101525

Hajdu, S. I. (2004). Greco-Roman Thought about Cancer. *Cancer*, *100*(10), 2048–2051. https://doi.org/10.1002/cncr.20198

Hanahan, D., & Weinberg, R. A. (2000). The hallmarks of cancer. *Cell*, *100*(1), 57–70. https://doi.org/10.1016/S0092-8674(00)81683-9

Hanahan, D., & Weinberg, R. A. (2011). Hallmarks of cancer: The next generation. *Cell*, *144*(5), 646–674. https://doi.org/10.1016/j.cell.2011.02.013

Hanaki, H., Yamamoto, H., Sakane, H., Matsumoto, S., Ohdan, H., Sato, A., & Kikuchi, A. (2012). An anti-Wnt5a antibody suppresses metastasis of gastric cancer cells in vivo by inhibiting receptor-mediated endocytosis. *Molecular Cancer Therapeutics*, *11*(2), 298–307. https://doi.org/10.1158/1535-7163.MCT-11-0682

Hao, H. X., Xie, Y., Zhang, Y., Zhang, O., Oster, E., Avello, M., … Cong, F. (2012). ZNRF3 promotes Wnt receptor turnover

in an R-spondin-sensitive manner. *Nature*, *485*(7397), 195–202. https://doi.org/10.1038/nature11019

Hardy, K. M., Garriock, R. J., Yatskievych, T. A., D'Agostino, S. L., Antin, P. B., & Krieg, P. A. (2008). Non-canonical Wnt signaling through Wnt5a/b and a novel Wnt11 gene, Wnt11b, regulates cell migration during avian gastrulation. *Developmental Biology*, *320*(2), 391–401. https://doi.org/10.1016/j.ydbio.2008.05.546

Härmä, V., Virtanen, J., Mäkelä, R., Happonen, A., Mpindi, J. P., Knuuttila, M., … Nees, M. (2010). A comprehensive panel of three-dimensional models for studies of prostate cancer growth, invasion and drug responses. *PLoS ONE*, *5*(5). https://doi.org/10.1371/journal.pone.0010431

Harnden, P., Shelley, M. D., Coles, B., Staffurth, J., & Mason, M. D. (2007). Should the Gleason grading system for prostate cancer be modified to account for high-grade tertiary components? A systematic review and meta-analysis. *Lancet Oncology*, *8*(5), 411–419. https://doi.org/10.1016/S1470-2045(07)70136-5

Harris, J. J. (1958). The Human Tumor Grown in the Egg. *Annals of the New York Academy of Sciences*, *76*(3), 764–774. https://doi.org/10.1111/j.1749-6632.1958.tb54894.x

Harris, L. J., Larson, S. B., Hasel, K. W., & McPherson, A. (1997). Refined Structure of an Intact IgG2a Monoclonal Antibody,. *Biochemistry*, *36*(7), 1581–1597. https://doi.org/10.1021/bi962514+

He, B., You, L., Uematsu, K., Xu, Z., Lee, A. Y., Matsangou, M., … Jablons, D. M. (2004). A Monoclonal Antibody against Wnt-1 Induces Apoptosis in Human Cancer Cells. *Neoplasia*, *6*(1), 7–14. https://doi.org/10.1016/s1476-5586(04)80048-4

He, D., Yue, Z., Liu, L., Fang, X., Chen, L., & Han, H. (2019). Long noncoding RNA ABHD11-AS1 promote cells proliferation and invasion of colorectal cancer via regulating the miR-1254-WNT11 pathway. *Journal of Cellular Physiology*, *234*(7), 12070–12079. https://doi.org/10.1002/jcp.27877

Heisenberg, C.-P., Tada, M., & Wilson, S. W. (2000). Silberblick/Wnt11 mediates convergent extension movements during zebrafish gastrulation. *Nature*, *405*(May), 1–6. Retrieved from papers2://publication/uuid/35F38944-9078-48EC-AF33-E7BB374FCEE9

Hirai, H., Matoba, K., Mihara, E., Arimori, T., & Takagi, J. (2019). Crystal structure of a mammalian Wnt–frizzled complex. *Nature Structural & Molecular Biology*, *3*. https://doi.org/10.1038/s41594-019-0216-z

Ho, S. Y., & Keller, T. H. (2015). The use of porcupine inhibitors to target Wnt-driven cancers. *Bioorganic and Medicinal Chemistry Letters*, *25*(23), 5472–5476. https://doi.org/10.1016/j.bmcl.2015.10.032

Holdsworth, G., Slocombe, P., Doyle, C., Sweeney, B., Veverka, V., Le Riche, K., … Robinson, M. K. (2012). Characterization of the interaction of sclerostin with the low density lipoprotein receptor-related protein (LRP) family of wnt co-receptors. *Journal of Biological Chemistry*, *287*(32), 26464–26477. https://doi.org/10.1074/jbc.M112.350108

Hsueh, Y., Hodgkinson, C., Pratt, R. E., & Dzau, V. J. (2020). *Abstract 15547: Sfrp2 Mediates Ipsc to Cardiomyocyte Differentiation via Competing Actions on Wnts*. *Circulation* (Vol. 142). https://doi.org/10.1161/circ.142.suppl_3.15547

Hu, J., Ishihara, M., Chin, A. I., & Wu, L. (2019). Establishment of xenografts of urological cancers on chicken chorioallantoic membrane (CAM) to study metastasis. *Precision Clinical Medicine*, *2*(3), 140–151. https://doi.org/10.1093/pcmedi/pbz018

Hua, Y., Yang, Y., Li, Q., He, X., Zhu, W., Wang, J., & Gan, X. (2018). Oligomerization of Frizzled and LRP5/6 protein initiates intracellular signaling for the canonical WNT/β-catenin pathway. *Journal of Biological Chemistry*, *293*(51), 19710–19724. https://doi.org/10.1074/jbc.RA118.004434

Hyun Woo, P., Kim, Y. C., Yu, B., Moroishi, T., Mo, J.-S., Plouffe, S. W., … Guan, K.-L. (2015). Alternative Wnt Signaling Activates YAP/TAZ. *Cell*, *13*(162 (4)), 780–794. https://doi.org/10.1016/j.cell.2015.07.013

Isaacson Velho, P., Wei, F., Hao, W., & S. Antonarakis, E. (2020). Wnt-pathway Activating Mutations Are Associated with Resistance to First-line Abiraterone and Enzalutamide in Castration-resistant Prostate Cancer. *Eur Urol*. https://doi.org/10.1016/j.eururo.2019.05.032.Wnt-pathway

Janda, C. Y., Waghray, D., Levin, A. M., Thomas, C., & Garcia, K. C. (2012). Structural basis of Wnt recognition by Frizzled. *Science*, *337*(July), 59–64. https://doi.org/10.1126/science.1222879.Structural

Jefferies, B., Lenze, F., Sathe, A., Truong, N., Anton, M., Von Eisenhart-Rothe, R., … Mayer-Kuckuk, P. (2017). Non-invasive imaging of engineered human tumors in the living chicken embryo. *Scientific Reports*, *7*(1), 1–9. https://doi.org/10.1038/s41598-017-04572-1

Jeong, W., Kim, S., Lee, U., Zhong, Z. A., Savitsky, M., Kwon, H., … Jho, E. (2020). LDL receptor-related protein LRP 6 senses nutrient levels and regulates Hippo signaling . *EMBO Reports*, *21*(9), 1–13. https://doi.org/10.15252/embr.202050103

Jiang, J., Lan, C., Li, L., Yang, D., Xia, X., Liao, Q., … Zeng, C. (2018). A novel porcupine inhibitor blocks WNT pathways and attenuates cardiac hypertrophy. *Biochimica et Biophysica Acta - Molecular Basis of Disease*, *1864*(10), 3459–3467. https://doi.org/10.1016/j.bbadis.2018.07.035

Jimeno, A., Gordon, M., Chugh, R., Messersmith, W., Mendelson, D., Dupont, J., … Smith, D. C. (2017). A first-in-human

phase I study of the anticancer stem cell agent ipafricept (OMP-54F28), a decoy receptor for wnt ligands, in patients with advanced solid tumors. *Clinical Cancer Research*, *23*(24), 7490–7497. https://doi.org/10.1158/1078-0432.CCR-17-2157

Joiner, D. M., Ke, J., Zhong, Z., Xu, H. E., & Williams, B. O. (2013). LRP5 and LRP6 in development and disease. *Trends in Endocrinology and Metabolism*, *24*(1), 31–39. https://doi.org/10.1016/j.tem.2012.10.003

Jumper, J., Evans, R., Pritzel, A., Green, T., Figurnov, M., Ronneberger, O., … Hassabis, D. (2021). Highly accurate protein structure prediction with AlphaFold. *Nature*, *596*(7873), 583–589. https://doi.org/10.1038/s41586-021-03819-2

Katoh, M. (2017). Canonical and non-canonical WNT signaling in cancer stem cells and their niches: Cellular heterogeneity, omics reprogramming, targeted therapy and tumor plasticity (Review). *International Journal of Oncology*, *51*(5), 1357–1369. https://doi.org/10.3892/ijo.2017.4129

Kawano, Y., & Kypta, R. (2003). Secreted antagonists of the Wnt signalling pathway. *Journal of Cell Science*, *116*(13), 2627–2634. https://doi.org/10.1242/jcs.00623

Kestler, H. A., & Kühl, M. (2008). From individual Wnt pathways towards a Wnt signalling network. *Philosophical Transactions of the Royal Society B: Biological Sciences*, *363*(1495), 1333–1347. https://doi.org/10.1098/rstb.2007.2251

Kim, J. H., Jung, E., Ahn, S. S., Yeo, H., Lee, J. Y., Seo, J. K., … Shin, S. Y. (2020). WNT11 is a direct target of early growth response protein 1. *BMB Reports*, *53*(12), 628–633. https://doi.org/10.5483/BMBRep.2020.53.12.052

Kirikoshi, H., Sekihara, H., & Katoh, M. (2001). Molecular cloning and characterization of human WNT11. *International Journal of Molecular Medicine*, *8*(6), 651–656. https://doi.org/10.3892/ijmm.8.6.651

Kobayashia, T., Koshidaa, K., Endob, Y., Imaoa, T., Uchibayashia, T., Sasakia, T., & Namikia, M. (1998). A Chick Embryo Model for Metastatic Human Prostate Cancer. *European Urology*, *920*, 154–160.

Kofron, M., Birsoy, B., Houston, D., Tao, Q., Wylie, C., & Heasman, J. (2007). Wnt11/β-catenin signaling in both oocytes and early embryos acts through LRP6-mediated regulation of axin. *Development*, *134*(3), 503–513. https://doi.org/10.1242/dev.02739

Koo, B. K., Spit, M., Jordens, I., Low, T. Y., Stange, D. E., Van De Wetering, M., … Clevers, H. (2012). Tumour suppressor RNF43 is a stem-cell E3 ligase that induces endocytosis of Wnt receptors. *Nature*, *488*(7413), 665–669. https://doi.org/10.1038/nature11308

Korinek, V., Barker, N., Morin, P. J., Van Wichen, D., De Weger, R., Kinzler, K. W., … Clevers, H. (1997). Constitutive transcriptional activation by a β-catenin-Tcf complex in APC(-/-) colon carcinoma. *Science*, *275*(5307), 1784–1787. https://doi.org/10.1126/science.275.5307.1784

Krishnamurthy, N., & Kurzrock, R. (2018). Targeting the Wnt/beta-catenin pathway in cancer: Update on effectors and inhibitors. *Cancer Treatment Reviews*, *62*, 50–60. https://doi.org/10.1016/j.ctrv.2017.11.002

Kuai, J., Mosyak, L., Brooks, J., Cain, M., Carven, G. J., Ogawa, S., … Pullen, N. (2015). Characterization of Binding Mode of Action of a Blocking Anti-Platelet-Derived Growth Factor (PDGF)-B Monoclonal Antibody, MOR8457, Reveals Conformational Flexibility and Avidity Needed for PDGF-BB to Bind PDGF Receptor-β. *Biochemistry*, *54*(10), 1918–1929. https://doi.org/10.1021/bi5015425

Kuek, V., Hughes, A. M., Kotecha, R. S., & Cheung, L. C. (2021). Therapeutic targeting of the leukaemia microenvironment. *International Journal of Molecular Sciences*, *22*(13), 1–32. https://doi.org/10.3390/ijms22136888

Kumon, H., Ariyoshi, Y., Sasaki, K., Sadahira, T., Araki, M., Ebara, S., … Nasu, Y. (2016). Adenovirus vector carrying REIC/DKK-3 gene: Neoadjuvant intraprostatic injection for high-risk localized prostate cancer undergoing radical prostatectomy. *Cancer Gene Therapy*, *23*(11), 400–409. https://doi.org/10.1038/cgt.2016.53

Kurash, M. M., Gill, R., Khairulin, M., Harbosh, H., & Keidar, Z. (2020). 68Ga-labeled PSMA-11 (68Ga-isoPROtrace-11) synthesized with ready to use kit: normal biodistribution and uptake characteristics of tumour lesions. *Scientific Reports*, *10*(1), 1–8. https://doi.org/10.1038/s41598-020-60099-y

Lako, M., Strachan, T., Bullen, P., Wilson, D. I., Robson, S. C., & Lindsay, S. (1998). Isolation, characterisation and embryonic expression of WNT11, a gene which maps to 11q13.5 and has possible roles in the development of skeleton, kidney and lung. *Gene*, *219*(1–2), 101–110. https://doi.org/10.1016/S0378-1119(98)00393-X

Lander, E. S., Linton, L. M., Birren, B., Nusbaum, C., Zody, M. C., Baldwin, J., … Chen, Y. J. (2001). Initial sequencing and analysis of the human genome: International Human Genome Sequencing Consortium. *Nature*, *412*(6846), 565–566. https://doi.org/10.1038/35087627

Lange, T., Oh-Hohenhorst, S. J., Joosse, S. A., Pantel, K., Hahn, O., Gosau, T., … Schumacher, U. (2018). Development and Characterization of a Spontaneously Metastatic Patient-Derived Xenograft Model of Human Prostate Cancer. *Scientific Reports*, *8*(1), 1–11. https://doi.org/10.1038/s41598-018-35695-8

Lee, H. J., Shi, D. L., & Zheng, J. J. (2015). Conformational change of dishevelled plays a key regulatory role in the wnt

signaling pathways. *ELife*, *4*(AUGUST2015), 1–15. https://doi.org/10.7554/eLife.08142

Lee, J. S., Hur, M. W., Lee, S. K., Choi, W. Il, Kwon, Y. G., & Yun, C. O. (2012). A novel sLRP6E1E2 inhibits canonical Wnt signaling, epithelial-to-mesenchymal transition, and induces mitochondria-dependent apoptosis in lung cancer. *PLoS ONE*, *7*(5). https://doi.org/10.1371/journal.pone.0036520

Lee, K. H., Johmura, Y., Yu, L. R., Park, J. E., Gao, Y., Bang, J. K., … Lee, K. S. (2012). Identification of a novel Wnt5a-CK1ε-Dvl2-Plk1-mediated primary cilia disassembly pathway. *EMBO Journal*, *31*(14), 3104–3117. https://doi.org/10.1038/emboj.2012.144

Lee, N. K., Zhang, Y., Su, Y., Bidlingmaier, S., Sherbenou, D. W., Ha, K. D., & Liu, B. (2018). Cell-type specific potent Wnt signaling blockade by bispecific antibody. *Scientific Reports*, *8*(1), 1–16. https://doi.org/10.1038/s41598-017-17539-z

Lee, P., Chandel, N. S., & Simon, M. C. (2020). Cellular adaptation to hypoxia through hypoxia inducible factors and beyond. *Nature Reviews Molecular Cell Biology*, *21*(5), 268–283. https://doi.org/10.1038/s41580-020-0227-y

Li, H. X., Lin, J., Jiang, B., & Yang, X. J. (2020). Wnt11 preserves mitochondrial membrane potential and protects cardiomyocytes against hypoxia through paracrine signaling. *Journal of Cellular Biochemistry*, *121*(2), 1144–1155. https://doi.org/10.1002/jcb.29349

Li, N., Lu, N., & Xie, C. (2019). The Hippo and Wnt signalling pathways: crosstalk during neoplastic progression in gastrointestinal tissue. *FEBS Journal*, *286*(19), 3745–3756. https://doi.org/10.1111/febs.15017

Li, X.-Y., & Green, M. R. (1996). Intramolecular inhibition of activating transcription factor-2 function by its DNA-binding domain. *Genes and Development*, *10*(5), 517–527. https://doi.org/10.1101/gad.10.5.517

Lin, C., Lua, W., Zhaia, L., Betheab, T., Berryb, K., Qua, Z., … Lia, Y. (2011). Mesd Is A General Inhibitor of Different Wnt Ligands In Wnt/LRP Signaling and Inhibits PC-3 Tumor Growth In Vivo. *FEBS Lett.*, *585*(19), 3120–3125. https://doi.org/10.1016/j.febslet.2011.08.046.Mesd

Lin, D., Wyatt, A. W., Xue, H., Wang, Y., Dong, X., Haegert, A., … Wang, Y. (2014). High fidelity patient-derived xenografts for accelerating prostate cancer discovery and drug development. *Cancer Research*, *74*(4), 1272–1283. https://doi.org/10.1158/0008-5472.CAN-13-2921-T

Lin, Y. C., Haas, A., Bufe, A., Parbin, S., Hennecke, M., Voloshanenko, O., … Bastians, H. (2021). Wnt10b-GSK3β-dependent Wnt/STOP signaling prevents aneuploidy in human somatic cells. *Life Science Alliance*, *4*(1), 1–12. https://doi.org/10.26508/LSA.202000855

Liu, C. C., Prior, J., Piwnica-Worms, D., & Bu, G. (2010). LRP6 overexpression defines a class of breast cancer subtype and is a target for therapy. *Proceedings of the National Academy of Sciences of the United States of America*, *107*(11), 5136–5141. https://doi.org/10.1073/pnas.0911220107

Liu, H., Du, S., Lei, T., Wang, H., He, X., Tong, R., & Wang, Y. (2018). Multifaceted regulation and functions of YAP/TAZ in tumors (Review). *Oncology Reports*, *40*(1), 16–28. https://doi.org/10.3892/or.2018.6423

Liu, L. (2018). Pharmacokinetics of monoclonal antibodies and Fc-fusion proteins. *Protein and Cell*, *9*(1), 15–32. https://doi.org/10.1007/s13238-017-0408-4

Livak, K. J., & Schmittgen, T. D. (2001). Analysis of relative gene expression data using real-time quantitative PCR and the 2-ΔΔCT method. *Methods*, *25*(4), 402–408. https://doi.org/10.1006/meth.2001.1262

Loh, K. M., van Amerongen, R., & Nusse, R. (2016). Generating Cellular Diversity and Spatial Form: Wnt Signaling and the Evolution of Multicellular Animals. *Developmental Cell*, *38*(6), 643–655. https://doi.org/10.1016/j.devcel.2016.08.011

Lokman, N. A., Elder, A. S. F., Ricciardelli, C., & Oehler, M. K. (2012). Chick chorioallantoic membrane (CAM) assay as an in vivo model to study the effect of newly identified molecules on ovarian cancer invasion and metastasis. *International Journal of Molecular Sciences*, *13*(8), 9959–9970. https://doi.org/10.3390/ijms13089959

Lu, R. M., Hwang, Y. C., Liu, I. J., Lee, C. C., Tsai, H. Z., Li, H. J., & Wu, H. C. (2020). Development of therapeutic antibodies for the treatment of diseases. *Journal of Biomedical Science*, *27*(1), 1–30. https://doi.org/10.1186/s12929-019-0592-z

Lu, W., & Li, Y. (2014). Salinomycin suppresses LRP6 expression and inhibits both Wnt/β-catenin and mTORC1 signaling in breast and prostate cancer cells. *J Cell Biochem.*, *115*(10), 1799–1807. https://doi.org/10.1002/jcb.24850.Salinomycin

Lu, W., Lin, C., King, T. D., Chen, H., Reynolds, R. C., & Li, Y. (2012). Silibinin inhibits Wnt/β-catenin signaling by suppressing Wnt co-receptor LRP6 expression in human prostate and breast cancer cells. *Cellular Signalling*, *24*(12), 2291–2296. https://doi.org/10.1016/j.cellsig.2012.07.009

Lu, W., Lin, C., Roberts, M. J., Waud, W. R., Piazza, G. A., & Li, Y. (2011). Niclosamide suppresses cancer cell growth by inducing Wnt co-receptor LRP6 degradation and inhibiting the Wnt/β-catenin pathway. *PLoS ONE*, *6*(12), 1–8. https://doi.org/10.1371/journal.pone.0029290

Lu, W., Liu, C. C., Thottassery, J. V., Bu, G., & Li, Y. (2010). Mesd is a universal inhibitor of wnt coreceptors lrp5 and lrp6 and blocks wnt/β-catenin signaling in cancer cells. *Biochemistry*, *49*(22), 4635–4643. https://doi.org/10.1021/bi1001486

Ma, J., Lu, W., Chen, D., Xu, B., & Li, Y. (2017). Role of Wnt Co-Receptor LRP6 in Triple Negative Breast Cancer Cell Migration and Invasion. *Journal of Cellular Biochemistry*, *118*(9), 2968–2976. https://doi.org/10.1002/jcb.25956

MacDonald, B. T., & He, X. (2012). Frizzled and LRP5/6 Receptors for Wnt/β-Catenin Signaling. *Cold Spring Harbor Perspectives in Biology*, *4*. https://doi.org/10.1101/cshperspect.a007880

MacDonald, B. T., Tamai, K., & He, X. (2009). Wnt/β-Catenin Signaling: Components, Mechanisms, and Diseases. *Developmental Cell*, *17*(1), 9–26. https://doi.org/10.1016/j.devcel.2009.06.016

Majumdar, A., Vainio, S., Kispert, A., McMahon, J., & McMahon, A. P. (2003). Wnt11 and Ret/Gdnf pathways cooperate in regulating ureteric branching during metanephric kidney development. *Development*, *130*(14), 3175–3185. https://doi.org/10.1242/dev.00520

Malinauskas, T., & Jones, E. Y. (2014). Extracellular modulators of Wnt signalling. *Current Opinion in Structural Biology*, *29*, 77–84. https://doi.org/10.1016/j.sbi.2014.10.003

Many, A. M., & Brown, A. M. C. (2014). Both canonical and non-canonical Wnt signaling independently promote stem cell growth in mammospheres. *PLoS ONE*, *9*(7), 1–9. https://doi.org/10.1371/journal.pone.0101800

Matsumura, Y., & Maeda, H. (1986). A New Concept for Macromolecular Therapeutics in Cancer Chemotherapy: Mechanism of Tumoritropic Accumulation of Proteins and the Antitumor Agent Smancs. *Cancer Research*, *46*(8), 6387–6392.

Matuszak, J., Dörfler, P., Zaloga, J., Unterweger, H., Lyer, S., Dietel, B., … Cicha, I. (2015). Shell matters: Magnetic targeting of SPIONs and in vitro effects on endothelial and monocytic cell function. *Clinical Hemorheology and Microcirculation*, *61*(2), 259–277. https://doi.org/10.3233/CH-151998

Maye, P., Zheng, J., Li, L., & Wu, D. (2004). Multiple mechanisms for Wnt11-mediated repression of the canonical Wnt signaling pathway. *Journal of Biological Chemistry*, *279*(23), 24659–24665. https://doi.org/10.1074/jbc.M311724200

McGough, I. J., Vecchia, L., Bishop, B., Malinauskas, T., Beckett, K., Joshi, D., … Vincent, J. P. (2020). Glypicans shield the Wnt lipid moiety to enable signalling at a distance. *Nature*, *585*(7823), 85–90. https://doi.org/10.1038/s41586-020-2498-z

Menshykau, D., Michos, O., Lang, C., Conrad, L., McMahon, A. P., & Iber, D. (2019). Image-based modeling of kidney branching morphogenesis reveals GDNF-RET based Turing-type mechanism and pattern-modulating WNT11 feedback. *Nature Communications*, *10*(1). https://doi.org/10.1038/s41467-018-08212-8

Metz, E. P., Wilder, P. J., Dong, J., Datta, K., & Rizzino, A. (2020). Elevating SOX2 in prostate tumor cells upregulates expression of neuroendocrine genes, but does not reduce the inhibitory effects of enzalutamide. *Journal of Cellular Physiology*, *235*(4), 3731–3740. https://doi.org/10.1002/jcp.29267

Micka, M., & Bryja, V. (2021). Can We Pharmacologically Target Dishevelled: The Key Signal Transducer in the Wnt Pathways? In *Handbook of Experimental Pharmacology* (pp. 1–19). Berlin, Heidelberg: Springer Berlin Heidelberg. https://doi.org/10.1007/164_2021_527

Mihara, E., Hirai, H., Yamamoto, H., Tamura-Kawakami, K., Matano, M., Kikuchi, A., … Takagi, J. (2016). Active and water-soluble form of lipidated wnt protein is maintained by a serum glycoprotein afamin/α-albumin. *ELife*, *5*(FEBRUARY2016), 1–19. https://doi.org/10.7554/eLife.11621

Mikami, I., You, L., He, B., Xu, Z., Batra, S., Lee, A. Y., … Jablons, D. M. (2005). Efficacy on Wnt-1 monoclonal antibody in sarcoma cells. *BMC Cancer*, *5*, 1–7. https://doi.org/10.1186/1471-2407-5-53

Mikels, A. J., & Nusse, R. (2006). Wnts as ligands: Processing, secretion and reception. *Oncogene*, *25*(57), 7461–7468. https://doi.org/10.1038/sj.onc.1210053

Miller, I., Min, M., Yang, C., Tian, C., Gookin, S., Carter, D., & Spence, S. L. (2018). Ki67 is a Graded Rather than a Binary Marker of Proliferation versus Quiescence Graphical Abstract HHS Public Access. *Cell Rep*, *24*(5), 1105–1112. https://doi.org/10.1016/j.celrep.2018.06.110.Ki67

Mix, E., Goertsches, R., & Zett, U. K. (2006). Immunoglobulins - Basic considerations. *Journal of Neurology*, *253*(SUPPL. 5), 9–17. https://doi.org/10.1007/s00415-006-5002-2

Miyamoto, D. T., Zheng, Y., Wittner, B. S., Lee, R. J., Zhu, H., Broderick, K. T., … Haber, D. A. (2015). RNA-Seq of single prostate CTCs implicates noncanonical Wnt signaling in antiandrogen resistance. *Science*, *349*(6254), 1351–1356. https://doi.org/10.1126/science.aab0917

Mochmann, L. H., Bock, J., Ortiz-Tánchez, J., Schlee, C., Bohne, A., Neumann, K., … Baldus, C. D. (2011). Genome-wide screen reveals WNT11, a non-canonical WNT gene, as a direct target of ETS transcription factor ERG. *Oncogene*, *30*(17), 2044–2056. https://doi.org/10.1038/onc.2010.582

Molenaar, M., Van De Wetering, M., Oosterwegel, M., Peterson-Maduro, J., Godsave, S., Korinek, V., … Clevers, H. (1996). XTcf-3 transcription factor mediates β-catenin-induced axis formation in xenopus embryos. *Cell*, *86*(3), 391–399. https://doi.org/10.1016/S0092-8674(00)80112-9

Moon, R. T., Campbell, R. M., Christian, J. L., McGrew, L. L., Shih, J., & Fraser, S. (1993). Xwnt-5A: A maternal Wnt that affects morphogenetic movements after overexpression in embryos of Xenopus laevis. *Development*, *119*(1), 97–111. https://doi.org/10.1242/dev.119.1.97

Moore, T. L., Rodriguez-Lorenzo, L., Hirsch, V., Balog, S., Urban, D., Jud, C., … Petri-Fink, A. (2015). Nanoparticle colloidal stability in cell culture media and impact on cellular interactions. *Chemical Society Reviews*, *44*(17), 6287–6305. https://doi.org/10.1039/c4cs00487f

Moorthy, B. S., Xie, B., Moussa, E. M., Iyer, L. K., Chandrasekhar, S., Panchal, J. P., & Topp, E. M. (2015). Structure of Monoclonal Antibodies. In *Biobetters: Protein Engineering to Approach the Curative* (pp. 81–89). https://doi.org/10.1007/978-1-4939-2543-8_6

Moparthi, L., Pizzolato, G., & Koch, S. (2019). Wnt activator FOXB2 drives the neuroendocrine differentiation of prostate cancer. *Proceedings of the National Academy of Sciences of the United States of America*, *116*(44), 22189–22195. https://doi.org/10.1073/pnas.1906484116

Mori, H., Yao, Y., Learman, B. S., Kurozumi, K., Joji, I., Ramakrishnan, S. K., … Shah, Y. M. (2016). Induction of WNT11 by hypoxia and hypoxia-inducible factor-1 α regulates cell proliferation , migration and invasion. *Scientific Reports*, *6*(February), 1–14. https://doi.org/10.1038/srep21520

Morin, P. J., Sparks, A. B., Korinek, V., Barker, N., Clevers, H., Vogelstein, B., & Kinzler, K. W. (1997). Activation of β-catenin-Tcf signaling in colon cancer by mutations in β-catenin or APC. *Science*, *275*(5307), 1787–1790. https://doi.org/10.1126/science.275.5307.1787

Moti, N., Yu, J., Boncompain, G., Perez, F., & Virshup, D. M. (2019). Wnt traffic from endoplasmic reticulum to filopodia. *PLoS ONE*, *14*(2), 1–15. https://doi.org/10.1371/journal.pone.0212711

Movsas, B., Chapman, J. D., Horwitz, E. M., Pinover, W. H., Greenberg, R. E., Hanlon, A. L., … Hanks, G. E. (1999). Hypoxic regions exist in human prostate carcinoma. *Urology*, *53*(1), 11–18. https://doi.org/10.1016/S0090-4295(98)00500-7

Mukherjee, S., Liang, L., & Veiseh, O. (2020). Recent advancements of magnetic nanomaterials in cancer therapy. *Pharmaceutics*, *12*(2). https://doi.org/10.3390/pharmaceutics12020147

Mullard, A. (2021). FDA approves 100th monoclonal antibody product. *Nature Reviews. Drug Discovery*, *20*(7), 491–495. https://doi.org/10.1038/d41573-021-00079-7

Munemitsu, S., Albert, I., Souza, B., Rubinfeld, D., & Polakis, P. (1995). Regulation of intracellular β-catenin levels by the adenomatous polyposis coli (APC) tumor-suppressor protein. *Proceedings of the National Academy of Sciences of the United States of America*, *92*(7), 3046–3050. https://doi.org/10.1073/pnas.92.7.3046

Murillo-Garzón, V., Gorroño-Etxebarria, I., Åkerfelt, M., Puustinen, M. C., Sistonen, L., Nees, M., … Kypta, R. M. (2018). Frizzled-8 integrates Wnt-11 and transforming growth factor-β signaling in prostate cancer. *Nature Communications*, *9*(1). https://doi.org/10.1038/s41467-018-04042-w

Murillo-Garzón, V., & Kypta, R. (2017). WNT signalling in prostate cancer. *Nature Reviews Urology*, (14), 683–696. Retrieved from https://spiral.imperial.ac.uk:8443/bitstream/10044/1/57966/7/Murillo_Kypta_Nature_Reviews_Urology_accepted version.pdf

Mygland, L., Brinch, S. A., Strand, M. F., Olsen, P. A., Aizenshtadt, A., Lund, K., … Waaler, J. (2021). Identification of response signatures for tankyrase inhibitor treatment in tumor cell lines. *IScience*, *24*(7). https://doi.org/10.1016/j.isci.2021.102807

Nagesh, P. K. B., Johnson, N. R., Boya, V. K. N., Chowdhury, P., Othman, S. F., Khalilzad-Sharghi, V., … Yallapu, M. M. (2016). PSMA targeted docetaxel-loaded superparamagnetic iron oxide nanoparticles for prostate cancer. *Colloids and Surfaces B: Biointerfaces*, *144*(2016), 8–20. https://doi.org/10.1016/j.colsurfb.2016.03.071

Nagy, I. I., Xu, Q., Naillat, F., Ali, N., Miinalainen, I., Samoylenko, A., & Vainio, S. J. (2016). Impairment of Wnt11 function leads to kidney tubular abnormalities and secondary glomerular cystogenesis. *BMC Developmental Biology*, *16*(1), 1–14. https://doi.org/10.1186/s12861-016-0131-z

Najdi, R., Proffitt, K., Sprowl, S., Kaur, S., Yu, J., Covey, T. M., … Waterman, M. L. (2012). A uniform human Wnt expression library reveals a shared secretory pathway and unique signaling activities. *Differentiation*, *84*(2), 203–213. https://doi.org/10.1016/j.diff.2012.06.004

Nakamura, Y., De Paiva Alves, E., Veenstra, G. J. C., & Hoppler, S. (2016). Tissue-and stage-specific Wnt target gene expression is controlled subsequent to β-catenin recruitment to cis-regulatory modules. *Development (Cambridge)*, *143*(11), 1914–1925. https://doi.org/10.1242/dev.131664

Nguyen, T. L., & Durán, R. V. (2016). Prolyl hydroxylase domain enzymes and their role in cell signaling and cancer metabolism. *International Journal of Biochemistry and Cell Biology*, *80*, 71–80. https://doi.org/10.1016/j.biocel.2016.09.026

Niehrs, C. (2010). On growth and form: A Cartesian coordinate system of Wnt and BMP signaling specifies bilaterian body axes. *Development*, *137*(6), 845–857. https://doi.org/10.1242/dev.039651

Niehrs, C. (2012). The complex world of WNT receptor signalling. *Nature Reviews Molecular Cell Biology*, *13*(12), 767–779. https://doi.org/10.1038/nrm3470

NIH National Cancer Institute. (2021). Cancer (NIH). Retrieved May 17, 2021, from www.cancer.gov/publications/dictionaries/cancer-terms/def/cancer

Nishioka, M., Ueno, K., Hazama, S., Okada, T., Sakai, K., Suehiro, Y., … Hinoda, Y. (2013). Possible involvement of Wnt11 in colorectal cancer progression. *Molecular Carcinogenesis*, *52*(3), 207–217. https://doi.org/10.1002/mc.21845

Nishita, M., Itsukushima, S., Nomachi, A., Endo, M., Wang, Z., Inaba, D., … Minami, Y. (2010). Ror2/Frizzled Complex Mediates Wnt5a-Induced AP-1 Activation by Regulating Dishevelled Polymerization. *Molecular and Cellular Biology*, *30*(14), 3610–3619. https://doi.org/10.1128/mcb.00177-10

Nusse Lab. (2021). The Wnt Homepage, Wnt target genes. Retrieved August 25, 2021, from https://web.stanford.edu/group/nusselab/cgi-bin/wnt/target_genes

Nusse, R., & Clevers, H. (2017). Wnt/β-Catenin Signaling, Disease, and Emerging Therapeutic Modalities. *Cell*, *169*(6), 985–999. https://doi.org/10.1016/j.cell.2017.05.016

Nusse, R., & Varmus, H. (2012). Three decades of Wnts: A personal perspective on how a scientific field developed. *EMBO Journal*, *31*(12), 2670–2684. https://doi.org/10.1038/emboj.2012.146

Nusse, R., & Varmus, H. E. (1982). Many tumors induced by the mouse mammary tumor virus contain a provirus integrated in the same region of the host genome. *Cell*, *31*(1), 99–109. https://doi.org/10.1016/0092-8674(82)90409-3

Nusse, R., & Varmus, H. E. (1992). Wnt genes. *Cell*, *69*(7), 1073–1087. https://doi.org/10.1016/0092-8674(92)90630-U

O'Brien, L. L., Combes, A. N., Short, K. M., Lindström, N. O., Whitney, P. H., Cullen-McEwen, L. A., … McMahon, A. P. (2018). Wnt11 directs nephron progenitor polarity and motile behavior ultimately determining nephron endowment. *ELife*, *7*, 1–25. https://doi.org/10.7554/eLife.40392

Ohkawara, B., & Niehrs, C. (2011). An ATF2-based luciferase reporter to monitor non-canonical Wnt signaling in xenopus embryos. *Developmental Dynamics*, *240*(1), 188–194. https://doi.org/10.1002/dvdy.22500

Ouko, L., Ziegler, T. R., Gu, L. H., Eisenberg, L. M., & Vincent, W. (2004). Wnt11 Signaling Promotes Proliferation, Transformation, and Migration of IEC6 Intestinal Epithelial Cells. *J. Biol. Chem.*, *279*(25), 26707–26715.

Öztürk, E., Hobiger, S., Despot-Slade, E., Pichler, M., & Zenobi-Wong, M. (2017). Hypoxia regulates RhoA and Wnt/β-catenin signaling in a context-dependent way to control re-differentiation of chondrocytes. *Scientific Reports*, *7*(1), 1–11. https://doi.org/10.1038/s41598-017-09505-6

Pacella, I., Cammarata, I., Focaccetti, C., Miacci, S., Gulino, A., Tripodo, C., … Piconese, S. (2018). Wnt3a neutralization enhances T-cell responses through indirect mechanisms and restrains tumor growth. *Cancer Immunology Research*, *6*(8), 953–964. https://doi.org/10.1158/2326-6066.CIR-17-0713

Pak, S., Park, S., Kim, Y., Park, J. H., Park, C. H., Lee, K. J., … Ahn, H. (2019). The small molecule WNT/β-catenin inhibitor CWP232291 blocks the growth of castration-resistant prostate cancer by activating the endoplasmic reticulum stress pathway. *Journal of Experimental and Clinical Cancer Research*, *38*(1), 1–13. https://doi.org/10.1186/s13046-019-1342-5

Petrova, V., Annicchiarico-Petruzzelli, M., Melino, G., & Amelio, I. (2018). The hypoxic tumour microenvironment. *Oncogenesis*, *7*(1). https://doi.org/10.1038/s41389-017-0011-9

Pettersen, E. F., Goddard, T. D., Huang, C. C., Couch, G. S., Greenblatt, D. M., Meng, E. C., & Ferrin, T. E. (2004). UCSF Chimera - A visualization system for exploratory research and analysis. *Journal of Computational Chemistry*, *25*(13), 1605–1612. https://doi.org/10.1002/jcc.20084

Pinson, K. I., Brennan, J., Monkley, S., Avery, B. J., & Skarnes, W. C. (2000). An LDL-receptor-related protein mediates Wnt signalling in mice. *Nature*, *407*(6803), 535–538. https://doi.org/10.1038/35035124

Piva, M., Domenici, G., Iriondo, O., Rábano, M., Simões, B. M., Comaills, V., … Vivanco, M. D. M. (2014). Sox2 promotes tamoxifen resistance in breast cancer cells. *EMBO Molecular Medicine*, *6*(1), 66–79. https://doi.org/10.1002/emmm.201303411

Plummer, R., Dua, D., Cresti, N., Drew, Y., Stephens, P., Foegh, M., … Sarker, D. (2020). First-in-human study of the PARP/tankyrase inhibitor E7449 in patients with advanced solid tumours and evaluation of a novel drug-response predictor. *British Journal of Cancer*, *123*(4), 525–533. https://doi.org/10.1038/s41416-020-0916-5

Pomerantz, M. M., Qiu, X., Zhu, Y., Takeda, D. Y., Pan, W., Baca, S. C., … Freedman, M. L. (2020). *Prostate cancer reactivates developmental epigenomic programs during metastatic progression*. *Nature Genetics* (Vol. 52). Springer US. https://doi.org/10.1038/s41588-020-0664-8

Postma, M., & Goedhart, J. (2019). Plotsofdata—a web app for visualizing data together with their summaries. *PLoS Biology*, *17*(3), 1–8. https://doi.org/10.1371/journal.pbio.3000202

Predoi, M. C., Mîndrilă, I., Buteică, S. A., Purcaru, Ș. O., Mihaiescu, D. E., & Mărginean, O. M. (2020). Iron oxide/salicylic acid nanoparticles as potential therapy for B16F10 melanoma transplanted on the chick chorioallantoic membrane. *Processes*, *8*(6). https://doi.org/10.3390/PR8060706

Prostate cancer foundation. (2021). *Prostate Cancer Patient Guide*, *2021* (Third). Retrieved from www.pcf.org www.manyvscancer.org

Qiu, W., Chen, L., & Kassem, M. (2011). Activation of non-canonical Wnt/JNK pathway by Wnt3a is associated with differentiation fate determination of human bone marrow stromal (mesenchymal) stem cells. *Biochemical and Biophysical Research Communications*, *413*(1), 98–104. https://doi.org/10.1016/j.bbrc.2011.08.061

Railo, A., Nagy, I. I., Kilpeläinen, P., & Vainio, S. (2008). Wnt-11 signaling leads to down-regulation of the Wnt/β-catenin, JNK/AP-1 and NF-κB pathways and promotes viability in the CHO-K1 cells. *Experimental Cell Research*, *314*(13), 2389–2399. https://doi.org/10.1016/j.yexcr.2008.04.010

Raisch, J., Côté-Biron, A., & Rivard, N. (2019). A role for the WNT co-receptor LRP6 in pathogenesis and therapy of epithelial cancers. *Cancers*, *11*(8), 1–23. https://doi.org/10.3390/cancers11081162

Rajan, P., Sudbery, I. M., Villasevil, M. E. M., Mui, E., Fleming, J., Davis, M., … Leung, H. Y. (2014). Next-generation sequencing of advanced prostate cancer treated with androgen-deprivation therapy. *European Urology*, *66*(1), 32–39. https://doi.org/10.1016/j.eururo.2013.08.011

Rao, D. M., Shackleford, M. T., Bordeaux, E. K., Sottnik, J. L., Ferguson, R. L., Yamamoto, T. M., … Sikora, M. J. (2019). Wnt family member 4 (WNT4) and WNT3A activate cell-autonomous Wnt signaling independent of porcupine O-acyltransferase or Wnt secretion. *Journal of Biological Chemistry*, *294*(52), 19950–19966. https://doi.org/10.1074/jbc.RA119.009615

Rasheed, S. A. K., Efferth, T., Asangani, I. A., & Allgayer, H. (2010). First evidence that the antimalarial drug artesunate inhibits invasion and in vivo metastasis in lung cancer by targeting essential extracellular proteases. *International Journal of Cancer*, *127*(6), 1475–1485. https://doi.org/10.1002/ijc.25315

Ratta, R., Guida, A., Scotté, F., Neuzillet, Y., Teillet, A. B., Lebret, T., & Beuzeboc, P. (2020). PARP inhibitors as a new therapeutic option in metastatic prostate cancer: a systematic review. *Prostate Cancer and Prostatic Diseases*, *23*(4), 549–560. https://doi.org/10.1038/s41391-020-0233-3

Rawla, P. (2019). Epidemiology of Prostate Cancer. *World Journal of Oncology*, *10*(2), 63–89. https://doi.org/10.14740/wjon1191

Redman, J. M., Hill, E. M., AlDeghaither, D., & Weiner, L. M. (2015). Mechanisms of action of therapeutic antibodies for cancer. *Molecular Immunology*, *67*(2), 28–45. https://doi.org/10.1016/j.molimm.2015.04.002

Ren, D., Dai, Y., Yang, Q., Zhang, X., Guo, W., Ye, L., … Song, L. (2018). Wnt5a induces and maintains prostate cancer cells dormancy in bone. *J. Exp. Med*, 1–28. https://doi.org/10.1084/jem.20180661

Ren, D. N., Chen, J., Li, Z., Yan, H., Yin, Y., Wo, D., … Zhu, W. (2015). LRP5/6 directly bind to Frizzled and prevent Frizzled-regulated tumour metastasis. *Nature Communications*, *6*. https://doi.org/10.1038/ncomms7906

Ren, Q., Chen, J., & Liu, Y. (2021). LRP5 and LRP6 in Wnt Signaling: Similarity and Divergence. *Frontiers in Cell and Developmental Biology*, *9*(May), 1–11. https://doi.org/10.3389/fcell.2021.670960

Ribatti, D. (2016). The chick embryo chorioallantoic membrane (CAM). A multifaceted experimental model. *Mechanisms of Development*, *141*, 70–77. https://doi.org/10.1016/j.mod.2016.05.003

Riley, R. S., & Day, E. S. (2017). Frizzled7 Antibody-Functionalized Nanoshells Enable Multivalent Binding for Wnt Signaling Inhibition in Triple Negative Breast Cancer Cells. *Small*, *13*(26), 1–10. https://doi.org/10.1002/smll.201700544

Robinson, D., Allen, E. M. Van, Wu, Y.-M., Schultz, N., Sawyers, C. L., & Chinnaiyan, A. M. (2015). Integrative clinical genomics of advanced prostate cancer. *Cell*, *161*(5), 1215–1228. https://doi.org/10.1016/j.cell.2015.05.001

Rodon, J., Argilés, G., Connolly, R. M., Vaishampayan, U., de Jonge, M., Garralda, E., … Janku, F. (2021). Phase 1 study of single-agent WNT974, a first-in-class Porcupine inhibitor, in patients with advanced solid tumours. *British Journal of Cancer*, *125*(1), 28–37. https://doi.org/10.1038/s41416-021-01389-8

Rodriguez-Hernandez, I., Maiques, O., Kohlhammer, L., Cantelli, G., Perdrix-Rosell, A., Monger, J., … Sanz-Moreno, V. (2020). WNT11-FZD7-DAAM1 signalling supports tumour initiating abilities and melanoma amoeboid invasion. *Nature Communications*, *11*(1). https://doi.org/10.1038/s41467-020-18951-2

Roslan, Z., Muhamad, M., Selvaratnam, L., & Ab-Rahim, S. (2019). The Roles of Low-Density Lipoprotein Receptor-Related Proteins 5, 6, and 8 in Cancer: A Review. *Journal of Oncology*, *2019*(Vldl), 1–7. https://doi.org/10.1155/2019/4536302

Ruenraroengsak, P., Kiryushko, D., Theodorou, I. G., Klosowski, M. M., Taylor, E. R., Niriella, T., … Porter, A. E. (2019). Frizzled-7-targeted delivery of zinc oxide nanoparticles to drug-resistant breast cancer cells. *Nanoscale*, *11*(27), 12858–12870. https://doi.org/10.1039/c9nr01277j

Säfholm, A., Tuomela, J., Rosenkvist, J., Dejmek, J., Härkönen, P., & Andersson, T. (2008). The wnt-5a-derived hexapeptide

Foxy-5 inhibits breast cancer metastasis in vivo by targeting cell motility. *Clinical Cancer Research*, *14*(20), 6556–6563. https://doi.org/10.1158/1078-0432.CCR-08-0711

Sandsmark, E., Hansen, A. F., Selnæs, K. M., Bertilsson, H., Bofin, A. M., Wright, A. J., … Rye, M. B. (2017). A novel non-canonical Wnt signature for prostate cancer aggressiveness. *Oncotarget*, *8*(6), 9572–9586. https://doi.org/10.18632/oncotarget.14161

Schindelin, J., Arganda-Carreras, I., Frise, E., Kaynig, V., Longair, M., Pietzsch, T., … Cardona, A. (2012). Fiji: An open-source platform for biological-image analysis. *Nature Methods*, *9*(7), 676–682. https://doi.org/10.1038/nmeth.2019

Scholten, D. J., Timmer, C. M., Peacock, J. D., Pelle, D. W., Williams, B. O., & Steensma, M. R. (2014). Down regulation of Wnt signaling mitigates hypoxia-induced chemoresistance in human osteosarcoma cells. *PLoS ONE*, *9*(10), 1–8. https://doi.org/10.1371/journal.pone.0111431

Schröder, F. H., Hermanek, P., Denis, L., Fair, W. R., Gospodarowicz, M. K., & Pavone-Macaluso, M. (1992). The TNM classification of prostate cancer. *The Prostate*, *21*(4 S), 129–138. https://doi.org/10.1002/pros.2990210521

Schulte, G., & Bryja, V. (2007). The Frizzled family of unconventional G-protein-coupled receptors. *Trends in Pharmacological Sciences*, *28*(10), 518–525. https://doi.org/10.1016/j.tips.2007.09.001

Semënov, M. V., Tamai, K., Brott, B. K., Kühl, M., Sokol, S., & He, X. (2001). Head inducer dickkopf-1 is a ligand for Wnt coreceptor LRP6. *Current Biology*, *11*(12), 951–961. https://doi.org/10.1016/S0960-9822(01)00290-1

Senior, A. W., Evans, R., Jumper, J., Kirkpatrick, J., Sifre, L., Green, T., … Hassabis, D. (2020). Improved protein structure prediction using potentials from deep learning. *Nature*, *577*(7792), 706–710. https://doi.org/10.1038/s41586-019-1923-7

Sharma, M., Castro-Piedras, I., Simmons, G. E., & Pruitt, K. (2018). Dishevelled: A masterful conductor of complex Wnt signals. *Cellular Signalling*, *47*, 52–64. https://doi.org/10.1016/j.cellsig.2018.03.004

Sharma, R. P., & Chopra, V. L. (1976). Effect of the wingless (wg1) mutation on wing and haltere development in Drosophila melanogaster. *Developmental Biology*, *48*(2), 461–465. https://doi.org/10.1016/0012-1606(76)90108-1

Shen, M. M., & Abate-Shen, C. (2010). Molecular genetics of prostate cancer: New prospects for old challenges. *Genes and Development*, *24*(18), 1967–2000. https://doi.org/10.1101/gad.1965810

Shi, H., Xu, X., Zhang, B., Xu, J., Pan, Z., Gong, A., … Xu, W. (2017). 3,3'-Diindolylmethane stimulates exosomal Wnt11 autocrine signaling in human umbilical cord mesenchymal stem cells to enhance wound healing. *Theranostics*, *7*(6), 1674–1688. https://doi.org/10.7150/thno.18082

Shimomura, Y., Agalliu, D., Vonica, A., Luria, V., Wajid, M., Baumer, A., … Christiano, A. M. (2010). APCDD1 is a novel Wnt inhibitor mutated in hereditary hypotrichosis simplex. *Nature*, *464*(7291), 1043–1047. https://doi.org/10.1038/nature08875

Shojima, K., Sato, A., Hanaki, H., Tsujimoto, I., Nakamura, M., Hattori, K., … Kikuchi, A. (2015). Wnt5a promotes cancer cell invasion and proliferation by receptor-mediated endocytosis-dependent and -independent mechanisms, respectively. *Scientific Reports*, *5*, 8042. https://doi.org/10.1038/srep08042

Siman-Tov, R., Zelikson, N., Caspi, M., Levi, Y., Perry, C., Khair, F., … Rosin-Arbesfeld, R. (2021). Circulating Wnt Ligands Activate the Wnt Signaling Pathway in Mature Erythrocytes. *Arteriosclerosis, Thrombosis, and Vascular Biology*, (May), E243–E264. https://doi.org/10.1161/ATVBAHA.120.315413

Singh, N., Jenkins, G. J. S., Asadi, R., & Doak, S. H. (2010). Potential toxicity of superparamagnetic iron oxide nanoparticles (SPION). *Nano Reviews*, *1*(1), 5358. https://doi.org/10.3402/nano.v1i0.5358

Sizemore, G. M., Pitarresi, J. R., Balakrishnan, S., & Ostrowski, M. C. (2017). The ETS family of oncogenic transcription factors in solid tumours. *Nature Reviews Cancer*, *17*(6), 337–351. https://doi.org/10.1038/nrc.2017.20

Sneha, S., Nagare, R. P., Priya, S. K., Sidhanth, C., Pors, K., & Ganesan, T. S. (2017). Therapeutic antibodies against cancer stem cells: a promising approach. *Cancer Immunology, Immunotherapy*, *66*(11), 1383–1398. https://doi.org/10.1007/s00262-017-2049-0

Sousa, F., Castro, P., Fonte, P., Kennedy, P. J., Neves-Petersen, M. T., & Sarmento, B. (2017). Nanoparticles for the delivery of therapeutic antibodies: Dogma or promising strategy? *Expert Opinion on Drug Delivery*, *14*(10), 1163–1176. https://doi.org/10.1080/17425247.2017.1273345

Stamos, J. L., & Weis, W. I. (2013). The β-catenin destruction complex. *Cold Spring Harbor Perspectives in Biology*, *5*(1), 1–16. https://doi.org/10.1101/cshperspect.a007898

Stanganello, E., & Scholpp, S. (2016). Role of cytonemes in Wnt transport. *Journal of Cell Science*, *129*(4), 665–672. https://doi.org/10.1242/jcs.182469

Steinhart, Z., & Angers, S. (2018). Wnt signaling in development and tissue homeostasis. *Development*, *145*(11), dev146589. https://doi.org/10.1242/dev.146589

Stoletov, K., Willetts, L., Paproski, R. J., Bond, D. J., Raha, S., Jovel, J., … Lewis, J. D. (2018). Quantitative in vivo whole genome motility screen reveals novel therapeutic targets to block cancer metastasis. *Nature Communications*, *9*(1), 1–12. https://doi.org/10.1038/s41467-018-04743-2

Sun, T., Huang, Z., Liang, W., Yin, J., Lin, W. Y., Wu, J., … Arron, J. R. (2021). TGF b 2 and TGF b 3 isoforms drive fibrotic disease pathogenesis. *Science Translational Medicine*, *0407*(August), 1–17.

Sussman, D. J., Klingensmith, J., Salinas, P., Adams, P. S., Nusse, R., & Perrimon, N. (1994). Isolation and characterization of a mouse homolog of the drosophila segment polarity gene dishevelled. *Developmental Biology*. https://doi.org/10.1006/dbio.1994.1297

Swadi, R. R., Sampat, K., Herrmann, A., Losty, P. D., See, V., & Moss, D. J. (2019). CDK inhibitors reduce cell proliferation and reverse hypoxia-induced metastasis of neuroblastoma tumours in a chick embryo model. *Scientific Reports*, *9*(1), 1–15. https://doi.org/10.1038/s41598-019-45571-8

Takada, R., Satomi, Y., Kurata, T., Ueno, N., Norioka, S., Kondoh, H., … Takada, S. (2006). Monounsaturated Fatty Acid Modification of Wnt Protein: Its Role in Wnt Secretion. *Developmental Cell*, *11*(6), 791–801. https://doi.org/10.1016/j.devcel.2006.10.003

Takada, S., Fujimori, S., Shinozuka, T., Takada, R., & Mii, Y. (2017). Wnt Signaling: Biological Functions and Its Implications in Diseases Differences in the secretion and transport of Wnt proteins. *Journal of Biochemistry*, *161*(1), 1–7. https://doi.org/10.1093/jb/mvw071

Takahashi, K., Tanabe, K., Ohnuki, M., Narita, M., Ichisaka, T., Tomoda, K., & Yamanaka, S. (2007). Induction of Pluripotent Stem Cells from Adult Human Fibroblasts by Defined Factors. *Cell*, *131*(5), 861–872. https://doi.org/10.1016/j.cell.2007.11.019

Tamai, K., Semenov, M., Kato, Y., Spokony, R., Liu, C., Katsuyama, Y., … He, X. (2000). LDL-receptor-related proteins in Wnt signal transduction. *Nature*, *407*(6803), 530–535. https://doi.org/10.1038/35035117

Tamai, K., Zeng, X., Liu, C., Zhang, X., Harada, Y., Chang, Z., & He, X. (2004). A Mechanism for Wnt Coreceptor Activation. *Molecular Cell*, *13*(1), 149–156. https://doi.org/10.1016/S1097-2765(03)00484-2

Tang, Z., Li, C. C., Kang, B., Gao, G., Li, C. C., & Zhang, Z. (2017). GEPIA: A web server for cancer and normal gene expression profiling and interactive analyses. *Nucleic Acids Research*, *45*(W1), W98–W102. https://doi.org/10.1093/nar/gkx247

Tao, Q., Yokota, C., Puck, H., Kofron, M., Birsoy, B., Yan, D., … Heasman, J. (2005). Maternal Wnt11 activates the canonical Wnt signaling pathway required for axis formation in Xenopus embryos. *Cell*, *120*(6), 857–871. https://doi.org/10.1016/j.cell.2005.01.013

Tenjin, Y., Kudoh, S., Kubota, S., Yamada, T., Matsuo, A., Sato, Y., … Ito, T. (2019). Ascl1-induced Wnt11 regulates neuroendocrine differentiation, cell proliferation, and E-cadherin expression in small-cell lung cancer and Wnt11 regulates small-cell lung cancer biology. *Laboratory Investigation*. https://doi.org/10.1038/s41374-019-0277-y

Terenzi, D. C., Verma, S., & Hess, D. A. (2021). Exploring the Clinical Implications of Wnt Signaling in Enucleated Erythrocytes. *Arteriosclerosis, Thrombosis, and Vascular Biology*, (May), 1654–1656. https://doi.org/10.1161/ATVBAHA.121.316169

Tian, S., Hu, J., Tao, K., Wang, J., Chu, Y., Li, J., … Wang, Z. (2018). Secreted AGR2 promotes invasion of colorectal cancer cells via Wnt11-mediated non-canonical Wnt signaling. *Experimental Cell Research*, *364*(2), 198–207. https://doi.org/10.1016/j.yexcr.2018.02.004

Tomlins, S. A., Laxman, B., Dhanasekaran, S. M., Helgeson, B. E., Cao, X., Morris, D. S., … Chinnaiyan, A. M. (2007). Distinct classes of chromosomal rearrangements create oncogenic ETS gene fusions in prostate cancer. *Nature*, *448*(7153), 595–599. https://doi.org/10.1038/nature06024

Tomlins, S. A., Laxman, B., Varambally, S., Cao, X., Yu, J., Helgeson, B. E., … Chinnaiyan, A. M. (2008). Role of the TMPRSS2-ERG Gene Fusion in Prostate Cancer. *Neoplasia*, *10*(2), 177-IN9. https://doi.org/10.1593/neo.07822

Toyama, T., Lee, H. C., Koga, H., Wands, J. R., & Kim, M. (2010). Noncanonical Wnt11 inhibits hepatocellular carcinoma cell proliferation and migration. *Mol Cancer Res.*, *8*(2), 254–265. https://doi.org/10.1158/1541-7786.MCR-09-0238.Noncanonical

Trabulo, S., Aires, A., Aicher, A., Heeschen, C., & Cortajarena, A. L. (2017). Multifunctionalized iron oxide nanoparticles for selective targeting of pancreatic cancer cells. *Biochimica et Biophysica Acta - General Subjects*, *1861*(6), 1597–1605. https://doi.org/10.1016/j.bbagen.2017.01.035

Trenevska, I., Li, D., & Banham, A. H. (2017). Therapeutic antibodies against intracellular tumor antigens. *Frontiers in Immunology*, *8*(AUG). https://doi.org/10.3389/fimmu.2017.01001

Tse, B. W. C., Cowin, G. J., Soekmadji, C., Jovanovic, L., Vasireddy, R. S., Ling, M. T., … Russell, P. J. (2015). PSMA-targeting iron oxide magnetic nanoparticles enhance MRI of preclinical prostate cancer. *Nanomedicine*, *10*(3), 375–386. https://doi.org/10.2217/nnm.14.122

Tsukiyama, T., Koo, B. K., & Hatakeyama, S. (2021). Post-translational Wnt receptor regulation: Is the fog slowly clearing?: The molecular mechanism of RNF43/ZNRF3 ubiquitin ligases is not yet fully elucidated and still controversial. *BioEssays*, *43*(4), 1–10. https://doi.org/10.1002/bies.202000297

Ulrich, F., Krieg, M., Schötz, E. M., Link, V., Castanon, I., Schnabel, V., … Heisenberg, C. P. (2005). Wnt11 functions in gastrulation by controlling cell cohesion through Rab5c and E-Cadherin. *Developmental Cell*, *9*(4), 555–564. https://doi.org/10.1016/j.devcel.2005.08.011

Uysal-Onganer, Kawano, Y., Caro, M., Walker, M. M., Diez, S., Darrington, R. S., … Kypta, R. M. (2010). Wnt-11 promotes neuroendocrine-like differentiation, survival and migration of prostate cancer cells. *Molecular Cancer*, *9*, 1–11. https://doi.org/10.1186/1476-4598-9-55

Uysal-Onganer, & Kypta. (2012). Wnt11 in 2011 - the regulation and function of a non-canonical Wnt. *Acta Physiologica*, *204*(1), 52–64. https://doi.org/10.1111/j.1748-1716.2011.02297.x

Valenta, T., Hausmann, G., & Basler, K. (2012). The many faces and functions of β-catenin. *EMBO Journal*, *31*(12), 2714–2736. https://doi.org/10.1038/emboj.2012.150

van Amerongen, R. (2012). Alternative Wnt pathways and receptors. *Cold Spring Harbor Perspectives in Biology*, *4*(10), 1–18. https://doi.org/10.1101/cshperspect.a007914

van Amerongen, R., & Berns, A. (2006). Knockout mouse models to study Wnt signal transduction. *Trends in Genetics*, *22*(12), 678–689. https://doi.org/10.1016/j.tig.2006.10.001

Van Der Sanden, M. H. M., Meems, H., Houweling, M., Helms, J. B., & Vaandrager, A. B. (2004). Induction of CCAAT/enhancer-binding protein (C/EBP)-homologous protein/growth arrest and DNA damage-inducible protein 153 expression during inhibition of phosphatidylcholine synthesis is mediated via activation of a C/EBP-activating transcription factor-r. *Journal of Biological Chemistry*, *279*(50), 52007–52015. https://doi.org/10.1074/jbc.M405577200

Veeman, M. T., Axelrod, J. D., & Moon, R. T. (2003). A second canon: Functions and mechanisms of β-catenin-independent Wnt signaling. *Developmental Cell*, *5*(3), 367–377. https://doi.org/10.1016/S1534-5807(03)00266-1

Velázquez, D. M., Castañeda-Patlán, M. C., & Robles-Flores, M. (2017). Dishevelled stability is positively regulated by PKCζ-mediated phosphorylation induced by Wnt agonists. *Cellular Signalling*, *35*(February), 107–117. https://doi.org/10.1016/j.cellsig.2017.03.023

Veltri, A., Lang, C., & Lien, W. H. (2018). Concise Review: Wnt Signaling Pathways in Skin Development and Epidermal Stem Cells. *Stem Cells*, *36*(1), 22–35. https://doi.org/10.1002/stem.2723

Veronika, W., Rene, D. R., Karolin, R., Tina, K., Gerd, U. N., Doris, W., & Dietmar, G. (2014). Live imaging of Xwnt5A-ROR2 complexes. *PLoS ONE*, *9*(10), 1–9. https://doi.org/10.1371/journal.pone.0109428

Vitorino, M., Silva, A. C., Inácio, J. M., Ramalho, J. S., Gur, M., Fainsod, A., … Kibar, Z. (2015). Xenopus Pkdcc1 and Pkdcc2 are two new tyrosine kinases involved in the regulation of JNK dependent Wnt/PCP signaling pathway. *PLoS ONE*, *10*(8), 1–25. https://doi.org/10.1371/journal.pone.0135504

Volante, M., Tota, D., Giorcelli, J., Bollito, E., Napoli, F., Vatrano, S., … Rapa, I. (2016). Androgen deprivation modulates gene expression profile along prostate cancer progression. *Human Pathology*, *56*, 81–88. https://doi.org/10.1016/j.humpath.2016.06.004

Voloshanenko, O., Schwartz, U., Kranz, D., Rauscher, B., Linnebacher, M., Augustin, I., & Boutros, M. (2018). β-catenin-independent regulation of Wnt target genes by RoR2 and ATF2/ATF4 in colon cancer cells. *Scientific Reports*, *8*(1), 1–14. https://doi.org/10.1038/s41598-018-20641-5

Vu, B. T., Shahin, S. A., Croissant, J., Fatieiev, Y., Matsumoto, K., Le-Hoang Doan, T., … Tamanoi, F. (2018). Chick chorioallantoic membrane assay as an in vivo model to study the effect of nanoparticle-based anticancer drugs in ovarian cancer. *Scientific Reports*, *8*(1), 1–10. https://doi.org/10.1038/s41598-018-25573-8

Wall, J. A., Klempner, S. J., & Arend, R. C. (2020). The anti-DKK1 antibody DKN-01 as an immunomodulatory combination partner for the treatment of cancer. *Expert Opinion on Investigational Drugs*, *29*(7), 639–644. https://doi.org/10.1080/13543784.2020.1769065

Wallingford, J. B., & Habas, R. (2005). The developmental biology of Dishevelled: An enigmatic protein governing cell fate and cell polarity. *Development*, *132*(20), 4421–4436. https://doi.org/10.1242/dev.02068

Wang, G., Zhao, D., Spring, D. J., & Depinho, R. A. (2018). Genetics and biology of prostate cancer. *Genes and Development*, *32*(17–18), 1105–1140. https://doi.org/10.1101/gad.315739.118

Wang, Jiani, & Xu, B. (2019). Targeted therapeutic options and future perspectives for her2-positive breast cancer. *Signal Transduction and Targeted Therapy*, *4*(1). https://doi.org/10.1038/s41392-019-0069-2

Wang, Jingcai, Gong, M., Zuo, S., Xu, J., Paul, C., Ashraf, M., & Xu, M. (2020). WNT11-Conditioned Medium Promotes Angiogenesis through the Activation of Non-Canonical WNT-PKC-JNK Signaling Pathway. *Genes*, (Mi), 1–17.

Wang, L., Dehm, S. M., Hillman, D. W., Sicotte, H., Tan, W., Gormley, M., … Kohli, M. (2018). A prospective genome-wide study of prostate cancer metastases reveals association of wnt pathway activation and increased cell cycle proliferation with primary resistance to abiraterone acetate-prednisone. *Annals of Oncology*, *29*(2), 352–360. https://doi.org/10.1093/annonc/mdx689

Wang, W., Li, X., Lee, M., Jun, S., Aziz, K. E., Feng, L., … Chen, J. (2015). FOXKs promote Wnt/β-catenin signaling by translocating DVL into the nucleus. *Developmental Cell*, *32*(6), 707–718. https://doi.org/10.1016/j.devcel.2015.01.031

Wang, X., Zou, Y., Chen, Z., Li, Y., Pan, L., Wang, Y., … Gong, H. (2021). Low-density lipoprotein receptor-related protein 6 regulates cardiomyocyte-derived paracrine signaling to ameliorate cardiac fibrosis. *Theranostics*, *11*(3), 1249–1268. https://doi.org/10.7150/thno.48787

Waterhouse, A. M., Procter, J. B., Martin, D. M. A., Clamp, M., & Barton, G. J. (2009). Jalview Version 2-A multiple sequence alignment editor and analysis workbench. *Bioinformatics*, *25*(9), 1189–1191. https://doi.org/10.1093/bioinformatics/btp033

Watson, G., Ronai, Z., & Lau, E. (2017). ATF2, a paradigm of the multifaceted regulation of transcription factors in biology and disease. *Pharmacological Research*, *119*, 347–357. https://doi.org/10.1016/j.phrs.2017.02.004

Wehrli, M., Dougan, S. T., Caldwell, K., O'Keefe, L., Schwartz, S., Valzel-Ohayon, D., … DiNardo, S. (2000). Arrow encodes an LDL-receptor-related protein essential for Wingless signalling. *Nature*, *407*(6803), 527–530. https://doi.org/10.1038/35035110

Wei, H., Wang, N., Zhang, Y., Wang, S., Pang, X., & Zhang, S. (2016). Wnt-11 overexpression promoting the invasion of cervical cancer cells. *Tumor Biology*, *37*(9), 11789–11798. https://doi.org/10.1007/s13277-016-4953-x

Wiese, K. E., Nusse, R., & van Amerongen, R. (2018). Wnt signalling: Conquering complexity. *Development (Cambridge)*, *145*(12), 1–9. https://doi.org/10.1242/dev.165902

Wilczewska, A. Z., Niemirowicz, K., Markiewicz, K. H., & Car, H. (2012). Nanoparticles as drug delivery systems systematic review. *Nanoparticles and Drugs*, (64), 1020–1037.

Willert, K., & Nusse, R. (2012). Wnt proteins. *Cold Spring Harbor Perspectives in Biology*, *4*(9), 1–13. https://doi.org/10.1101/cshperspect.a007864

Wise, D. R., Schneider, J. A., Armenia, J., Febles, V. A., McLaughlin, B., Brennan, R., … Sawyers, C. L. (2020). Dickkopf-1 Can Lead to Immune Evasion in Metastatic Castration-Resistant Prostate Cancer. *JCO Precision Oncology*, *4*. https://doi.org/10.1200/PO.20.00097

Witzel, S., Zimyanin, V., Carreira-Barbosa, F., Tada, M., & Heisenberg, C. P. (2006). Wnt11 controls cell contact persistence by local accumulation of Frizzled 7 at the plasma membrane. *Journal of Cell Biology*, *175*(5), 791–802. https://doi.org/10.1083/jcb.200606017

Wolfram, J., Zhu, M., Yang, Y., Shen, J., Gentile, E., Paolino, D., … Zhao, Y. (2015). Safety of Nanoparticles in Medicine. *Current Drug Targets*, *16*(14), 1671–1681. https://doi.org/10.2174/1389450115666140804124808

World Health Organization. (2021). Cancer (WHO). Retrieved May 17, 2021, from https://www.who.int/health-topics/cancer

Wu, L., Zhao, J. C., Kim, J., Jin, H.-J., Wang, C.-Y., & Yu, J. (2013). ERG Is a Critical Regulator of Wnt/LEF1 Signaling in Prostate Cancer. *Cancer Research*, *73*(19), 6068–6079. https://doi.org/10.1158/0008-5472.CAN-13-0882

Yamamoto, H., Oue, N., Sato, A., Hasegawa, Y., Yamamoto, H., Matsubara, A., … Kikuchi, A. (2010). Wnt5a signaling is involved in the aggressiveness of prostate cancer and expression of metalloproteinase. *Oncogene*, *29*(14), 2036–2046. https://doi.org/10.1038/onc.2009.496

Yamamoto, Hideki, Awada, C., Hanaki, H., Sakane, H., Tsujimoto, I., Takahashi, Y., … Kikuchi, A. (2013). The apical and basolateral secretion of Wnt11 and Wnt3a in polarized epithelial cells is regulated by different mechanisms. *Journal of Cell Science*, *126*(13), 2931–2943. https://doi.org/10.1242/jcs.126052

Yan, X., Lin, Y., Yang, D., Shen, Y., Yuan, M., Zhang, Z., … Liu, Q. (2003). IMMUNOBIOLOGY A novel anti-CD146 monoclonal antibody , AA98 , inhibits angiogenesis and tumor growth. *IMMUNOBIOLOGY*, *102*(1), 184–191. https://doi.org/10.1182/blood-2002-04-1004.Supported

Yao, C. Q., Liu, S. K., Yamaguchi, T. N., Sabelnykova, V. Y., Lesurf, R., Livingstone, J., … Espiritu, S. M. G. (2019). Molecular landmarks of tumor hypoxia across cancer types. *Nature Genetics*, *51*(2), 308–318. https://doi.org/10.1038/s41588-018-0318-2

Yao, Q., An, Y., Hou, W., Cao, Y.-N., Yao, M.-F., Ma, N.-N., … Zhang, B. (2017). LRP6 promotes invasion and metastasis of colorectal cancer through cytoskeleton dynamics. *Oncotarget*, *8*(65), 109632–109645. https://doi.org/10.18632/oncotarget.22759

Yazici, Y., McAlindon, T. E., Fleischmann, R., Gibofsky, A., Lane, N. E., Kivitz, A. J., … Hochberg, M. C. (2017). A novel Wnt pathway inhibitor, SM04690, for the treatment of moderate to severe osteoarthritis of the knee: results of a 24-week, randomized, controlled, phase 1 study. *Osteoarthritis and Cartilage*, *25*(10), 1598–1606. https://doi.org/10.1016/j.joca.2017.07.006

Yin, Y., Ding, L., Hou, Y., Jiang, H., Zhang, J., Dai, Z., & Zhang, G. (2019). Upregulating MicroRNA-410 or Downregulating Wnt-11 Increases Osteoblasts and Reduces Osteoclasts to Alleviate Osteonecrosis of the Femoral Head (Nanoscale Research Letters, (2019), 14, 1, (383), 10.1186/s11671-019-3221-6). *Nanoscale Research Letters*, *16*(1). https://doi.org/10.1186/s11671-020-03465-z

Yost, C., Torres, M., Miller, J. R., Huang, E., Kimelman, D., & Moon, R. T. (1996). The axis-inducing activity, stability, and subcellular distribution of β-catenin is regulated in Xenopus embryos by glycogen synthase kinase 3. *Genes and Development*, *10*(12), 1443–1454. https://doi.org/10.1101/gad.10.12.1443

Zhang, M., Haughey, M., Wang, N. Y., Blease, K., Kapoun, A. M., Couto, S., … Xie, W. (2020). Targeting the Wnt signaling pathway through R-spondin 3 identifies an anti-fibrosis treatment strategy for multiple organs. *PLoS ONE*, *15*(3), 1–21. https://doi.org/10.1371/journal.pone.0229445

Zhang, P., Cai, Y., Soofi, A., & Dressler, G. R. (2012). Activation of Wnt11 by transforming growth factor drives mesenchymal gene expression through non-canonical Wnt protein signaling in renal epithelial cells. *Journal of Biological Chemistry*, *287*(25), 21290–21302. https://doi.org/10.1074/jbc.M112.357202

Zhang, S., Chen, L., Wang-Rodriguez, J., Zhang, L., Cui, B., Frankel, W., … Kipps, T. J. (2012). The onco-embryonic antigen ROR1 is expressed by a variety of human cancers. *American Journal of Pathology*, *181*(6), 1903–1910. https://doi.org/10.1016/j.ajpath.2012.08.024

Zhang, S., Zhang, H., Ghia, E. M., Huang, J., Wu, L., Zhang, J., … Kipps, T. J. (2019). *Inhibition of chemotherapy resistant breast cancer stem cells by a ROR1 specific antibody*. *Proceedings of the National Academy of Sciences of the United States of America* (Vol. 116). https://doi.org/10.1073/pnas.1816262116

Zhang, Y., Toneri, M., Ma, H., Yang, Z., Bouvet, M., Goto, Y., … Hoffman, R. M. (2016). Real-Time GFP Intravital Imaging of the Differences in Cellular and Angiogenic Behavior of Subcutaneous and Orthotopic Nude-Mouse Models of Human PC-3 Prostate Cancer. *Journal of Cellular Biochemistry*, (January 2016), 2546–2551. https://doi.org/10.1002/jcb.25547

Zhang, Z., Cheng, L., Li, J., Farah, E., Atallah, N. M., Pascuzzi, P. E., … Liu, X. (2018). Inhibition of the Wnt/β-Catenin Pathway Overcomes Resistance to Enzalutamide in Castration-Resistant Prostate Cancer. *Cancer Research*, *78*(12), 3147–3162. https://doi.org/10.1158/0008-5472.CAN-17-3006

Zheng, M., Tian, C., Fan, T., & Xu, B. (2019). Fibronectin regulates the self-renewal of rabbit limbal epithelial stem cells by stimulating the Wnt11/Fzd7/ROCK non-canonical Wnt pathway. *Experimental Eye Research*, *185*(April), 107681. https://doi.org/10.1016/j.exer.2019.05.021

Zhong, Q., Zhao, Y., Ye, F., Xiao, Z., Huang, G., Xu, M., … Ma, D. (2021). Cryo-EM structure of human Wntless in complex with Wnt3a. *Nature Communications*, (12). https://doi.org/10.1038/s41467-021-24731-3

Zhu, H., Mazor, M., Kawano, Y., Walker, M. M., Leung, H. Y., Armstrong, K., … Kypta, R. M. (2004). Analysis of Wnt gene expression in prostate cancer: Mutual inhibition by WNT11 and the androgen receptor. *Cancer Research*, *64*(21), 7918–7926. https://doi.org/10.1158/0008-5472.CAN-04-2704

Zhu, J. H., Liao, Y. P., Li, F. S., Hu, Y., Li, Q., Ma, Y., … Su, Y. X. (2018). Wnt11 promotes BMP9-induced osteogenic differentiation through BMPs/Smads and p38 MAPK in mesenchymal stem cells. *Journal of Cellular Biochemistry*, *119*(11), 9462–9473. https://doi.org/10.1002/jcb.27262

Zhu, L., Zhou, Z., Mao, H., & Yang, L. (2017). Magnetic nanoparticles for precision oncology: Theranostic magnetic iron oxide nanoparticles for image-guided and targeted cancer therapy. *Nanomedicine*, *12*(1), 73–87. https://doi.org/10.2217/nnm-2016-0316

Zijlstra, A., Lewis, J., DeGryse, B., Stuhlmann, H., & Quigley, J. P. (2008). The Inhibition of Tumor Cell Intravasation and Subsequent Metastasis via Regulation of In Vivo Tumor Cell Motility by the Tetraspanin CD151. *Cancer Cell*, *13*(3), 221–234. https://doi.org/10.1016/j.ccr.2008.01.031

Zijlstra, A., Mellor, R., Panzarella, G., Aimes, R. T., Hooper, J. D., Marchenko, N. D., & Quigley, J. P. (2002). A quantitative analysis of rate-limiting steps in the metastatic cascade using human-specific real-time polymerase chain reaction. *Cancer Research*, *62*(23), 7083–7092.

Zinzalla, V., Drobits-Handl, B., Savchenko, A., Rinnenthal, J., Bauer, M. J., Sanderson, M., … Kraut, N. (2019). *Abstract DDT01-01: BI 905677: A first-in-class LRP5/6 antagonist targeting Wnt-driven proliferation and immune escape*. *Cancer Research* (Vol. 79). American Association for Cancer Research. https://doi.org/10.1158/1538-7445.AM2019-DDT01-01

Zuo, S., Jones, W. K., Li, H., He, Z., Pasha, Z., Yang, Y., … Xu, M. (2012). Paracrine Effect of Wnt11-Overexpressing Mesenchymal Stem Cells on Ischemic Injury. *Stem Cells and Development*, *21*(4), 598–608. https://doi.org/10.1089/scd.2011.0071

Resumen extendido

Introducción

El cáncer de próstata es el segundo cáncer más diagnosticado en la población masculina a nivel mundial, afectando en 2020 a más de 1.4 millones de personas y causando la muerte de aproximadamente 300 000 hombres (Rawla, 2019). La mayor parte de los tumores de próstata son adenocarcinomas de tipo acinar. El cáncer de próstata se detecta de forma precoz gracias al análisis de los niveles sanguíneos de antígeno específico de próstata (PSA) e inicialmente se considera un cáncer poco agresivo. El crecimiento del tumor suele ser dependiente de andrógenos, lo que hace de la deprivación androgénica (ADT) una de las principales líneas terapéuticas para su tratamiento. No obstante, el cáncer puede desarrollar mecanismos de resistencia a la terapia, convirtiéndose en cáncer de próstata resistente a la castración (CRPC), lo cual va acompañado de un incremento en su agresividad y capacidad de metastatizar (Attard et al., 2016).

En estadio CRPC son necesarias dianas terapéuticas independientes de las relacionadas con la señalización por andrógenos. Uno de los mecanismos de resistencia es la reactivación de cascadas de señalización del desarrollo (Shen & Abate-Shen, 2010). En este contexto, alteraciones en la ruta de señalización por Wnt ha mostrado ser importante para la progresión del cáncer de próstata y su activación aberrante ocurre mediante factores específicos de tejido (Murillo-Garzón & Kypta, 2017). Entre ellos, la expresión de Wnt-11 se encuentra aumentada en cáncer de próstata, especialmente en estadios avanzados, y se ha demostrado que promueve la progresión tumoral activando la diferenciación neuroendocrina, la migración e invasión celular (Uysal-Onganer et al., 2010; H. Zhu et al., 2004). FZD8 ha sido descrito como uno de sus receptores en cáncer de próstata y, además, media la cooperación con la ruta de señalización por TGF-β, activando la transición epitelio mesénquima (EMT) y promoviendo la agresividad de la enfermedad (Murillo-Garzón et al., 2018).

Alteraciones en la ruta de señalización por Wnt se encuentran de forma frecuente en múltiples cánceres (Anastas & Moon, 2013). Por ello, se han desarrollado múltiples

mecanismos para la inhibición de esta señalización a distintos niveles como posibles terapias, aunque ninguna se encuentra en uso clínico. Entre estos destacan los inhibidores de secreción de Wnt, los moduladores de la actividad de β-catenina y los anticuerpos terapéuticos contra receptores y coreceptores de Wnt, como son Vantictumab y Cirmtuzumab. No obstante, debido a la implicación de Wnt-11 en la progresión del cáncer de próstata, inhibidores selectivos serían de interés para su tratamiento.

Algunos estudios han descrito el uso de anticuerpos comerciales anti-Wnt-11 para su inhibición pero ninguno ha sido explorado como agente terapéutico (Dwyer et al., 2010; Hsueh et al., 2020; Ouko et al., 2004; Jingcai Wang et al., 2020; Zuo et al., 2012). En contexto de aplicación en la clínica, es atractiva la conjugación de los potenciales anticuerpos terapéuticos con nanopartículas magnéticas (MNP), ya que se ha descrito que la funcionalización mejora su estabilidad y capacidad de ser distribuido de forma selectiva al tumor sin afectar a las propiedades de neutralización de antígeno (Dulińska-Litewka et al., 2019; Sousa et al., 2017).

Hipótesis y objetivos

Este trabajo se basa en los antecedentes que indican a Wnt-11 como una posible diana terapéutica en el cáncer de próstata avanzado y en la viabilidad de los anticuerpos anti-Wnt-11 generados en el laboratorio del Dr. Kypta como agentes capaces de bloquear su señalización y función aberrante. Adicionalmente, se hipotetiza que su conjugación a nanopartículas magnéticas puede mejorar sus potenciales propiedades terapéuticas. Así, se proponen los siguientes objetivos:

1. Determinar los efectos de los anticuerpos anti-Wnt-11 y los conjugados con nanopartículas magnéticas en modelos de cáncer de próstata *in vitro* e *in vivo*.
2. Explorar el mecanismo de acción de los anticuerpos en el bloqueo de función y señalización por Wnt-11.

Materiales y métodos

Para este estudio se han empleado diversos métodos y técnicas de biología celular y molecular. Se ha llevado a cabo el cultivo de líneas celulares de cáncer de próstata en los que se ha analizado el efecto de la transfección de plásmidos, del silenciamiento génico y del tratamiento con los anticuerpos anti-Wnt-11 y sus nanoformulaciones en ensayos de proliferación, migración e invasión celular. También se han empleado análisis RNA por PCR

en tiempo real cuantitativa (RT-PCR) y de proteína por western blot, así como ensayos de inmunoprecipitación (IP), inmunofluorescencia (IF), inmunohistoquímica (IHC), de clasificación de células activadas por fluorescencia (FACS) y de gen reportero, entre otros. Se ha empleado el modelo *in vivo* de membrana corioalantoidea de pollo (CAM) para estudios de formación de tumor.

Resultados

Capítulo I: Caracterización de anticuerpos anti-Wnt-11 y sus conjugados con nanopartículas magnéticas (MNP)

Se lleva a cabo la caracterización en contexto celular del reconocimiento por parte de los anticuerpos anti-Wnt-11 E8 y F10, que reconocen el mismo epítopo de Wnt-11. Se demuestra por western blot de proteína recombinante, que el anticuerpo anti-Wnt-11 E8 es específico para Wnt-11 al no detectar la proteína homologa Wnt-3a. E8 también detecta por inmunofluorescencia las células que expresan Wnt-11 en el modelo de sobreexpresión estable en células de próstata C4-2B (C4-2B-WNT11), mostrando co-localización con un anticuerpo comercial anti-Wnt-11. La interacción en contexto celular también se analiza por un método indirecto basado en FACS. Para esto, células HEK 293 que expresan Wnt-11 son teñidas con E8 para su clasificación por FACS en base a niveles de tinción alto/bajo. Estas dos poblaciones se procesan para el análisis por western blot y se demuestra que las células que presentan una alta intensidad de tinción de E8 expresan mayores niveles de la proteína diana Wnt-11.

Por otro lado, se realiza una caracterización preliminar de las nanopartículas magnéticas (MNP) conjugadas con los anticuerpos anti-Wnt-11. Para ello se emplean células de cáncer de próstata VCaP, que presentan altos niveles de expresión de Wnt-11 endógeno, se incuban con las MNP funcionalizadas y se realiza una tinción de Prussian Blue para la detección del hierro presente en las MNP. Así, las células incubadas con las MNP-E8 muestran una tinción de MNP en membrana, compatible con la detección de Wnt-11, la cual es superior en intensidad a la obtenida usando las MNP no funcionalizadas o funcionalizadas con IgG como control.

Capítulo II: Efectos de los anticuerpos anti-Wnt-11 y sus conjugados con MNP en células de cáncer de próstata *in vitro*

Se procede a analizar los efectos de los anticuerpos y nanopartículas funcionalizadas en ensayos *in vitro* que, se ha visto en otros estudios, pueden estar mediados por Wnt-11. Así, se detecta una inhibición limitada en el crecimiento en adherencia de células de cáncer de próstata PC3 y DU145 en ensayos a 7 días, solo a dosis altas de los anticuerpos. Por otro lado, se observa que células PC3 cultivadas en condiciones para el estudio de células madre en ensayos de formación de esferas, aumentan la expresión de la proteína y del mRNA de Wnt-11. Además, el mRNA de Wnt-11 mantiene una correlación con el marcador de células madre SOX2 lo que sugiere una implicación de Wnt-11 en este contexto. Por ello, se estudia el efecto de los anticuerpos ant-Wnt-11 en ensayos de formación de esferas y se determina que son capaces de inhibir la formación de esferas de PC3 y DU145 de forma superior a la capacidad de estos de inhibir la proliferación en adherencia.

Wnt-11 es conocido por tener un papel importante en la migración e invasión celular (Uysal-Onganer et al., 2010). Se observa que el silenciamiento génico de *WNT11* reduce la migración de células PC3 medida por ensayos de cicatrización de herida (*wound healing*) y se determina que los anticuerpos anti-Wnt-11 producen una inhibición similar en este contexto. Se confirma por ensayos de migración celular en *transwell* la reducción en la migración de células PC3 y DU145 tratadas con los anticuerpos anti-Wnt-11. En células C4-2B-WNT11, que sobreexpresan Wnt-11, se observa que éste induce la invasión celular y se determina que el tratamiento con los anticuerpos anti-Wnt-11 revierte este fenotipo, reduciendo la invasión celular.

Además, Wnt-11 ha demostrado tener un papel relevante en la respuesta a la hipoxia celular, donde sus niveles se ven aumentados en hipoxia y promueve la migración e invasión celular (Mori et al., 2016). Se estudia por tanto su papel en células PC3 tratadas con el hipoximimético DMOG y se detecta un aumento en la expresión de Wnt-11 y un incremento en la migración celular. El empleo de los anticuerpos anti-Wnt-11 en este contexto es capaz de revertir parcialmente el incremento en la migración celular en células PC3 sometidas a hipoxia. Se realiza un estudio por RT-PCR de la expresión de otros componentes de la ruta Wnt en condiciones de hipoxia y se determina que también se incrementan la expresión mRNA del receptor de Wnt-11, *FZD8* (Murillo-Garzón et al., 2018).

Se estudian de forma paralela los efectos de las MNP conjugadas con los anticuerpos anti-Wnt-11. Se observa que ninguno de los conjugados MNP reducen la viabilidad de células PC3. También se demuestra que las nanopartículas magnéticas conjugadas con E8 (MNP-E8) producen una reducción en la migración de células PC3 medida por ensayos de cicatrización de herida, y, que las MNP-F10 muestran una tendencia no significativa de reducción.

Capítulo III: Efectos de los anticuerpos anti-Wnt-11 y sus conjugados con MNP en células de cáncer de próstata *in vivo*

Los efectos del anticuerpo E8 y de las nanopartículas son estudiados en el modelo *in vivo* de la membrana corioalantoidea de pollo CAM en ensayos de formación de tumor con células PC3. El tratamiento con E8 de los tumores de PC3 en la CAM produce una disminución significativa tanto en el área del tumor y como en el peso del tumor cuando se compara con los tumores tratados con el control de IgG. Adicionalmente, se determina por inmunohistoquímica que los niveles nucleares de expresión del marcador de proliferación Ki67 se encuentran reducidos en los tumores tratados con E8 lo cual apoya corrobora los resultados en la reducción del crecimiento tumoral.

Los conjugados con nanopartículas magnéticas, especialmente MNP-E8, también son capaces de reducir la formación de tumor de PC3 en la CAM, aunque de forma más modesta que E8 sin conjugar, lo cual puede ser debido a la menor dosis empleada en comparación. De forma preliminar también se observa una reducción en la intensidad de la expresión de Ki67 nuclear en los tumores tratados con MNP-E8 comparado con los tratados con MNP-IgG y, además, se emplea la tinción por Prussian Blue para demostrar la presencia y localización de las MNP en los tumores.

Capítulo IV: Mecanismo de acción de los anticuerpos anti-Wnt-11

Por último, se explora el mecanismo de acción de los anticuerpos anti-Wnt-11. Primero, se detecta mediante ensayos de cambio en la movilidad electroforética, que en células PC3 tratadas con E8 y F10 los niveles de fosforilación del mediador de Wnt, Dishevelled (DVL) se encuentran reducidos con respecto al tratamiento con IgG control. También se demuestra en base uso del inhibidor de secreción de Wnt, Wnt-C59, que la fosforilación de DVL en células PC3 es dependiente de Wnt; y, que la regulación de DVL mediada por los anticuerpos anti-Wnt-11 ocurre a nivel de proteína y no de mRNA.

Para el estudio del potencial papel de la región epítopo en Wnt-11, se genera un mutante (AE, *Epítopo del Anticuerpo delecionado*) delecionando parte del epítopo de los anticuerpos ΔL101-T108 (`LLDLERT`). Para no afectar a la estabilidad de la proteína se estudia que la región no forme estructura secundaria y además se conjetura que es esta secuencia la que media la mayor parte del reconocimiento de los anticuerpos. Para apoyar esto, se confirma que el mutante AE se expresa, secreta y se encuentra en la membrana de forma similar a la proteína Wnt-11 nativa. Además, por ensayos de FACS se determina que la unión de E8 a este mutante es mínima comparándose con la unión a Wnt-11 nativo.

La expresión exógena de Wnt-11 aumenta la migración de células PC3M, en cambio cuando se expresa el mutante AE la migración no aumenta, sugiriendo que su función está impedida y que el epítopo es esencial para la actividad mediada por Wnt-11. A nivel de señalización se demuestra que la expresión exógena de Wnt-11 aumenta la fosforilación de DVL de manera dependiente de tratamiento con el inhibidor Wnt-C59, mientras que el mutante AE es incapaz de promover una fosforilación similar. Además, se observa que, mientras la expresión exógena de Wnt-11 reduce la activación de la transcripción dependiente de β-catenina/TCF activada por Wnt-3a en ensayos de gen reportero, el mutante AE es incapaz de mediar la inhibición. Estos resultados sugieren que la señalización por Wnt-11 se encuentra impedida.

La visualización del epítopo en la región homóloga de la estructura resuelta para otros Wnts, mediante alineamiento de sus secuencias proteicas, demuestra que éste se encuentra lejos de las regiones de interacción con FZD y relativamente cerca de la zona que ha sido propuesta para la interacción con el correceptor LRP6 (Hirai et al., 2019). En base a esto se estudia la interacción por inmunoprecipitación, primero de Wnt-11 con FZD8 y, se observa que la unión del mutante AE no se encuentra impedida. Se analiza la interacción de Wnt-11 con LRP6 y se detecta que se unen y además que la interacción con el mutante AE se encuentra reducida. Esto se demuestra con la proteína LRP6 completa, con la región exclusivamente extracelular o ectodominio (LRP6N) y en células PC3 y HEK 293. Se confirma este hallazgo por ensayos de co-localización por inmunofluorescencia, en los que se observa una menor co-localización del mutante AE respecto a Wnt-11 nativo.

A nivel de señalización mediada por receptores y coreceptores de Wnt, se observa que Wnt-11 inhibe la activación mediada por LRP6 de la transcripción dependiente de β-catenina/TCF; mientras que el mutante AE no es capaz de inhibir esta activación. Se explora el posible papel de LRP6 en la transducción de la ruta dependiente de ATF2 en la que Wnt-11 se ha descrito

como mediador de su activación (Murillo-Garzón et al., 2018). Se observa que la expresión de LRP6 no activa la transcripción dependiente de ATF2, ni tiene una actividad aditiva con Wnt-11 en células PC3. En cambio, en un modelo de HEK 293 con LRP5 y LRP6 inactivados genícamente (LRP5/6$^{-/-}$), se demuestra que LRP6 es capaz de cooperar en la señalización dependiente de ATF2 inducida por la expresión exógena de Wnt-11/FZD8, mientras que no coopera en la actividad inducida por AE/FZD8. Así, se propone que el LRP6 endógeno es el principal factor causante de las diferencias descritas cuando se emplea el mutante AE y que la región epítopo está implicada en la interacción y señalización mediada por el coreceptor LRP6.

Conclusiones

Los resultados obtenidos en esta tesis permiten concluir lo siguiente:

1. Dos anticuerpos monoclonales, E8 y F10, se unen al mismo epítopo en Wnt-11 e inhiben procesos mediados por Wnt-11 como son la fosforilación de DVL, la formación de esferas de células de cáncer de próstata, la migración celular en normoxia e hipoxia y la invasión celular.
2. Nanopartículas magnéticas de óxido de hierro (MNP) funcionalizadas con los anticuerpos neutralizantes anti-Wnt-11 inhiben la migración de células de cáncer de próstata sin afectar a la viabilidad.
3. El anticuerpo E8 y su nanoformulación MNP-E8 reducen el crecimiento de tumor de células de cáncer de próstata PC3 *in vivo* en el modelo de la membrana corioalantoidea de pollo (CAM).
4. La región epítopo de los anticuerpos anti-Wnt-11 es necesaria para la inducción de la fosforilación de DVL y la migración de células de cáncer de próstata PC3M.
5. La deleción de la región epítopo de los anticuerpos anti-Wnt-11 reduce su interacción con el correceptor de Wnt LRP6 y limita la capacidad de Wnt-11 de inhibir la actividad transcripcional β-catenina/TCF y de potenciar la actividad transcripcional FZD8/LRP6/ATF2.
6. Los anticuerpos neutralizantes de Wnt-11 y sus nanoformulaciones tienen el potencial para ser explorados como agentes terapéuticos en el tratamiento de pacientes con cáncer de próstata avanzado.